

# Fracture Mechanics of Nanostructured Polymer Blends with Janus Particles

Von der Fakultät für Ingenieurwissenschaften  
der Universität Bayreuth  
zur Erlangung der Würde eines  
Doktor-Ingenieurs (Dr.-Ing.)  
genehmigte Dissertation

von

*M.Sc. (hons) Ronak Bahrami*

aus

*Teheran*

Erstgutachter:	Professor Dr.-Ing. Volker Altstadt
Zweitgutachter:	Professor Dr. Axel HE. Müller
Tag der mündlichen Prüfung:	26.04.2018

Lehrstuhl für Polymere Werkstoffe  
Universität Bayreuth  
2018

## Short Summary

For the first time, novel Janus nanoparticles (JPs) were used in sufficiently large quantities for industrial scale blend compatibilization experiments. Several 100 g batches of JPs were prepared and successfully employed as compatibilizers in technologically relevant poly(2,6-dimethyl-1,4-phenylene ether)/poly(styrene-*co*-acrylonitrile) (PPE/SAN) blends. The obtained small PPE droplet sizes of less than 300 nm (at 10 wt.% JPs in the blend) greatly outperformed the co-continuous neat blend but also the blend compatibilized with a linear SBM (polystyrene-*block*-polybutadiene-*block*-poly(methyl methacrylate)) triblock terpolymer as benchmark material. This clearly shows the outstanding performance of JPs as compatibilizers in polymer blends. Additionally, huge discrepancies in the blend morphology depending on the blending equipment was found (mini-compounder (g scale) vs. extruder (kg scale)). This demonstrates the importance of large-scale experiments before considering possible applications. The optimum JP content, necessary to achieve a homogenous morphology after compatibilization, was found to be between 2-5 wt.%, which is significantly lower than the amount needed for SBM triblock terpolymers (10 wt.%).

Fracture mechanics analysis of JP compatibilized blends revealed significantly stronger interface bonding compared to the neat and SBM compatibilized blends. The JP compatibilized blends show higher strength and stiffness at the interface compared to the SBM compatibilized blends, which results in lower toughness of the material when used solely in the blend as compatibilizers. However, it is possible to tailor the nano/micro structure *via* a combination of JPs and SBM triblock terpolymers to tune the macro properties such as toughness. Combination of JPs with a SBM triblock terpolymer as compatibilizer in the blend resulted in a fine morphology with small PPE droplets with radius of 100 nm, which homogenized the deformation in the blend. The toughness as well as resistant against crack growth of the blend was significantly improved over a wide range of crack propagation rates, revealing the synergistic effect of a reduced PPE domain size (mediated by JPs) and an elastic interface (mediated by the SBM triblock terpolymer). Furthermore, understanding the deformation micromechanisms of each compatibilizer is the key point to design blend morphologies with tailored mechanical properties.

As an outlook, JPs were also employed in foaming PPE/SAN blends to observe their potential as highly active foam nucleating agents. The JPs increase the melt strength of the blend and stabilize the cellular structure with smaller cell sizes. The strong JP mediated linkage at the interface could also produce homogenous foams with a partially open cellular structure. The average foam cell size was decreased over 50 % to 900 nm compared to the neat blend and the minimum foam density reached was 550 kg/m<sup>3</sup> (compared to the neat blend with densities of around 900 kg/m<sup>3</sup>).

## Kurzzusammenfassung

Neuartige Janus-Partikel (JP) wurden zum ersten Mal in technologisch relevanten Mengen (mehrere 100 g) synthetisiert und für die Herstellung von Polymerblends im industriellen Maßstab eingesetzt. Die JP wurden als Phasenvermittler in unverträglichen Poly(2,6-dimethyl-1,4-phenylenether)/Poly(styrol-co-acrylnitril) (PPE/SAN) Polymerblends im industrie-relevanten Maßstab durch Extrusion verarbeitet. Im Vergleich zum reinen co-kontinuierlichen PPE/SAN-Blend und dem mit SBM Triblockterpolymer (10 Gew-%) kompatibilisierten Blend, konnte mit JP eine wesentlich kleinere PPE-Tröpfchengröße (unter 300 nm bei 10 Gew-% JP) und eine homogenere Verteilung der PPE Tröpfchen in der SAN-Matrix erreicht werden. Dies manifestiert die ausgezeichnete Einsatzbarkeit von JP als Verträglichkeitsvermittler in Polymerblends. Es muss hierbei allerdings berücksichtigt werden, dass die Blendmorphologie sehr stark von der Art der Verarbeitung und den verwendeten Geräten (Mini-Compounder (g-Maßstab) gegenüber Extruder (kg-Maßstab)) abhängt. Dies zeigt, dass Extrusionen im industrierelevanten Maßstab unabdinglich sind um mögliche Anwendungsfelder zu erschließen.

Bruchmechanische Untersuchungen haben gezeigt, dass die mit JP kompatibilisierten Blends eine viel stärkere Grenzflächenanbindung besitzen als das reine oder mit SBM Triblockterpolymer kompatibilisierte Blendsystem. Dies führt zu einer höheren Festigkeit und Steifigkeit der Phasengrenzfläche in den JP basierenden Blends, die allerdings mit einer im Vergleich zum SBM kompatibilisierten Blend wesentlich niedrigeren Zähigkeit einhergeht. Um Synergien in den mechanischen Eigenschaften zu erreichen, kann die Mikro-/Nanostruktur der Blends aber durch eine Mischung aus JP und SBM Triblockterpolymer maßgeschneidert und so die Zähigkeit wesentlich verbessert werden. Diese Kombination aus JP und SBM Triblockterpolymer als Phasenvermittler resultiert in einer pseudo co-kontinuierlichen Morphologie und sowohl die Verkleinerung der PPE-Tröpfchengröße (durch JP) als auch die elastischere Grenzfläche (durch SBM) des PPE/SAN-Blends führt insgesamt zu einer erheblich verbesserten Beständigkeit gegen Ermüdungsrissausbreitung. Für die Entwicklung von Polymerblends mit maßgeschneiderten mechanischen Eigenschaften ist es daher essentiell, die wirksamen Deformationsmechanismen für jeden einzelnen Phasenvermittler zu kennen um die Morphologie der Blend-Systeme exakt an die Anforderungen anpassen zu können.

JP können zudem als hocheffiziente Nukleierungsmittel in PPE/SAN-Schäumen verwendet werden, was das große Potential von JP in technologisch relevanten Anwendungen unterstreicht. Die JP erhöhen die Schmelzefestigkeit während der Verarbeitung, wodurch Zellstrukturen mit kleineren Schaumzellen effizient stabilisiert werden können. Die durch JP vermittelte starke Anbindung zwischen den PPE und SAN Phasen führt zudem zu sehr homogenen Schäumen mit einer partiell offenen Zellstruktur. Im Vergleich zum reinen PPE/SAN Schaum konnte die Zellgröße im JP kompatibilisierten Schaum um 50 % auf 900 nm reduziert werden und die Zelldichte nahm insgesamt um etwa 40 % von 900 kg/m<sup>3</sup> auf 550 kg/m<sup>3</sup> ab.

## Acknowledgement

I would like to express my especial appreciation to Prof. Dr.-Ing. Volker Altstädt for not only supervision of PhD studies, having creative approaches, and his management style, which gives one freedom to grow, also for being a great mentor. I have learned a lot from him and am so honoured and grateful for the opportunity of working together. I am also very thankful to Prof. Dr. H. E. Müller who co-supervised the project, for his great scientific advices and inputs on our publications. I am also grateful to Dr. Holger Schmalz in the Macromolecular Chemistry II department of Bayreuth university for his novel ideas and constant support during the project, as well as correcting the first version of the dissertation. I also thank Dr. Tina Löbling, my project partner and dear friend, not only for her magical Janus particles, but the great collaboration we had in the way to our PhDs. I would like to thank the German research foundation as well for the financial support of the project within the framework of AL 474/21-1 and MU896/39-1.

It takes a lot more than a small team to get a PhD degree; I am thankful to all members of the Polymer Engineering department in University of Bayreuth during my time there, who provided an open atmosphere for research. Specifically, I would like to name Markus Schirmer and Sebastian Gröschel for their support during polymer processing. Ute Kuhn for interesting rheological discussions and so many DMA measurements. Melanie Förtsch (Müller), Annika Pfaffenberger, and last but not least Annelisa Lang for the amazing job of capturing so many wonderful TEM and SEM images. I owe lots of my interpretations and conclusions to the clear images they captured. I heartfully thank Andreas Mainz and Alexander Brückner for introducing me to the challenging world of fracture toughness measurements and I am grateful for their support. Further on I like to thank Jacqueline Uhm for indirectly linking me to the past and helping with challenges I faced that have already been previously encountered. I also thank Sven Polatzek (Altstädt) for support with the co-kneader processes in Hamburg. In the end, I thank Theresa Adelhardt and Kerstin Mosig who have been always there for administrative support. I also thank all my Diploma and Master students (Stefanie Bärwinkel whose work contributed to the outlook of my dissertation, Jasmin Walther, Christoph Callsen, and Jessica Pater) together with all other students with project works, and student assistants that taught me to trust with delegating. I like to mention my officemates Michaela, Bianca, and later Christoph. It would have been very difficult to go through some days without our occasional office “laugh/nag” sessions.

In loving memory of Ms. Alireza, my first chemistry teacher in high school, who introduced me to the world of polymers and greatly influenced my life path.

In the end, I would like to express my ultimate gratitude to my mother, Soraya, my father, Mohsen, and my dearest little sister Roya for their love and encouragement. I have been blessed with a loving, supportive family that have always believed in me and taught me that I could do anything I set my mind up to. Without them and their support I wasn't the person I am today, and couldn't have achieved what I have now. Last but definitely not least, I thank my love, my best friend, and my dear husband Amir, who has shared this entire amazing journey with me and has been there every single step and has seen me through the ups and downs of the entire process. Without his smile every morning, I would start my days as a much grumpier person; without his love and kindness, I would lose balance.

Writing this dissertation would not have been possible (or half as much fun) without the support of all my family, friends, colleagues, and mentors. Thanks, Danke, سپاسگزارم

# Table of contents

<b>1</b>	<b>Introduction and motivation</b>	<b>1</b>
<b>2</b>	<b>State of the art</b>	<b>4</b>
2.1	Polymer blends	4
2.1.1	Thermodynamics	5
2.1.2	Morphology and rheology of polymer blends	10
2.2	Compatibilization of polymer blends	15
2.2.1	Compatibilization <i>via</i> graft and block copolymers	19
2.2.2	Hierarchical self-assembly of ABC triblock terpolymers in bulk and solution	21
2.2.3	Janus particles	22
2.3	Mechanical properties of polymer blends	24
2.3.1	Deformation mechanisms in polymer blends	25
2.3.2	Fracture mechanics of polymer blends	26
2.4	Chemical resistance of polymer blends	33
2.4.1	Measures to improve chemical resistance	34
2.4.2	Methods of determining the chemical resistance of polymers	34
<b>3</b>	<b>Goals and approaches</b>	<b>36</b>
<b>4</b>	<b>Materials and experimental methods</b>	<b>40</b>
4.1	Materials	40
4.1.1	Matrix polymers	40
4.1.2	Compatibilizers	41
4.2	Experimental methods	44
4.2.1	Melt processing of polymer blends	44
4.2.2	Morphological characterization	45
4.2.3	Rheological characterization	46
4.2.4	Thermal and thermomechanical characterization	47
4.2.5	Mechanical characterization	48
4.2.6	Chemical resistance	49
<b>5</b>	<b>Results</b>	<b>51</b>
5.1	Characterization of neat blends and compatibilizers	51
5.1.1	Why PPE/SAN?!	51
5.1.2	Characterization of the compatibilizers	56
5.1.3	Optimization of the melt blending process	58

---

5.1.4	Conclusion.....	62
5.2	Micromechanics of blends compatibilized with SBM triblock terpolymers.....	64
5.2.1	Morphological characterization of SBM compatibilized blends.....	64
5.2.2	Rheological characterization of SBM compatibilized blends.....	70
5.2.3	Mechanical characterization of SBM compatibilized blends.....	71
5.2.4	Conclusion.....	88
5.3	Blends compatibilized with Janus Particles.....	89
5.3.1	Morphological characterization of JP compatibilized blends.....	89
5.3.2	Rheological characterization of JP compatibilized blends.....	100
5.3.3	Mechanical characterization of JP compatibilized blends.....	102
5.3.4	Conclusion.....	111
5.4	Synergistic effects on toughness of blends compatibilized with JPs and SBMs....	114
5.4.1	Morphological characterization of mixed blends.....	114
5.4.2	Rheological characterization of mixed blends.....	117
5.4.3	Mechanical properties of mixed blends.....	118
5.4.4	Conclusion.....	134
<b>6</b>	<b>Summary and Outlook.....</b>	<b>138</b>
6.1	Summary.....	138
6.2	Outlook.....	139
6.2.1	Nanocellular foams from JP compatibilized blends.....	139
6.2.2	Different JPs and JP modified structures.....	143
<b>7</b>	<b>Bibliography.....</b>	<b>145</b>

## Abbreviations

ABS	Acrylonitrile butadiene styrene
AN	Acrylonitrile
CPE	Chlorinated polyethylene
CT	Compact tension
CTOD	Crack tip opening displacement
DMA	Dynamic mechanical analysis
DSC	Differential scanning calorimetry
EPDM	Ethylene propylene diene monomer
FCP	Fatigue crack propagation
FESEM	Field emission scanning electron microscopy
GPC	Gel permeation chromatography
HIPS	High impact polystyrene
JPs	Janus particles
LLDPE	Linear low density polyethylene
MCM	Multi compartment micelle
PA	Polyamide
PA6	Polyamide 6
PAN	Polyanilin
PB	Polybutadiene
PBT	Poly(butylene terephthalate)
PC	Polycarbonate
PDLLA	Poly(D, L-lactide acid)
PE- <i>g</i> -MA	Polyethylene- <i>graft</i> -maleic anhydride
PLA	Poly(lactide acid)
PMMA	Poly(methyl methacrylate)
PP	Polypropylene
PPE	Poly(2,6-dimethyl-1,4-phenylene ether)
PS	Polystyrene
PS-E	Polystyrene-extrusion grade
PS-I	Polystyrene-injection molding grade
PVC	Poly(vinyl chloride)
SAN	Poly(styrene- <i>co</i> -acrylonitrile)
SAN- <i>g</i> -MA	Poly(styrene- <i>co</i> -acrylonitrile)- <i>graft</i> -maleic anhydride
SBM	Polystyrene- <i>block</i> -polybutadiene- <i>block</i> -poly(methyl methacrylate)
SEM	Scanning electron microscopy
TEM	Transmission electron microscopy
TPV	Thermoplastic vulcanizate

## Symbols

$\Delta G_m$	Gibbs free energy of mixing
$\Delta H_m$	Enthalpy of mixing
$\Delta S_m$	Entropy of mixing
$T$	Temperature
$\Phi$	Volume fraction of a polymer chain
$i$	Blend component i
$P_r$	Pressure
$R$	Ideal gas constant
$V$	Volume (total)
$\chi$	Flory-Huggins interaction parameter
$\delta$	Solubility parameter
$z$	Number of contacts between polymers
$\Delta w$	Energy increment
$k$	Boltzman factor
$n_i$	Number of moles in Polymer i
$Ca$	Capillary number
$Ca_c$	Critical capillary number
$\eta$	Viscosity
$\dot{\gamma}$	Shear rate
$r$	Radius of the dispersed phase
$\Gamma$	Interfacial tension
$M_c$	Critical molecular weight of entanglement
$R$	Radius of the dispersed phase or particle
$K_I$	Stress intensity factor
$K_{IC}$	Critical stress intensity factor
$\sigma_f$	Failure stress
$a$	Crack length
$\alpha$	Geometrical parameter
$da/dN$	Fatigue crack propagation
$\sigma$	Applied time dependent stress
$Y_I$	Geometrical factor
$R_s$	Stress ratio
$N$	Number of load cycles
$\Delta K$	Stress intensity factor range
$C$	Material constant
$n$	Material constant
$T_g$	Glass transition temperature
$M_w$	Weight averaged molecular weight
$M_n$	Number averaged molecular weight
$OsO_4$	Osmium tetroxide
$F$	Force
$B$	Thickness of the specimen
$w$	Width of the specimen
$CCl_4$	Carbon tetrachloride

---

$P$	Viscosity ratio
$\Phi_m$	Maximum packing volume fraction
wt. %	Weight percent
$\bar{D}_M$	Molar Mass Dispersity
$\Delta E_{desorb.}$	Energy required to desorb JPs from the blend interface
$\gamma_{PPE/SAN}$	Interfacial tension between the blend components
$R_g$	Radius of gyration
$f_{JP}$	JP content as compatibilizer
$A$	Interface area
$\rho$	Density
$CO_2$	Carbon dioxide

# 1 Introduction and motivation

Multifunctionality is known to be one of the most important factors in current innovations. The idea to design a material that has multiple tailored properties is the key to eliminate unnecessary components within a given device. This can improve the performance while keeping the design simplicity and remaining sustainable. Implementing the idea of multifunctionality requires tailoring the material down to the molecular level and design of materials with macro properties targeted for specific applications. Nanostructured materials are perfect examples of multifunctional designs which can combine multiple properties in a single high performance material. The “nano effect” [1–4] in these structures provides much larger surfaces and interfaces for interactions and plays an important role in materials properties. Nanostructured materials can consist of one or several components depending on their design and manufacturing methods. Examples of single nanostructured materials can include self-assembled particles and structures, whereas for multicomponent nanostructures, polymer nanocomposites, or polymer blends can be named. The way different components interact with each other in these materials would determine the macro properties of the system.

Nanostructured polymer blends are among the most complex, yet most efficient designs for new applications. The idea of using available materials and combining them to produce advanced materials with multiple properties for new applications is of high economical, industrial, as well as scientific interests [5–9]. Recently, several nanostructured blends produced in small scales and via solvent based methods have been introduced and discussed in the literature. Solution based methods provide a medium for self-assembly and allow a more precise control of the structure. However, in order to be able to transfer the knowledge to industrial applications, more economic methods such as melt blending of such materials needs yet to be established. Controlling the morphology and the blend structure during these processes requires understanding of the complex thermodynamical and rheological interactions as well as design of the elements producing the mixing forces between the components.

In the current study, the casing of chemical pumps (**Figure 1**) has been chosen as an example for designing new multifunctional nanostructured materials. The material needs to fulfil several functions such as processability, good mechanical properties under long term vibrations produced by the pump, as well as high chemical resistance against certain solvents. Poly(2,6-dimethyl-1,4-phenylene) ether (PPE) and polystyrene (PS) polymer blends (PPE/PS) are the

commercially available materials for such applications. While blending the highly viscous but ductile PPE with PS has improved the blend processability and provides good mechanical properties for these materials, the chemical resistance of the blend is less than ideal and often additional protection layers are needed. In order to improve the chemical resistance in such blend systems, one can replace PS by a material with similar viscosity to maintain the processability, but showing a better chemical resistance. For this purpose, poly(styrene-co-acrylonitrile) (SAN), which is a copolymer of styrene with acrylonitrile (AN), is a suitable candidate. However, while PPE/PS is a homogenous miscible blend, the alternative PPE/SAN blend is immiscible. Immiscibility in polymer blends usually results in inhomogeneous structures, in which unmodified blend interfaces often act as stress concentration points that can weaken the material's mechanical properties. Hence, compatibilizers, which improve the blend homogeneity and often modify the blend interfaces, have to be added to immiscible blend systems in order to fulfil the required mechanical properties.



**Figure 1** Casing of a chemical pump made of PPE/PS [10]

State of the art compatibilizers for PPE/SAN blend systems are polystyrene-*block*-polybutadiene-*block*-poly(methyl methacrylate), SBM, triblock terpolymers, which are discussed in the literature [11–13]. Adding them to the blend will result in nanostructured materials, in which the morphology can be tuned via different parameters such as block lengths, molecular weight, etc. Recently, newer and novel structures such as Janus particles (JPs) are introduced as possible highly effective compatibilizers for similar systems [14]. JPs are also synthesized from triblock terpolymers, however they are multicompartment micelles with 3D, double faced structures. They combine the amphiphilicity of common surfactants with the Pickering effect of particles and as a result show higher surface activities. Unlike triblock terpolymers that only stabilize the morphology via emulsification, JPs promote the so-called Pickering effect as well

which makes them more effective. However, all studies of JPs up to now have been performed on laboratory scale and often via solution based methods. Hence, it is of high scientific interest to study the behaviour of JPs in the engineering plastic blend systems like PPE/SAN. In addition, it is important to evaluate their performance during large-scale melt blending processing methods, compared to the studies up to now. The PPE/SAN blend compatibilized with JPs is an example of a multifunctional material which requires tailored nanostructures and motivates the current study to explore the performance and effect of JPs on the blend properties.

Looking back at the targeted application area, one finds out that the compatibilized blends would undergo vibrations during their lifetime as casings of pumps. This means that the fracture mechanic behaviour of the blends, specifically the crack propagation mechanisms are of high importance. Therefore, the fracture toughness of the blends, as well as their fatigue crack propagation behaviour of them will be deeply studied.

## 2 State of the art

This chapter gives an overview on polymer blends and their compatibilization, especially with block copolymers. The morphology of triblock terpolymers in bulk and hierarchical self-assembly in solution will be shortly addressed and novel Janus particles will be introduced. Later on, the effect of compatibilization on mechanical properties of blends, focusing on fracture mechanics will be discussed. First, immiscible polymer blends with their complex structures are introduced and the influence of thermodynamical incompatibility and rheological properties on their morphologies are reviewed. Further on, different compatibilization methods for polymer blends, with a focus on recent advances with Janus particles are explained. Additionally, previous studies on PPE/SAN blends and their compatibilization are also discussed to provide a knowledge base for the current study. In the end, deformation mechanisms in polymer blends and their mechanical properties are discussed. The focus would be on the effect of the blend morphology, blend interface, and compatibilization on fracture mechanics.

### 2.1 Polymer blends

The blending of polymers is a well-established and versatile concept to economically unify desirable material properties of multiple components within new materials and builds the foundation of an entire industry [15–17]. It is one of the methods to produce polymer materials with tailored properties chosen from two or more of its polymer components. Another driving force to blend polymer materials is to improve the handling in production and processability. Today, there is already a huge number of polymers with wide range of properties available to industries for commercialization. Hence, there is less need for elaborate development of new polymers, but one can target new, growing applications using available resources *via* the blending of polymers. The possibility of using a minor fraction of high performance polymers to tailor the properties of the major fraction of commodity polymers is extremely cost effective and makes blending attractive for manufactures. These benefits have caused a fast growth of the polymer blending industry for the past four decades [17,18].

The design and development of polymer blends strongly depends on two major parameters: The control of blend morphology and interface. As most polymers are inherently immiscible,

blending often results in formation of multiphase materials with complex structures. The size, shape and distribution of one phase in the other one depends on material parameters (such as the blend composition, viscosity ratio, elasticity ratio and interfacial tension) as well as on processing conditions (*i.e.*, temperature, time, intensity of mixing and the nature of the flow). Therefore, the greatest challenge in the field of multiphase polymer blends is to control the blend morphology *by* tailoring the melt flow during processing and the interfacial interactions between the components to stabilize the produced morphology [19]. In the following sections, fundamentals that allow for understanding the complex interactions between the blend components are discussed. These information's are essential to control the blend morphology and the interactions at the interface. Tailoring nanostructured polymer blends with improved macro properties for specific applications is of high scientific as well as industrial interest.

### 2.1.1 Thermodynamics

A polymer blend is defined as a mixture of at least two polymers or copolymers containing more than 2 wt.% of each component [20]. Polymer blends can be classified into three groups: Miscible, partially miscible and immiscible polymer blends (examples are given in **Table 1**). Most polymers are incompatible, *i.e.*, they do not mix and immiscible blends are formed. A miscible blend forms one phase (homogenous structure), whereas an immiscible blend separates into two phases (inhomogeneous structure). The partially miscible blend shows both, phase-separated and homogeneously mixed regions.

**Table 1** Examples of different blend types

Miscible	Partially miscible	Immiscible
<b>PPE/PS</b>	<b>PC/SAN</b>	<b>PPE/SAN</b>
<b>PVC/PCL</b>	<b>PET/PHB</b>	<b>PC/ABS</b>
<b>PMMA/SAN</b>	<b>PMMA/PVC</b>	<b>PE/PP</b>

Miscibility is governed by some specific characteristics of each component. If the polarities of polymers are similar, it is more likely that they are miscible with each other. By introducing specific interactions, like hydrogen bonding, Van-der-Waals and ionic forces, the miscibility can

specifically be favoured towards one polymer. Miscibility also depends on the molecular weight and is usually higher between blend components of lower molecular weights. This is due to the larger effect of entropy compared to enthalpy in a polymer blend system [21].

The thermodynamic requirement for miscibility in a polymer blend can be expressed by the Gibbs free energy of mixing ( $\Delta G_m$ ), shown in equation 1 [18].

$$\Delta G_m = \Delta H_m - T\Delta S_m \quad (1)$$

If  $\Delta G_m$  is negative, the polymers would be miscible. This requirement, however, is not enough and the second deviation of  $\Delta G_m$  with respect to the concentration has to be considered as well. This means that the behaviour of the Gibbs free energy as a function of volume fraction should be a concave curve which has a maximum point. The miscibility of two polymers can be sum up in the equations 2 and 3. Where  $\phi_i$  is the volume fraction of polymer  $i$  in the blend, and  $P_r$  represents the pressure.

$$\Delta G_m \leq 0 \text{ and } \left( \frac{\partial^2 \Delta G_m}{\partial \phi_i^2} \right)_{T, P_r} > 0 \quad (2) \text{ and } (3)$$

For partially miscible blends, the Gibbs free energy is also negative. Here, in contrast to miscible blends, the second derivative of the Gibbs free energy is negative as well. This leads to equation 4 and 5 which describe the partially miscible blends.

$$\Delta G_m \leq 0 \text{ and } \left( \frac{\partial^2 \Delta G_m}{\partial \phi_i^2} \right)_{T, P} < 0 \quad (4) \text{ and } (5)$$

Partially miscible blends, have an area in their phase diagram where they separate into two phases (one is rich in blend component 1 and the other phase is rich in blend component 2). In this case, the temperature plays a key role in determining the blend miscibility. Increasing the temperature leads to a larger  $T\Delta S_m$  term which could drive the  $\Delta G_m$  to more negative values and result in increased miscibility. However, for higher molecular components, the  $T\Delta S_m$  is relatively small and there are other factors effecting the  $\Delta H_m$  term more significantly. This would lead to a reverse behaviour, meaning that by increasing the temperature, miscibility would decrease. Polymer blends belonging to the first group mentioned, exhibit upper critical solution temperatures (UCST) behaviour, and by increasing temperature, their miscibility increases. The latter group has lower critical solution temperature (LCST) behaviour, meaning that by increasing the temperature, the miscibility decreases and the phase separation happens.

In most cases, polymer blends are immiscible and equation 6 is for them valid.

$$\Delta G_m > 0 \quad (6)$$

The positive value of the Gibbs free energy in immiscible blends results in phase separation and formation of multiphase structures.

Among well-known examples of miscible polymer blends are PPE/PS blends, which are miscible over a complete composition range [22,23]. The interactions between the  $\pi$ -electron donor site (aromatic rings) in PS and electron deficient methyl groups of PPE has been proposed as the cause for miscibility [24]. Blending with PS has facilitated the processability of the PPE, which is difficult to process due to its high  $T_g$  and viscosity. This has made PPE/SAN blends available for several applications such as electronics (due to the inherent fire-retardant behaviour of PPE) under the trademark Noryl [25]. Another example of miscibility between polymers are blends of polymethylmethacrylate (PMMA) and SAN. Here, the miscibility window is observed in a composition range of 9-33 wt.% AN in SAN [26–28]. The miscibility is suggested to happen due to the repulsion effect between styrene and acrylonitrile units in SAN and other intermolecular interactions [29,30]. Even though SAN is a copolymer of PS and has a relatively similar structure to it, the incorporation of AN strongly reduces its interactions with PPE. This leads to the immiscibility of PPE/SAN blends for AN contents of more than 11 wt.% in SAN [31]. This miscibility window of the SAN with PPE with respect to the interfacial energy of the blend is shown in **Figure 2**. Commercially available SAN grades have AN contents of 18-32 wt.% and fall into the immiscible region.

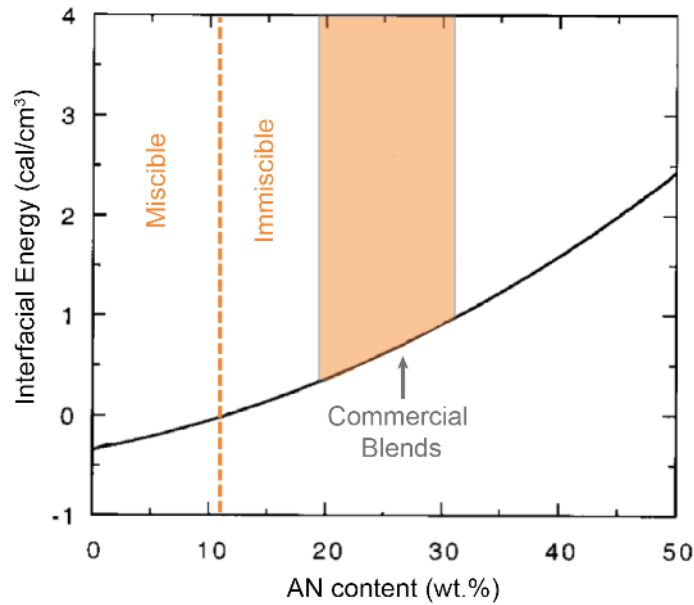


**Figure 2** Interaction energy of PPE/SAN blends as a function of AN content in SAN [31]

#### 2.1.1.1 Flory-Huggins theory

Flory and Huggins proposed the most popular theory for the thermodynamics of polymer mixtures in 1941 [32,33]. They developed a simple expression for the Gibbs free energy of mixing based on an empiric approach to describe the enthalpy ( $\Delta H_m$ ) and entropy ( $\Delta S_m$ ) of mixing. For describing the entropy, a lattice as a basis is defined and it is assumed that the interactions between the polymer components in a mixture happens in this lattice. The second assumption defines the polymer as a flexible chain with connected segments that consists of molecules with the same size, as can be seen in **Figure 3** [21,34,35].

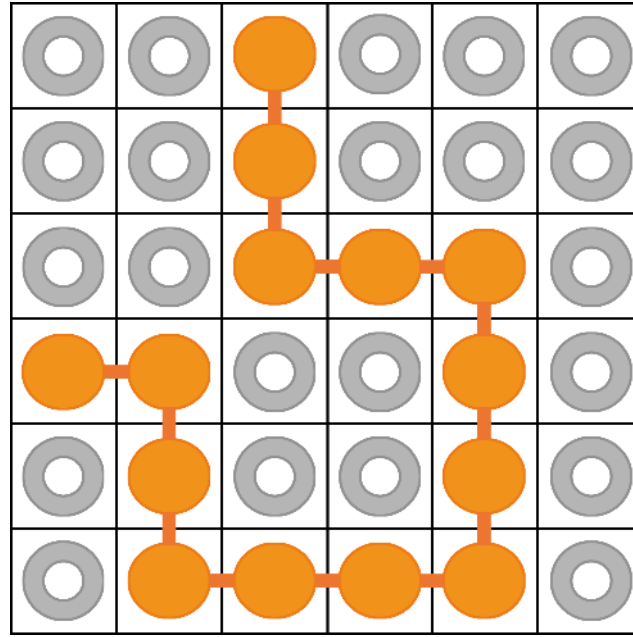


**Figure 3** Schematic model of the Flory-Huggins Theory

Based on equation 1, in order to calculate the Gibbs free energy, the mixing enthalpy and mixing entropy should be calculated separately. The entropy of mixing in a Flory-Huggins theory is calculated based on the number of configurations that a collection of polymer chains with a known number of segments (monomers) can have on the lattice. The change in entropy of mixing is calculated based on statistical mechanics and the increase in spatial uncertainty as a result of mixing the polymer with a solvent. Hence, the entropy of mixing represents the probability of a given random lattice site being occupied by a polymer segment or a solvent molecule.

In order to calculate the enthalpy of mixing, different interactions (bonds) between the molecules, which can change the internal energy of the system, should be taken into considerations. The change in enthalpy is equal to the change in the monomer-solvent interaction multiplied by the number of such interactions. Here, the Flory-Huggins interaction parameter,  $\chi$ , is introduced as a unitless equivalent of the solubility parameter,  $\delta$ , which is related to the molecular energy of interaction between the components of a binary system. For a mixture consisting of polymer A and B, following equation describing the free energy of mixing is proposed:

$$\Delta G_m = RTV \times \left( \frac{\phi_A}{V_A} \ln \phi_A + \frac{\phi_B}{V_B} \ln \phi_B + \phi_A \phi_B \frac{\chi_{AB}}{V_r} \right) \quad (7)$$

Where  $R$  is the ideal gas constant, and  $v$  the total volume. The first two terms on the left side of the equation 7 represent the entropy of mixing. Thereby  $v_i$ , represents the molar volume of Polymer A and B, and  $v_r$  shows the molar volume of a specific segment. The third term represents the enthalpy of mixing and contains the Flory-Huggins interaction parameter.  $\chi$ , is the only material-specific parameter in this model and describes the interaction between two polymers in the solid state. It is a critical value indicating the miscibility of polymers and describes the thermodynamic phase behaviour with equation 8. Here,  $z$  is the number of contacts between polymers,  $\Delta w$  is energy increment per monomer (A)-monomer (B) contact,  $k$  is the Boltzmann factor, and  $n_A$  is the number of moles in polymer A. If the interaction parameter has negative values, the polymer blend components are miscible. However, in most cases, the  $\chi$  values are larger than zero which indicate immiscibility.

$$\chi_{A,B} = \frac{z \times \Delta w}{k \times T} \quad (8)$$

$$\Delta H_m = k \times T \times n_A \times \phi_B \times \chi_{A,B} \quad (9)$$

The equation 8 shows that by increasing temperature and/or decreasing the amount of contacts, the interaction parameter decreases. When inserting this decreased value in equation 9, it would also decrease the change in enthalpy. Looking at equation 1, one can conclude that this would result in lower  $\Delta G_m$  and improved miscibility of the blend.

Most interactions in polymer mixtures can be discussed based on the Flory-Huggins parameter. Even though other parameters such as pressure and the volume influence the miscibility, they are not considered in the Flory-Huggins theory but appear in more advanced models like the equation of state theory [18,19,36,37].

### 2.1.2 Morphology and rheology of polymer blends

One important factor to consider for immiscible polymer blends is their morphology. The term “morphology” refers to the shape and organization above the atomic level, however, the morphology of polymer blends indicates the size, shape and spatial distribution of one blend phase with respect to the other [19]. Most of the properties of polymer blends (mechanical, rheological, optical, dielectrical) are highly dependent on the blend morphology. Hence, morphology control is of prime importance and has been a challenging task in the past years [16,37–40]. When two immiscible polymers are mixed, the size, shape and distribution of blend

phases depend on material parameters (*i.e.*, blend composition, viscosity ratio, elasticity ratio and interfacial tension) as well as processing conditions (*i.e.*, temperature, time and intensity of mixing, and the nature of the flow) [19]. **Figure 4** shows common morphologies of immiscible polymer blends. Other possible complex structures include fibrillar [41–43], core-shell [44–46] and onion ring like morphologies [19,47]. Each morphology can contribute to the enhancement of different blend properties.

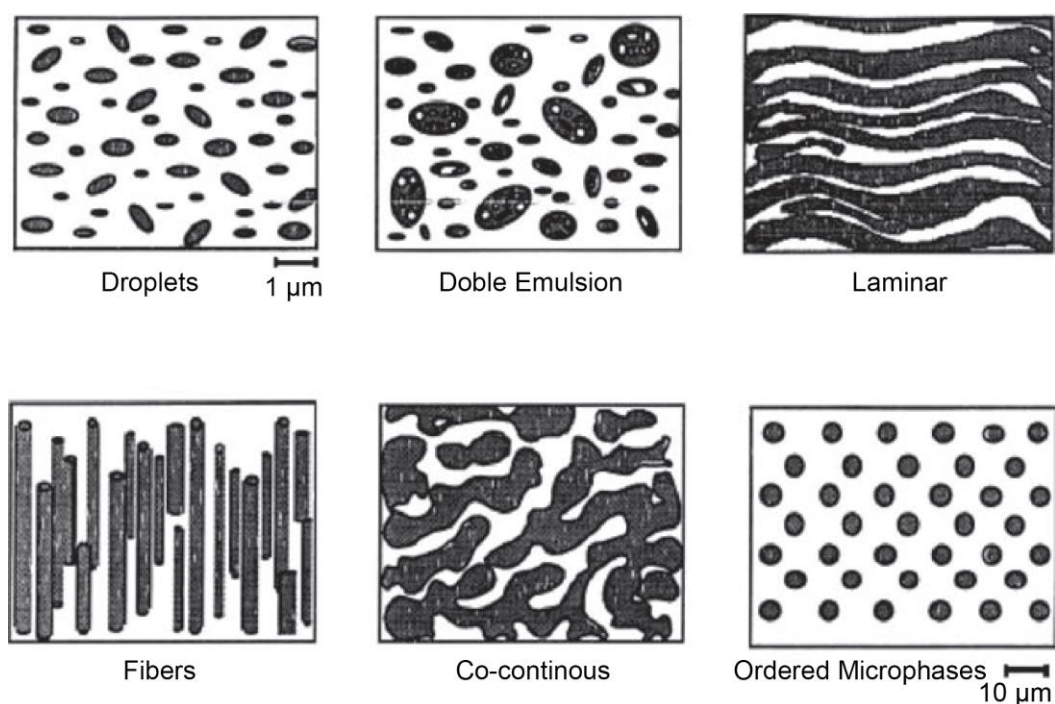


**Figure 4** Schematic representation of common polymer blend morphologies [38]

### 2.1.2.1 Morphology development in immiscible polymer blends

The phase morphology development in immiscible polymer blends during melt mixing and processing is an important topic to discuss. Even in a simplest assumption of dispersing one polymer system in another, complex deformation, breakup and coalescence mechanisms should be considered. At relatively high concentrations of the minor phase, the final morphology results from a competition between break up and coalescence. Whereas, at low concentrations, the droplet break up is the dominant effect that dictates the lower limit of particle size. In certain composition ranges, dispersed droplets and semi continuous fibrils can coexist [48,49]. The final

morphology depends on the fibril stability and whether nodules are formed *via* Rayleigh instability or phase inversion has happened by coalescence of stable fibrils. The Rayleigh break up mechanism defines the thread break up of one blend components into droplets by capillary instabilities during melt mixing [50–52].

In order to be able to predict the morphologies in the blend system, the mechanisms leading to such morphologies need to be considered. In case of immiscible polymer blends the second phase can form different morphological structures such as droplets, fibers, laminar layers and co-continuous phases during melt processing. Superior mechanical properties in terms of toughness and stiffness can be obtained when one phase is dispersed as droplets in the matrix of the other blend component [38]. In addition, it is much easier to investigate the toughening micromechanisms on a system with droplet morphology rather than other structures (*i.e.* co-continuous). The droplet breakup behaviour during melt blending depends on several parameters, like interfacial properties, flow type (shear, elongation, and hyperbolic), etc. In a simple shear flow, four different polymer droplets break up mechanisms can happen as shown in **Figure 5**: 1. The droplets may form a sheet parallel to the flow direction and further on, expand and break up (sheet break up); 2. The droplets may erode at the surface slowly due to high viscosity of one of the matrices (erosion); 3. The droplets may stretch in the perpendicular direction and be cut by sheets in the other direction and break up; and 4. The droplets may spit out small droplets *via* a tip streaming mechanism [19].

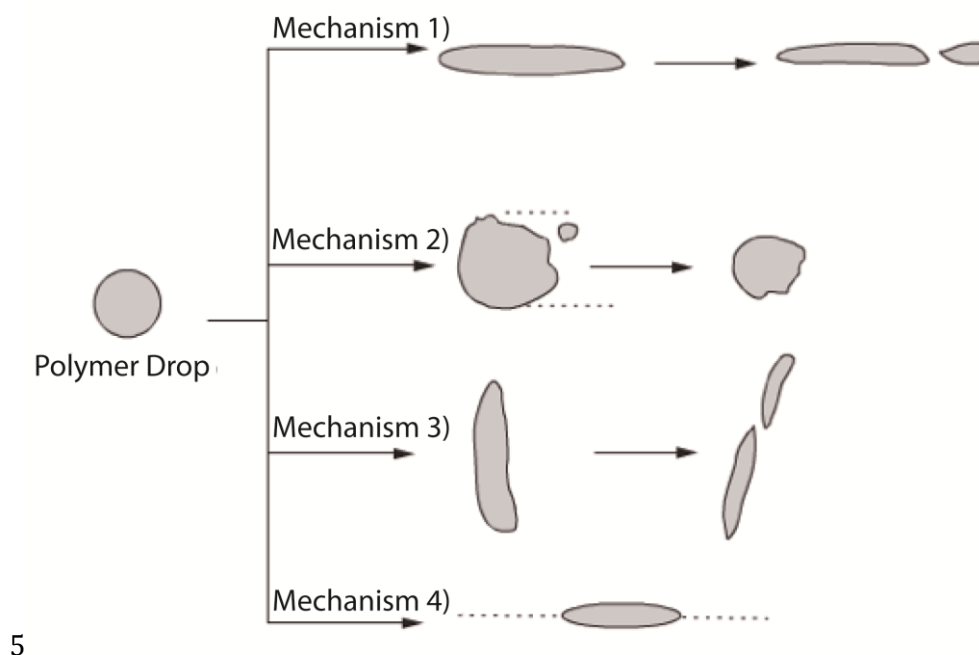


**Figure 5** Droplet break up mechanism in polymer melt blends: 1) Parallel flow direction break up,  $0.05 < \eta_r < 9$ ; 2) Erosion,  $0.05 < \eta_r < 60$ , 3) Perpendicular flow direction break up,  $\eta_r \sim 7.5$  and 4) Tip streaming  $0.05 < \eta_r < 3$  [19]

Usually, the morphology of polymer blends depends on the composition. It was found experimentally for most polymer blends that at low concentration of component 2, the particles of component 2 are dispersed in the matrix of component 1. With increasing concentration of component 2, a partially continuous structure of 2 appears at first, and then, a fully co-continuous structure is formed. After that, phase inversion occurs and component 2 forms the matrix and component 1 the dispersed phase [52,53]. Control of the morphology during processing is the key issue for the production of new materials with improved properties compared to the neat components. The size, shape and spatial distribution of the phases result from a complex interplay between viscosity (and elasticity) of the phases, interfacial properties, blend composition and processing conditions.

### 2.1.2.2 Rheology of immiscible polymer blends

Other factors such as rheological properties of the blend components (mainly their viscosity ratio), interfacial tension between the components, and the processing conditions (the type and

amount of shear forces introduced) also play an important role in determining the final blend morphology. These properties define the droplet size and the complex break up and coalescence mechanisms. Palierne [54,55] has proposed the Palierne's model, which relates the linear viscoelastic material functions of the blend to: 1. rheological properties of its components, 2. interfacial tension between the blend components, and 3. droplet size distribution of the blend inclusions. This most common model predicts higher elasticity at low frequencies, and can explain the relaxation of the dispersed phase. The model has been used successfully to predict the interfacial tension between the components by fitting values to the known data [56–59] or estimation of the droplet size for systems with known interfacial tensions [60,61].

In case of two viscous polymers, drop formation is mainly governed by the capillary number. The dimensionless capillary number ( $Ca$ ) in equation 10 represents the relative effect of viscous forces (coming from shear fields produced during processing) versus surface tension (parameter of the blend system) and summarizes all important factors influencing the blend morphology.

$$Ca = \frac{\eta_m \times \dot{\gamma} \times R}{\Gamma} \quad (10)$$

Where  $\eta_m$  is the viscosity of the matrix,  $\dot{\gamma}$  is the shear rate applied to the system during processing,  $R$  is the radius of the dispersed phase and  $\Gamma$  is the interfacial tension. For each system, a critical value ( $Ca_c$ ) exists, above which the phases break up into droplets. Values smaller than  $Ca_c$  result in elongated phases in a co-continuous system, where there is no droplet break up [62,63]. **Figure 6** shows the critical capillary number as a function of the viscosity ratio of the dispersed phase to the matrix ( $P=\eta_d/\eta_m$ ) for shear flow. It shows that for a certain blend material (with defined matrix viscosity and interfacial tension), a higher shear rate is needed in order to increase the capillary number to induce break up. A higher difference in the viscosity of the blend components (high viscosity ratios) induces a transient mechanism that applies the maximum shear stress directly to the drop. Hence, the droplet goes through stretching and finally breaks up into a finer blend morphology [64]. In reality, the melt viscosity of polymer blends highly depends on the interactions at the interface and the phase morphology. These properties can be tailored and modified *via* addition of an interfacial agent (such as compatibilizer) and will be discussed in the next section.

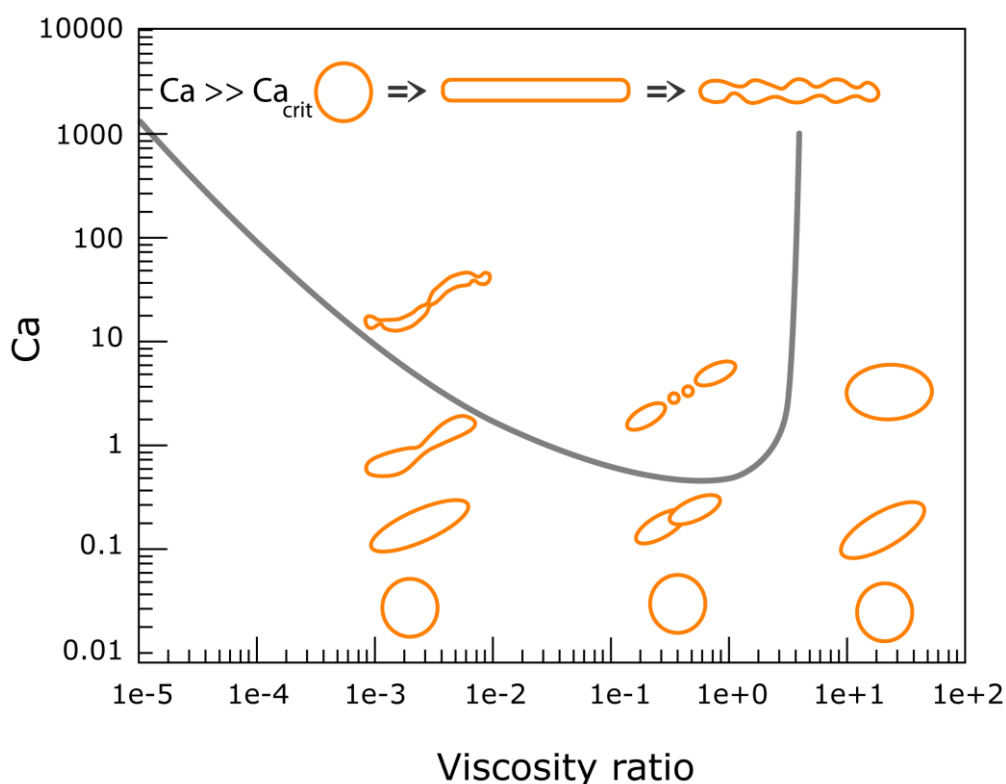


**Figure 6** Critical capillary number to move from a co-continuous to a droplet-matrix morphology for blends with different viscosity ratios (assumption of having a shear flow) [51]

## 2.2 Compatibilization of polymer blends

The inherent immiscibility of polymers usually demands the careful design of blend recipes, processing conditions and/or the addition of compatibilizers to control the blend morphology [35,65,66]. Most immiscible polymers tend to form macrophase-separated regions after blending, that results in a decreased homogeneity in the final blend. The large interfacial tension induces phase coarsening phenomena such as coalescence and Ostwald ripening [67,68]. Furthermore, the poor interfacial adhesion between the blend components causes inferior mechanical properties in the solid state. In addition, one should always keep in mind that there is a chance that the blend would melt further again after compounding (during molding, etc.). Hence, a rapidly cooled system which is quenched as a homogenous system can separate into a multi-phase system due to coalescence of its blend components. Using small amounts of materials known as compatibilizers will help to stabilize the morphology [69] and preserve the desired properties. **Figure 7** [47,70] schematically shows the morphology development of immiscible polymer blends in the presence of compatibilizers. Compatibilizers may add further

functionality to the blend and range from organic molecules to block and graft copolymers [47,71], nanoparticles [72–75] and carbon based reinforcement agents [76,77]. Nanoparticle reinforced composites have evolved into a vivid field of research, owing to the selective localization of particles and, thus, functional matter at the blend interface [8,65,78,79]. In some cases, using compatibilizers can even promote synergistic effects, e.g. compatibilization in combination with enhancing the toughness of the system [39,80]. Compatibilizers are defined as functional additives exhibiting interfacial activities in immiscible polymer blends. The compatibilization process often pursues 3 main goals: (1) Optimization (often reduction) of the interfacial tension between the phases, (2) stabilization of the morphology against high stresses and phase coarsening during processing and forming, and (3) enhancement of adhesion between the phases in the solid state [16,81–83].

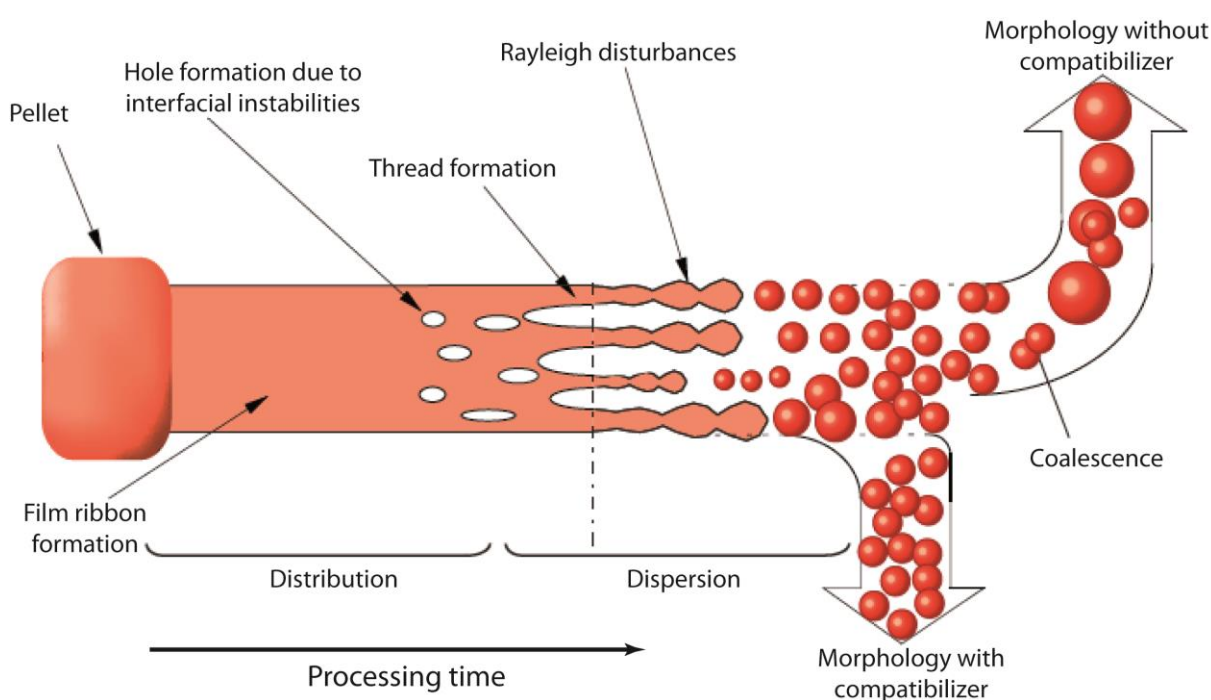


**Figure 7** Morphology development in immiscible polymer blends [84]

### **Influence of compatibilization on the morphology**

The goal here is to decrease the interfacial tension between the blend components and control the blend morphology by influencing the break up and coalescence mechanisms. It is expected for the blend with compatibilizer to result in finer morphologies with droplets of smaller sizes

dispersed in the polymer matrix. The role of compatibilizers is to delay the formation of Rayleigh disturbances on the generated polymer threads by decreasing the interfacial tension [83]. The lower the interfacial tension, the longer the time where the deformation tension would be higher than the interfacial tension, *i.e.*, the thread would stretch for longer times. As a result, the diameter of the thread would get smaller and the droplets generated from it would be also smaller. On the other hand, the compatibilizer at the interface also prevents the coalescence of the droplets occurring during the absence of shear forces and subsequent processing. Reduction of the domain size after compatibilization has often been reported in the literature [85–91].

### **Influence of compatibilization on rheology**

It is expected that the blend phases are somehow attached to each other after compatibilization, which provides extra hindrance against flow. Therefore, effective compatibilization would result in a higher viscosity of the blends compared to the neat (not compatibilized) ones. Moreover, the elastic properties of neat blends depend on energy storage mechanisms at the interphase, as the relaxation of the dispersed phase is often much longer than the relaxation of the polymer chains of the individual components [92,93]. The increase in blend viscosity after compatibilization is discussed in several publications [94–97]. Stary et. al showed that even addition of only 1 wt.% styrene-butadiene-styrene triblock copolymer as compatibilizer to a PS/LLDPE blend lead to a pronounced increase of the stationary elongational viscosity and stabilises the droplets against breakup during flow at  $Ca_{Cr}$  [98].

### **Different compatibilization techniques**

There are several methods for compatibilization of immiscible blends. Depending on their modification strategy, they have been organized into 4 different groups:

1. Compatibilization *via* addition of graft or block copolymers

Emulsification of polymer blends has been proposed as the most efficient tool for obtaining a fine morphology as well as good mechanical properties [99–104]. Since this thesis is also based on the addition of triblock terpolymers and Janus particles, synthesized from triblock terpolymer precursors, this technique will be reviewed in more detail in section 2.2.1.

2. Compatibilization *via* reactive processing

This method is based on the addition of a reactive polymer, which is preferably miscible with one component and reactive towards the functional groups in the other component. During the

reaction, *in-situ* formed block or graft copolymers would compatibilize the blend. Another approach is the addition of low molecular weight polymers such as peroxides (polymeric epoxies), bifunctional chemicals, or a mixture of both to form a compatibilizer (block or graft) during the reactive blending process. Here, the competition between *in-situ* compatibilization, crosslinking and degradation controls the blend properties. In case of polyesters, interchange reactions could also be used to compatibilize immiscible blends. In thermoplastic/elastomer blends selective crosslinking agents can be added to promote vulcanization of one phase and results in thermoplastic vulcanizates (TPVs).

### 3. Mechanochemistry

This method is based on the degradation of the polymers under mechanical shear, which results in formation of free radicals and oxidative degradation. The radicals can combine and form bonds between the blend components. This method is mainly used for elastomers, as they are prone to mastification.

### 4. Incorporation of functional groups/addition of miscible polymers

These less discussed methods of compatibilizing polymer blends include **a)** introduction of specific interactions (where the goal is to modify the blend components in a way that Van der Waals interactions or hydrogen bonds could be induced). Specific interactions between the polymer chains changes the enthalpy of mixing, reduces the interfacial tension and increase the interphase thickness [83]. An example would be compatibilization of the PDLLA/PS blends through specific interactions of the modified PS with carbonyl groups of PDLLA. Here, incorporation of the -OH groups in the PS by copolymerization with hydroxystyrene causes the specific OH...O=C interactions [105]. Another example would be copolymerizing styrene with *p*-(hexafluoro-2-hydroxy-isopropyl)styrene to improve the miscibility of PS with hydrogen acceptor containing polymers such as PMMA, SAN, PET, etc. [106]. **b)** Addition of ionomers for promoting miscibility between the blend components. Similar to the previous method, ionic functional groups could be used to achieve specific interactions such as ion-dipole, hydrogen bonding or transition metal complexation with complementary functional groups on the other polymer. Also, the repulsive interactions between the ionic and non-ionic species of ionomers (that are random copolymers) suggest that the charged polymers may mix with the other polymers through a copolymer effect [107]. Some examples include compatibilization of PBT/PP blends by adding side-chain liquid crystalline ionomers with quaternary pyridinium groups. This resulted in a finer and more uniform distribution of the PP phase in PBT as a result of better intermolecular interactions [107]. Additionally, sulfonated polyester ionomers are commonly

used as compatibilizers for amorphous polyester/polyamide blends and effectively reduce the domain size of the dispersed phase and enhance the mechanical properties [108]. **c)** Addition of a third polymer, (partially) miscible with all blend phases, can also compatibilize immiscible polymer blends. The third component is usually chosen as a common “solvent” for the other 2 components and results in the formation of ternary blends. The miscibility is then dictated based on the blend composition, hence, the phase diagram of such blends gives important information regarding the miscibility regions. Typical examples would be addition of chlorinated polyethylene, CPE, to the blends of PVC with different elastomers (such as ethylene propylene diene monomer, EPDM), in order to improve the miscibility and mechanical properties of the elastomer modified PVC [109]. The incorporation of nanoparticles to produce compatibilized blend nanocomposites can also be included in this category [110–114].

### 2.2.1 Compatibilization *via* graft and block copolymers

The basic interest when using graft or block copolymers is the unique possibility to tailor their characteristic features in a controlled way to (1) decrease the interfacial tension, and more importantly, (2) impart a strong mutual anchoring of the phases [83]. There are several parameters, such as macromolecular architecture of the compatibilizer (graft, linear, star-shaped...), effect of relative length of the blocks in block polymers, amount of added compatibilizer, etc. that influence the efficiency of such compatibilizers and their effect on the morphology and mechanical properties of blends [83]. A critical point here is the molecular weight of each block that has to be higher than the critical molecular weight of entanglement ( $M_c$ ) [115,116] to ensure sufficient attachment to the blend phases.

Block copolymers with selective miscibility of the blocks with each blend components are used as compatibilizers to improve the adhesion in immiscible blends. The location of the block copolymer compatibilizers at the interface stabilizes the morphology and results in finer blend structures as demonstrated in various studies [16,37,117–125]. Lee et. al [126] reported the use of maleic anhydride grafted SAN as a suitable compatibilizer that results in small, uniform dispersed domains and increases both flexural and tensile strengths of PC/PLA blends. Similarly, compatibilizing blends of LDPE/doped Polyanilin (PAN) with polyethylene grafted maleic anhydride (PE-*g*-MA) caused a large increase in the blend ductility [127]. More examples of block copolymer compatibilizers and their influence on the mechanical properties, especially toughness, of the material are discussed in section 2.3.

In the particular case of PPE/SAN blends, SM diblock copolymers and later on SBM triblock terpolymers have shown to enhance dispersion and load transfer between the PPE and SAN phases by selective entanglement of the PS and PMMA blocks in the interfacial region [13,128,129]. Addition of the SBM triblock terpolymers, result in formation of the raspberry morphology [118], which contains discontinuous PB blocks at the blend interface. **Figure 8** shows a scheme of the raspberry structure for a PPE/SAN blend compatibilized by SBM triblock terpolymers. The system has been subjected to many studies on such blends produced *via* solvent-mediated as well as melt processing manufacturing methods. Therefore, the well studied SBM triblock terpolymers are chosen as benchmark material of the current study.

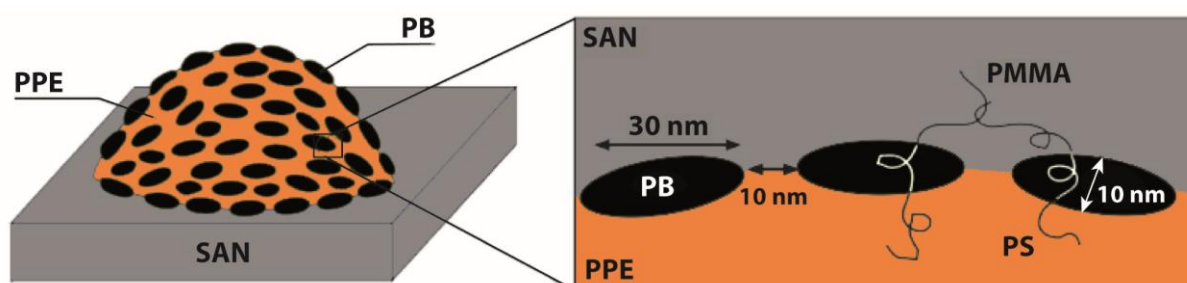


**Figure 8** Raspberry structure of PPE/SAN blends compatibilized by SBM triblock terpolymers [128]

Among disadvantages of block copolymers are their high tendencies to form micelles in the bulk phase (especially during melt blending). Several micelle formation mechanisms (**Figure 9**) have been proposed [11] that result in a decreasing compatibilization efficiency, since the compatibilizer is not located at the interface any more. The proposed mechanisms are based on different values of Flory-Huggins interaction parameters of the compatibilizer end blocks and the blend components. Hence, there is a need for the development of more efficient compatibilizers. The most promising options are discussed in the next section.

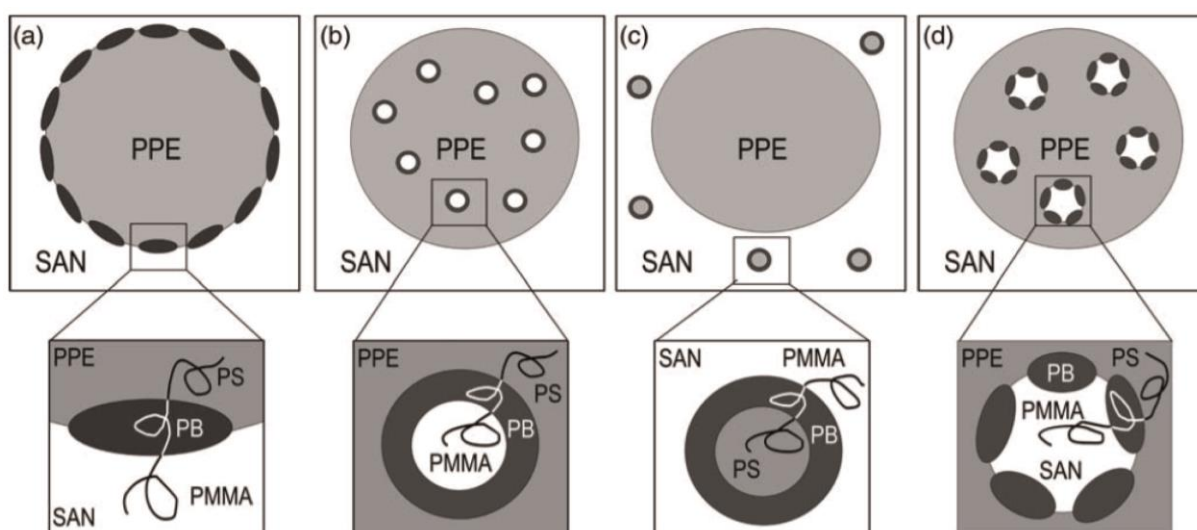


**Figure 9** Possible micelle formation mechanisms in SBM compatibilized PPE/SAN blends: a) SBM at the interface (raspberry morphology, effective compatibilization), b) SBM micelles in PPE, c) SBM micelles in SAN, and d) complex core-shell structures in PPE also known as double emulsion morphology. (b to d are ineffective compatibilization) [11]

### 2.2.2 Hierarchical self-assembly of ABC triblock terpolymers in bulk and solution

Self-assembly of macromolecules in both bulk and solutions enables the formation of well-controlled nanostructures. ABC triblock terpolymers such as SBM show various exotic morphologies in bulk [121] as a result of the balance between enthalpic (interfacial energy) and entropic (chain stretching) contributions of block components. In general, the system tries to minimize the interfacial energy by minimizing the interfacial area between the blocks. Here, the morphologies mainly depend on the polymer-polymer interaction parameters of the blocks with each other as well as the weight fraction of each block. Stadler et al. studied the self-assembly of SBM triblock terpolymers in detail and showed diverse complex structures such as sphere on sphere, sphere on cylinder, and sphere on lamella, as well as helix on cylinder, gyroid, and a “knitting pattern” morphology [120,130–132].

The hierarchical self-assembly of such ABC triblock terpolymers in solution have gain scientific attention recently [133,134]. Different bulk morphologies can be targeted in solution as well when the proper volume ratios and stability regions are chosen. Gröschel has suggested a ternary phase diagram for the morphologies that can appear in the solution (analogue to the bulk morphologies discussed above). The phase separation here also strongly depends on the

volume fraction of the blocks, interfacial tension between the blocks and the interaction parameter. Additionally in solution, surface curvature and interfacial tension at the core-solvent interface have to be considered as influencing factors [135]. Triblock terpolymers rearrange themselves into multi compartment micelles (MCMs) in shape of complex morphologies such as hamburger, football, clovers, or worm like structures [133]. Müller et. al [133,136] have demonstrated a wide array of self-assembled structures using different organic particles (mainly different block copolymers). By changing the parameters mentioned, assemblies such as linear strings of particles, kicked chains, and lattice like networks can be produced [137]. In the following section, one of the spherical MCMs, that is chosen as the compatibilizer for the PPE/SAN system in this work, is discussed in more detail.

### 2.2.3 Janus particles

Janus particles (JPs) are 3D, non-centrosymmetric, anisotropic, colloidal particles with two strictly phase separated hemispheres, differing in their chemical and/or physical properties **Figure 10**. Due to their unique structure, they combine the amphiphilicity of common surfactants with the Pickering effect of nanoparticles, resulting in a superior surface and interfacial activity compared to homogenous particles [138]. Colloidal particles have often been demonstrated to be very efficient in emulsion stabilization [139] and so-called Pickering emulsions can be stable indefinitely. The effect of the amphiphilic nature of JPs on their interfacial behaviour compared to that of homogenous particles was studied in detail by Blinks et. al [138]. They showed that the interfacial adsorption energy of JPs can be up to three times higher than that of homogenous particles of the same size and average wettability (depending on the wettability differences of the two Janus sides). Due to pinning of the contact line on the dividing line between the regions, JPs can retain their interfacial activity at wettability's approaching 0 or 180°. This is different from homogenous particles, as their interfacial adsorption energy becomes very small for extreme wettabilities. Therefore, JPs are generally considered to be more "interfacially active" and to adsorb more likely at the interface compared to the homogenous particles.

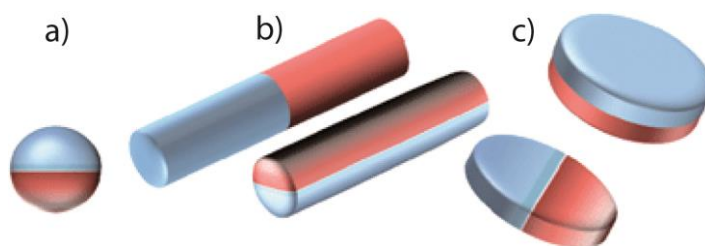


**Figure 10** Overview of possible Janus structures: a) Spheres, b) Cylinders, c) Discs [140]

In that regard, JPs have received much less attention, despite their known exceptional performance in applications that specifically rely on the minimization of interfacial energies (emulsions, suspensions, melts) [141–144]. JPs are the colloidal analogue of surfactants and amphiphilic block copolymers and feature different physical properties on opposing hemispheres [145–147]. The combination of amphiphilicity and particulate character (Pickering effect) favours strong and selective adsorption to interfaces. Among others, this is considered challenging when applying nanoparticle compatibilizers in polymer melts [138,148]. Previous work on PS/PMMA blends compatibilized by JPs with matching PS and PMMA hemispheres served as an ideal small-scale model for comprehensive studies on JP location, blending efficiency and morphological evolution [14]. Since then, only a handful of theoretical works advanced this prospective research field [149–151]. Studies involving JPs mostly focus on blend polymers that allow convenient handling (in experiments and calculations) as to understand underlying mechanisms, while studies on blends with material properties appealing for practical applications have remained beyond laboratories' reach.

There are several works addressing the interfacial activity of JPs derived from ABC triblock terpolymers at liquid-liquid [152–154] and polymer-polymer blend interfaces [130,138]. But despite the tremendous progress in JP synthesis and application of this special particles in solutions [135,140,157–159], their behaviour in polymer melts and their ability to perform and stabilize morphologies under high shear forces has been rarely addressed in literature [14,160]. Specifically, JPs synthesized from a SBM precursor synthesized by the same group [161] will be used in this study. This gives us a similar chemical base of JPs to SBM triblock terpolymers as benchmark materials. The synthesis of the JPs from their SBM precursor is based on the selective precipitation of PB middle block which produces individual micellar particles comprised of several copolymer chains (PB core and PS/PMMA grafted chains). Later on, the PS chains are selectively precipitated and the PB cores are partially crosslinked to form a MCM.

Upon addition of a good solvent for both PS and PMMA, these MCMs yield dispersed JPs that can be freeze dried into a powder form for later processing (schematically shown in **Figure 11**). The detailed methodology is published in various studies [155,161] and discussed in more detail in section 4.1.2.

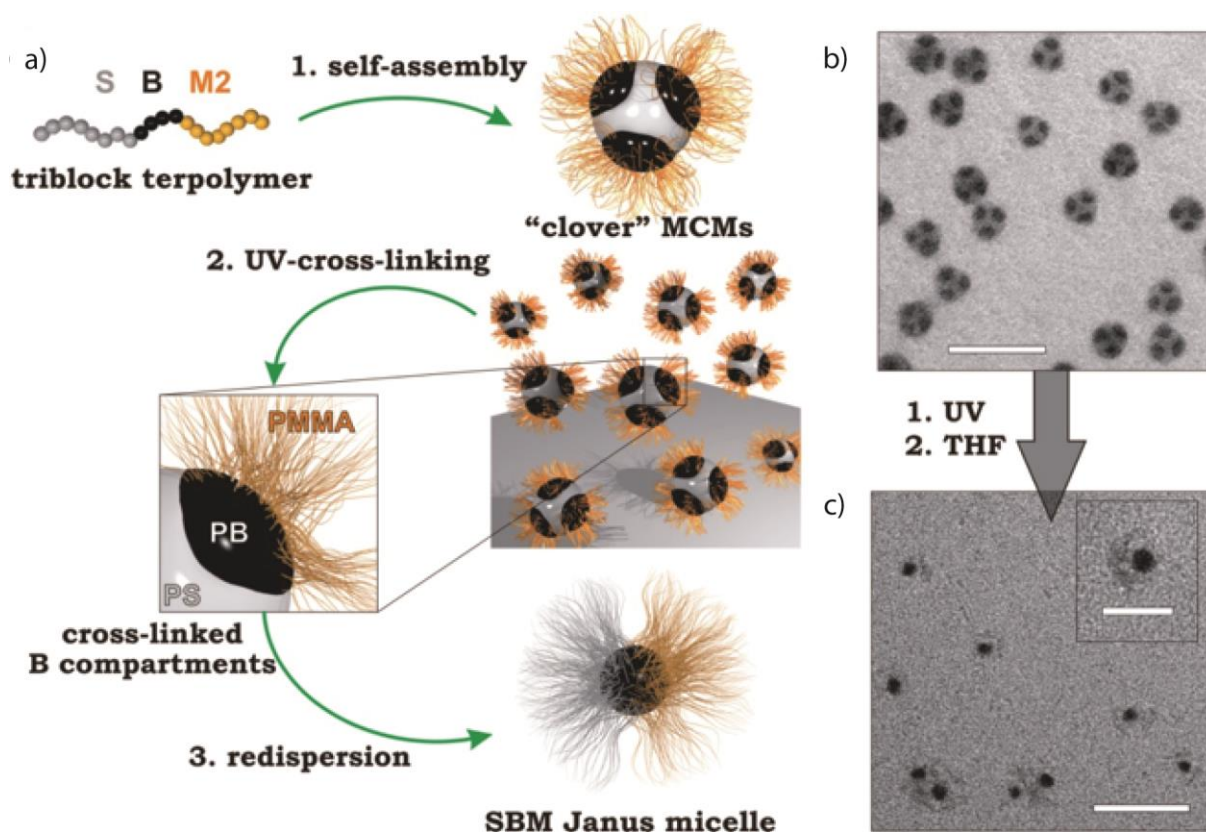


**Figure 11** Preparation of SBM Janus micelles from SM triblock terpolymers: a) Self-assembly of multicompart ment micelles (MCMs), subsequent cross-linking of the compartments and redispersion in the solvent, b) TEM images of clover MCMs, and c) single JPs (bottom). Scale bars are 200 nm and 50 nm in the inset. [162]

### 2.3 Mechanical properties of polymer blends

Polymer blends have a complex structure, which is usually composed of the matrix, the dispersed phase and the interface. In order to be able to transfer the stress between the phases, compatibilizers located at the interface are needed, which further add to the complexity of the system. The deformation mechanisms, and as a result mechanical properties of the blends,

mainly depend on the morphology and size of the dispersed phase, as well as the interface properties such as its mobility (flexibility). In this section, the different deformation mechanisms in polymer blends are introduced first, followed by an introduction into methods of fracture toughness and fatigue crack propagation measurements as important tools for investigating the micromechanics of materials. Later on, the relevant literature focusing on compatibilized blends, is reviewed. However, there are not many studies yet available in this field.

### 2.3.1 Deformation mechanisms in polymer blends

Plastic deformation in polymers happens when the elasticity limit of the polymer is reached. In case of polymer blends, it is important that the stress is transferred through an interface from the matrix to the dispersed phase. Therefore, the properties of the interface play an important role in determining the blend behaviour. The lack of sufficient interactions at the blend interface and between the blend components results in a detachment of the phases. Even though a weak adhesion is not efficient enough to transfer the stress, it can cause some friction or generate debonding of the phases. On the other hand, a strong bond at the interface prevents slipping between the matrix and droplets and ensures efficient stress transfer between the phases. The deformation mechanisms mainly depend on the characteristic polymer properties such as entanglement density, chain flexibility, in addition to the measurement conditions such as temperature, deformation speed, loading mode, geometry, etc. However, employing standard testing methods for the comparison of polymers, the first two polymer characteristics stay the dominant parameters influencing the behaviour.

The deformation in microscale can be divided into three main categories: (1) Crazes, (2) shear bands and (3) shear deformation zones [162,163]. Crazes are crack-like sharply localized bands of plastically deformed material that are initiated when an applied tensile stress causes microvoids to nucleate at points of high stress concentrations created by heterogeneities [162,164–166]. They usually form in planes normal to the direction of maximum tensile stress and consist of highly orientated polymer fibrils of approximately 5-15 nm. Crazes are in fact highly localized yielded regions and are capable of load transfer and commonly develop and propagate *via* two processes: (1) Craze tip advance that allows fibril generation and craze width growth [162] and (2) craze thickening that involves more volume of the bulk polymer at the interface. In this way, more material would be present in the plastic deformation zone, hence craze thickening keeps molecular stretch uniform within the craze. There are many theories and

models available on initiation and growth of crazes [163,165,167–169], but in summary one can say that lower entanglement densities are favourable for craze initiation. Increasing the entanglement density of the molecular network in a polymer will lead to an increase in the surface energy per area of a void surface. Hence, the craze initiation stress [162] will also increase. Multiple crazing is referred to the increased concentration of crazes and often happens in rubber toughened polymers [164]. Numerous crazes are usually initiated at the interface of cavitated rubber particles due to a high stress concentration [164,170]. Presence of sharp cracks, notches, defects, or in case of blends unmodified interface, favours craze initiation leading to brittle fracture. This is opposite to a bulk shear yielding mechanism that commonly results in a ductile behaviour [162]. Shear bands and shear deformation zones (made of thick bands and coalescing shear bands) are a result of shear processes and can be localized or diffuse in the bulk. In both cases, their interface with the materials is much thicker than of crazes. Shear yielding involves displacement of matter (*i.e.* molecules sliding past each other) during deformation [162]. The stress needed to initiate the shear yielding highly depends on the temperature and, hence, the chain flexibility (mobility). The higher the chain stiffness, the lower the chain mobility and therefore the higher the yield initiation stress [171,172].

The competition between crazing and shear yielding usually defines the behaviour of the material (brittle or ductile). The entanglement density (influencing crazing phenomena) and the chain flexibility (influencing shear yielding phenomena) are the key parameters to determine the macro mechanical properties of the polymers, such as toughness. Additionally, the interface between the blend components is a possible source of cavitation or debonding of phases. Both phenomena result in the creation of new surfaces, which dissipate a large amount of energy.

### 2.3.2 Fracture mechanics of polymer blends

Toughness is the ability of resisting fracture by absorbing and dissipating energy during deformation prior to ultimate fracture [164]. Commonly, promoting the plastic deformations to increase the toughness would result in a reduction of stiffness and strength. In case of polymer blends with raspberry morphology this does not happen, probably due to the discontinuous placement of the rubber patches at the interface [12,118,119,173]. Toughness is usually higher for morphologies that allow lots of local yielding points simultaneously in the entire material (similar to the raspberry morphology). There are several strategies to improve the toughness, such as blending with other materials [174], copolymerization, addition of elastomer particles to

increase the craze nucleation (such as HIPS and ABS), inducing shear yielding in semi-ductile polymers and addition of rigid particles.

Since interfaces in immiscible polymer blends usually act as weak spots and are prone to high stress concentrations, the possibility of having a crack in these materials is very high. Once the crack is formed and when it reaches a certain critical length, it can propagate very fast (catastrophically) in the material and cause failure. This phenomenon can happen at stresses much lower than that normally causing yielding or failure in a tensile test. This, together with the application of PPE/SAN blends in casing of pumps, which go through constant vibration that can speed up the crack growth, are the main reasons that make the understanding of the materials' behaviour in the presence of a crack to the main aspect of the current thesis. "Fracture Mechanics" refers to a specialization within solid mechanics, in which the presence of a crack is assumed and one attempts to find quantitative relations between the crack length, the material's inherent resistance to crack growth and the stress at which the crack propagates at high speed to cause failure [175,176]. In this thesis, the two methods of 2.3.2.1 measuring fracture toughness and 2.3.2.2 fatigue crack propagation were used to evaluate and compare the SBM and Janus compatibilized blends. The principles of these methods will be discussed in the following sections.

### 2.3.2.1 Fracture toughness ( $K_{Ic}$ )

There are two common approaches for quantifying the fracture process: (1) the energy balance method suggested by Irwin [177] and Orowan [178,179] and (2) the stress intensity method that directly examines the stress state near the tip of a sharp crack [175,176]. The latter method has proven more useful in engineering practice and allows to correlate the crack opening stresses in mode  $I$  (tensile) to the so-called stress intensity factor,  $K_I$ , where  $I$  dictates the crack opening mode. The  $K_I$  factor contains the dependence on applied stress, crack length and specimen geometry, and represents the overall intensity of the stress distribution. The materials can withstand crack tip stresses up to a critical value of stress intensity,  $K_{Ic}$ , and beyond this value the crack propagates rapidly. Reaching  $K_{Ic}$  means that the size of the plastic zone is so large that it cannot grow further due to molecular mobility or microstructure constrains and unstable crack propagation happens. Hence, the critical stress intensity factor is a measure of material toughness. The failure stress ( $\sigma_f$ ) is related to the crack length ( $a$ ) and fracture toughness ( $K_{Ic}$ ) by the following equation 11.

$$\sigma_f = \frac{K_{Ic}}{\alpha\sqrt{\pi a}} \quad (11)$$

Where  $\alpha$  is a geometrical parameter usually equal to 1 for edge cracks and many other situations. The equation is valid for plain strain condition. Here, the size of the plastic zone is small and neither interacts with specimen's free boundaries nor destroys the basic nature of the singular stress distribution. Measurement details in ASTM standards (D5054, E 399-83 and E 399-90) [180,181] specify the methods and geometries needed to ensure this condition and are taken into consideration during this work.

Even though fracture toughness measurements are able to precisely correlate the morphological features and the microstructure with the macroscopic mechanical properties, only few studies have so far focused on these correlations in case of thermoplastic polymer blends [182–187]. By studying the fractured surfaces of ABS copolymers toughened with core shell particles, Michler [183] suggested core-fibrillation mechanisms for the first time, consisting of fibrillation at the craze interface during craze thickening in glassy polymers. Tiejune et al. [184] investigated complex shear band formation mechanisms combined with rubber cavitation in PC/ABS blends. Handge et al. [182,185] investigated the micromechanical deformations of PA6/SAN blends, which were compatibilized with maleic anhydride grafted poly(styrene-*co*-acrylonitrile) (SAN-*g*-MA), *via* in-situ tensile tests on semi-thin TEM specimens. In the blend with a ductile matrix and rigid particles, local failure is initiated by rupture and crazing of the interface between the constituents. They concluded that the mechanical properties of the SAN-*g*-MA compatibilized PA6/SAN system improve due to an improved interfacial adhesion between the blend phases. This effect was very pronounced and exceeded the influence of the particle size on the mechanical properties.

In the current study, fracture toughness measurements are chosen as the first tool to obtain information on the mechanical behaviour of the blends (especially toughness). Firstly, the effect of domain size on these properties is studied for SBM compatibilized PPE/SAN blends at different blend ratios. By keeping the interface flexibility constant (*via* having only one type of compatibilizer, SBM) for the blends, one is able to exclude the effect different behaviour of SBM triblock terpolymers compared to JPs. In the next step, one blend ratio is chosen and the effect of different amounts of JPs on the fracture toughness behaviour of the blends are further investigated. However, due to the high degree of complexity of the JP compatibilized blends, other methods which can deliver more information are chosen as well, which will be discussed in the next section.

### 2.3.2.2 Fatigue crack propagation ( $da/dN$ )

Cracks will grow under dynamical loading, even though the applied load maximum is far below the material's strength determined by static testing. Fatigue crack propagation (FCP) is proven to be the most sensible test in mechanics to study micromechanical deformation and fracture mechanism of the materials [188,189].

The methodology for determination of the FCP behaviour or the resistance of a material against stable cracking under dynamic load has been described in detail by Hertzberg and Manson [190]. In this thesis FCP behaviour is investigated by determination of crack propagation speed,  $da/dN$ , as a function of the amplitude of the stress intensity factor,  $\Delta K$ . The measurement method makes it possible to determine the FCP behaviour over several decades of crack growth speeds. As a result of the variation of  $\Delta K$ , the rate of crack growth in the sample changes from 1 nm/s up to 1 mm/s which requires advanced software and hardware test equipment. One should mention that these values are calculated from the fatigue crack propagation measurements per oscillation cycle and are therefore frequency dependent. In this work, the test frequency of 10 Hz is applied, which represents the vibrations happening in a chemical pump. One of the two standardized specimen shapes for determination of the fatigue crack propagation behaviour is the compact tension (CT) geometry that is schematically illustrated together with the load direction in **Figure 12a**. If the resulting data is illustrated by a double logarithmic plot, a characteristic curve with three discrete regimes is obtained for rigid and semi-rigid materials (black curve in **Figure 12b**).

In region I, after exceeding the threshold value,  $\Delta K_{th}$ , the fatigue crack propagation is initiated. For stress intensity ranges below this value, crack propagation is not possible [191]. Region II, which is also known as the Paris region, represents the stable crack propagation. In this range, the FCP behaviour can be described by the Paris law [192] shown in equation 12.

$$\frac{da}{dN} = C \times \Delta K^n \quad (12)$$

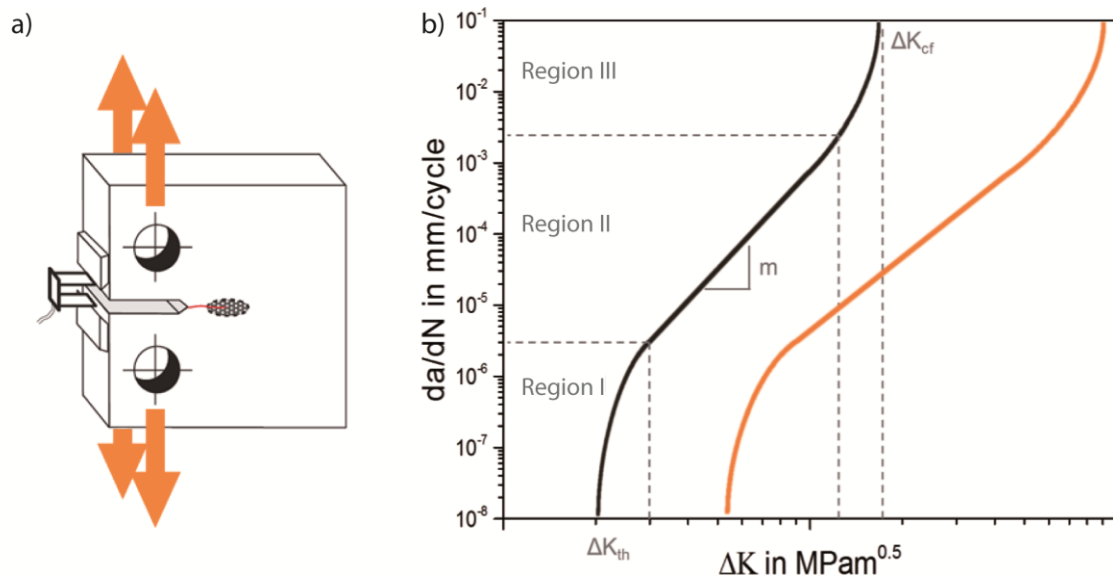


**Figure 12** Schematic illustration of a) a compact tension specimen with vertical load direction, and b) typical  $da/dN$ - $\Delta K$  traces at frequency of 10 Hz (orange trace corresponds to improved fatigue crack propagation behaviour) [188]

According to the Paris law, fatigue crack propagation per cycle ( $da/dN$ ) in the region of stable crack growth is described by the applied  $\Delta K$ , a material constant  $C$ , and the Paris parameter  $n$ . In a double-logarithmic plotted diagram of  $da/dN$ - $\Delta K$ ,  $n$  corresponds to the slope of the curve in the area of the stable crack preparation. Since the area of the stable crack preparation is strongly material-dependent, a general area in the curve for determination of  $n$  can not be defined. In section III, crack propagation is unstable. The amplitude of the stress intensity factor, which above is the onset of unstable crack growth, is called  $\Delta K_{cf}$ , indicating critical failure. A specimen with improved fatigue crack propagation behaviour, as illustrated by the orange curve in **Figure 12b**, is characterized by an increase in  $\Delta K_{th}$  and  $\Delta K_{cf}$  as well as a decreased slope ( $n$ ), which results in a shift of the curve to the right side [188,193].

Since fatigue crack propagation is not a common test for thermoplastic materials, the fundamentals of the test are briefly discussed here. The FCP behaviour is investigated on CT specimens as a function of the amplitude of the stress intensity factor,  $\Delta K$ . The load on the sample is a cyclic sinusoidal one with a defined frequency and stress ratio,  $R_s$ , as shown in equation 13. The stress ratio corresponds to the relation of minimum stress,  $\sigma_{min}$ , to the maximum stress,  $\sigma_{max}$ , in the cyclic loading.

$$R_s = \frac{\sigma_{min}}{\sigma_{max}} = \frac{K_{min}}{K_{max}} \quad (13)$$

The amplitude of the stress intensity factor,  $\Delta K$ , is the difference of the maximum stress intensity factor,  $K_{max}$ , and minimum stress intensity factor,  $K_{min}$ , as shown in equation 14.

$$\Delta K = K_{max} - K_{min} \quad (14)$$

$K_{max}$  and  $K_{min}$  values are calculated from equations similar to the equation 11, that is previously discussed for critical stress intensity factor (equations 15 and 16). Here as well  $\alpha$  represents the geometrical factor and  $a$  is the crack length.

$$K_{max} = \sigma_{max} \times \alpha \sqrt{\pi a} \quad (15)$$

$$K_{min} = \sigma_{min} \times \alpha \sqrt{\pi a} \quad (16)$$

In order to calculate the  $da/dN$  values at different  $\Delta K$ , one should have the applied force and crack length at each time. The crack length can be calculated *via* the compliance method [189,194]. Compliance ( $C$ ) is the ratio of the deformation to the applied load and during the test, it is calculated with the known values of the crack opening displacements (COD) and applied force. Considering the sample thickness, tensile modulus, and the compliance, one can calculate the crack length ( $a$ ) at each time during the test. Knowing the crack length and the number of cycles,  $N$ , the crack propagation speed can be calculated according to equation 17.

$$\frac{da}{dN} = \frac{a_{n+1} - a_n}{N_{n+1} - N_n} \quad (17)$$

A notch is machined in the centre of the specimen and then an actual fatigue crack is induced at the base of the notch by applying a stress. Commonly a low stress range is used to induce the fatigue cracking. Employing high stresses (in order to speed up the process) can cause a large area of plastically deformed material to form ahead of the fatigue crack, which makes the test result invalid. After the test, studying the fatigue crack surface is necessary to determine the validity or the failure of the test. If the crack is not in a single plane, or at an angle to the machined notch, or if the crack is not in the proper region, the test would be invalid. The crack must be also long enough to pass through any area displaying plastic deformation [195–197].

Fatigue crack propagation (FCP) measurements have proven to be a strong and sensitive tool to study the role of interfacial adhesion and blend morphology in complex blend structures. The behaviour during several decades of loading speeds can be detected and disentanglement and

even rupture of polymer chains are possible. The materials may exhibit a significantly different mechanical behaviour when subjected to dynamic loadings. Understanding the molecular motion and energy dissipation processes in complex blend structures is of significant importance and could be directly correlated to their macro properties such as ductility [198].

FCP behaviour of PS/HDPE blends were studied in detail by Bureau et. al [199]. The results showed that several parameters such as loading direction (for injection molded parts), morphology and orientation of the phases, blend composition, and testing conditions strongly effect the FCP behaviour. Increasing the HDPE content as the minor component in blend leads to progressive reduction of the fatigue crack growth rates, especially when SEBM terpolymer is added as a compatibilizer [199,200]. The main mechanism contributing to this behaviour is formation of large dimples around the HDPE particles, ahead of the microscopic crack (similar to multiple crazing). In case of injection molded specimens, FCP rates are lower when samples are tested parallel to the melt flow direction compared to normal direction. This is correlated to the oriented co-continuous morphology in absent of compatibilizer, and very oriented and elongated minor phase morphology after addition of SEBS parallel to the FCP direction [98].

It was previously shown that in fine blend morphologies, where the dispersed phase forms droplets smaller than a certain size (1-2  $\mu\text{m}$ ), the process of crack propagation appears to be uniform across the crack front [201]. The size of the droplets varies for different blends; however, there have been only few studies providing such fine morphologies with droplets smaller than 1  $\mu\text{m}$  to prove this theory. The deformation mechanisms during fatigue crack propagation of a miscible PPE/PS system, where the PS phase is modified with rubber particles of 1.5  $\mu\text{m}$  has been previously investigated by Morelli et al. [202]. The lack of fine morphologies with phase sizes smaller than 1  $\mu\text{m}$ , due to the larger size of the added rubber particles, hinders the formation of effective deformation mechanisms and causes craze growth termination which can deteriorate the toughness. Similarly, Wyzgoski et al [203] investigated the fatigue resistance of different nylon 6,6 blends with PA and PPE. They concluded that the main deformation mechanism, which is craze coalescence in their case, is not affected by blending nylon 6,6 with other materials, since the morphological features of the blend hinders occurrence of other mechanisms. Surprisingly, addition of EPDM rubber particles did not improve the fatigue crack growth behaviour and ductility of the blends. Here, the cavitation of the rubber particles retards the craze breakdown and coalescence process and, hence, cannot blunt the crack tip. To understand the transition in deformation modes, Ramstein et al. [204] investigated the plastic deformation mechanisms in high impact PS (HIPS) after FCP test in low and high speed regions.

They showed that polymer chains in thermoplastic materials disentangle mainly at low deformation speeds, whereas plastic deformations and chain scission dominate at higher speeds. Therefore, the deformation speed (local crack propagation rate) is another important factor that influences the blend interface and resulting deformation mechanisms.

The fatigue crack growth behaviour of SBM compatibilized PPE/SAN blends with 60/40 (w/w) ratio has been studied before [205]. However, due to the co-continuous structure of the blends and excessive micelle formation that leads to rubber particles not locating at the interface, the deformation mechanisms and the effect of the raspberry morphology could not be exactly identified. Besides, the interface effect and role of JPs correlating the microstructure to the macroscopic properties of the blend material has not been investigated yet. There are only few studies investigating the relationship between the size of the dispersed phase and the mechanical properties, especially FCP behaviour, of polymer blends [206–209]. The size of the blend phases and the ratio of their moduli plays an important role in determining such properties. Thus, a comprehensive study of the interface properties with different compatibilizers and the deformation mechanisms in JP compatibilized systems with such fine morphologies is still missing.

In the current study, the influence of JPs on the FCP behaviour of the PPE/SAN blends will be thoroughly investigated. In the last step, the hypothesis of having synergistic effects by combining the SBM triblock terpolymers together with the JPs as compatibilizers would be proposed and tested *via* different methods.

## 2.4 Chemical resistance of polymer blends

Polymer materials can be attacked by different chemicals such as acids, alkalis, fuels, fats, oils, solvents, and even water. Even if these materials do not react with the polymer and change its chemical structure, they can penetrate in the polymer and interact with it in the form of absorption and swelling, plasticization, and dissolution. In our case, due to the application of the studied PPE/PS blends in casings of chemical pumps, the absorption of certain chemicals by the blends is of special interest.

The interactions between chemicals and polymers are mainly based on van der Waal's forces, which can lead to an absorption of the chemical by the polymer [210]. For amorphous polymers, the chemicals are accumulating in the specific free volume of the polymer after absorption. This

results in “swelling”, *i.e.*, an increase in the volume of the polymer relative to its original state prior to the interaction with the chemical [211,212]. The degree of swelling depends on the chemical structure of the molecule and polymer, size of the molecule, crystallinity, degree of crosslinking, filler content, etc.

#### **2.4.1 Measures to improve chemical resistance**

Developing different protection mechanisms for polymers against chemicals has not advanced compared to other stabilisation methods such as thermal oxidation, photo oxidative, or biological degradation. This is probably due to the fact that modifications to the composition and possibly the structure of the polymer would be necessary which requires efforts and expenses comparable to the development of a completely new polymeric materials [213,214]. For certain materials one can look into crosslinking, increasing crystallinity, or playing with molecular orientation [214]. However, these options are not available for many amorphous structures, or require special manufacturing methods and complex mold design. Alternatively, blending has proven to be an effective way to improve the chemical resistance of polymers [17,215–220]. The exposure of a blend system to a certain chemical can not only improve the chemical resistance, but also influence the mechanical properties of the blend with respect to that of the neat polymers [221].

#### **2.4.2 Methods of determining the chemical resistance of polymers**

There are very few standard test methods (ASTM D1239-07, ASTM D3681-06, ASTM D4398-07, ASTM D1417-10) for quantitative measurement of the chemical resistance. Due to the large number of applications and conditions applied, which make them impractical, scientists usually develop their own tests to compare materials [210]. Determination of the level of attack and possible damages to the materials is usually done by evaluation of the following parameters after immersion of the polymer in the solvent, acid, base, or other chemical for a certain amount of time: (1) Appearance of the specimen before and after testing, (2) Weight change of the specimen due to exposure, (3) Performing mechanical tests (tensile, impact) after the chemical resistance tests.

---

In our case, the complex nature of the PPE/SAN blends compatibilized with triblock terpolymers or JPs, brings up the need for a more accurate evaluation. The chosen solvents can influence one or both phase, and the PB middle block and its crosslinking density can also influence the penetration and absorption of the chemicals. Hence, a method based on the molecular weight ( $M_w$ ) and the glass transition temperature  $T_g$  of the polymers is proposed and explained in chapter 4.2.6 (experimental section). Molecular weight can directly confirm the degradation of polymer chains, and  $T_g$  can provide information about the degree of the interaction between each blend component and the chemicals.

### 3 Goals and approaches

The goal of this thesis is to achieve a fundamental understanding of the behaviour of JPs in immiscible PPE/SAN blends. The influence of JPs on the morphological, rheological and mechanical properties of such blends will be investigated in detail. JPs synthesized from SBM triblock terpolymer precursors combine Pickering effect with the biphasic structure (amphiphilicity). JPs have been shown to have higher surface activities compared to triblock terpolymers. Additionally, they have shown to act as efficient compatibilizers for PS/PMMA blends, therefore, it is of high interest to study them in engineering blend systems such as PPE/SAN. SBM triblock terpolymers are well-known compatibilizers for PPE/SAN blends, hence, they are chosen as the benchmark compatibilizers for comparison with JPs. The SBM triblock terpolymers are known to result in the formation of the raspberry morphology [118] in PPE/SAN blends. Therefore, it is important to investigate whether JPs could also induce similar structures. One of the application areas of PPE/SAN blend material is as casing of chemical pumps. This work focuses on the mechanical properties of the JP compatibilized blends, especially their toughness and fatigue crack propagation (FCP) behaviour which are relevant for the application. Additionally, the influence of the type and amount of compatibilizer as well as the blend morphology on the mentioned properties will be studied. Understanding the structure property relationships in such nanostructured immiscible blends allows to tune their macro properties *via* the use of tailor-made compatibilizers, enabling the use of existing materials in emerging applications. In complex systems, like JP or SBM compatibilized PPE/SAN blends, it is important to analyse and distinguish the effects influencing the deformation micromechanics. In the current study we correlate the formed blend morphology to the micro-mechanical and finally macro-mechanical properties of the blends. In particular, the effect of JPs at the interface on micro-mechanics is thoroughly characterized with special emphasis on the fracture toughness.

Following sub-goals are derived for the current work:

- 1. Understanding the morphology development in JP compatibilized PPE/SAN blends compared to SBM triblock terpolymers as benchmark materials.** After finding the optimum processing conditions and choosing the suitable blend ratio for the investigations, the influence of the JPs on the blend morphology is compared to the bench mark materials.

Different amounts of JPs are added to PPE/SAN blends as compatibilizers and compared with the blend compatibilized with optimum amounts of SBM triblock terpolymers based on previous studies [11,222]. Detailed morphological investigations confirm the formation of raspberry morphology in JP compatibilized blends, similar to SBM triblock terpolymers.

**2. Understanding the deformation mechanisms in JP compatibilized blends, emphasizing on the raspberry morphology, during fracture.** Influence of blend morphology in JP and SBM compatibilized blends on micromechanics are studied and explained. Correlations between the two important parameters (domain size of the blends and interface flexibility) and the induced plastic deformation in the blend systems are made.

**3. Improving the fracture mechanical properties of PPE/SAN blends after compatibilization.** With the gathered information up to this point, a strategy is proposed to improve the materials toughness and FCP behaviour. The goal is to improve these behaviours without deteriorating the modulus of the materials. A Hypothesis is proposed that predicts combination of JPs and SBM triblock improves the fracture toughness behaviour of the system. This hypothesis is confirmed *via* experiments and the parameters contributing to this positive behaviour are explained and correlated. In the end, a system with tailored nanostructured is introduced for the targeted application. The morphological, rheological, and mechanical behaviour of this optimum system is compared with the JP, as well as SBM compatibilized blends to confirm the hypothesis of having synergistic effects by combining compatibilizers.

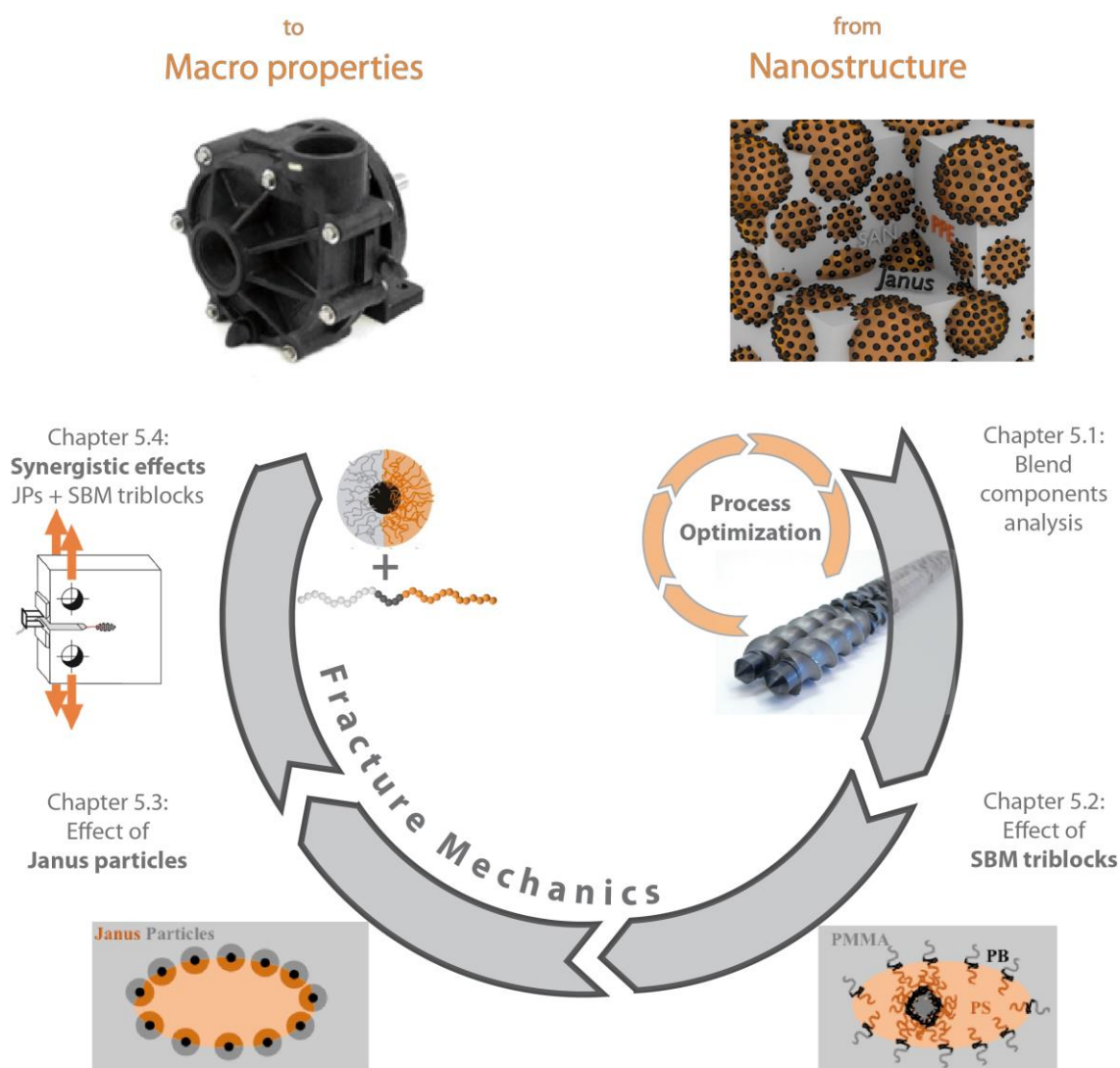


**Figure 13** Graphical abstract of the thesis summarizing the chapters in the result section

**Figure 13** gives a schematic overview of the strategy development in this thesis. Different motivations for choosing PPE/SAN blends instead of state of the art PPE/PS blends will be discussed in chapter 5.1. The blend components as well as compatibilizers will be analysed and the optimum processing parameters and conditions such as blend ratios for further investigations will be chosen. In chapter 5.2, different blend ratios that result into different blend morphologies are compatibilized with benchmark SBM triblock terpolymers. The effect of compatibilization and different domain sizes on the mechanical properties will be investigated. An optimum blend ratio will be chosen for further studies with JPs. In chapter 5.3 the JPs (which produce a stiff interface) are compared to the SBM triblock terpolymers (that result in a flexible interface) in detail. Morphological, rheological, and mechanical aspects of JPs are compared to

---

the benchmark material. The effect of different JP contents on the mentioned properties are studied as well. After understanding the deformation mechanisms in blends with flexible (SBM triblock terpolymer) and stiff (JPs) interfaces, respectively, a strategy to tailor the macro properties *via* changing the nanostructure is proposed in chapter 5.4. A blend containing both JPs and SBM triblock terpolymers as compatibilizers with improved mechanical properties (both modulus and toughness) is produced. The formation of a fine blend morphology and its correlation to the rheological properties is determined and explained. Last but not least, deformation mechanisms in the blends, at different crack growth rates during FCP measurements are identified.

The contents of chapters 5.2, 5.3, 5.4, and 6.2.1 are partially published by the author in the form of 4 peer reviewed articles. Permissions to reprint the text and figures from them for this dissertation are obtained from each journal.

## 4 Materials and experimental methods

### 4.1 Materials

#### 4.1.1 Matrix polymers

Commercial grade PPE (PX100F) was obtained as powder from Mitsubishi Engineering Plastics Europe, Düsseldorf, Germany. It is important to mention that PPE is pure and without any PS addition and therefore has a high viscosity. The weight averaged molecular weight  $M_w = 12.9$  kg/mol and the molar mass dispersity  $\mathcal{D}_M = 1.63$  of PPE was determined by GPC with THF as eluent at a flow rate of 1.0 ml/min (columns at 40 °C) using an UV detector and narrowly distributed polystyrene standards for calibration.

The commercially available SAN with an acrylonitrile content of 19 wt.% was purchased as pellets from BASF AG, Ludwigshafen, Germany (SAN VLL 19100). The  $M_w = 97.1$  kg/mol and  $\mathcal{D}_M = 2.13$  of SAN was determined the same way as mentioned above *via* GPC measurements. The low acrylonitrile content of the polymer ensures homogenous miscibility of the SAN with the PMMA blocks of the compatibilizers at the relevant processing conditions [26,223].

Extrusion grade (PS 158K) polystyrene (PS-E), were supplied by BASF AG, Ludwigshafen, Germany. Injection moulding grade (PS 124 N/L) polystyrene (PS-I) was kindly donated by INEO Styrolution GmbH. The name, grade and abbreviations of the materials used in this thesis is listed in table **Table 2**.

**Table 2** Different blend components used in this work

Material/Grade	Abbreviation
<b>PPE PX100F</b>	<b>PPE</b>
<b>SAN VLL 19100</b>	<b>SAN</b>
<b>PS 158K</b>	<b>PS-E</b>
<b>PS 124N/L</b>	<b>PS-I</b>

A 2:1 mixture of Irganox 1010 and Irgafos 168 (0.1 wt.% in total) from BASF, Germany, was used as stabilizer to prevent polymer heat degradation during the process. **Figure 14** shows the chemical structure of the matrix polymers. It is important to note that the oxidation process of the methyl side groups in PPE starts at 125 °C. Hence, the resident times during the extrusion process should be kept as short as possible due to the limited thermal stability of PPE.

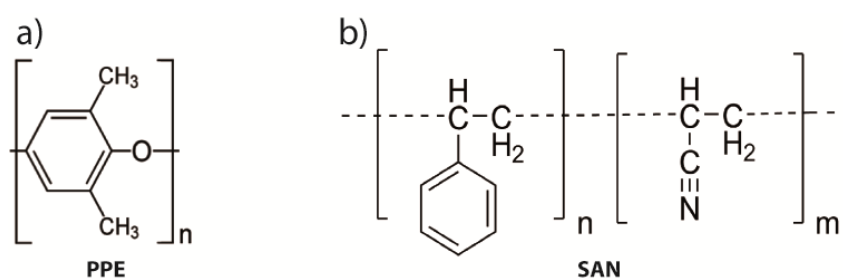


**Figure 14** Chemical structure of the blend components: a) PPE, and b) SAN

#### 4.1.2 Compatibilizers

All solvents used were of analytical grade. Dialysis tubes of regenerated cellulose with a molecular weight cut-off (MWCO) of 12,000 – 14,000 g/mol were purchased from Carl Roth™, equilibrated in deionized water for 30 min and washed with excess dioxane before use. The photo-crosslinker, 2,4,6-trimethylbenzoyldiphenyl-phosphineoxide ( $\lambda_{\max} \approx 360$  nm) was obtained from BASF AG, Ludwigshafen, Germany (Lucirin TPO®).

#### Synthesis of the SBM triblock terpolymer

The polystyrene-*block*-polybutadiene-*block*-poly(methyl methacrylate), (SBM), triblock terpolymer was synthesized *via* sequential living anionic polymerization as reported elsewhere in detail [11]. The used  $S_{32}B_{36}M_{32}^{93}$  triblock terpolymer (subscripts denote the weight fraction of the respective block and the subscript gives the number averaged molecular weight in kg/mol) has a number averaged molecular weight of  $M_n = 93$  kg/mol and a molar mass dispersity of  $D_M = 1.04$ . The  $S_{40}B_{20}M_{40}^{108}$  triblock terpolymers were synthesized *via* a similar method and were used as precursors for synthesizing the Janus particles. Both triblock terpolymers were

prepared in several 1 kg scale batches, making them optimum for using in technologically relevant conditions.

### Synthesis of the Janus nanoparticles

Janus particles (**Figure 15**), used as compatibilizer, were synthesized from a  $S_{40}B_{20}M_{40}^{108}$  triblock terpolymer. The JPs feature a cross-linked PB core and equally sized PS/PMMA hemispheres. The polymer chains of the hemispheres are above the critical entanglement lengths,  $M_c$ , with  $M_{n,PS} = 42$  kg/mol ( $M_{c,PS} = 34$  kg/mol) [224] and  $M_{n,PMMA} = 42$  kg/mol ( $M_{c,PMMA} = 18$  kg/mol) [225] ensuring sufficient interaction between JPs and the blended polymers.

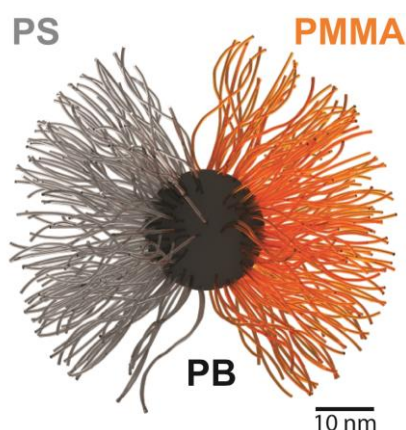


**Figure 15** Schematic structure of a single Janus Particle (JP) with PS and PMMA chains on both sides and a partially crosslinked PB core

The Janus nanoparticles were prepared according to a recipe modified from the earlier report to satisfy the requirements of industry blending equipment [148]. In a typical experiment, 100 g of SBM triblock terpolymer was dissolved in 1 L THF to yield a concentration of  $c = 100$  g/L. After complete dissolution, the concentrated polymer solution was dialyzed against 10 L acetone/isopropanol (60/40 v/v) (selective solvent for PMMA). The solvent mixture was changed twice to generate JP clusters (spherical multicompartiment micelles that consist of JPs). After dialysis, the phase-separated state of the micelles was permanently fixed by cross-linking

of the PB block. Therefore, 0.25 equivalent (compared to the PB double bonds) of photo-crosslinker, 2,4,6-trimethylbenzoyldiphenyl-phosphineoxide (Lucirin TPO®;  $\lambda_{max} \approx 360$  nm), were dissolved in 1 L acetone/isopropanol (60/40 v/v) and added to the dispersion of the JP clusters to dilute the highly viscous dispersion from 100 g/L to 50 g/L. The sample was then irradiated for 24 h using a UV lamp with a cut-off filter of  $\lambda = 300$  nm. Continuous stirring ensured homogeneous cross-linking of the opaque solution. The JPs were recovered by precipitation into 20 L methanol. **Figure 16** shows the different steps in JP synthesis from SBM triblock terpolymers.



**Figure 16** Illustration of the preparative steps in JP synthesis (100 g scale): a) Dissolution of 100 g S<sub>40</sub>B<sub>20</sub>M<sub>40</sub><sup>108</sup> triblock terpolymer in 1 L THF yields a polymer concentration of

10 wt.%, b) dialysis into acetone/isopropanol (60/40 v/v) as selective solvent for PMMA forms patchy multi-compartment micelles (JP clusters), c) turbid colloidal dispersion of JP cluster of defined size, d) addition of 0.25 equiv. Lucirin TPO™ photo-crosslinker ( $\lambda_{max} = 360$  nm) and UV irradiation (cut-off  $\lambda = 300$  nm) for 24 h, e) dispersion after cross-linking, f) purification of JPs *via* precipitation into excess methanol [155]

## 4.2 Experimental methods

### 4.2.1 Melt processing of polymer blends

Before melt blending of the homopolymers, the PPE powder and the SAN granulates were dried at 80 °C for at least 12 h under vacuum. For SBM triblock terpolymers and JPs a lower temperature of 40 °C was chosen due to the sensitivity of the PB block to degradation when longer exposed to oxygen atmosphere at elevated temperatures. In case of JPs, residues of the crosslinker could promote further crosslinking of the PB middle block at higher temperatures. In addition, the SBM and JP compatibilizers were cryo-grinded into a powder to facilitate the dry mixing process. Prior to melt blending, PPE and SAN were dry blended with SBM or JPs using powder mixers. The PPE/SAN ratios of the different blends were 50/50, 60/40, and 70/30 (w/w). The amount of SBM compatibilizer, used as the benchmark material, was 10 wt.%. The employed amounts of JP compatibilizers were 1, 2, 5, and 10 wt.%. An additional blend containing a combination of both compatibilizers, 5 wt.% of each compatibilizer, was also compounded for further investigation. The stabilizers were added and mixed into the dry mixture before compounding.

#### Lab-scale melt processing (batch)

On a small scale and for initial investigations, melt blending of the compounds was performed on a micro-compounder (Xplore DSM) with co-rotating conical twin-screw setup and volume capacity of 15 mL. This process is comparable to a batch mixing process. The temperature inside the micro-compounder was kept constant at 260 °C, the screw speed at 85 rpm and the mixing time was 5 min (similar to the residence time in the extruder). The melt strands were cooled down and cut into granulates.

### Large-scale melt processing (continuous)

A continuous scale, co-rotating twin-screw extruder (Brabender DSE 20/40) with a screw diameter of 20 mm and a screw length of 600 mm ( $L/D=30$ ) was used to compound the polymer blends. The screw configuration is shown in **Figure 17**. After optimizing process parameters such as screw speed on the neat blend, all mixtures were extruded with the maximum barrel and nozzle temperature fixed at 250 °C and 245 °C, respectively. The screw speed was kept constant at 85 rpm with a constant throughput of 1 kg/h using a gravimetric feeding. Therefore, the mean residence time of the blends in the extruder was around 5 min. The blends were air-cooled and pelletized after extrusion.



**Figure 17** Screw design of the twin-screw extruder used for compounding the blends

### Sample preparation

Specimens for shear rheology, dynamic mechanical analysis (DMA), and  $K_{Ic}$  were compression molded to eliminate the strong effect of any orientation of the blend phases (PPE) during the injection molding process, based on previous studies [222]. The compounded granulates were dried at 80 °C in a vacuum oven for at least 4 h and then compression molded using a hydraulic hot press (Paul Weber) under vacuum conditions for 5 min with 100 kN at 260 °C (pure PPE at 270 °C and pure SAN at 160 °C), and subsequently cooled down in a cold press with 30 kN compression load.

## 4.2.2 Morphological characterization

### Transmission electron microscopy (TEM)

Ultrathin sections (50-80 nm) were cut of the blended materials at room temperature using an ultra-microtome (Leica UC7 ultramicrotome (Leica Microsystems, Germany)) equipped with a diamond knife. To ensure sufficient contrast between the phases, the particles and ultrathin sections were stained with  $OsO_4$  for 30 s in vacuum in case of SBM compatibilized blends and 3 h

at ambient conditions [128] in case of JP compatibilized blends. Due to this staining method SAN appears as the brighter and PPE as the darker phase, while the PB block (or core) of SBM (JPs) appears black (selectively stained with OsO<sub>4</sub>). Bright field transmission electron microscopy was carried out using Zeiss CEM 902 and 922 OMEGA EFTEM electron microscopes (Carl Zeiss Microscopy, Jena, Germany) operated at acceleration voltages of 80 and 200 kV, respectively. Both microscopes were equipped with IS Megaview III CCD-camera with AnalySIS image processing.

Number averaged diameters of the PPE droplets and their distributions were obtained by measuring at least 500 droplets in TEM micrographs using ImageJ software. First, the area of each PPE droplet was measured using the software, then, assuming that the droplets have a perfect spherical shape and the TEM cuts have gone through the middle of each droplet, the radius corresponding to the area was back calculated. Of course, these assumptions cannot be 100 % fulfilled, hence, resulting in relatively large standard deviations of the measurements.

#### **Field emission scanning electron microscopy (FESEM)**

The fractured surface of the blends after compounding and mechanical testing was analysed *via* bright field emission scanning electron microscopy using a Leo 1530 Gemini from Zeiss equipped with a secondary electron detector and operated at an acceleration voltage of 10 kV. The samples were sputtered with a 1.3 nm thick platinum layer prior to the measurement.

#### **4.2.3 Rheological characterization**

Rheological properties were investigated employing a stress controlled dynamic-mechanical rheometer RDA III from Rheometric Scientific with plate-plate geometry under nitrogen atmosphere. The pressed samples had a diameter of 25 mm and thickness of 1.5 mm and were analysed isothermally at 260 °C. The complex moduli and the complex viscosity of the blend systems were measured as a function of frequency within the range of 0.01–500 rad/s at 260 °C. Prior to each measurement, the linear viscoelastic region was determined by carrying out an amplitude sweep at a deformation range of 0.1–100 %, at frequencies of 1 and 50 rad/s. Subsequently, the deformation applied for the frequency sweeps was set to be within the linear viscoelastic region. The rheological measurements of neat PPE and SAN were performed on

samples, which were prepared by extrusion applying the same condition as for the blends. Each measurement was repeated at least three times to minimize the experimental errors.

#### 4.2.4 Thermal and thermomechanical characterization

##### Differential scanning calorimetry (DSC)

The glass transition temperature ( $T_g$ ) of the neat materials and the immiscible blend systems were measured using a Mettler Toledo DSC 1. The method consists of a heating-cooling-heating cycle under nitrogen atmosphere from 25 - 250 °C at a scanning rate of 10 K/min. The values of the second heating cycle were evaluated in order to calculate the  $T_g$ .

Additionally, modulated DSC measurements (TA Instrument DSC Q1000) at low temperature were done with pure JPs and with PPE/SAN + 10 wt.% JP to analyse the influence of compatibilization and to determine the effect of cross-linking of the PB core in the JPs. The measured temperature range was -150 - 150 °C at a heating rate of  $(3 \pm 1)$  K/min under nitrogen atmosphere. This method gives information on the reversing and non-reversing characteristics of thermal events. Especially, the polybutadiene domains in the blend with low amounts of compatibilizer can be detected.

##### Dynamic mechanical analysis (DMA)

The dynamic mechanical analysis (DMA) of the blend systems was performed in the dual-cantilever mode on hot-pressed rectangular specimens with dimensions of  $25 \times 6 \times 1$  mm<sup>3</sup>, using a Mettler Toledo DMA/SDTA 821e. The frequency of the measurement was constant at 1 Hz and the test setup applied tensile forces to the specimens. The applied strain was kept small enough to ensure linear-elastic behaviour of all systems. The samples were heated from -100 °C (after establishment of equilibrium) to 230 °C at a constant heating rate of 2 K/min. The same device was used to investigate the non-linear behaviour of the blends with the Payne test. The Payne strain sweeps were all performed with the constant frequency of 1 Hz at 150 °C. The onset of the decrease in modulus was defined as the intersection of the tangents on the traces.

Additionally, several DMA measurements under tension load were performed with different amplitudes of the applied strain (0.05%, 0.1%, 0.2%, and 0.3%) in order to investigate the structural networks formed in the blends. Due to higher strain values, these measurements were performed on a Gabo Eplexor 500N with a larger dynamic load cell (150 - 500 N), due to the

high stiffness of the samples. However, here also the frequency and temperature were kept constant at 1 Hz and 150 °C, respectively in order to make comparisons possible.

#### 4.2.5 Mechanical characterization

##### Tensile characterization

Tensile measurements were performed according to DIN EN ISO 527-2 at 23 °C and 50 % relative humidity using a Zwick 1485 universal testing machine with 10 kN load cell. A minimum number of 10 specimens (with 1BA geometry) were used for each individual material composition and the average values are reported. Samples had a thickness of 2, width and length of narrow section of 5 and 30, and maximum length between the grip zone of 57.5 mm. The Young's modulus (tensile modulus) was determined at a crosshead speed of 1 mm/min. Reaching a sample deformation of 0.25%, the crosshead speed was increased to 5 mm/min and was kept constant until fracture of the specimens occurred.

##### Critical stress intensity factor ( $K_{Ic}$ )

Fracture toughness measurements were conducted according to the standard test method ISO 13586 to obtain the mode I critical stress intensity factor ( $K_{Ic}$ ) of the polymer blends at 23 °C. Compact tension (CT) specimens had width and thickness of 33 and 2 mm, respectively. For each sample, pushing a new razor blade into the machined V-notch generated a sharp crack. Samples were afterwards loaded under tension mode so the crack can grow until the end of the specimen. The crack opening displacement (COD) during crack growth is measured using a clip extensometer (632.29-30, MTS Sensor Technology GmbH & Co. KG, Germany). At least 5 notched, compact tension specimens were tested at a strain rate of 10 mm/min. The thickness of the specimens was 2 mm. The tests were carried out on a Zwick BZ2.5/TN1S universal testing machine to ensure reliable results. The critical stress intensity factor was calculated using the following equation 18:

$$K_{IC} = \frac{F}{B\sqrt{w}} * f(a/w) \quad (18)$$

Where  $F$  represents the force required for the crack to start propagation,  $B$  and  $w$  are the thickness and width of the specimen, respectively,  $a$  is the initial crack length and  $f$  is the geometrical term.

### **Fatigue crack propagation (FCP)**

The fatigue crack propagation (FCP) behaviour was determined on CT specimens with width and thickness of 33 and 2 mm, respectively [206]. The tests were performed based on ISO 15850/ASTM E647 at 23 °C and a relative humidity of 50 %. The samples were loaded dynamically (frequency of 10 Hz) in tension-tension mode, using a servo hydraulic testing machine (IST Hydro Pulse MHF) from Schenck, Germany. The amplitude of the cyclic stress intensity factor ( $\Delta K = K_{\max} - K_{\min}$ ) was increased as a function of crack length. The minimum to maximum load ratio,  $R_s$ , was set at 0.1. Prior to the measurement, an initial natural sharp pre-crack is introduced into the machined V-notch of the specimen by a sharp razor blade. The compliance was continuously measured by the crack opening displacement method using a transducer (632.13F-20, MTS, Sensor Technology GmbH & Co. KG, Germany) fixed to the front of the CT specimen with rubber bands. From this, the crack length was calculated continuously by equations published by Saxena and Huduk [194]. Each measurement was repeated at least three times to minimize the experimental errors and an averaged curve is generated to be shown here. A detailed description of the methodology can be found elsewhere [194,226] and schematic diagrams explaining different regions in a typical FCP curve and the sample geometry are given in chapter 2.3.2.

#### **4.2.6 Chemical resistance**

The samples (granulates) were immersed in the chosen solvent ( $CCl_4$ ) for a certain time period (1, 7, and 30 days). The physical state of the samples (including visual form and size of the granulates, colour and clarity of the solvents) immersed in the solvent was monitored and reported. Afterwards, they were removed from the solvent and air dried. Due to the complexity of the blends with multiple components, the molecular weight and glass transition temperature were additionally chosen as key properties for comparison of the air-dried samples. The molecular weight was chosen as an indicator for possible chain degradation and was determined by gel permeation chromatography (GPC). Since blends containing PPE couldn't be solved in PS

solvent based GPC, the  $T_g$  measurements ended to be more useful for interpretation. The glass transition temperatures of the samples before and after exposure were measured using the same method explained in chapter 2.4.2 and compared with each other.

## 5 Results

### 5.1 Characterization of neat blends and compatibilizers

This chapter aims to explain the reason of selecting the blend system and the processing conditions in the future chapters. Later, the two main motivations behind the approach of this thesis in choosing the PPE/SAN system over the state of the art PPE/PS blends currently used in commercial applications such as chemical pump casings, are discussed. The advantages of the SAN over the PS, in terms of its rheological and chemical resistant properties are explained. Later on, based on screening the viscosity of different PPE/PS blends, three PPE/SAN blends with different weight ratios are chosen to achieve the suitable morphology (droplets dispersed in matrix) for further investigations of the mechanical properties and micromechanics of deformation in the next chapters.

#### 5.1.1 Why PPE/SAN?!

##### **1<sup>st</sup> Motivation: Better processability**

Good processability is the key parameter for industrialization and commercial applications. The rheological features of the blend, especially the viscosity, play an important role here. Hence, the rheological properties of the blend components will be discussed first. The high viscosity of PPE compared to that of SAN, extrusion grade PS (PS-E) and injection molding grade PS (PS-I) is clearly visible in **Figure 18**. Blending PPE polymer with lower viscous materials would improve its processability tremendously. The lower the viscosity of the other blend component, the lower the overall viscosity of the blend and the better its processability. Here, the viscosity of both PS-E and PS-I are higher than SAN, meaning that SAN is more effective in decreasing the blend viscosity and improving its processability. This is the first motivation for our approach to move towards PPE/SAN blends instead of PPE/PS.

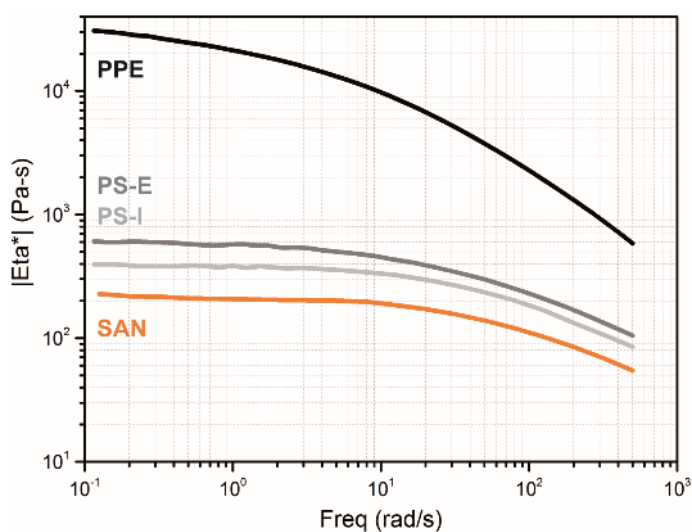


**Figure 18** Absolute shear viscosity of neat polymers (blend components)

Previous studies [227,228] used PS-I with a lower viscosity to produce ternary PPE/PS/SAN blends and tailor the microstructure to improve materials foamability. They determined an area within the ternary blend phase diagram as un-processable with standard melt blending approaches using twin-screw extruders. The mentioned area includes blends with equal or more than 80 wt.% PPE. In this thesis, a co-kneader was used instead of the commonly employed extrusion with twin screw extruders to study the rheological properties of PPE/PS-E and PPE/PS-I blends in dependence of their composition. The amount of PPE in the blends was kept above 50 wt.% to ensure good mechanical properties, as PPE is the more ductile phase.

The use of a co-kneader instead of a twin-screw extruder proved as a successful method to process blends with above 80% PPE contents. One can confirm the processability of even pure PPE with the change of force fields from shear to extensional forces during the process. The viscosities of PPE/PS-E and PPE/PS-I blends at different blend ratios compared to the viscosity of the neat blend components are shown in **Figure 19a, b**. Even though PPE/PS blends are miscible and the blends are expected to have one single phase, there is a clear increase (jump) in the viscosities from the blends with 70/30 ratios to the blends with higher PPE amounts. The difference between the blend viscosities is more profound in the higher frequency region, which represents the viscosity during the melt blending process. Due to the higher viscosity of PS-E in comparison to PS-I, its 80/20 blend also shows a larger difference in the low frequency region compared to the blends with lower amounts of PPE (**Figure 19a**).

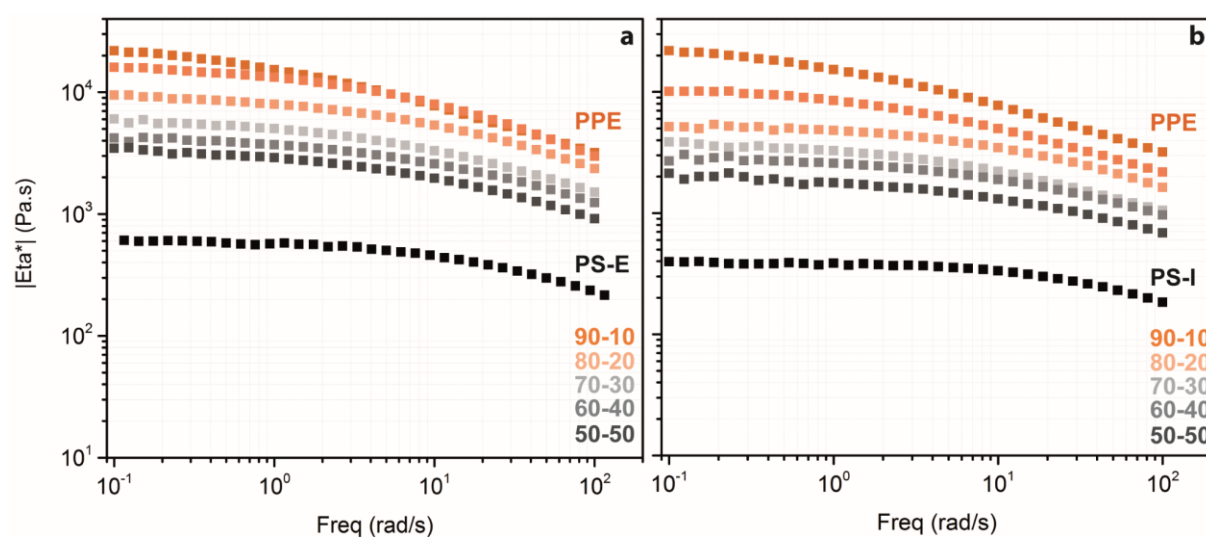


**Figure 19** Absolute shear viscosity of a) PPE/PS-E and b) PPE/PS-I blends at different blend ratios

It is important to notice that the force fields are different in twin-screw extruders (shear fields) and co-kneaders (extensional forces). Therefore, we confirm as well that the blends with PPE contents above 80 wt.% are not going to be processable in the twin-screw extruder. So far only miscible PPE/PS blends are compared over a wide range of blend ratios. Producing PPE/SAN blends *via* this compounding method (co-kneader) would not provide useful information as extensional forces could highly affect the morphology of the immiscible blends. Based on this information and as blends with 80 wt.% PPE show a jump and increase in their viscosity, one can predict that the at 80 wt.% of PPE phase inversion would happen in immiscible blends with similar viscosity ratios (such as PPE/SAN). Therefore, for investigations in the next sections, PPE/SAN blends are produced and investigated in blend ratios close to the phase inversion (50/50, 60/40, and 70/30).

## 2<sup>nd</sup> Motivation: Improved chemical resistance

The second motivation to replace PPE/PS by PPE/SAN blends is to increase their chemical resistance. SAN has a better chemical resistant against several solvents compared to PS due to its AN content and, thus, also improves the chemical resistance of PPE/SAN blends. Here, the chemical resistance of the neat materials, as well as the blends are discussed. For comparison between the two blend types, an aggressive solvent system ( $CCl_4$ ) was chosen. As discussed, the

glass transition temperature ( $T_g$ ) of a polymer is useful indicator to determine the influence of solvents on the molecular structure. When exposed to solvents polymers usually swell, the degree of swelling and interaction between the polymer chain and solvent depends on the affinity of the materials towards each other. This affinity should be low for polymers with a high chemical resistance and consequently less or no swelling would happen.

The GPC measurements (based on PS standard calibration curve) of the PS-I, PS-E, and SAN samples before and after solvent exposure were compared and showed no significant influence of solvent. This could be due to the fact that hydrodynamic volumes of polymer coils before and after exposure to the solvents do not differ much. Hence, other methods, such as  $T_g$  measurements could be used to compare the materials.

The  $T_g$  of the neat polymers (blend components) was compared before and after exposure to  $CCl_4$  for 7 days. After the exposure and before measuring the  $T_g$ , the materials were air dried to remove excess solvent. After solvent evaporation, the free volume of the polymer decreases as the slow evaporation allows chain movements. The chains have time during long evaporation times to rearrange themselves and reduce the free volume. As a result of this lower free volume, the  $T_g$  values are expected to increase [229–232]. Thus, swelling shows similar effect as annealing on the  $T_g$ , where the material is kept at elevated temperatures for a period of time. An increase in  $T_g$  shows higher affinity that causes stronger swelling and consequently indicates lower chemical resistance against the solvent. **Figure 20** shows no interaction and influence on  $T_g$  of SAN after exposure, whereas there is an increase in  $T_g$  of 13 and 7% for PS-I, and PS-E, respectively. This indicates a high interaction and therefore lower resistance of these materials towards the solvent. In addition, the change in the heat capacity of the polymers after exposure has broadened the glass transition. This broader  $T_g$  step indicates heterogeneity in the molecular clusters [233] that could be the result of possible partial damage to the polymer chains *via* solvent exposure. Visual observations show that granulates of PS-E and PS-I were dissolved and after solvent evaporation, the  $T_g$  of the resulting films were measured. The  $T_g$  of PPE also shows a slight increase, indicating the lack of chemical resistance towards the solvent. Even though some swelling was visible, the PPE granulates still kept their shape and were not completely dissolved. The SAN granulates didn't show any change in their form and shape and there was no visual sign of swelling during and after solvent exposure.

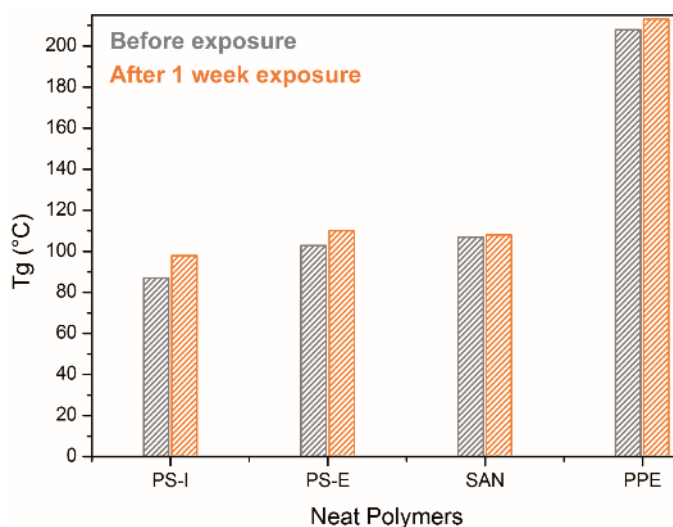


**Figure 20**  $T_g$  values of blend components before and after 7 days of exposure to  $CCl_4$

The  $T_g$  of PPE blends (with PS-I, PS-E, and SAN) after exposure to  $CCl_4$  were investigated in an analogous manner. In case of both PPE/PS blends (**Figure 21**), where only one  $T_g$  is visible due to full miscibility, a large increase by 21% and 13% is visible for PS-I and PS-E, respectively. Visually the granulates deformed, swelled, and were partially dissolved in the solvent, indicating that miscibility of the PPE/PS system extends the degree of solvent polymer interaction and negatively influences the chemical resistance of the blends. In case of the PPE/SAN blends, due to component's immiscibility, there are two  $T_g$  values, corresponding to the PPE and SAN phases, available. The  $T_g$  of the SAN phase is as expected constant before and after exposure. After blending, the solvent influence on the  $T_g$  of the PPE phase is reduced. This means that the SAN phase encapsulates the PPE phase (more details on blend morphology, which has continuous SAN phase, follows in the next chapters) and, thus, minimizes its contact to the solvent, resulting in an improved chemical resistance of the blend.

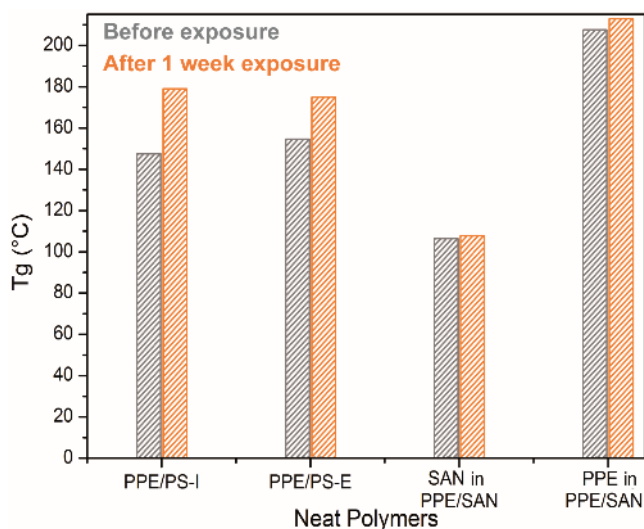


**Figure 21**  $T_g$  values of PPE/PS and PPE/SAN blends (with same blend ratio of 60/40) before and after 7 days of exposure to  $CCl_4$

With these two motivations, PPE/SAN blends are chosen as main material of the current study. Unlike miscible PPE/PS blends, the PPE/SAN is immiscible, hence the system needs a third component, known as compatibilizer, in order to have good mechanical properties (stiffness as well as toughness). The compatibilizers used in this work and their differences are discussed in the next section.

### 5.1.2 Characterization of the compatibilizers

In this work, the influence of JPs as compatibilizers on the mechanical properties of PPE/SAN blends will be investigated. SBM triblock terpolymers are state of the art compatibilizers for this system [11,12,118,173] and are used as benchmark materials for comparison. Even though the SBM triblock terpolymers are precursors for synthesizing the JPs, there are some differences between them that should be discussed. These differences play an important role on the mechanical properties and activation of deformation mechanisms in the blends, which are the main subject of this work. This is due to the fact that the JPs and SBM triblock terpolymers are located at the PPE/SAN interface in the raspberry morphology formed by the blends.

JPs are synthesized from SBM triblock terpolymers and have similar chemical structures, however, there are significant differences between them in terms of their morphological

features. The SBM triblock terpolymers are linear polymer chains, whereas JPs are multicompartment micelles with each side containing several polymer chains. This is expected to increase the entanglement density at the blend interface after compatibilization with JPs. In addition, partial crosslinking of the PB middle block during JP synthesis [155] changes the elasticity of the soft middle block (in SBM triblock terpolymers) to a stiffer one in case of JPs. **Figure 22** shows the dynamic mechanical analysis (DMA) of JPs and the  $S_{32}B_{36}M_{32}^{93}$  triblock terpolymers (representing the benchmark, standard SBM compatibilizers). The influence of partial crosslinking on the  $T_g$  of each block and stiffness of each compatibilizer can be observed. The JPs can only be formed from symmetric SBM triblock terpolymers with a maximum PB content around 20% [161]. Hence, the SBM precursors of the JPs ( $S_{40}B_{20}M_{40}^{108}$  triblock terpolymers) are also included for comparison with JPs and standard SBM compatibilizers. The uncrosslinked PB blocks in SBM triblock terpolymers have a  $T_g$  of around  $-80$  °C, whereas the partially crosslinked PB core of the JPs has a glass transition temperature of around  $0$  °C. As the  $T_g$  shifts to  $0$ °C for the crosslinked PB core of the JPs the steep decrease in modulus, observed at the  $T_g$  of the PB block in SBM, vanishes. Hence, the JPs have a higher modulus and as a result a higher stiffness compared to the SBM triblock terpolymers in a broad temperature range, including room temperature, where the mechanical properties are investigated. The higher the degree of crosslinking, the higher the modulus of the PB core, and the higher the modulus of the JPs corresponding to the core. This is an important point to consider later on, as the interface elasticity defines the deformation mechanisms and macro properties of the blends, such as resistance to crack growth. One could assume that this large difference (around 65 % decrease) in the modulus could be the result of lower amount of the PB middle block (20 % in JPs compared to the 36 % in the SBM triblock terpolymers). However, DMA analysis of the SBM triblock terpolymers with similar PB amount as JPs also shows a larger step and steep decrease in the modulus at the  $T_g$  of the PB block, compared to the multicompartment micelles. Hence, the difference is surely a result of different synthesis process of the JPs and their 3D structure.

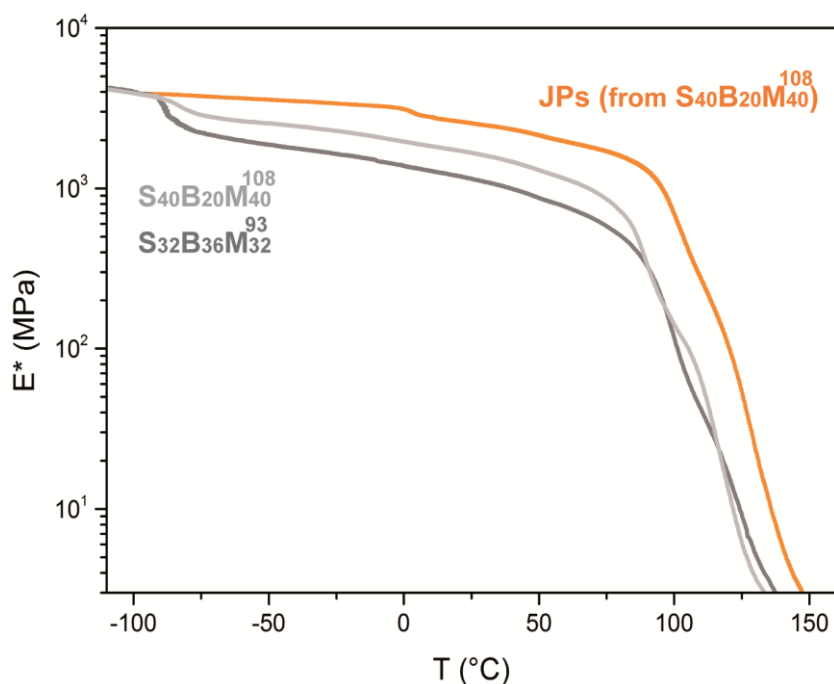


**Figure 22** Complex modulus of compatibilizers (JPs and SBM triblock terpolymers) and SBM precursors used to synthesis JPs

### 5.1.3 Optimization of the melt blending process

Polymer processing in extruders is one of the most common ways of melt blending different polymers. In terms of polymer blends, although some studies have focused on the effect of processing parameters on the final blend morphologies [234], many studies have concluded that the morphology development mechanisms are similar for batch mixers and twin screw extruders and, thus, the final morphology at matched conditions would be also similar [235–238]. This could be the case for many common polymer blends with blend viscosity ratios within the range of 1. However, one should take into account that the generated shear field is unique for a certain equipment and has different effects on the polymer blend. An example was shown before, where the different force fields in the co-kneader compared to the twin screw extruder made the production of PPE/PS blends with more than 80 wt.% PPE possible. In particular, the processing conditions must be closely observed while down scaling and working with special blend systems (*i.e.* with higher viscosity ratios). Morphology and possible droplet breakup mechanisms are strongly dependent on the viscosities and the viscosity ratio ( $P$ ) of the blend components, especially for PPE/SAN blends due to the much higher viscosity of PPE compared to that of SAN. The viscosity ratio of the PPE/SAN system in dependence of frequency (based on

rheological measurements) is shown in **Figure 23**. The P value is at all frequencies higher than 10 (the upper end of the viscosity ratio range for normal blends). This calls for special attention at the processing conditions chosen to compound these polymer blends.

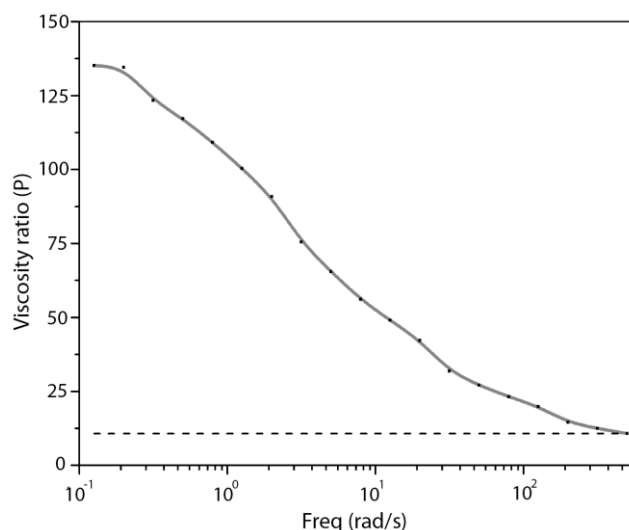


**Figure 23** Viscosity ratio of the PPE/SAN (60/40 w/w) system at different frequencies (based on the absolute shear viscosity data of the neat components in Figure 18)

In order to get a preliminary idea about the effect of JPs on the PPE/SAN blend system, and due to limitations in synthesizing JPs in large amounts, a DSM micro compounder was chosen as compounding device to produce blends on a smaller scale, first. The morphology of the neat PPE/SAN (60/40 w/w) blend and the blends with 10 wt.% SBM (standard compatibilizer with 36% PB and equal block sizes), and 10 wt.% JPs was analysed with TEM. The amount of 10 wt.% compatibilizer was chosen based on the previous studies by Ruckdäschel [228], and the 60/40 blend was selected as a system with medium viscosity. The TEM images in **Figure 24** compare neat, SBM, and JP compatibilized blends. The brighter phase is SAN and the PPE phase appears as the dark phase due to the staining process explained in the experimental section. The stained PB block in SBM triblock terpolymers or JPs would show up as black spots (not visible at current magnifications), however, the morphologies of the blend systems are discussed in more detail in the next sections. The blends do not differ much in their morphologies, although in the compatibilized blends the SBM triblock terpolymers or JPs are located at the interface. In all three cases a co-continuous morphology with little differences in the domain areas is observed. This is in contrast to the results of Walther et al. [14], who observed droplet morphologies in

PS/PMMA blends produced with the same type of micro compounder under comparable processing conditions.

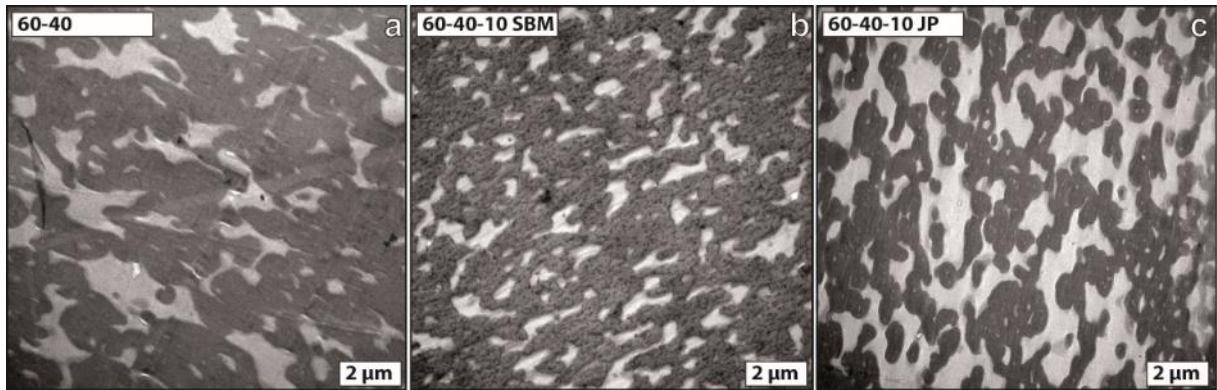


**Figure 24** TEM images of PPE/SAN (60/40) blends from a lab-scale micro compounder: a) neat, b) SBM compatibilized and c) JP compatibilized blends

By comparing the PPE/SAN and PS/PMMA systems, the only major difference (beside the chemistry of the components) that can cause this phenomenon is the difference in viscosity ratios. The viscosity ratio for the PPE/SAN blend is larger than 10, whereby that of the PS/PMMA blend is around 0.08 [239]. There are several studies that investigate the effect of viscosity ratio on structure evolution in miscible and immiscible blends [240–243]. Looking at the morphologies obtained in the micro compounder, and the relevant mechanisms for droplet formation, it can be concluded that the shear forces were not strong enough to break up the in plane PPE and SAN sheets in the polymer melt, resulting in the formation of a co-continuous phases in blend morphology.

The capillary number (equation 10) is a dimensionless number that represents the relative effect of viscous forces, coming from the force fields (in this case shear) produced during processing, versus surface tension (property of the blend system). For each system, a critical value  $Ca_c$  exists, above which the one blend phase breaks up into droplets. In case of smaller values, the phases elongate into a co-continuous structure and there is no droplet break up [62]. In this study, two strategies were chosen to overcome this challenge and produce blends with droplet morphologies: (1) The blend components were compounded for longer times in order to break up more PPE domains into droplets, (2) A higher amount of compatibilizer is used to further reduce the interfacial tension and increase the capillary number. However, both

strategies failed to produce the desired droplet morphology and the blends always showed co-continuous morphologies.

At a certain viscosity ratio, if all parameters of the system are constant, the capillary number needs to be increased in order to move out of the stability regime for the co-continuous blend structure. The variable that can be changed *via* choosing the right processing method is the shear rate. By moving from a micro compounder to a twin-screw extruder employing screw design with a sufficient number of kneading blocks, the applied shear rate will increase and one can move out of the co-continuous zone and achieve a droplet morphology. The TEM micrographs of the 60/40 neat blends, produced with a twin-screw extruder and the micro compounder, respectively, and a schematic graph showing the critical capillary number as a function of the viscosity ratio for shear flow are shown in **Figure 25**. It is clear that by increasing the shear rate, and as a result capillary number, the morphology of the neat blend has changed into PPE droplets dispersed in a SAN matrix (**Figure 25a**). The difference is visible by comparison with the same blend produced in the micro compounder (**Figure 25b**), which has smaller capillary number. The measured torque values during the process were 5 and 45 Nm for the micro compounder and twin-screw extruder, respectively. This confirms low and high shear forces during processing. Therefore, even though compounding on a small scale has the advantage of using lower amounts of materials, for such special systems like PPE/SAN with large viscosity ratios, compounding in close to industrial scale compounders is inevitable.

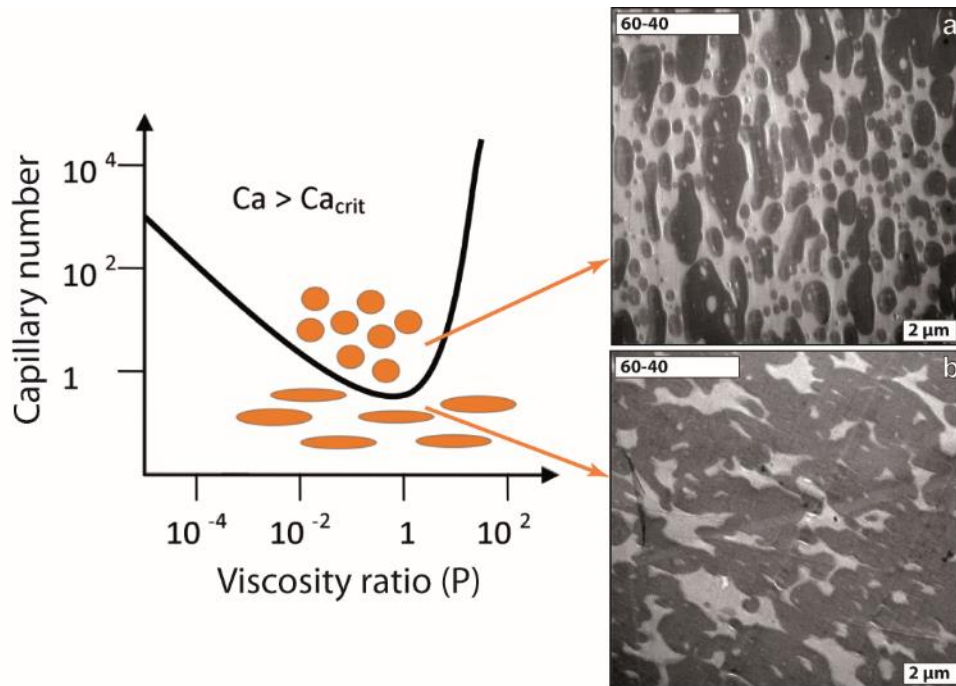


**Figure 25** Schematic dependence of the capillary number on the viscosity ratio under shear flow as shown in 2.1.2.2. TEM images of PPE/SAN (60/40) blends obtained from a) twin-screw extruder and b) micro-compounder

#### 5.1.4 Conclusion

The main motivations behind the current work and study of the PPE/SAN blends were introduced and discussed. The lower viscosity of SAN facilitates the processing of PPE and reduces the blend viscosity. Besides, the higher chemical resistance of SAN compared to PS, which is the state of the art material for blending with PPE, improves the chemical resistance of the blends. Rheological measurements suggest the use of 50/50, 60/40, and 70/30 (w/w) PPE/SAN blend ratios for future investigations of this work.

JPs and SBM triblock terpolymers (benchmark) are introduced as compatibilizers for the PPE/SAN blend systems. The  $T_g$  of the crosslinked PB core in the JPs is almost 80 °C higher than that of the PB block in SBM triblock terpolymers and JPs exhibit a higher modulus at room temperature compared to their triblock terpolymer precursors. This difference in stiffness is important, as the compatibilizers are located directly at the blend interface in the raspberry morphology and strongly influence the mechanical properties.

---

The melt blending process and its parameters were optimized for the PPE/SAN blend system. Entirely different morphologies were obtained for lab-scale and industry-scale processing, underlining the importance of large-scale studies on systems involving specialized materials. The high viscosity ratio of the blend necessitates the use of a twin screw extruder (higher accessible shear forces) as the convenient processing method to achieve the desired morphology (PPE droplets dispersed in a SAN matrix). Hence, all blend systems, studied in this thesis with respect to their morphological, rheological and mechanical properties, were produced on an industrial scale using a twin-screw extruder.

## 5.2 Micromechanics of blends compatibilized with SBM triblock terpolymers

Toughening mechanisms in polymer blends depend highly on the size of the domains dispersed in the matrix as well as the interface properties. Therefore, it is difficult to simultaneously monitor these effects in a new system such as JP compatibilized blends. Therefore, the role of the domain size is first investigated in a known system with the benchmark material, while the interface properties are kept constant (all compatibilized with SBM triblock terpolymers). Three different PPE/SAN blend systems with 50, 60, and 70 wt.% of PPE (50/50, 60/40, and 70/30) are compatibilized with 10 wt.% of the state of the art SBM triblock terpolymers. Their morphological, rheological and mechanical properties are compared to the neat, uncompatibilized blends. The goal of the chapter is to understand the effect of domain size on the toughening micromechanisms and at the end, to select a blend ratio for comparing the JPs to the SBM triblock terpolymers.

### 5.2.1 Morphological characterization of SBM compatibilized blends

The morphology of an immiscible polymer blend depends strongly on the rheological properties of the blend components. Based on previous rheological investigations in section 5.1.3, it is expected that the large viscosity differences between the blend components result in unusual morphology of the immiscible blends. It is also expected that high viscosity ratio shifts the phase inversion region for having a PPE matrix far from the expected 50/50 blend ratio [243]. The phase inversion of this system can be predicted with the aid of two models proposed by Chen [244](equation 19) and Utracki [243] (equation 20). The models calculate a threshold value for the viscosity ratio, which above that PPE can no longer form the continuous matrix. Under these conditions, even though PPE is the dominant component in the blend and has weight fractions of more than 50%, a PPE matrix is rheologically not possible.

$$\frac{\phi_{PPE}}{\phi_{SAN}} = 1.2 \left( \frac{\eta_{PPE}}{\eta_{SAN}} \right)^{0.3} \quad (19)$$

$$P = \frac{\eta_{PPE}}{\eta_{SAN}} = \left( \frac{\phi_m - \phi_{SAN}}{\phi_m - \phi_{PPE}} \right) \eta^* \phi_m \quad (20)$$

Where  $P = \frac{\eta_{PPE}}{\eta_{SAN}}$  is the viscosity ratio,  $\phi_m$  is the maximum packing volume fraction equal to 0.84 for most polymer blends [17],  $\phi_{SAN}$  and  $\phi_{PPE}$  are the SAN and PPE weight fractions respectively, and  $\eta$  represents the corresponding viscosities.

In case of 50/50, 60/40 and 70/30 PPE/SAN blends, the predicted threshold values are shown in **Table 3**. A comparison between these predicted values with the measured viscosity ratios (**Figure 23**) suggests a continuous SAN phase with PPE droplets for all chosen blend ratios. The viscosity ratio of the blend at high frequencies discussed in the previous chapter is around 12. This represents the value at high shear rates in the extruder. According to these values, PPE contents of above 70 wt.% are necessary to achieve a continuous PPE phase with dispersed SAN droplets. The chosen blend systems (50/50, 60/40, 70/30) all deliberately have the same droplets dispersed in matrix morphologies, (SAN matrix with dispersed PPE droplets), which facilitates the direct comparison of the micromechanical properties between them.

**Table 3** Viscosity ratio ( $P$ ) of the blends calculated *via* different models: all values are smaller than 12 (measured threshold limit for PPE/SAN blends)

Blend ratio	Chen's Model [244]	Utracki's Model [243]
<b>50/50</b>	<b>0.5</b>	<b>1</b>
<b>60/40</b>	<b>2.1</b>	<b>2.6</b>
<b>70/30</b>	<b>9.2</b>	<b>8.6</b>

Based on this information and the fact that PPE droplets are expected to be dispersed in the SAN matrix, the TEM micrographs of the neat and compatibilized blends are investigated. Firstly, the neat and SBM compatibilized PPE/SAN blends are compared at the 50/50 blend ratio (**Figure 26**). As mentioned previously, due to the staining process, the brighter matrix phase represents SAN, the PPE phase appears as the darker phase, and the PB block shows up as the black dots. The neat blend shows relatively random PPE structure dispersed in the SAN matrix with very large as well as very small PPE phases (**Figure 26a**). Using SBM triblock terpolymers, the blend morphologies become more homogeneous, and it looks that the PPE phase forms droplets

instead of a semi-continuous structure in **Figure 26b** [155]. It is expected that the PPE droplet sizes decrease after compatibilization, as the interfacial energy between the blend components decreases. Here, even though the droplets have a much more homogenous shape after compatibilization, their sizes are not significantly reduced. This may be due to SBM micelle formation within the PPE phase resulting from a slight preferential interaction of the PS block with PPE (Flory-Huggins segment-segment interaction parameter  $\chi_{PS/PPE} = -0.044$ ) compared to PMMA/SAN ( $\chi_{PS/PPE} = -0.008$ ) [31]. The different micelle formation mechanisms has been also reported before [11]. Beside thermodynamical interaction parameter and interfacial tension of the compatibilizer, the blend viscosity and shear forces during compounding also play a significant role in determining the final blend morphology and formation of micelles. **Figure 26c**, which shows the SBM compatibilized 50/50 blend at a higher magnification, clearly shows SBM micelles (marked by orange arrows) in the PPE phase as well as SBM triblock terpolymer chains located at the PPE/SAN interface. The core of the micelles consists of PMMA and PB, and the PS shell points to the PPE. At high SAN contents such as this blend, the blend viscosity is comparably low, and the initially formed smaller PPE droplets can coalesce and form larger PPE droplets. Consequently, there is excess SBM that cannot assemble at the interface and thus forms micelles. Additionally, SBM located at the interface of smaller PPE droplets may be trapped inside larger PPE domains as a micelle, during the coalescence process. This extensive micelle formation reduces the compatibilizer efficiency, as the amount of effective SBM triblock terpolymer chains at the interface is reduced (the SBM micelles can be counted as ineffective compatibilizer). Preventing coalescence in blends of low viscosities by either higher shear forces, or more efficient compatibilizer with higher surface activity like Janus particles [155], would lead to smaller PPE droplets without SBM micelle formation.

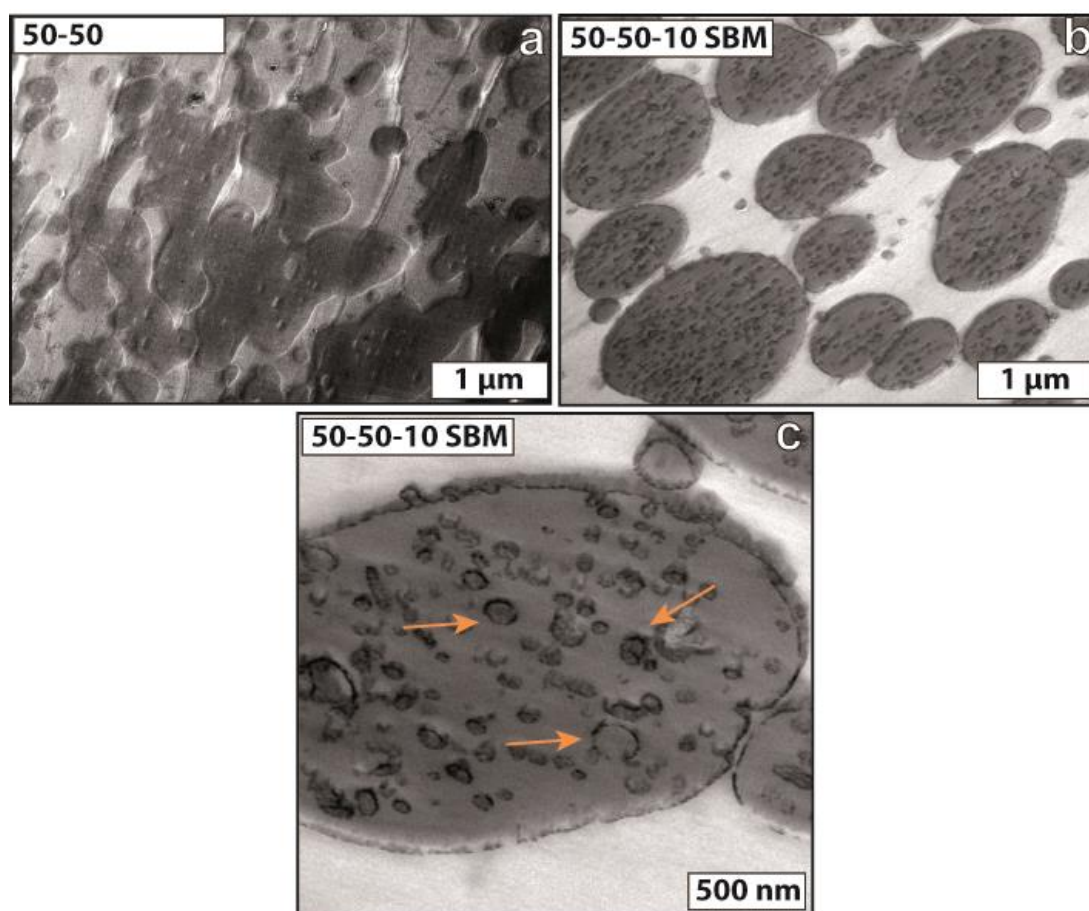


**Figure 26** TEM images of PPE/SAN (50/50) blends: a) neat, b) SBM compatibilized blends, and c) location of SBM triblock terpolymers at the interface and micelle formation in PPE phase

In case of the blend with 60/40 weight ratios, the neat blend again shows random morphology of PPE droplets with inhomogeneous sizes in the SAN matrix (**Figure 27a**). After compatibilization with SBM, the PPE domains are more homogeneous and presumably only present in form of droplets in the SAN matrix (**Figure 27b**). The blend shows less number of micelles (marked by orange arrows) in the PPE matrix (**Figure 27c**) compared to the 50/50 blend, however, still doesn't show significant reduction in PPE domain size after compatibilization due to these ineffective SBM compatibilizers trapped in the PPE phase. The higher viscosity of the 60/40 blend (due to its higher PPE content) reduces SBM mobility and droplet coalescence rate during extrusion, hence less micelles are trapped within the PPE domains.

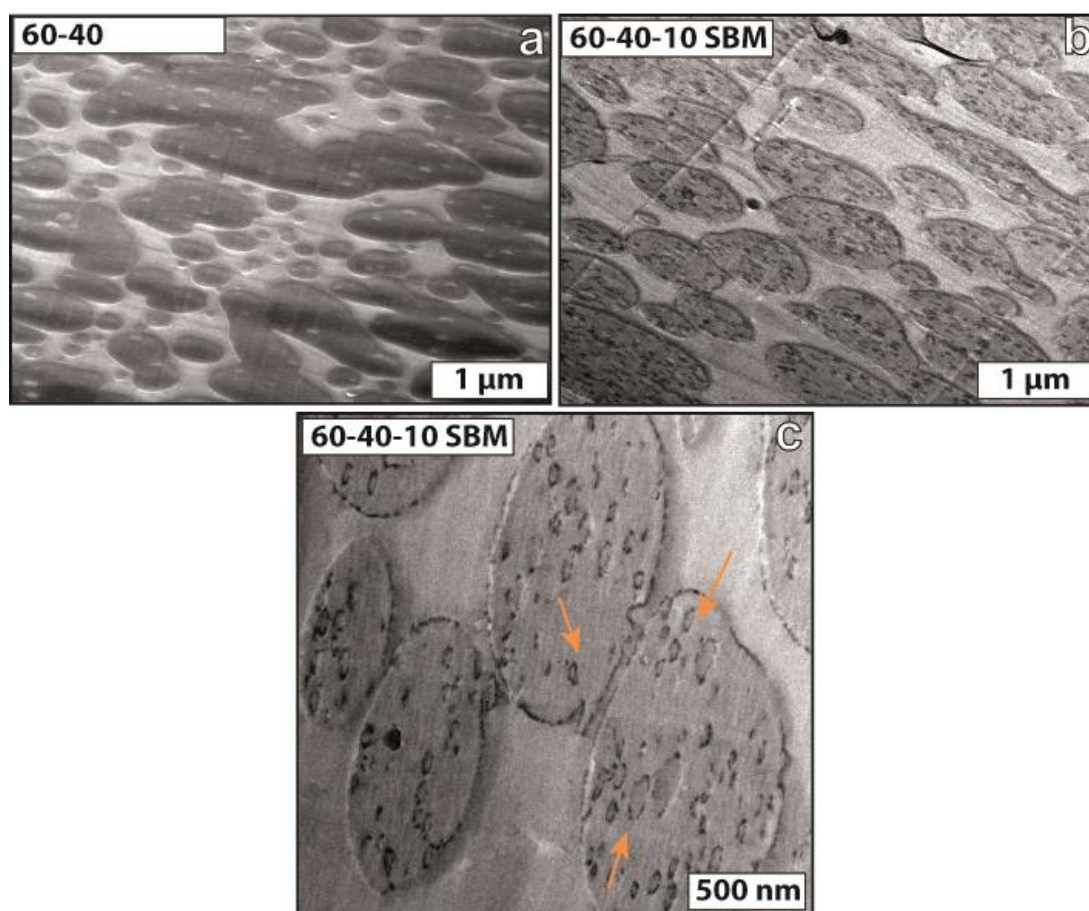


**Figure 27** TEM images of PPE/SAN (60/40) blends: a) neat, b) SBM compatibilized blends, and c) less number of micelles in PPE phase compared to the 50/50 blend

In case of the 70/30 blends in **Figure 28**, the total blend viscosity is higher than all previous blends, hence due to the higher internal shear forces produced during the extrusion process, higher droplet break up rates exists. Here, even the neat blend shows smaller PPE phases (**Figure 28a**). In the SBM compatibilized blends, the PPE domain size after compatibilization is also very small (**Figure 28b**), and there are almost no micelles in the PPE phases (**Figure 28c**). The triblock terpolymer chains are exclusively located at the interface between the blend phases, however, due to the high amount of PPE fraction, the number of SBM triblock terpolymers are probably not high enough to sufficiently cover all of the PPE domains. Therefore, the perfectly covered PPE domains are much smaller than of the partially covered ones, and there is a relatively large PPE domain size distribution available for this blend.

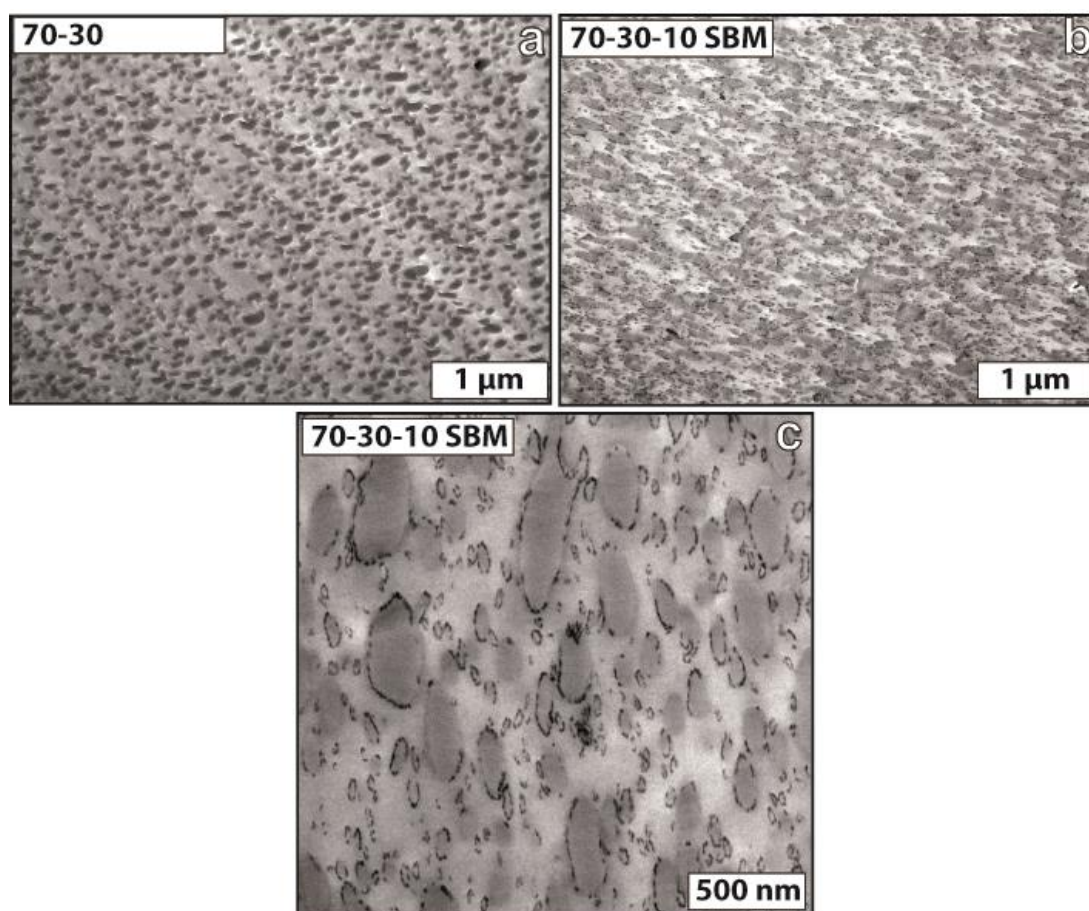


**Figure 28** TEM images of PPE/SAN (70/30) blends: a) neat, b) SBM compatibilized blends, and c) exclusive location of SBM triblock terpolymers at the interface and no micelle formation

In Summary, the PPE domain size decreases with increasing the PPE content from 50 to 70 wt.% (in both neat and compatibilized blends). At the same time, in the SBM compatibilized blends, the number of micelles in the PPE matrix decreases as the PPE content and the viscosity of the system increase. Investigating these blends with different domain size and same interface properties, allows to solely understanding the role of the domain size on the toughening micromechanisms in the next sections. Later on while comparing the JPs with the SBM triblock terpolymers, one can eliminate the differences in their domain sizes with this knowledge and solely compare the influence of the interface.

### 5.2.2 Rheological characterization of SBM compatibilized blends

In order to confirm the mentioned assumptions in regard of the droplet break up in correlation with higher viscosity of the blends with more PPE, shear rheological measurements of polymer blends are performed. Rheology is an important tool to compare the interfacial adhesion between the phases after compatibilization. The viscosity of a blend system depends on the viscosities of its components and their weight fractions, as well as the behaviour of the interface between them. If the interfacial adhesion is strong, the stress can be transferred from one phase to the other upon applying shear forces. Hence, the higher viscous phase (which is attached to the lower viscous phase) hinders its flowability and increases the viscosity of the system. In our case, the more viscous PPE phase hinders the deformation of the SAN matrix and, thus, increases the viscosity of the blends. **Figure 29** shows the shear viscosity of the neat and compatibilized blend systems. As expected, increasing the PPE amount from 50 to 70 wt.% leads to an increase in viscosity of the neat blends (without compatibilizer). In addition, after compatibilization with SBM triblock terpolymers, an increase in the viscosity relative to the neat blends is also observed, indicating the presence of the triblock terpolymer chains at the interface and better stress transfer between the phases.

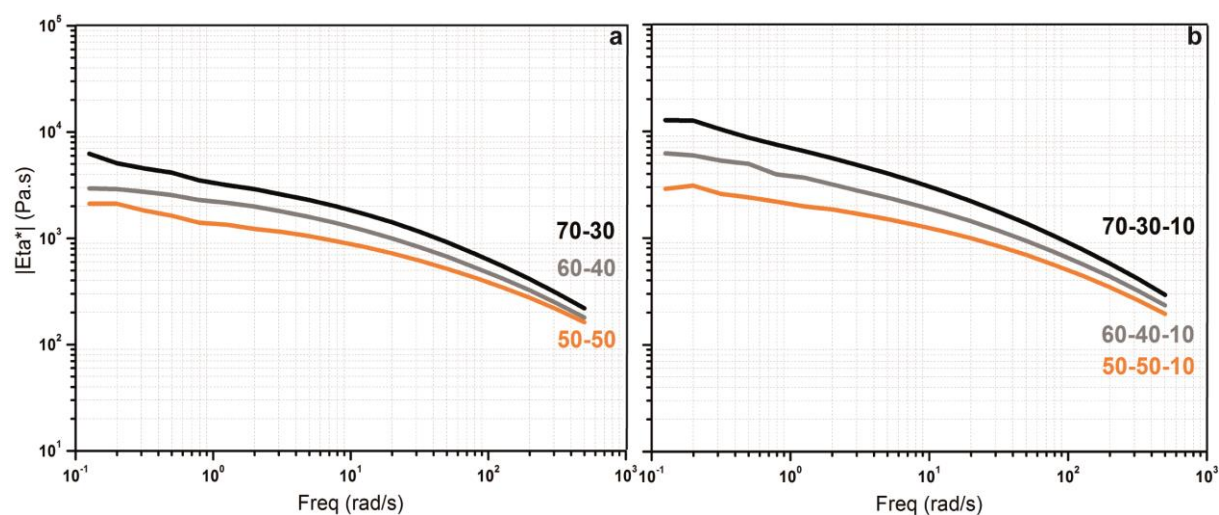


**Figure 29** Absolute shear viscosity of a) neat and b) SBM compatibilized PPE/SAN blends at different blend ratios

The increase in the viscosity after compatibilization is more pronounced in the 60/40 and 70/30 blends at lower frequencies. This is due to the decrease in PPE droplet size, which results in a

higher amount of PPE droplets. Consequently, there is a considerable increase in interfacial area, which strongly influences the viscosity of the blends especially at low frequencies. In order to better understand the viscosity differences before and after compatibilization shown in a logarithmic scale, the absolute shear viscosity values of all 6 blends at the frequency of 10 rad/s are representatively shown in **Table 4**.

**Table 4** Absolute shear viscosity of neat and SBM compatibilized blends at the frequency of 10 rad/s

Blend ratio	Neat blends viscosity (Pa.s)	SBM compatibilized blends viscosity (Pa.s)
50/50	938	1332
60/40	1386	2048
70/30	1995	3358

### 5.2.3 Mechanical characterization of SBM compatibilized blends

#### Dynamic Mechanical Analysis (DMA)

Dynamic mechanical analysis is an efficient way to investigate the mechanical properties, namely complex modulus in a wide temperature range. **Figure 30** shows the complex modulus of neat and compatibilized blends in dependence of temperature. In the DMA curves of the neat blends, two sharp and distinct steps are visible indicating the  $T_g$  of SAN and PPE, respectively. The discontinuous distribution of the elastic PB phase around the PPE domains in the compatibilized blends (raspberry morphology) prevents reduction of the modulus and stiffness of the material after toughness modification [173]. Therefore, at temperatures below the glass transition temperature of SAN, the complex modulus of the neat and compatibilized blends remains almost constant.

Right above the glass transition of SAN, the complex modulus shows a pronounced drop as the temperature increases, which is in accordance with the morphological results showing SAN as the continuous phase. The second reduction step in the complex modulus curves correlates to

the  $T_g$  of the PPE phase. After compatibilization, a shift in  $T_g$  of PPE to lower temperatures is observed for all blend compositions. This may be explained by the higher miscibility of PS/PPE and the high difference between the  $T_g$  values of both polymers (ca. 103 for PS and 210 °C for PPE). In addition, SBM micelles located in the PPE domains would further contribute to the reduction of its  $T_g$ . In contrast, SAN and PMMA have  $T_g$  values close to each other (ca. 110 °C for SAN and 100 °C for PMMA) and, hence, no significant change in  $T_g$  is expected.

The trend of the DMA trace above the  $T_g$  of the SAN matrix is a direct indication of the blend morphology. As a result of pseudo co-continuity in the neat 50/50 blend, a pronounced second plateau is visible around complex modulus of 250 MPa. After compatibilization with SBM, the morphology changes into droplets dispersed in the SAN phase (which is only 50 wt.-% of the specimen), hence a significant drop and continuous decrease of the modulus is observed until the  $T_g$  of the PPE is reached. Therefore, the difference in the complex modulus of the neat and SBM compatibilized blends at 50/50 weight ratio is very large in the temperature range above the  $T_g$  of SAN (**Figure 30a**).

In case of the neat 60/40 blend the pseudo co-continuous morphology [155] is preserved and visible in the DMA curve as plateau above the  $T_g$  of SAN at complex modulus of around 800 MPa. After compatibilization, the TEM (and also SEM images in the next section) show a morphology consisting of PPE droplets dispersed in the SAN matrix. However, the DMA curve of the compatibilized blend still shows a plateau at around 600 MPa instead of the expected fast decrease like in the compatibilized 50/50 blend. This phenomenon can be explained by the very large difference in the  $T_g$  values of the blend components, as well as the bonding at the interface *via* SBM. After softening of the SAN matrix, the PPE droplets, which represent the main fraction in the blend, are still in their glassy state and are able to hold the specimen together. In addition, as the droplet size decreases, the interfacial area between the phases increases. Hence, there is a strong linkage at the interface attaching the small glassy PPE domains to the SAN matrix and compared to the neat blend, only a small decrease in the plateau after compatibilization is observed (**Figure 30b**). This theory is later confirmed in the next chapter where DMA measurements with higher deformation amplitude are performed.

In the neat 70/30 blend, even though the morphology shows no co-continuity, there is a plateau visible above the  $T_g$  of SAN at a large complex modulus of 1000 MPa. The reason may be the high fraction of the PPE phase, resulting in densely packed small PPE particles within the SAN matrix. The hard glassy PPE domains in this region have an effect comparable to that of fillers in a highly filled polymer composite [245,246]. In this case one can think analogically of a highly filled

polymer (with mineral fillers like glass spheres). Even though the glass spheres are dispersed in a molten polymer matrix, due to their high amount (70 wt.%), they form a structural network and hold the material together. Here, the PPE droplets form a network providing structural viscosity to the blend, preventing its collapse (since the SAN phase has already softened) and holding the specimen together. After compatibilization, the same phenomenon as described above is observed. In comparison to the other blend ratios, the difference between the complex modulus of neat and compatibilized 70/30 blends is rather small (both have values around 1000 MPa), which is due to the large effect of higher PPE fraction (**Figure 30c**). The increase in the plateau values (from 600 in the 60/40 blend to 1000 MPa in the 70/30 blend) with increasing PPE content confirms that the PPE droplets act as glassy fillers in the SAN matrix.

It is worth to mention that in an attempt to be able to better interpret the results and their correlation to the morphology, attempts were made to freeze the specimens at different steps of the DMA measurements. The aim was to solve one of the phases in a good solvent for it (here THF for SAN) and look at the morphology of the remaining phase under the microscope. However, due to complexity of the blend morphology and instability of the remaining phase, it was not possible to gather fulfilling results.

In order to better understand the differences in the complex modulus before and after compatibilization shown in a logarithmic scale, these values at different temperatures (-50, 0, 50, 100, 150 °C) are representatively shown in **Table 5**.

**Table 5** Complex modulus of neat and compatibilized blends at different temperatures

Blend ratio		E* (MPa) at different temperatures									
Neat	SBM	-50 °C		0 °C		50 °C		100 °C		150 °C	
<b>50/50</b>	<b>50/50/10</b>	<b>2791</b>	<b>2551</b>	<b>2648</b>	<b>2246</b>	<b>2422</b>	<b>2066</b>	<b>1613</b>	<b>1456</b>	<b>220</b>	<b>27</b>
<b>60/40</b>	<b>60/40/10</b>	<b>2699</b>	<b>2628</b>	<b>2448</b>	<b>2524</b>	<b>2347</b>	<b>2304</b>	<b>1591</b>	<b>1628</b>	<b>669</b>	<b>474</b>
<b>70/30</b>	<b>70/30/10</b>	<b>2483</b>	<b>2924</b>	<b>2350</b>	<b>2692</b>	<b>2188</b>	<b>2396</b>	<b>1588</b>	<b>1693</b>	<b>962</b>	<b>888</b>

---

In conclusion, the high difference between the  $T_g$  of the blend components, sizes of the droplets in the matrix (which influences the interfacial area), and the quality/strength of the interface play important roles in determining the properties of the blend materials in DMA analysis. Here, the quality of the interface has been deliberately kept constant (always the same type of SBM triblock terpolymer) and the effect of the droplet size has been investigated. Smaller densely packed droplets seem to build a strong network holding the matrix together, and after compatibilization they attach to the matrix polymer effectively *via* a stronger interface through SBM chains. Therefore, finer PPE/SAN morphologies can improve the stability and modulus of the blend at higher temperatures.

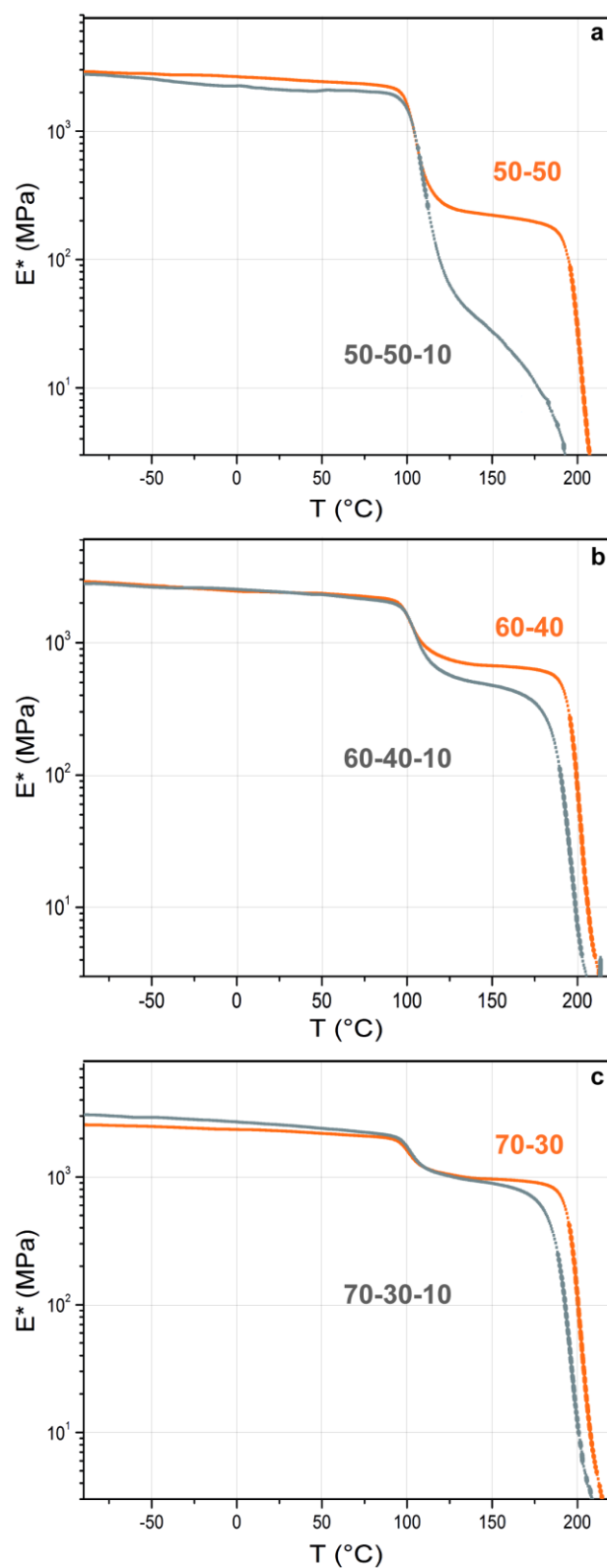


**Figure 30** Complex modulus of neat and compatibilized PPE/SAN blends, from DMA analysis, at different blend ratios: a) 50/50, b) 60/40, and c) 70/30 (w/w)

---

In order to further confirm the pseudo co-continuity of the blend structures before compatibilization and the change in morphology on a macro scale after compatibilization, Payne tests (strain sweep at constant temperature) were performed on all blends (**Figure 31 a-c**). The test is performed at 150 °C since this temperature is within the second plateau in the complex modulus of blends, above the  $T_g$  of SAN. The Payne effect [247] is mostly defined for filled rubber systems in which the filler particles form clusters and interact in a filler network. In such systems, the storage modulus depends on the amplitude of the applied strain. After applying high deformations (increasing the strain) the filler network can be disturbed and destroyed, and a decrease in the modulus occurs at a certain point during the strain sweep [248]. This analogy can be applied to our blend systems with their unique structures. In case of the neat blends, the pseudo co-continuous structure cannot be destroyed easily *via* strain, as it is partially connected through the elongated PPE domains. However, after compatibilization, the dispersed PPE particles resemble fillers that form a structural network in the blend system. This network can be destroyed at higher strains (Payne strain) compared to neat blends.

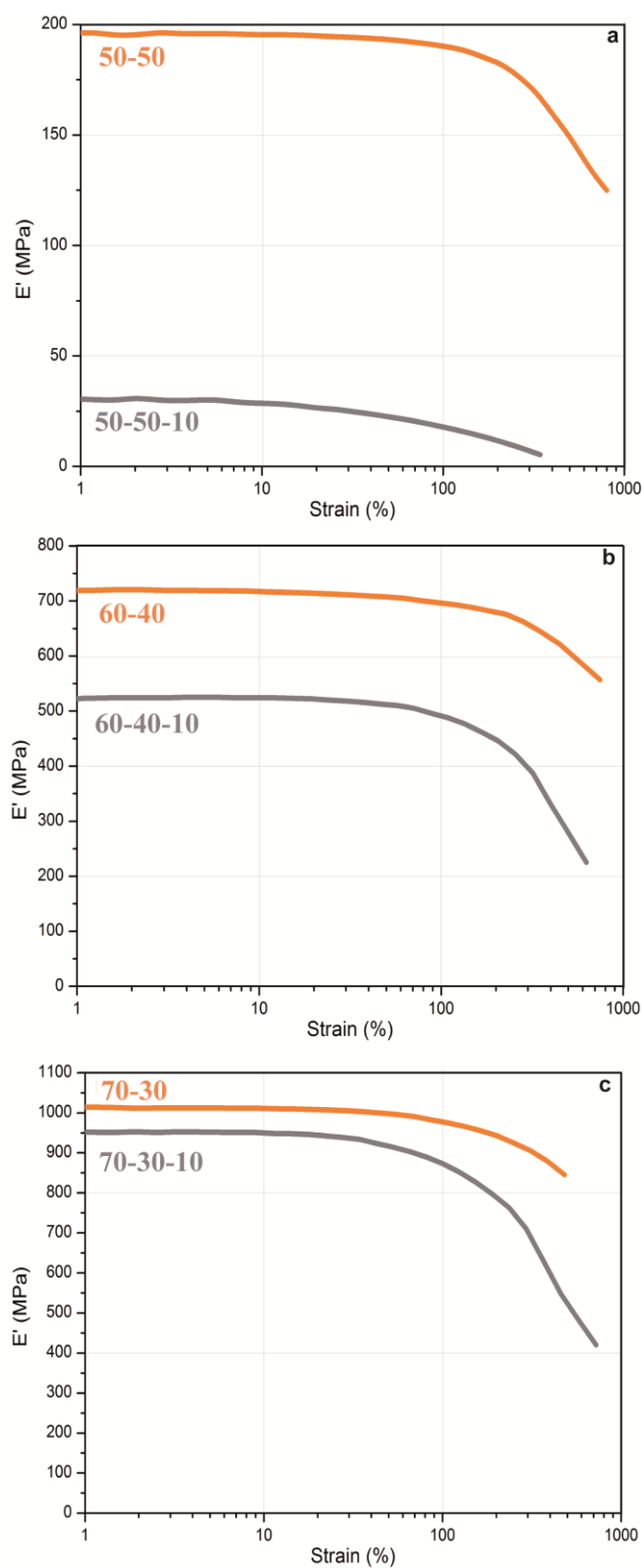


**Figure 31** Storage modulus of neat and compatibilized PPE/SAN blends in dependence of the applied strain at 150 °C at different blend ratios: a) 50/50, b) 60/40, c) 70/30 (w/w)

This behaviour is shown in **Figure 32**, where complex modulus of each blend system, at the point where the sharp decrease in modulus during the Payne test begins, is compared with each other. At 50/50 blend ratio, the difference between neat and compatibilized blends is quite large. The neat blend has much higher modulus at the start of the sharp drop compared to the SBM compatibilized blend due to its pseudo co-continuous structure. The addition of SBM improves the interface interaction between the matrix and dispersed phase and may result in the decrease of complex modulus. A similar trend but at a smaller scale is visible for the 60/40 blends, where the decrease in modulus appears for the SBM compatibilized blends compared to neat blend. The smaller difference between the moduli of the neat and compatibilized blends has similar reasons to what has been discussed for **Figure 30**. In case of the 70/30 blends, the complex modulus at the drop point is almost the same for the neat and SBM compatibilized blends (as expected due to lack of any co-continuity in the blend morphologies). The slight, lower complex modulus value for the SBM compatibilized blends could be due to the fact that compatibilization with block copolymers resulted in larger reductions of the storage modulus in the Payne test as reported by Wang et. al [249]. The Payne tests and their results for all blend systems is discussed in more detail in the published article by author [206].

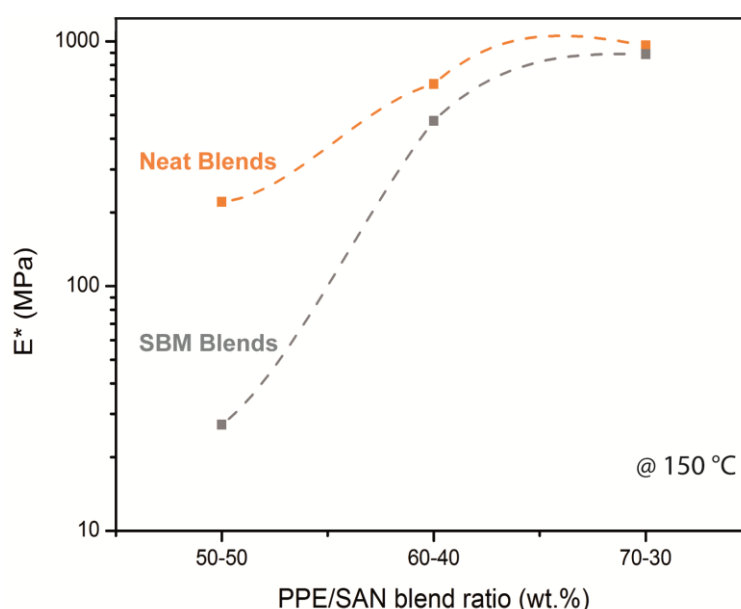


**Figure 32** Complex modulus of PPE/SAN neat and compatibilized blends from Payne test at 150 °C

### Elastic properties (Low strain behaviour)

The tensile properties of the polymer blends depend on the property of each phase, their contents and their mechanical behaviours; also very important is the resulting morphology. Tensile modulus (dog-bone specimens) of neat and compatibilized blends were tested compared as the function of the PPE weight content in **Figure 33**. Tensile properties of the SBM compatibilized blends, and comparison with different mechanical models have been previously investigated in detail by Ruckdäschel [222]. Here, the focus is on the behaviour after SBM compatibilization that results in droplets and correlation to the raspberry morphology. The moduli of the blends stay constant after compatibilization (compared to their equivalent neat blends). As mentioned in previous structures with raspberry morphology [11,118,173], due to formation of the discontinuous PB phase at the interface, the tensile moduli of the compatibilized and neat blends do not change significantly after compatibilization. The PB content in the SBM triblocks is ca. 30 %. Since 10 wt.% SBM is added to the blend, one can roughly say that there is around 3 wt.% PB rubber is available in total in the compatibilized blend structures. In an attempt to explain this phenomenon, fractured surface of the neat and compatibilized 60/40 blends after the tensile test, as an example, are looked at in more detail in **Figure 34**.

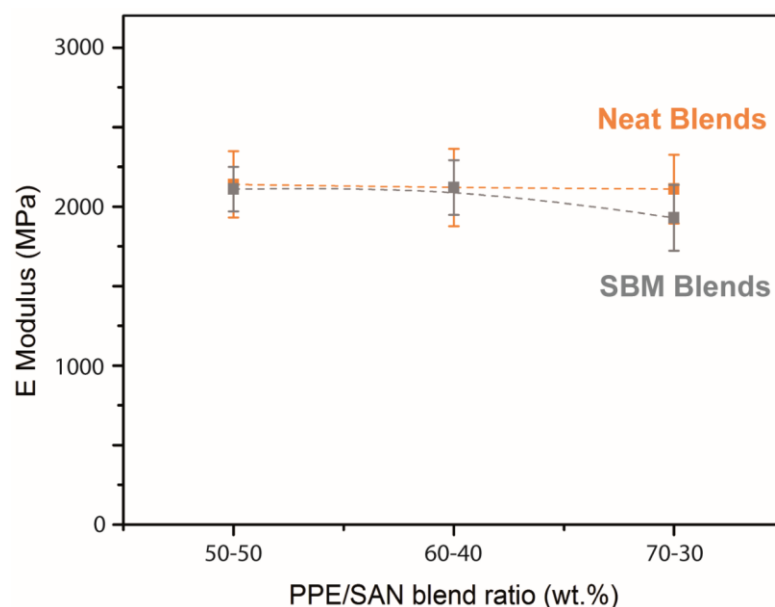


**Figure 33** Tensile modulus of neat and SBM compatibilized PPE/SAN blends

In case of the neat blend, the ductile PPE domains have no contact point or bonding to the SAN matrix, hence even at small strains, PPE domains debond and deform drastically as shown in **Figure 34a**. In case of the SBM compatibilized blend, the interface needs to deform to allow for PPE deformations. The deformation at the area around the interface, results in fibrillation of the SBM triblock terpolymers at the interface, however, the elastic nature of the butadiene middle block and its low modulus results in tear and debonding right after fibrillation of the interface (**Figure 34b**), followed by debonding of the PPE particles from the SAN matrix. The tear of the small area of each elastomeric part, would not result in instant failure of the material, but would produce a similar situation like the neat blend (deformation of the PPE which is debonded from the SAN matrix, yet still connected to the PPE network in the  $y$  direction). Therefore, the modulus of the material, which represents the behaviour of the material in small strain ranges, stays constant. In case of core shell particles, for example, rupture of the elastomeric core or shell will lead to instant failure, since rupture happens in a large area around the PPE particles and can act as a defect point, and reduces the modulus.

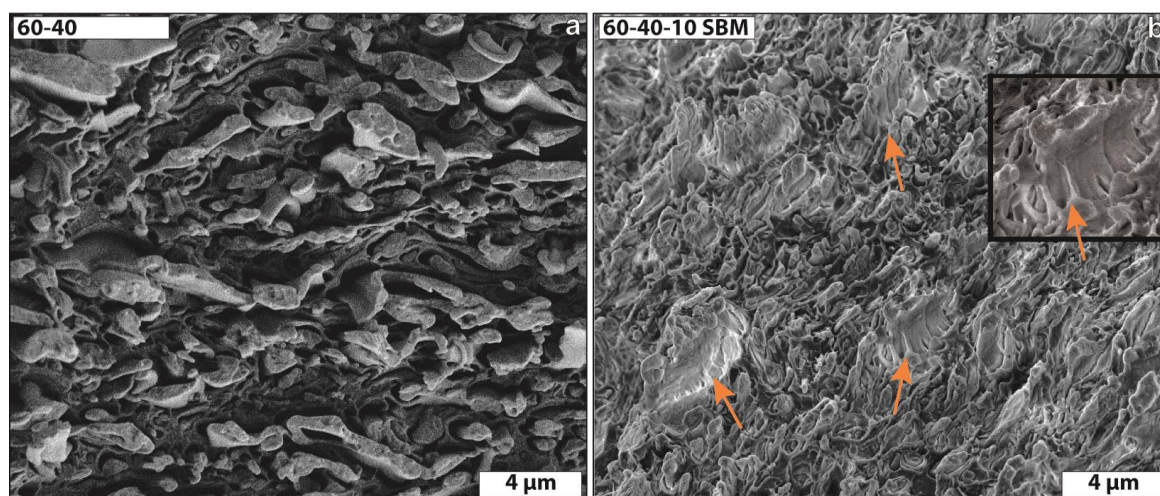


**Figure 34** SEM images of fracture surfaces of PPE/SAN (60/40) blends after tensile tests: a) neat and b) SBM compatibilized blends. Orange arrows point to the SBM fibrillation at the PPE/SAN interface. The inset shows a magnification of the PPE/SAN interface area with stretched SBM fibrils (scale bar 2  $\mu\text{m}$ )

### Fracture toughness characterizations

Fracture toughness measurements can provide important information about the toughness of materials. In addition, by investigating the fractured surfaces different toughening mechanisms for each blend system are identified. In order to be able to correlate the micro/nano-structure to the measured macro mechanical properties of polymer blends with complex morphologies, it is important to understand the micromechanical deformation mechanisms taking place in each phase. Any polymer material can withstand crack tip stresses up to a critical value of stress intensity (critical stress intensity factor,  $K_{Ic}$ ). Beyond this point, the crack propagates rapidly in the sample. The critical stress intensity factor is a measure of the material toughness. **Figure 35** shows the critical stress intensity factor ( $K_{Ic}$ ) value of the neat and compatibilized blends as a function of their PPE contents.

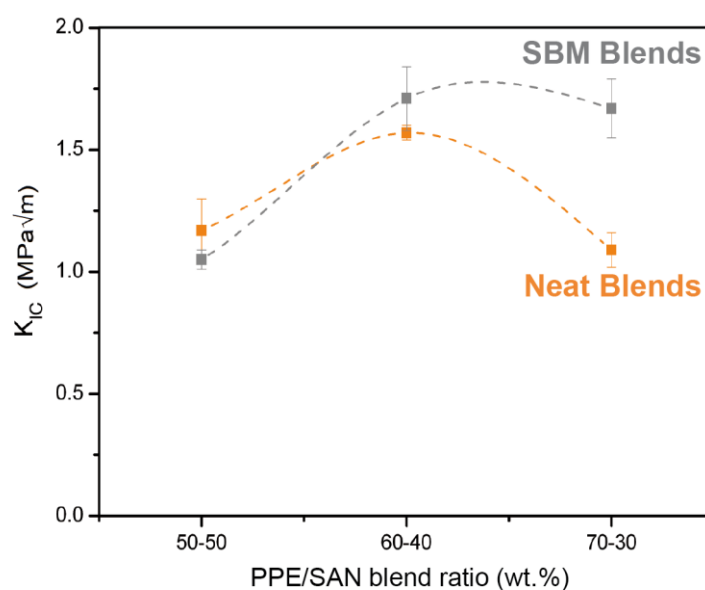


**Figure 35** Critical stress intensity factor of neat and SBM compatibilized PPE/SAN blends at different blend ratios

### Investigation of the fracture surface of the neat blends

In case of the neat blends, it is expected that increasing the PPE content (as the more ductile phase) should result in higher toughness values. In our case, this is valid when moving from the 50/50 to the 60/40 blend. However, a further increase of the PPE content (in case of the 70/30 blend) results in a significant reduction of toughness as compared to the 60/40 blend. In order

to understand and explain this behaviour of the neat blends, morphologies of the fractured surfaces (after  $K_{Ic}$  experiments) were investigated (**Figure 36**). It is worth to mention that the scale of the images in the figure are not the same due to the fact that the PPE domain sizes are different in blends with different blend ratios. Yet, it is important to compare them all together in one figure.

The larger PPE domains in the neat 50/50 and 60/40 blends (**Figure 36a, c**) have formed some fiber-like structures inside the SAN matrix, probably due to their pseudo co-continuous structure before compatibilization. It is known that elongated particles, which are parallel or perpendicular to the crack growth direction, are capable of affecting the crack more pronounced than spherical particles [250]. These elongated particles can plastically deform during crack growth and sometimes even hinder the crack propagation. In general, if the interface is strong enough, the fiber-like phase can also promote plastic deformations of the surrounding matrix. However, this is not the case here, since the neat blends have weak and detached interfaces. The PPE domains in the neat 50/50 and 60/40 blends can be assumed as elongated ductile particles, which can improve the toughness of the SAN matrix. In addition, since the interface between two immiscible polymers is weak, debonded PPE domains are visible in the fractured surface of the 50/50 (**Figure 36b**) and more pronounced in the 60/40 (**Figure 36d**) blends. This debonding leads to the pull out of PPE domains from the matrix, therefore contributing to plastification in the material as a toughening mechanism. In case of the 50/50 and 60/40 blends, both mechanisms (deformation of non-spherical PPE domains, and pull out of these domains from the matrix) consume large amounts of energy during fracture, leading to an increase in the toughness of the material. The necking phenomena observed in the PPE phases (specifically visible in case of the 60/40 blends is also clear indication of energy consumption and increased toughness of the blends. In case of the 70/30 blend, the PPE domains are more spherical and smaller in size (**Figure 36e, f**), despite of their higher fraction in the blend. These spherical PPE particles are more stable compared to the elongated ones in the 50/50 and 60/40 blends, as they have a smaller surface area to volume ratio. In other words, the size of the dispersed particles has a dramatic effect on their deformation behaviour in blend systems [251,252], and finer dispersions are more stable and more resistant to deformations due to lower resultant stress concentrations [252,253]. Generally, smaller particles are easier to deform (plain stress) than larger (thicker) ones (plain strain). Furthermore, in the 70/30 blend, the interparticle distance between the PPE domains is so small that the deformation of the SAN matrix is prevented. Therefore, there are only debonded PPE domains visible due to lack of compatibilization. Hence, due to absence of the aforementioned toughening mechanisms (lack of

PPE domain plastic deformation or pull out, and limited SAN matrix deformations), the  $K_{IC}$  value of the 70/30 blend decreases in comparison with blend systems with lower PPE contents.

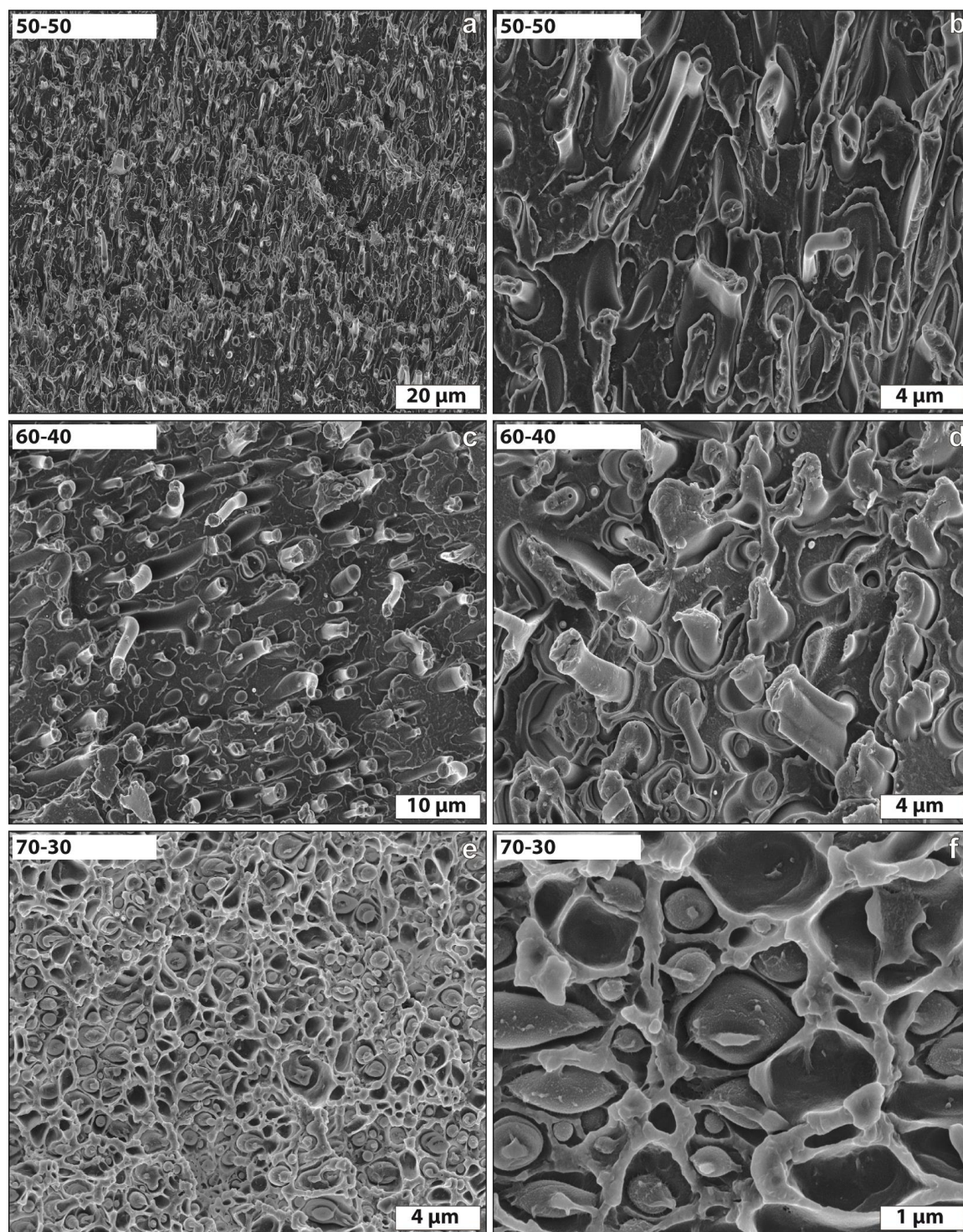


**Figure 36** SEM images of neat PPE/SAN blends with different blend ratios and magnifications after fracture toughness measurement: a, b) 50/50, c, d) 60/40, e, f) 70/30. The images are from the area right after the crack initiation point

### Investigation of the fracture surface of the SBM compatibilized blends

After effective compatibilization, it is expected to have an enhanced stress transfer from one phase to the other resulting in higher toughness values. According to **Figure 35**, in case of the 50/50 blend, the  $K_{IC}$  values remain almost constant after compatibilization. The fractured surface in **Figure 37** shows that the addition of SBM homogenizes the morphology and produces spherical PPE domains (oppose to the random non-spherical ones in neat blend) as seen in **Figure 26**. These PPE domains, containing SBM triblock terpolymers at their interface with SAN, show other toughening mechanisms (**Figure 37a**). The PPE domains are partially embedded in the SAN matrix (due to partial SBM coverage) and are, to some extent, capable of transferring the stress to the more brittle SAN at the points where SBM connects the two phases. At a higher magnification (**Figure 37b**), one can see the partial coverage of the PPE domains with SBM (white points representing SBM micelles). When the SBM connects the phases, some matrix deformations are visible in forms of crazes. However, the deformations of the spherical PPE domains in the compatibilized 50/50 blend are not as effective as the anisotropic PPE domains in the neat blend [250]. In addition, due to the different morphology (larger spherical PPE domains instead of smaller anisotropic ones), the interfacial area between PPE and SAN is smaller. Thus, the new toughening mechanisms provided by the SBM compatibilized interface are not sufficient to result in better  $K_{IC}$  values. In addition, the stronger adhesion between the phases after compatibilization prevents pull out of the PPE droplets from the SAN matrix that would consume a lot of energy and contribute to the toughening of the system as well. Here as well the scale of the images in the figure are not the same due to the fact that the PPE domain sizes are different in blends with different blend ratios. Yet, one can compare the single images of the figure with the previous one to understand the differences between neat and compatibilized blends.

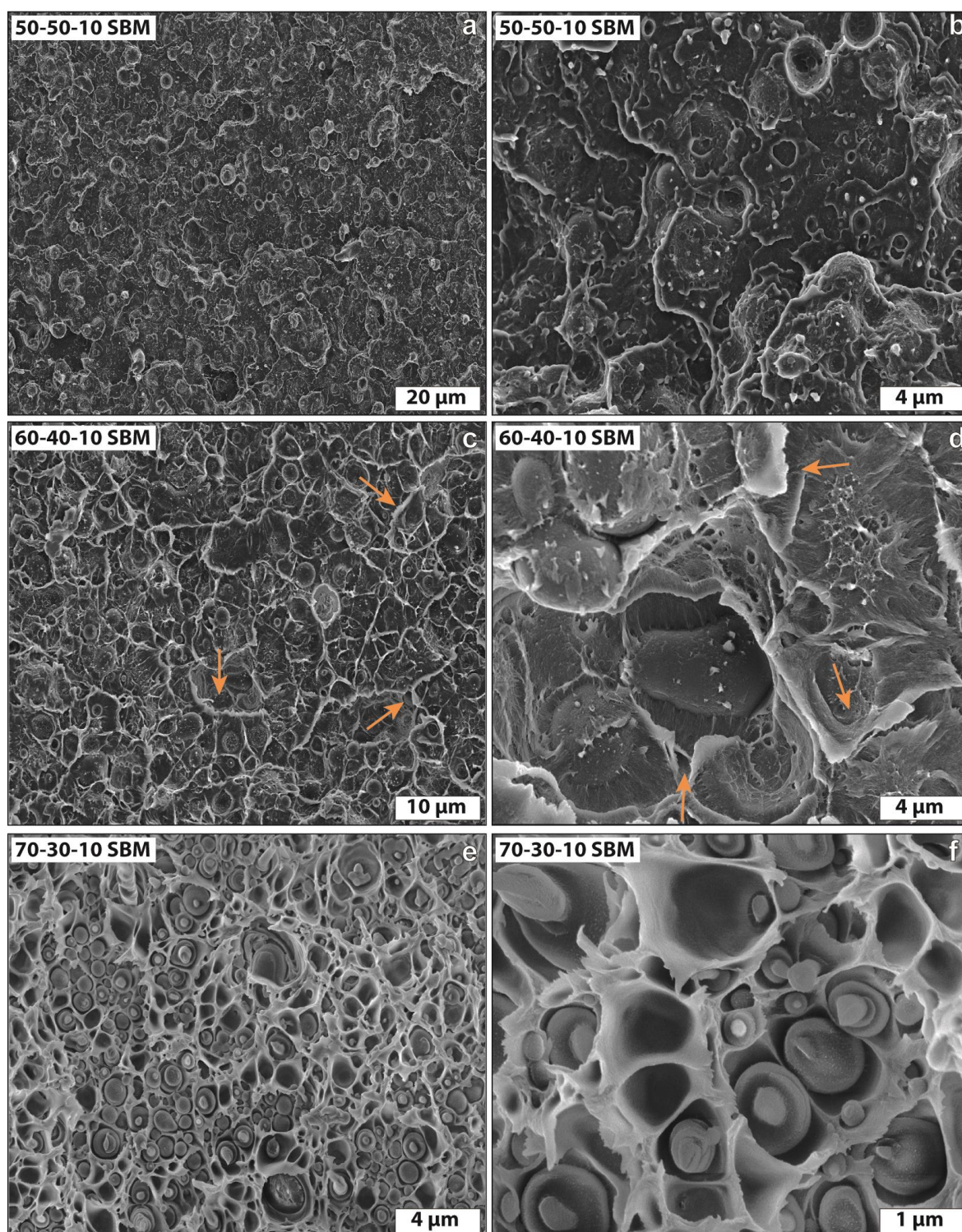


**Figure 37** SEM images of SBM compatibilized PPE/SAN blends with different blend ratios and magnifications after fracture toughness measurement: a, b) 50/50, c, d) 60/40, e, f) 70/30. The images are from the area right after the crack initiation point

The 60/40 blend shows an increase in the  $K_{Ic}$  value after compatibilization. According to **Figure 37c, d**, the stress is transferred from the SAN phase to the PPE phase more effectively compared to the 50/50 blend. Some shear bands are visible in the SAN matrix (white branched strips in the SEM images marked with arrows). Due to the location of SBM triblock terpolymer chains at the interface, the stress can be easily transferred from one phase to the other leading to more shear bands in the SAN matrix. In addition, the smaller sizes of the PPE domains after compatibilization play an important role during plastification, as the size of the dispersed phase determines the main deformation mechanism in the material. Due to the higher weight fraction and the smaller PPE droplet size, the overall interfacial area between PPE and SAN is significantly larger as compared to the 50/50 blend. Soft PPE domains promote crazing in the less ductile SAN matrix and craze formation happens at the early stage of deformation. At higher magnification, the PPE domains with SBM (white patches) and SBM fibrils that attach the phases to each other are visible. However, the increase of toughness after compatibilization in the 60/40 blend is not so profound. This again may be explained by the change in the geometries of PPE domains in the compatibilized blend (spherical) compared to the neat blend (anisotropic elongated structure), which affects the plastic deformation mechanisms of the PPE particles.

In case of the 70/30 blend, the increase in toughness (compared to the neat blend) after compatibilization is much more significant. This is expected since entire localization of the SBM chains at the interface causes a more effective stress transfer to the SAN matrix and the formation of small PPE droplets is observed. Shear yielding deformations are visible only in some regions of the SAN matrix (**Figure 37e, f**), probably due to the fact that small interparticle distances between PPE particles results in small SAN areas. This SAN layer between the PPE domains has a high potential to deform due to its small thickness and plain stress conditions. These shear bands can form a shear yielding network all over the sample, which can result in PPE droplets detaching from the SAN matrix and contribute to the toughening of the polymers *via* debonding mechanisms. Additionally, the necking phenomena of the PPE phase, which consumes a lot of energy and increase the toughness is here visible. Hence, the increase in toughness of the 70/30 blend is much larger compared to the other blends, due to multiple toughening mechanisms.

It has to be mentioned that conclusions on the effect of domain size after compatibilization on the toughness of the polymer blends can only be drawn if the fractured surfaces show similar toughening mechanisms. In other cases, fractured surfaces need to be carefully investigated as each material can act differently. Here, the 60/40 blends show the most number of deformation

mechanisms (also different types of mechanisms) and hence, are chosen for further investigations with Janus particles in the next sections.

#### 5.2.4 Conclusion

Immiscible PPE/SAN blends at blend ratios close to the phase inversion region were successfully compatibilized with a SBM triblock terpolymers. The morphologies of the blends, before and after compatibilization, with a special focus on the droplet size, were studied in detail. Micelle formation is observed in the blend systems with lower viscosities, whereas higher viscous blends show smaller PPE droplets in the blend morphologies with SBM triblock terpolymers exclusively located at the interface. DMA analysis revealed that the complex moduli of the blend systems show a plateau even above the  $T_g$  of SAN. This is explained by the strong difference between the  $T_g$  values of the components. The high viscosity mismatch of the system, and the linkage between the SAN and PPE phases at the interface mediated by the SBM triblock terpolymer further contribute to this matter. The dispersed PPE particles still in their glassy state build a network structure that hold the softened SAN matrix together and can be analogically compared to a highly filled composite system. The pseudo co-continuous structure of the neat blends compared to the fully droplets in SBM compatibilized blends was confirmed using a Payne test. A theory is proposed that explains the reason behind the constant tensile modulus of the blends with raspberry morphology after compatibilization. After fracture toughness measurements, characterization of the fractured surfaces showed complex and multiple deformation mechanisms strongly depending on the size of the dispersed PPE droplets. It could be concluded that smaller PPE domain sizes after compatibilization only can contribute to the toughness improvement of the material when the main deformation mechanisms stay constant before and after compatibilization.

Among the studied blend compositions, the 60/40 blend composition combines excellent toughness with good processability (low viscosity) and, thus, may be suited with regard to possible industrial applications. Hence, based on the results of this chapter, this blend composition is chosen for further studies and comparison of the efficiency of Janus particles with and state of the art SBM triblock terpolymers. The size of the PPE droplets in the 60/40 blend is small enough to form a network in the melt state and allow DMA measurements at temperatures above the  $T_g$  of the SAN. However, they are large enough to promote several deformation mechanisms during the fracture mechanic studies of the blends.

### 5.3 Blends compatibilized with Janus Particles

A solution-based synthesis of nano-sized Janus Particles (JPs) has been recently reported, which opens the way to significantly larger quantities of JPs [161]. The JPs have shown to have higher surface activities than the SBM triblock terpolymers [145] and therefore it is important to investigate their behaviour not only in solutions, but also during melt blending. The PPE/SAN blends with blend ratio of 60/40 are chosen for compatibilization. This particular blend ratio has not only well-processable medium viscosity and demonstrated convincing blend performance in earlier studies as well as the results discussed in the previous chapter [31,77,119,222]. The 60/40 blends were compatibilized with 1, 2, 5, and 10 wt.% of the JPs with industrial scale twin screw extruder with the parameters explained previously. **Figure 38** shows the schematic overview of the procedure to produce the blends.

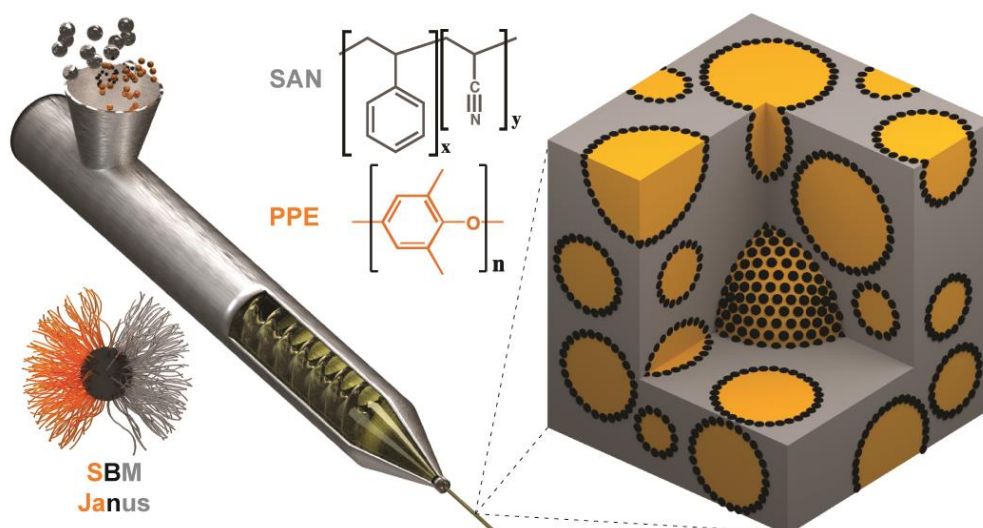


**Figure 38** Schematic procedure of producing JP compatibilized PPE/SAN blends on a large scale twin-screw extruder

#### 5.3.1 Morphological characterization of JP compatibilized blends

In the first step, the blend compatibilized with maximum amount of JPs is compared to the neat blend. Using 10 wt.% of compatibilizers has previously shown to be effective for SBM triblock terpolymers [228]. In order to analyse the blend morphology, TEM images of the JP compatibilized (10 wt.%) blend compared to the neat blend are shown in **Figure 39**. Since the

TEM images are performed on the extruded granulates, inhomogeneities in the neat blends are expected, depending on the cut direction during sample preparation. We find a substantial improvement of the blend homogeneity after addition of 10 wt.% JPs (**Figure 39b**) compared to the neat blend system (**Figure 39a**), when samples are cut parallel to the extrusion direction. The neat blend shows elongated, non-regular shaped droplets that frequently coagulate and resemble a co-continuous phase (parallel to extrusion direction), whereas the JP blend shows an entirely different small drop morphology. The morphology in **Figure 39b** shows small PPE droplets (dark) embedded in a continuous SAN matrix (bright). **Figure 39c, d**, show the TEM images of the blends that are cut perpendicular to the extrusion direction. Here also, the PPE droplets in case of neat blend are larger and have irregular shapes compared to the JP compatibilized blend. Strikingly after compatibilization, the droplets are able to pack densely without coagulation despite the harsh processing conditions (temperature, pressure, high viscosity) and the strong arising shear forces. Although the PPE droplets collide and deform as evident from their not fully spherical shape, the JPs at the interface provide efficient stabilization and repulsion for the droplets. The size of most droplets is well below 1  $\mu\text{m}$  as a direct result of efficient reduction of interfacial energy. Despite the excess of PPE in the feed (compared to SAN), we still find PPE droplets in a SAN matrix, because the high viscosity ratio,  $\eta_{\text{PPE}}/\eta_{\text{SAN}} > 10$ , shifts phase inversion far from a feed ratio of 50/50 as discussed in 5.2.1. This peculiarity is well known for PPE/SAN, where the less viscous SAN always forms the matrix [31,222].

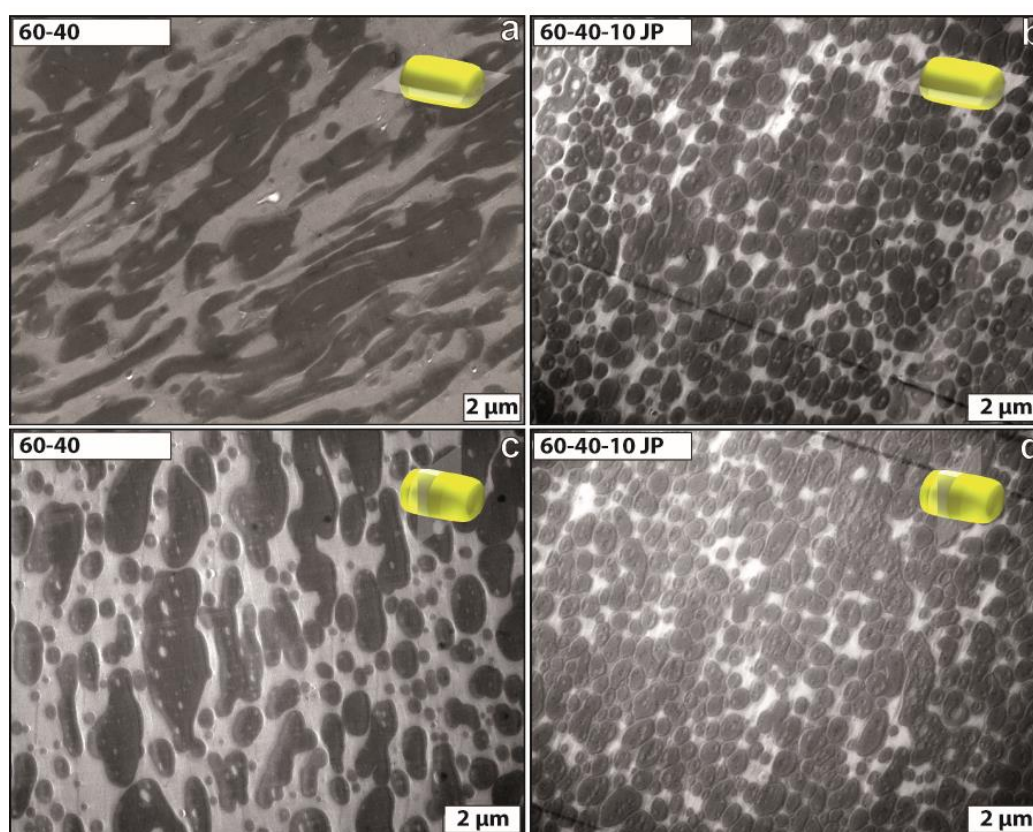


**Figure 39** TEM images of neat and JP compatibilized PPE/SAN (60/40) blends a, b) parallel and c, d) perpendicular to the extrusion direction

In order to get a better overview of the blend structures, SEM images (surface of fractured granulates) of the neat and JP compatibilized blends are compared in **Figure 40**. Here again the difference in blend structures shows a clear transition from a random co-continuous structure to a homogenous droplet structure. The morphological difference is also clearly demonstrated when comparing horizontal (parallel to extrusion direction) fractures for neat (**Figure 40a**) and JP compatibilized (**Figure 40b**) blends. Similarly, vertical (perpendicular to extrusion direction) fractures of the neat blends (**Figure 40c**) compared to the JP compatibilized blends (**Figure 40d**) would help to evaluate the homogeneity throughout the samples. The JP blend displays sub-micron features in both directions proving isotropic distribution of the blend components. Compared to that, the neat blend contains micron-sized elliptical domains in the horizontal, but distinctly different elongated cylindrical domains in the vertical cross-section attributed to anisotropic shearing of the PPE phase. This difference in morphological homogeneity should have profound effects on the stability of the blend when subjected to stress and macro mechanical properties.

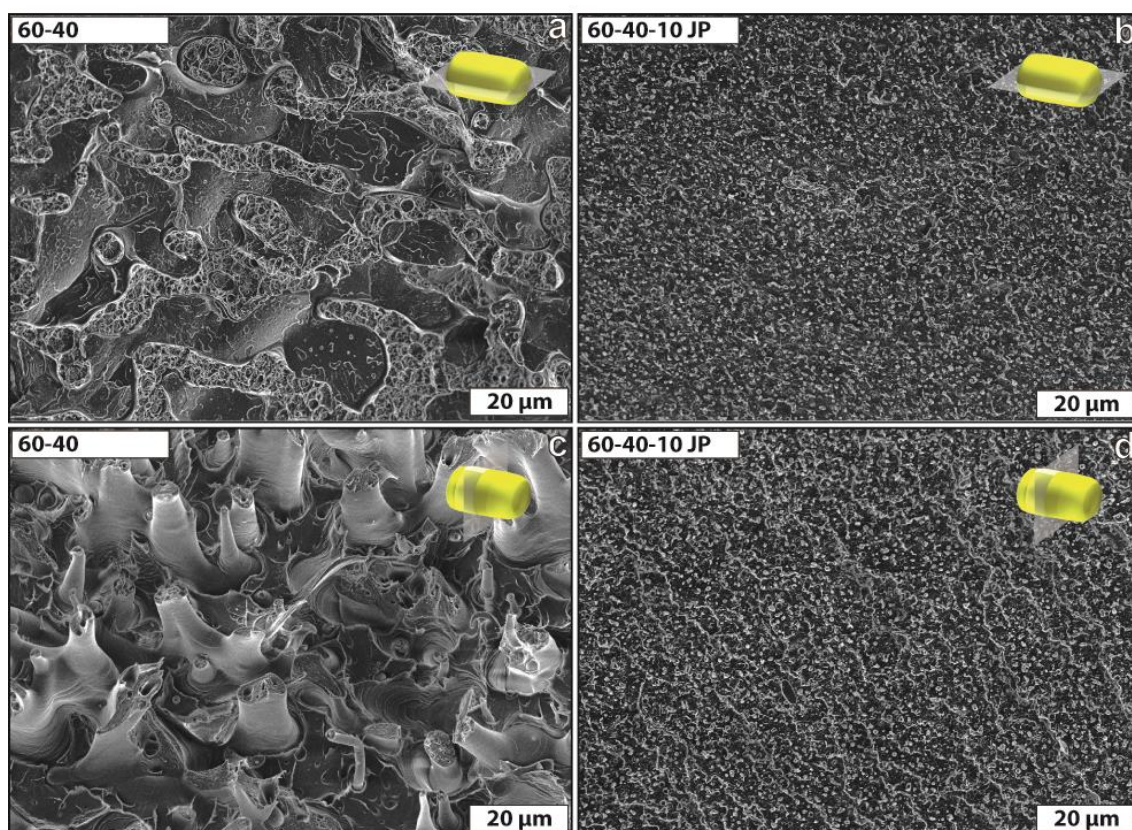


**Figure 40** SEM images of neat and JP compatibilized PPE/SAN (60/40) blends a, b) parallel and c, d) perpendicular to the extrusion direction

On closer inspection of the droplet morphology in **Figure 41a**, one observes brighter SAN droplets inside the darker PPE droplets, suggesting a double emulsion morphology, usually found close to phase inversion [38], *i.e.*, SAN droplets in PPE matrix. The TEM close-up in **Figure 41b** corroborates the double emulsion morphology. Here, the larger PPE droplet engulfs smaller SAN droplets, while all interfaces are densely covered with JPs visible as black dots (OsO<sub>4</sub> staining of remaining PB double bonds). The origin of this morphology and the narrow droplet size distribution will be discussed in more detail later in this chapter.

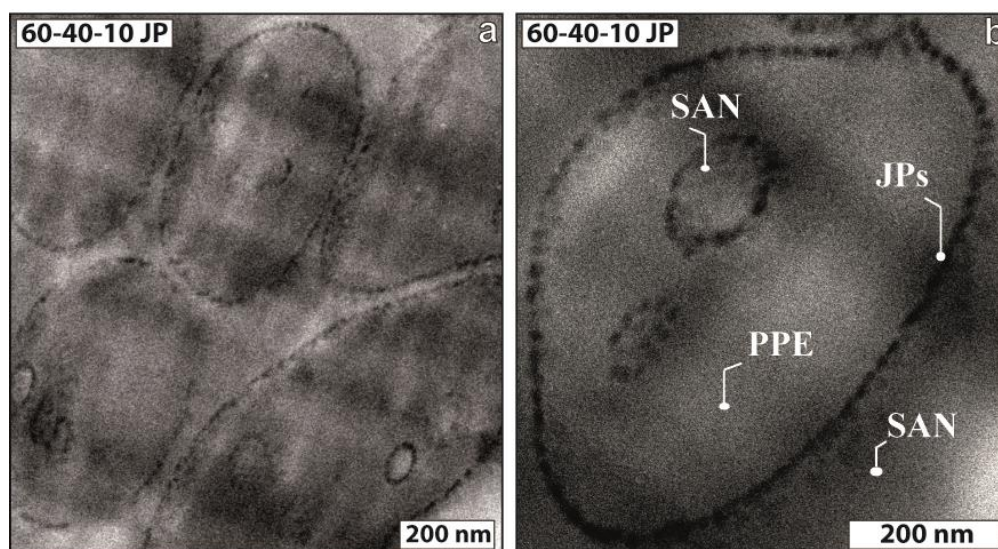


**Figure 41** TEM images of a) SAN droplets engulfed inside the darker PPE droplets in JP compatibilized (10 wt.%) PPE/SAN blend (60/40), b) Double emulsion morphology of the blend

The droplet morphology of the JP compatibilized blend in SEM shows up as a random distribution of dents and bumps corresponding to droplets and holes left behind by detached PPE droplets (**Figure 42a**) marked by light and dark orange arrows. The droplets show a multiscale structure as they are fully covered with JPs, forming raspberry-like structures in a SAN matrix. We clearly identify the JPs at the blend interface in SEM (**Figure 42b**). After cryo-fracturing of the blend, the droplet surface is fully decorated with small spherical particles corresponding to the JPs. The inset in **Figure 42b** shows a tendency for hexagonal close packing with inter-particle distances of 30 nm attributed to the JP size in the collapsed state [161].

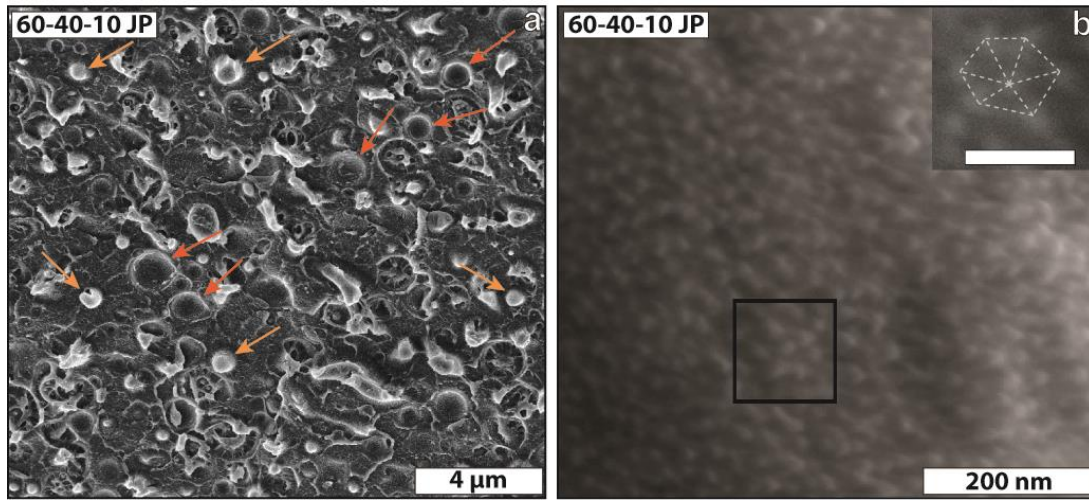


**Figure 42** a) Fully JP covered PPE droplets in SAN matrix (light orange arrows) and the dents left behind by them (dark orange arrows), b) Surface of a PPE droplet covered in JPs showing the raspberry morphology. The inset is a further magnification of the region marked by the black square and shows the hexagonal packing tendency of the JPs at the interface (scale bar is 100 nm)

Although very similar packing has been observed in the PS/PMMA blend [14], the PPE/SAN blend inherits a set of entirely different physical properties. The fact that JPs still selectively locate at the interface is remarkable and explained by the energy,  $\Delta E_{desorb}$ , required to desorb the JPs from the blend interface in the following equation 21 (the calculations leading to deriving the equation is already published in [155]).

$$\Delta E_{desorb} = 3\pi R_{JP}^2 \gamma_{PPE/SAN} \quad (21)$$

$\Delta E_{desorb}$  increases with the square of the particle radius,  $R_{JP}$ , and the interfacial tension between the blend components,  $\gamma_{PPE/SAN}$  [14,138]. The interfacial tension between two polymers can be estimated from the Flory-Huggins polymer-polymer interaction parameter,  $\chi$ , applying the relation  $\gamma \propto \chi^{1/2}$  (for  $\chi > 0$ ). In the studied system all parameters favour JP location at the interface [119], *i.e.*, high incompatibility of the blend components,  $\chi_{PPE/SAN} > 0.5$ , and good compatibility between blend components and the respective JP corona blocks,  $\chi_{PPE/PS} = -0.044$  and  $\chi_{SAN/PMMA} = -0.008$  [11] (for 19 wt.% AN in SAN). To further increase  $\Delta E_{desorb}$ , we chose JPs to be considerably larger than the radius of gyration of the blended polymers ( $R_{g,polymer} < 10$  nm vs.  $R_{JP,TEM} = 19$  nm;  $V_{JP}/V_{polymer} \geq 7$ ). Although an exact calculation of  $\Delta E_{desorb}$  is elusive, the quantitative adsorption of JP to the blend interface suggests that  $\Delta E_{desorb}$  must be sufficiently

high to overcome the thermal energy impacting the particles at 260°C during extrusion. The droplets locate themselves in the interface right after the blend components are melted in the extruder. Yet, as the materials move along towards the die, applying high shear will continuously decrease the droplet size and JPs are able to stabilize this small PPE particle sizes.

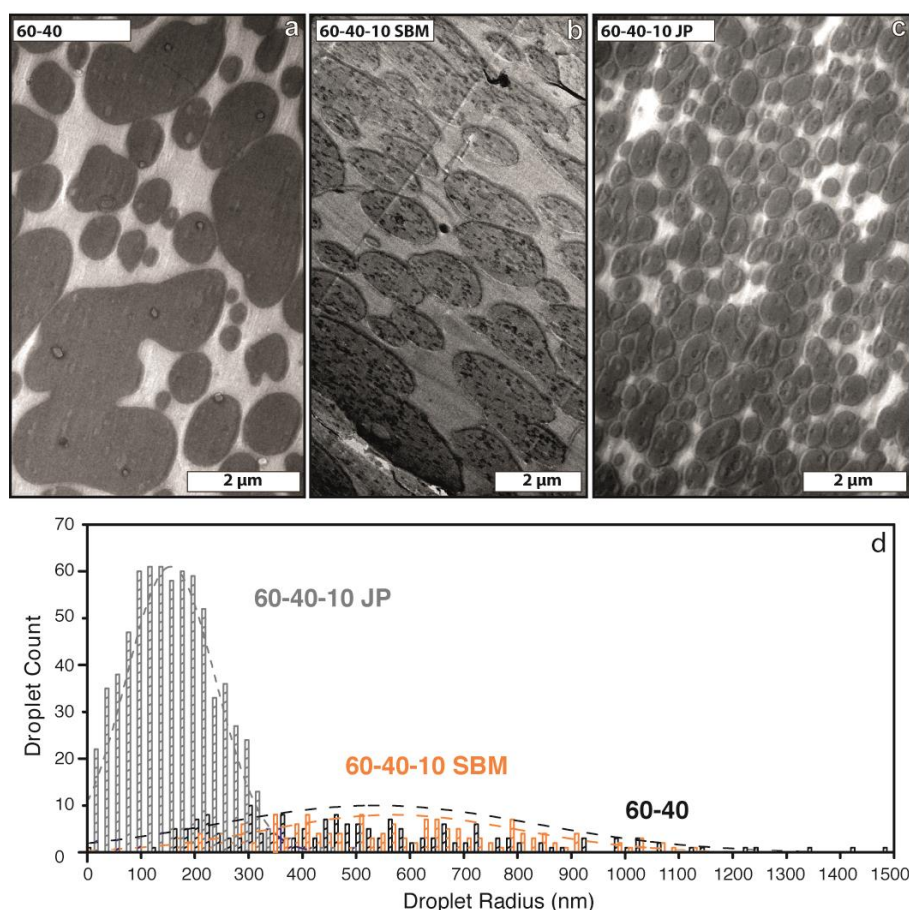


**Figure 43** Comparison of the a) neat blend morphology with b) SBM compatibilized (10 wt.%), and c) JP compatibilized (10 wt.%) PPE/SAN blends (60/40) in respect to the compatibilization efficiency, d) PPE droplet size distribution in the blends (at least 500 droplets are counted for each blend)

**Figure 43** summarizes the efficiency with which the JPs compatibilize this blend system compared to the state of the art SBM triblock copolymers. Here, the morphology of the neat blend without additive, compatibilized with 10 wt.% SBM triblock terpolymer and with 10 wt.% JPs are compared together. Slight contrast differences originate from varying film thicknesses,

and all other processing parameters were kept constant to allow reliable comparison. The JPs considerably reduce the droplet size as compared to the neat blend and also significantly outperform the SBM triblock terpolymers (**Figure 43a-c**).

For each system the radii of 500 PPE droplets in TEM micrographs of ultrathin cuts are analysed. The radius of each droplet is calculated from the cross-sectional area (determined using ImageJ software), assuming spherical shape. The average droplet radius,  $R_{PPE}$ , and standard deviation strongly decrease from  $R_{PPE;SBM} = 670 \pm 230$  nm to  $R_{PPE;JP} = 155 \pm 85$  nm underlining the superior stabilization capabilities of JPs as compared to the SBM terpolymer (**Figure 43d**). Both compatibilizers are amphiphilic in nature and exhibit the same interactions with the blend polymers, which is why we consider the Pickering effect and the accompanying high interfacial activity of the JPs mostly responsible for the significant improvement. The droplet radius for the neat blend,  $R_{PPE-neat} = 540 \pm 300$  nm, was determined for the sake of completeness, but does not adequately reflect the occasional large multi micron-sized droplets. Without any additive, the neat blend yields entirely unpredictable and irreproducible morphologies that may change at any given point even within the same extrusion experiment. In addition, reasonable droplet evaluation was complicated by excessive droplet coagulation, commonly observed for insufficient or missing surface stabilization. The difference between the SBM terpolymer and the neat blend is surprisingly small: both show broad distributions without significant shift of the average radius. It is known that a considerable fraction of the SBM terpolymer is actually present as micelles or micelle clusters that manifest as black spots inside PPE droplets in **Figure 43b** as discussed in previous sections. With SBM there is a high probability that the triblock gets destroyed and PS-PB diblocks turn into micelles. This of course highly depend on the processing conditions. These micelles in the SBM compatibilized blends are a reason for reduced efficiency of SBM during compatibilization (probably due to lower activity compared to JPs). These trapped SBM polymer chains in PPE, do not contribute to the stabilization of interfaces. Therefore, the difference between neat and SBM blends is only a more homogeneous morphology without smaller droplet sizes. JPs are probably less prone to get destroyed during processing as they have a 3D structure with semi crosslinked core.

**Figure 44** illustrate the morphological evolution of the blend as a function of the Janus particle content, *i.e.* at different JP weight fractions of 1, 2, and 5 wt.%. After compatibilization with only 1 wt.% JPs, the size of the PPE droplets does not vary much, even though the JPs (black dots) locate themselves at the blend interface (**Figure 44a, b**). By increasing the compatibilizer amount to 2 wt.%, already a reduction in the PPE droplet size is visible (**Figure 44c**), however a

closer look reveals that the number of JPs is not enough to fully cover the blend interface (**Figure 44d**). At 5 wt.% of JPs, the PPE droplet sizes reduces homogenously and partially double emulsion morphologies show up. This is probably due to the high number of JPs that are fully covering the blend interface (**Figure 44e, f**).

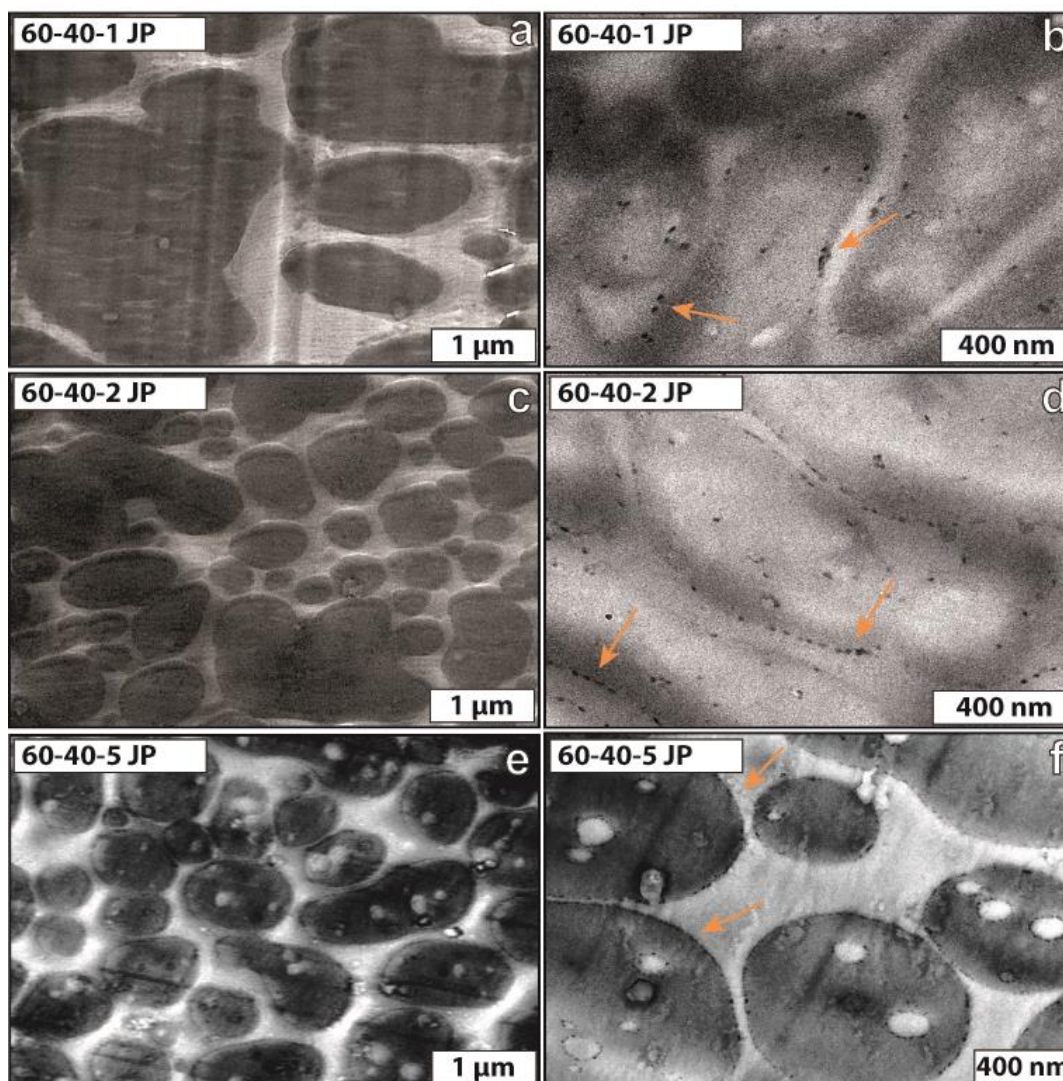


**Figure 44** TEM images of the PPE/SAN (60/40) blends compatibilized with JPs showing the evolution of the PPE droplet size reduction by increasing the compatibilizer amount from a, b) 1 to c, d) 2, and e, f) 5 wt.%

The occasional too large or too small particles visible in the blends with 1 and 2 wt.% JPs are not visible in blends with 5 (and 10 wt.%) JPs. The homogeneity of the blend morphologies would

result in homogenous macro mechanical properties and is of great industrial interest. As already discussed, at blends with 10 wt.% JPs (and at a lower extent in the blend with 5 wt.% JP) the morphology is reminiscent of a double emulsion with SAN inclusions inside PPE droplets (containing either PMMA, which in case of JPs can happen rarely) or a blend of of PMMA/SAN). We hypothesize that the system creates additional interface due to excess stabilization capability of the large amount of JP added. The second interface in the core of the droplet also suggests that the droplet already reached its optimum curvature and the involved interfacial energies. Assuming a dense packing of the JPs on the droplet interface area,  $A_{PPE}$ , simple geometric relations show that the radius of the PPE droplets should scale with the inverse square root of the JP content,  $f_{JP}$ , as shown in equation 22:

$$A_{PPE} = 4\pi R_{PPE}^2 \propto f_{JP}^{-1}$$

$$\therefore R_{PPE} \propto f_{JP}^{-\frac{1}{2}} \text{ or } R_{PPE} \propto f_{JP}^{\frac{1}{2}} = \text{Const.} \quad (22)$$

**Table 6** shows that (with the exception of  $f_{JP} = 5$  wt.%) the product  $R_{PPE}\sqrt{f_{JP}}$  is indeed constant, confirming our assumption that the JPs densely pack at the interface, irrespective of the JP content.

**Table 6** Dependence of average droplet size and stabilization efficiency on the JP content

$f_P$ (wt.%)	$R_{PPE}$ (nm) <sup>a</sup>	$R_{PPE}\sqrt{f_{JP}}$ (nm)
0	540 ± 300	-
1	440 ± 350	440
2	340 ± 190	480
5	270 ± 100	600
10	150 ± 80	474

The histograms in **Figure 45** show a distinct trend for the evolution of droplet radius in dependence of JP content. We found out that the addition of only 0.5 (not shown) and 1 wt.% JPs is not able to provide the necessary coverage to stabilize the interface and besides irregular droplet shape and large average droplet radii droplets still partly coagulate into the co-

continuous PPE/SAN morphology (**Figure 45a**). It is visible that by increasing the JP content from 2 to 5, and 10 wt.% (**Figure 45b, c, and d**), not only the PPE domain size gets smaller, but also the homogeneity of the blend morphologies improves and the droplet size distribution histogram gets narrower.

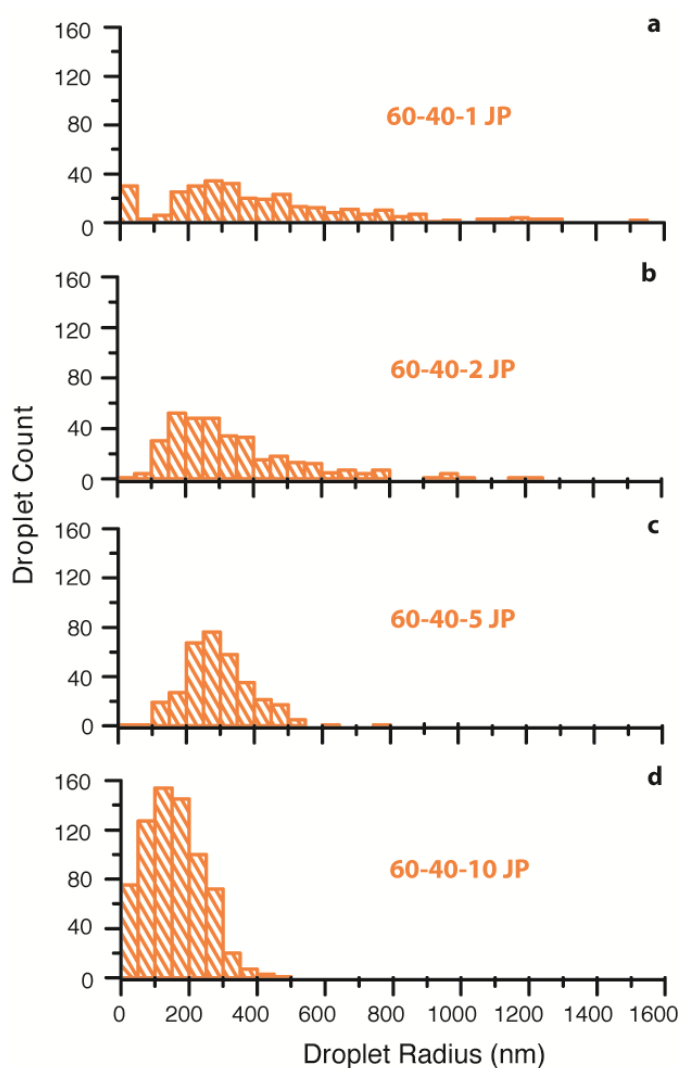


**Figure 45** The histogram of the PPE droplet size in PPE/SAN (60/40) blends compatibilized with a) 1, b) 2, c) 5, and d) 10 wt.% of JPs

**Figure 46** compares the evolution of average PPE droplet size by addition of JPs with neat blend. The inhomogeneities in the neat, and blends with lower amounts of JPs, result in large

standard deviations. However, the trend shows a clear decrease in the droplet size, by increasing the JP amount.

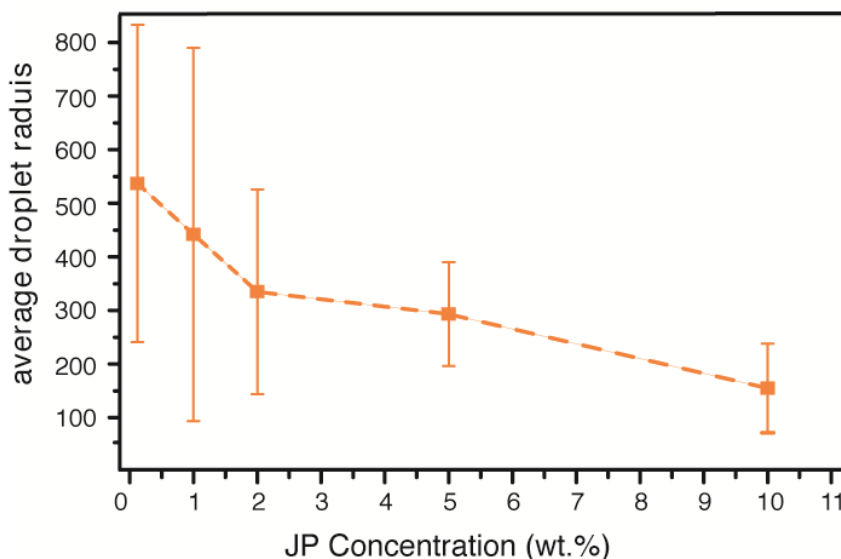


**Figure 46** Average PPE droplet radius of neat and JP compatibilized blends

The SAN inclusions are only visible in the blends with 5 wt.% JPs or more and are less in number compared to the significant micelle and micellar cluster formation observed in the SBM compatibilized blend previously. In order to understand the reason behind the formation of the SAN inclusions in the 5 and 10 wt.% blends, shear rheology measurements of neat and the JP compatibilized blends were performed and discussed in the next section.

### 5.3.2 Rheological characterization of JP compatibilized blends

The shear viscosity of the JP compatibilized blends compared to the neat blend is shown in **Figure 47**. The increase in viscosity after the addition of JPs indicates effective compatibilization as a result of better stress transfer between the phases in the blends with 1, 2, and 5 wt.% JPs. In case of the blend with 10 wt.% JPs, the viscosity does not change significantly in the high frequency range as compared to the neat blend. However, at lower frequencies, an increase in the viscosity is visible, indicating some network-like structure formations. The 3D network forms through structure build-up of the PPE droplets in the matrix once their sizes drop below a

critical value [254]. We assume that at high JP concentration during extrusion, at first the particles cover all PPE droplet interface and minimize droplet size, while excess JPs are still present as clusters in one of the phases (for equal hemispheres cluster formation is equally probable in both phases). These excess JPs which form clusters (super-micelles) are freely dispersed in the blend, and since they are small spherical particles, they can facilitate low friction sliding between the PPE droplets and the overall viscosity of the blend is reduced to that of the neat blend. In case of the blend with 5 wt.% JPs, we observe a similar phenomenon at smaller scale, also corroborating that the most economic amount of Janus particles to realize full compatibilization of the blend is indeed  $f_{JP} = 2-5$  wt.%. Another consequence of the excess amounts of JPs in the 5 and 10 wt.% blend is that the system tries to build up extra surface to accommodate excess JPs and hence, SAN inclusions form within the PPE droplets. In addition, lower viscosity of the blend at higher shear rates further facilitates the formation of such SAN inclusions during coalescence mechanisms.

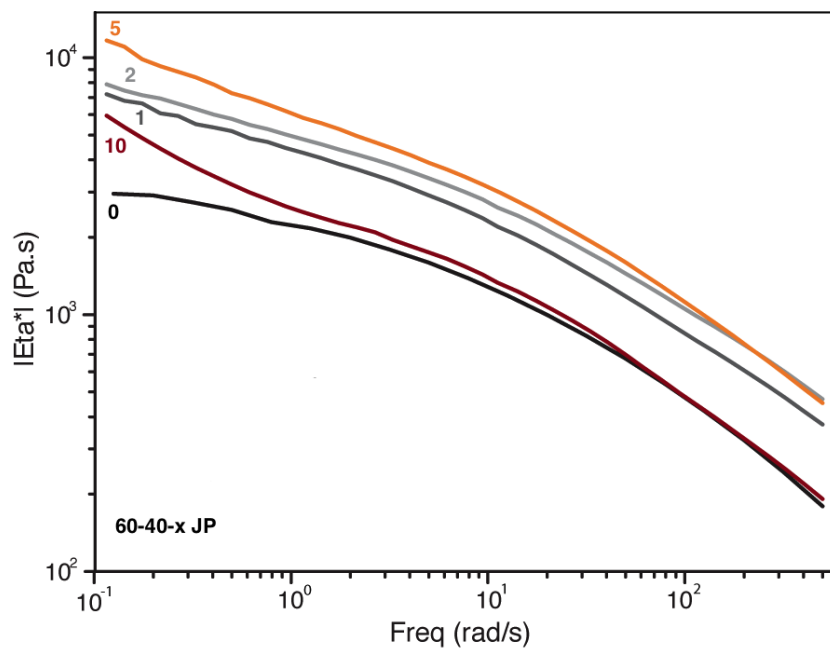


**Figure 47** Absolute shear viscosity of JP compatibilized PPE/SAN (60/40) blends

### 5.3.3 Mechanical characterization of JP compatibilized blends

#### DMA analysis of JP blends

Similar to SBM compatibilized blends, the complex modulus of the JP compatibilized blends after DMA measurements are discussed and compared. **Figure 48** shows that addition of 1 or 2 wt.% JPs almost do not significantly influence the modulus under a wide temperature range. Similar to the neat blend, a plateau is visible in temperatures above the first  $T_g$  (SAN) and no further drop in the modulus is visible until the  $T_g$  of PPE due to the pseudo-continuous structure of PPE phase that holds the SAN matrix together (as discussed in the previous chapter). In case of addition of 5 wt.% JPs, the modulus increases slightly at temperatures below the  $T_g$  of SAN due to the higher stiffness of JPs. Above the first  $T_g$  of the blend, slight drop in the modulus happens and the plateau “softens” a little bit. This happens due to the lack of intercontinuity in the PPE phase as a result of effective compatibilization, which solely produces PPE droplets in the form of single raspberry structures. By increasing the JP amount to 10 wt.%, the increase in the modulus at temperatures below the  $T_g$  of SAN is bigger, and even around 0 °C, a small step (representing the  $T_g$  of the PB middle block) shows up. Accordingly, above the  $T_g$  of SAN, a more significant drop in the modulus is observed, indicating fully droplet-domain morphology of the blend.

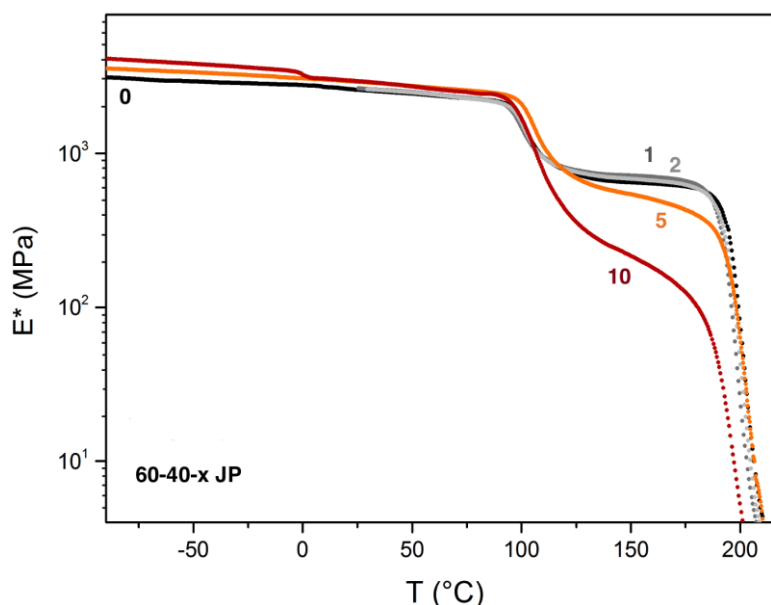


**Figure 48** Complex modulus of JP compatibilized blends at different JP contents. By increasing the JP amount, the co-continuity of the system decreases and the second drop in the modulus ( $T_g$  of the PPE) is shifted to lower temperatures

In order to prove the difference between pseudo co-continuous morphology and the physical network of the densely packed PPE particles, further DMA analysis on one blend composition (as a representative) have been performed. If the plateau after the  $T_g$  of SAN is only due to similar effects in highly filled thermoplastics, then one should be able to disrupt the network at higher strains. The focus is to confirm the lack of co-continuity in the JP blends compared to the SBM compatibilized blends. **Figure 49** compares the complex modulus of the 60/40 blends compatibilized with 10 wt.% SBM (**Figure 49a**) and 10 wt.% JPs (**Figure 49b**) under different strains. We have discussed that due to the co-continuity of the 60/40 blend compatibilized with SBM, a plateau after the  $T_g$  of SAN (matrix) appears. This is valid for the measurements at all strains and the sample and its structure wouldn't be deformed even at higher strains (deformations). Here, by increasing the strain during measurements, the pseudo co-continuity of the PPE phase will be intact and a second plateau is always visible for the blend (**Figure 49a**). In case of JP compatibilized blends, the formation of plateau can be disturbed at higher strains, indicating complete 3D droplet domain morphology of the system. By increasing the strain, since PPE droplets can freely move in the SAN matrix, a sliding effect is observed and the drop in the complex modulus is shifted to lower temperatures (the length of the plateau shortens until it eventually disappears). This proves that densely packed PPE particles only form a structural network. It is also worth to mention that measurements at higher strains were not possible due to mechanical limitations of the measurement device.

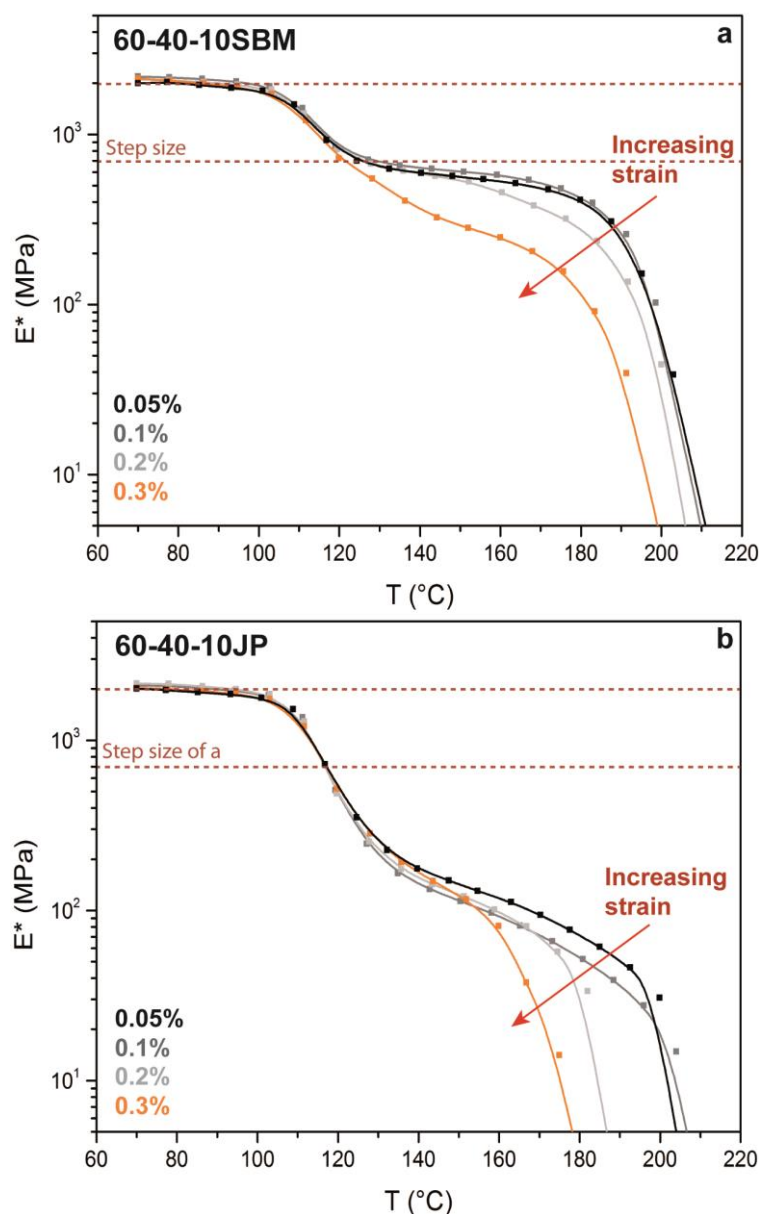


**Figure 49** Complex modulus of PPE/SAN (60/40) blends compatibilized with 10 wt.% a) SBM triblock terpolymers, and b) JPs under different strains

### Low strain (tensile) properties of JP blends

The tensile moduli of the JP compatibilized blends are compared to the neat 60/40 blend in **Figure 50**. As expected, the distribution of the discontinuous elastomeric phase at the interface due to the formation of the raspberry morphology prevents any decrease in the modulus after compatibilization. The slight increase with increasing the JP content is attributed to the higher

modulus of the JPs due to their partially crosslinked PB middle block as discussed in section 5.1.2.

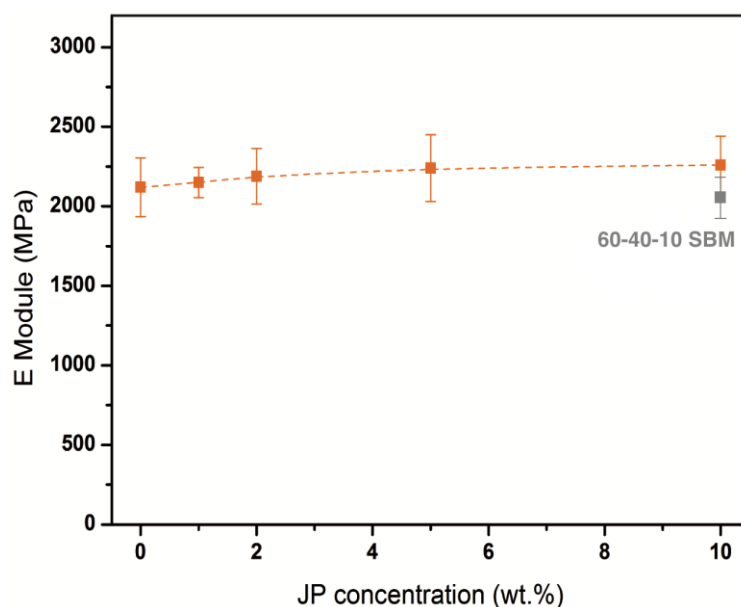


**Figure 50** Tensile modulus of neat and JP compatibilized PPE/SAN (60/40) Blends

### Fracture toughness of JP blends

The  $K_{Ic}$  values of the JP compatibilized blends as a function of the JP content are shown in **Figure 51**. Surprisingly, unlike SBM triblock terpolymers, by increasing the compatibilizer content after compatibilization, the  $K_{Ic}$  of the blends decreases. This is in contrast to the expectation of improvement in the toughness after compatibilization. We have also observed in the previous chapter that SBM compatibilized blends have shown an improvement in the materials toughness, depending on the blend ratio. In order to be able to understand this result, the fractured surface of the specimens after test were observed under the microscope.

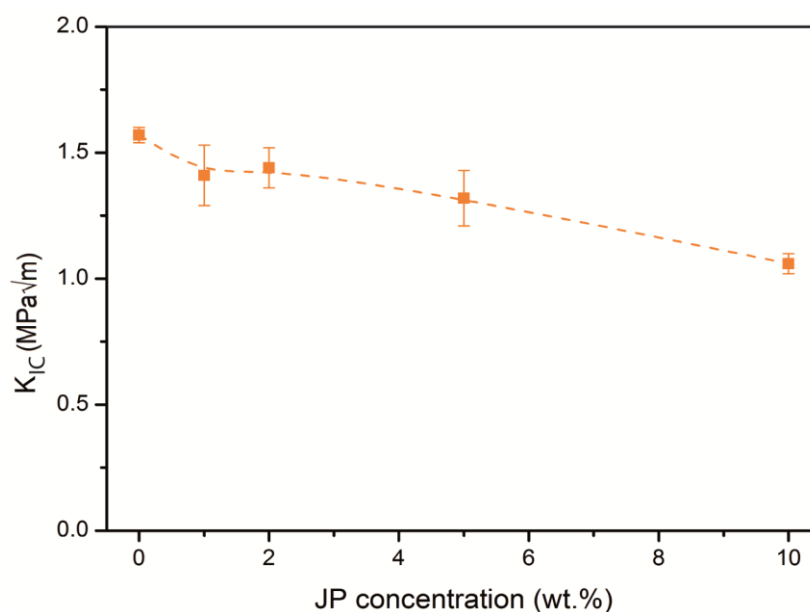


**Figure 51** Critical stress intensity factor of neat and JP compatibilized PPE/SAN (60/40) blends

The fractured surface of the blend compatibilized with 10 wt.% of JPs after  $K_{IC}$  test is representatively shown in **Figure 52**. In the first view, the small PPE droplets dispersed in the SAN matrix resemble the 70/30 blend discussed in the previous chapter (**Figure 37e**). There are high contrast white areas visible representing the shear yielding of the SAN matrix (**Figure 52a**). At higher magnification it is shown that these areas (marked by orange arrows) are formed where PPE droplets are fully debonded and has retained a dent (hole) behind (**Figure 52b**). The small interparticle distance between the PPE droplets push the SAN matrix between them outwards and produces shear yielding in these areas. However, the number of debonded particles are quite few compared to the whole volume of the specimen as the JPs provide a very strong bond between the PPE and SAN. Hence, even though shear yielding is induced as the dominant deformation mechanism, it is not enough to use up as much energies as the deformation mechanisms in the neat 60/40 blend (discussed previously). The strong linkage between the phases by JPs, which hinders the deformation is shown in **Figure 52c** (marked by orange arrows).

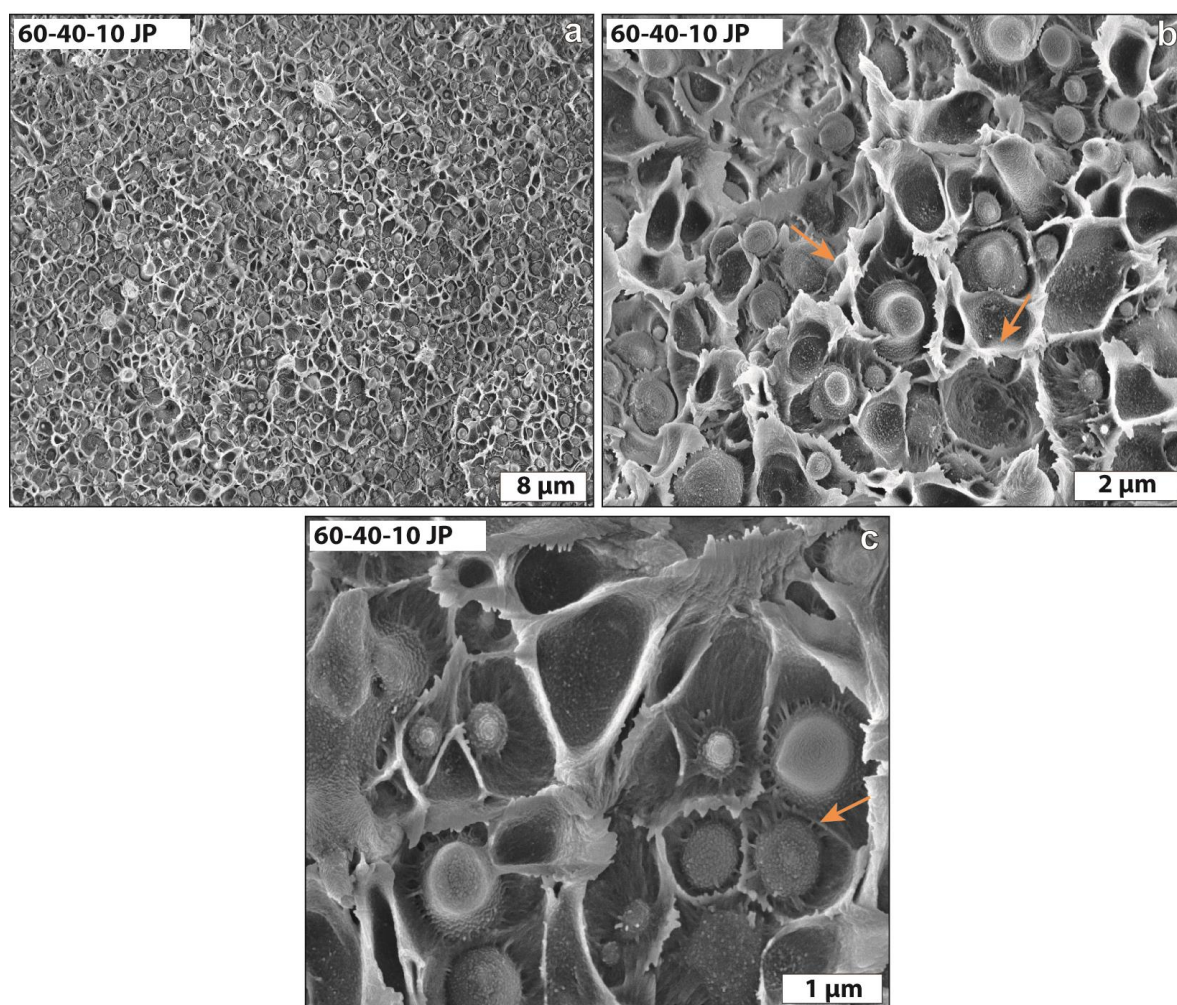


**Figure 52** SEM images of JP (10 wt.%) compatibilized PPE/SAN (60/40) after fracture toughness: a) shear yielding (white contrasted areas), b) dents left behind by detached raspberries, and c) Strong JP linkage at the interface preventing deformation. The images are from the area right after the crack initiation point

### Fatigue crack propagation (FCP) in JP compatibilized blends

Due to the complexity of structure, performing FCP measurements can allow us to obtain more information on the mechanical properties and deformation mechanisms at various crack propagation speeds. The fatigue crack growth behaviour of the JP compatibilized PPE/SAN blends in comparison to the neat blend is shown in **Figure 53**. Here, the fatigue crack growth rate,  $da/dN$ , is plotted in double logarithmic scale as a function of the stress intensity factor ratio,  $\Delta K$ , at the crack tip. In case of the JP compatibilized blends, the behaviour of the material upon compatibilization does not differ significantly from the neat blend in the first and second

region. In contrast, at higher crack propagation rates (region III), the neat blend performs better. The crack propagates faster in the JP compatibilized blends indicating deterioration of materials' behaviour (and its resistance against crack growth) after compatibilization. This means even though JPs have proven to be highly effective compatibilizers in nanostructuring the morphology during melt blending [14,155], they fail to improve the mechanical properties of the blends (specifically toughness) at fast crack propagation rates. This result is in agreement with the fracture toughness ( $K_{Ic}$ ) values discussed previously.

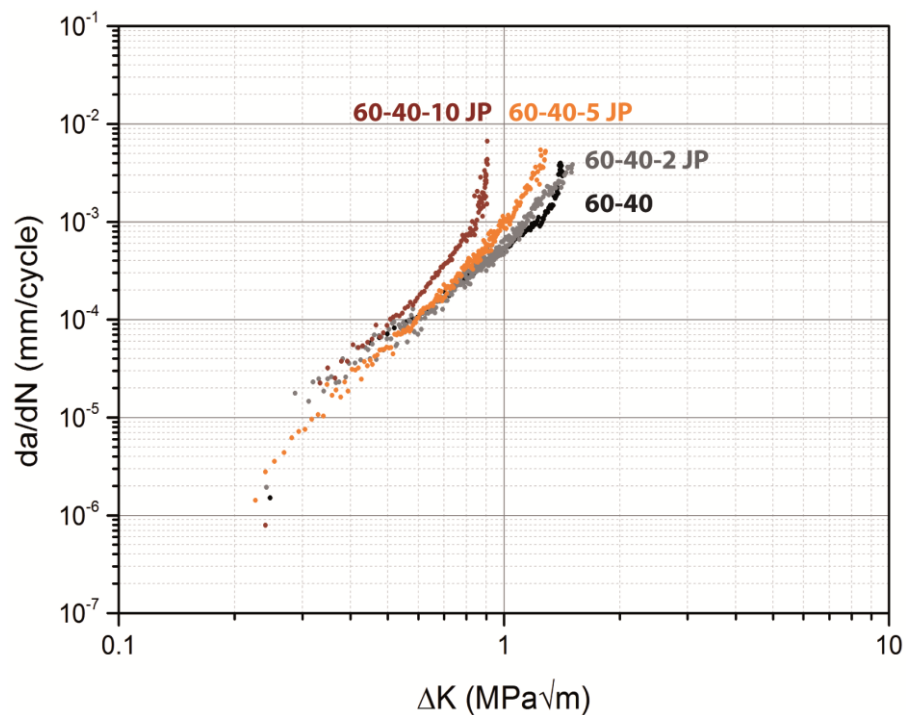


**Figure 53** FCP behaviour of neat and JP compatibilized PPE/SAN (60/40) blends

This phenomenon is better visible in **Figure 54**, where the stress intensity factors of the JP compatibilized blends are compared to the neat blends at in the threshold ( $\Delta K_{th}$ ) and critical fracture ( $\Delta K_{cf}$ ) regions. The  $\Delta K_{th}$  and  $\Delta K_{cf}$  values represent the first and last measured point of the curves, respectively. In the threshold region (region I, slow crack propagation speed),  $\Delta K_{th}$  is not influenced by addition of JPs and the value is not a function of the JP amounts. However, in the third region (high crack propagation speed) the  $\Delta K_{cf}$  values decrease by increasing the JP content, implying deterioration of the FCP behaviour.

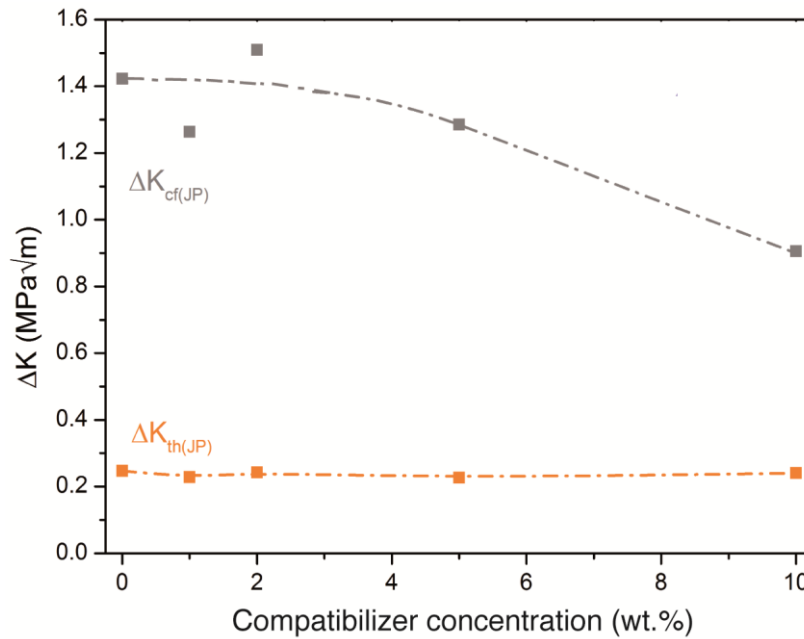


**Figure 54** The  $\Delta K_{th}$  and  $\Delta K_{cf}$  values of neat and JP compatibilized PPE/SAN (60/40) blends

In order to understand the reason for JP behaviours in region III, the fractured surface of the neat blend is compared to the blends compatibilized with 5, and 10 wt.% JPs in region III (**Figure 55**). In case of neat blend (**Figure 55a**), the large PPE regions are clearly visible in the SAN matrix. Their debonding all over the interface seems to be the main deformation mechanisms in this region. As discussed before for SBM compatibilized blends, this is an effective deformation mechanism which uses up a lot of energy. In case of the blend compatibilized with 5 wt.% JPs (**Figure 55b**), the PPE droplets are much smaller and are covered with JPs. This means that individual raspberries (marked by orange arrow) pin the SAN matrix at different points and prevent the formation of larger cracks (formation of new surface and massive energy usage). Hence, the areas undergoing deformation reduce and as a result the FCP behaviour is deteriorated compared to the neat blend. In case of the blend with 10 wt.% JPs (**Figure 55c**), the JP linkage between the phases is more dominant and instead of just pinning the matrix at various points, completely hinder the SAN deformation at a macro scale. The crazing and fibril formation at the small interface areas around the raspberries uses much less energy compared to debonding in neat blends. Therefore, by increasing the JP content, the degree of freedom of the SAN matrix is reduced by JP induced linkages and the resistance of the system towards cracks (and its ductility) reduces. SEM images in **Figure 55** are very similar to

the ones in **Figure 52** as the deformation mechanisms in Region III are much alike to the ones during  $K_{IC}$  measurements. This is since specimens in both tests undergo relatively fast crack propagations. It is worth to mention that measurements up to very high crack propagation speeds of almost 0.1 77/cycle, which is unusual for thermoplastics (due to their ductile behaviour) is possible due to strong JP mediated linkage.

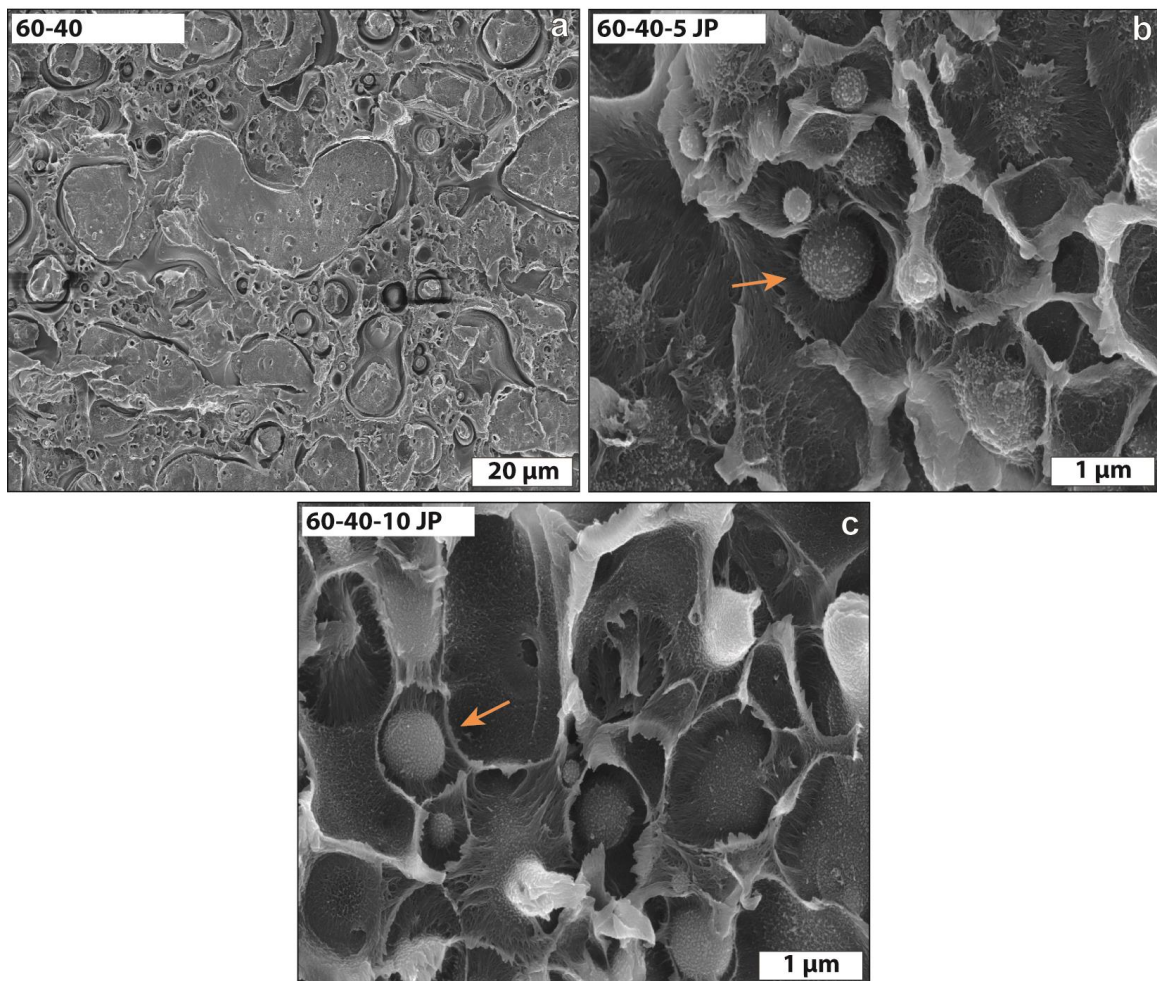


**Figure 55** SEM images of fractured surfaces of PPE/SAN (60/40) blends after FCP measurements from region III: a) neat, compatibilized with b) 5, and c) 10 wt.% JPs

The difference in the raspberry structure of the blends with 5 and 10 wt.% JPs is more clearly visible in **Figure 56**. The number of JPs on the PPE droplet surface is less in case of the blend with 5 wt.% JPs (**Figure 56a**) compared to the 10 wt.% JPs (**Figure 56b**). This gives the SAN matrix around the PPE particles more ability to deform and higher degree of freedom. On the

other hand, the strong JP linkage in case of the blend compatibilized with 10 wt.% JPs, produces more fibril crazings in the interface area and partial shear yielding of the SAN phase.

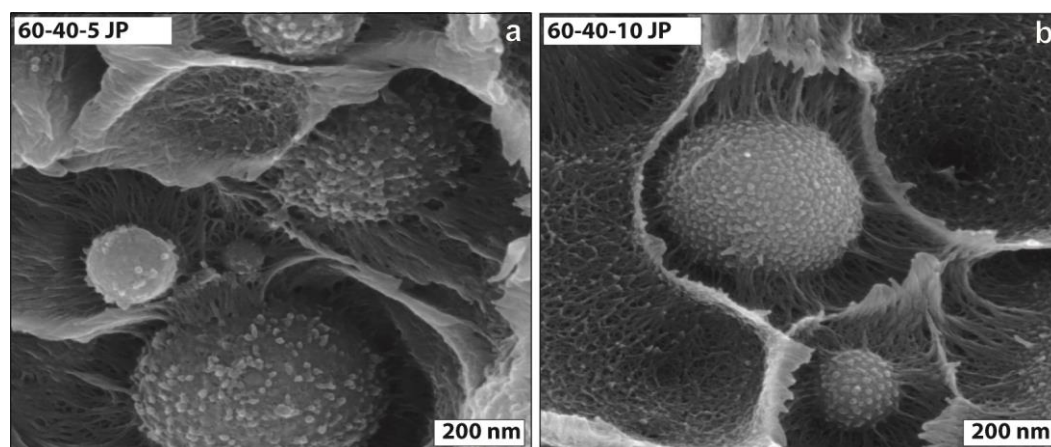


**Figure 56** SEM images of PPE/SAN (60/40) blends fractured surface after FCP test (region III) showing the raspberries in the structure with a) 5, and b) 10 wt.% JPs

### 5.3.4 Conclusion

Janus nanoparticles (JPs) demonstrate superior compatibilization capabilities compared to the corresponding SBM triblock terpolymers, attributed to the combined intrinsic properties, amphiphilicity and the Pickering effect. The Pickering effect significantly contributes to particle adsorption by overcoming the high thermal energy of the particles in the polymer melt. Straight forward mixing and extrusion protocols yield multiscale blend morphologies with “raspberry-like” structures of JPs-covered PPE phases in a SAN matrix. The JPs densely pack at the blend interface providing the necessary steric repulsion to suppress droplet coagulation and coalescence during processing. The efficiency of JP compatibilization is determined by droplet size evaluation and the smallest average droplet size of  $R \approx 150$  nm is reached at 10 wt.% of added JPs. The optimum fraction of JPs necessary for sufficient droplet stabilization without formation of double emulsion morphology was determined to be in the range of 2 to 5 wt.%. In case of excess JPs, rheological properties of the system are changed by a formation of a structural network since the droplet size and the inter droplet distance decreases significantly. The PPE droplet size decreased by increasing the JP content from 2-10 wt.% JPs were exclusively located at the interface of the blends. The large-scale synthesis of JPs, the low required weight fractions and their exceptional stability against extensive shear and

temperature profiles during industrial extrusion process make JP promising next generation compatibilizers.

Complex modulus from the DMA analysis of the JP compatibilized blends showed higher values for blends with 5 and 10 wt.% JPs due to higher stiffness of them. In addition, the plateau between the  $T_g$  of each blend component disappeared as the JP concentrations increased to 10 wt.%. This is correlated to disappearance of pseudo co-continuity and confirms the full droplet morphology of blends at 10 wt.% JP. In addition, DMA analysis with different strain rates of SBM and JP compatibilized blends (10 wt.%) confirmed that the presence of the plateau between the  $T_g$  values is due to the semi-continuous structure of the blends (in case of ineffective compatibilization). A schematic comparison of the 60/40 blend structures before and after compatibilization with 10 wt.% SBM and JPs is shown in **Figure 57**.

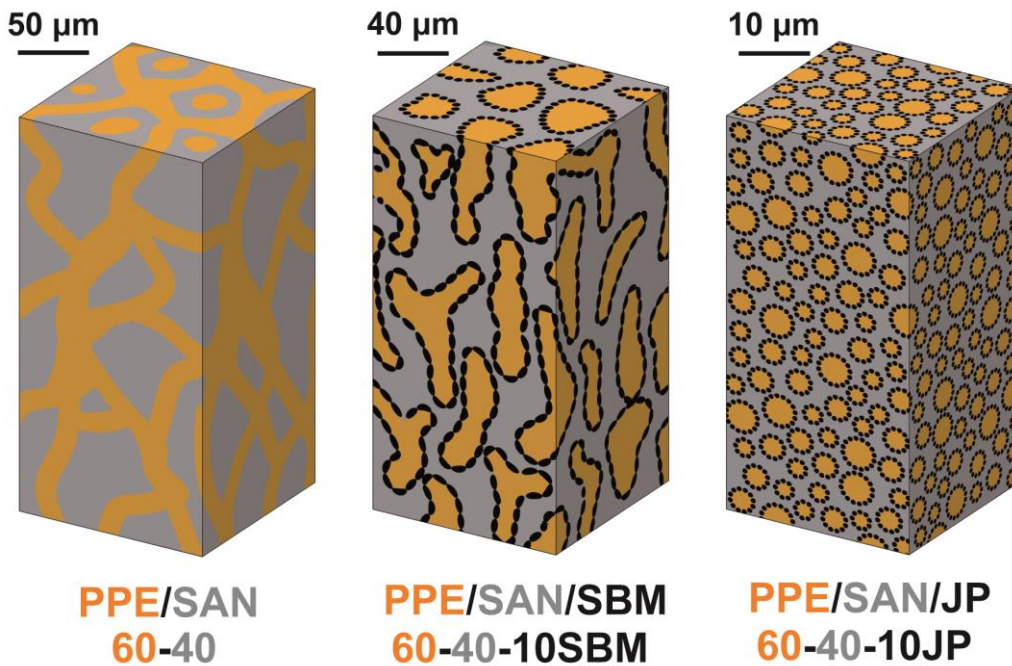


**Figure 57** Schematic 3D blend morphology of 60/40 PPE/SAN blends: a) co-continuous structure in neat, b) pseudo co-continuous structure in SBM (10 wt.%), and c) droplet structure in JP (10 wt.%) compatibilized blends

The effect of polymeric JPs as compatibilizers on the mechanical properties of PPE/SAN blends is investigated. Tensile properties and fracture toughness studies of the blends have proven an increase in the modulus and a reduction of the materials fracture toughness after compatibilization with JPs. The FCP behaviour of the blends compatibilized with JPs was investigated and compared to the neat blend. Neat blend contained large areas of debonded PPE as the main deformation mechanism. The JPs do not influence the FCP behaviour in the threshold region (region I) compared to the neat blends. However, addition of 10 wt.% JPs to the blend shows a negative influence at high crack propagation rates (region III) due to the reduction of the SAN potential to plastically deform by pinning it at different points *via* the raspberry structures (JP covered PPE droplets).

A more economic use of the Janus nanoparticles may be realized by admixing specific amounts of SBM triblock terpolymer. In order to investigate this idea and with the goal of producing JP compatibilized blend systems with improved mechanical behaviour, another blend system is introduced in the next chapter. Its mechanical properties are then investigated and compared to the neat and state of the art SBM triblock compatibilized blends in the following section.

## 5.4 Synergistic effects on toughness of blends compatibilized with JPs and SBMs

It has so far been shown that how elastic and stiff interfaces (chapters 5.2, and 5.3, respectively) as well as the domain size (chapter 5.2) each influence the macro-mechanical properties. From TEM analysis we know that JPs are very effective compatibilizers to produce small, homogeneously dispersed PPE droplets. Although a strong interfacial adhesion has been observed in the SEM images of the fractured surfaces which results in deteriorated FCP properties compared to neat blend. On the other hand, the SBM triblock terpolymers showed positive effect on the fracture toughness behaviour of the blend. Thus, the question is whether the advantages of the SBM and JPs could be combined in a synergistic way by preparing blends with both compatibilizers. In addition, by using SBM triblock terpolymer and JPs simultaneously, both soft (non-crosslinked) and hard (crosslinked) PB segments would be available at the interface and can generate multiple/new deformation mechanisms in the blend system.

In this chapter, PPE/SAN blends compatibilized with 5 wt.% JPs + 5 wt.% SBM triblock terpolymers (10 wt.% in total) are investigated and compared with blends containing only 10 wt.% JPs or 10 wt.% SBM triblock terpolymers.

### 5.4.1 Morphological characterization of mixed blends

**Figure 58** shows TEM micrographs of the PPE/SAN blend containing 5 wt.% SBM triblock terpolymer and 5 wt.% JPs. The total amount of compatibilizer in the blend is kept constant at 10 wt.% in order to allow further comparison of its properties to the blends with 10 wt.% of each compatibilizer discussed before. The combination of SBM and JP compatibilizers produces a fine blend morphology with smaller PPE droplets ( $R_{PPE} = 100 \pm 50$  nm) dispersed in the SAN matrix (**Figure 58a, b**) compared to the blends compatibilized with 10 wt.% SBM ( $R_{PPE} = 670 \pm 230$ , **Figure 58c**) and 10 wt.% JPs ( $R_{PPE} = 155 \pm 85$ , **Figure 58d**). The PPE droplets are densely packed and in some cases the interfaces even come into close contact with each other (**Figure 58b**). Since there are no SBM micelles or SAN inclusions visible in the PPE domains, it can be concluded that both the SBM and JPs are located exclusively at the interface. This is supported by the dark black line around each PPE phase, which is visible in **Figure 58b**, corresponding to the PB phase of the compatibilizers. However, it is difficult to distinguish between the two

compatibilizers (JP or SBM) as both appear black after selective staining of the PB segments and, thus, it is assumed that always a mixture of both compatibilizers is available at the interface.

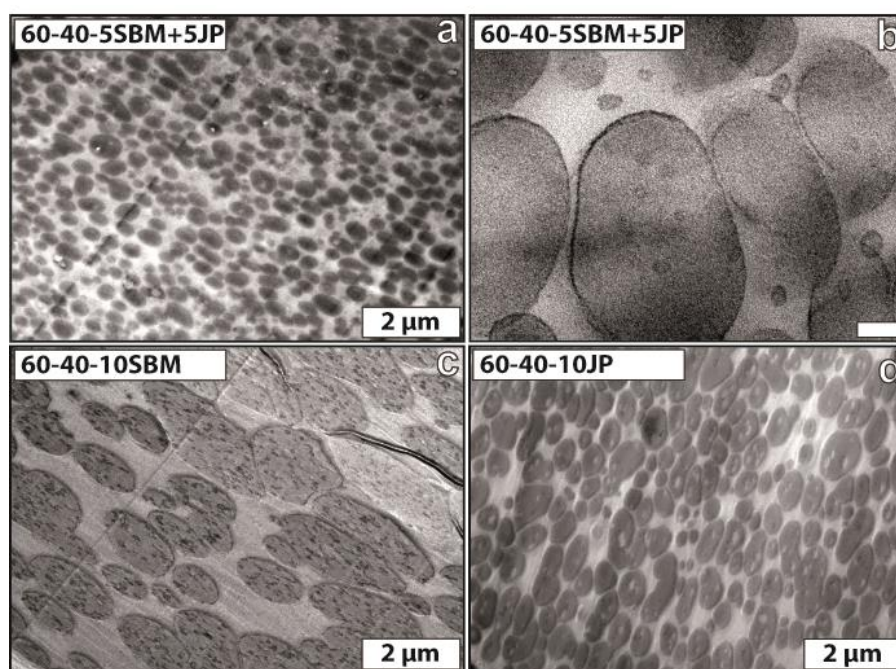


**Figure 58** TEM images of mixed (5 wt.% SBM + 5 wt.% JP compatibilized) PPE/SAN (60/40) blends: a) small PPE droplets finely dispersed in the SAN matrix, b) stained black blend interface (scale bar represents 50 nm); c) SBM (10 wt.%), and d) JP (10 wt.%) compatibilized PPE/SAN (60/40) blends discussed in previous chapters

The summary of the average PPE droplet sizes in blends containing 10 wt.% of compatibilizers compared to the neat blend is shown in **Table 7**. Aside from the neat blend (which has uncontrolled, non-reproducible morphology), using JPs alone or in combination with SBM triblock terpolymers effectively reduces the droplet size in blends. Additionally, it proves that using multiple compatibilizers in one system promotes synergistic effects on the morphology of the blend systems compared to using only JPs. After the addition of compatibilizers, the blend morphology is further homogenized (shown by the reduction in the standard deviation values in the table).

**Table 7** Average PPE droplet size in the blends with 10 wt.% compatibilizers

$f_p$ (wt.%)	$R_{PPE}$ (nm)
<b>0*</b>	<b>540 ± 300*</b>
<b>10 SBM</b>	<b>670 ± 230</b>
<b>10 JP</b>	<b>155 ± 85</b>
<b>5 SBM+5JP</b>	<b>100 ± 50</b>

\*As mentioned in 5.3.1, droplet radius of neat blend is determined for the sake of completeness, and does not adequately reflect the occasional large multi micron-sized droplets in a co-continuous morphology

With a similar method of calculating the radii of 500 PPE droplets in TEM micrographs (used in chapter 5.3.1), the PPE droplet size distribution of the blend with mixed compatibilizers is calculated and compared to the blend with smallest PPE droplets (10 wt.% JPs). **Figure 59** shows that even though both blends have very narrow droplet size distributions, combination of JPs and SBM triblock terpolymers confirms synergistic effects that further reduces the average droplet size to smaller values.

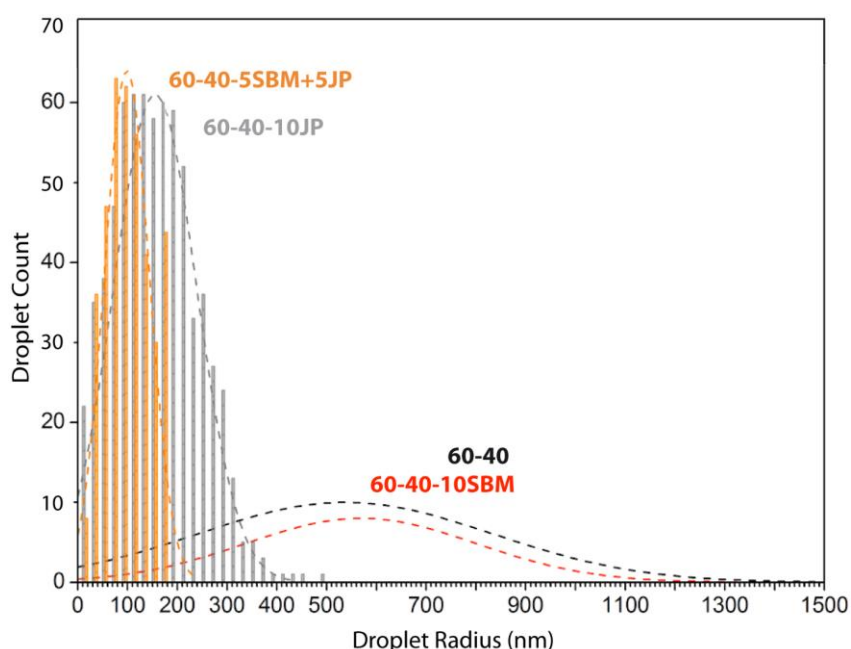


**Figure 59** PPE droplet size distribution of mixed blend (5 wt.% SBM + 5 wt.% JP) compared to SBM (10 wt.%) and JP (10 wt.%) compatibilized blends as well as the neat blend

### 5.4.2 Rheological characterization of mixed blends

In order to explain the interesting finer morphology of the blend with both compatibilizers, its viscosity is compared to that of the blends with 10 wt.% of only the SBM triblock terpolymer and JPs as compatibilizers (**Figure 60**). At higher frequencies, the viscosity of the “mixed” (JPs + SBM) blend is higher compared to the other blends. Hence, higher shear forces occur during the extrusion process, which allows the formation of very small PPE droplets and a fine morphology. At lower frequencies, an increase in viscosity and a yield point is visible due to the densely packed small PPE particles which build a structural network, as discussed in detail previously [155] (also with diameters below the critical value of 500 nm [254]). Since the PPE droplets are smaller than those of the other blends, the PPE/SAN interfacial area is increased and, thus, there is no excess compatibilizer in the system available to reduce the viscosity due to slipping effects, as observed in JP compatibilized blends [155]. Thus, by tailoring the rheological properties of the blend, during the extrusion process a blend with customized fine morphology can be produced, leading to improved mechanical properties.

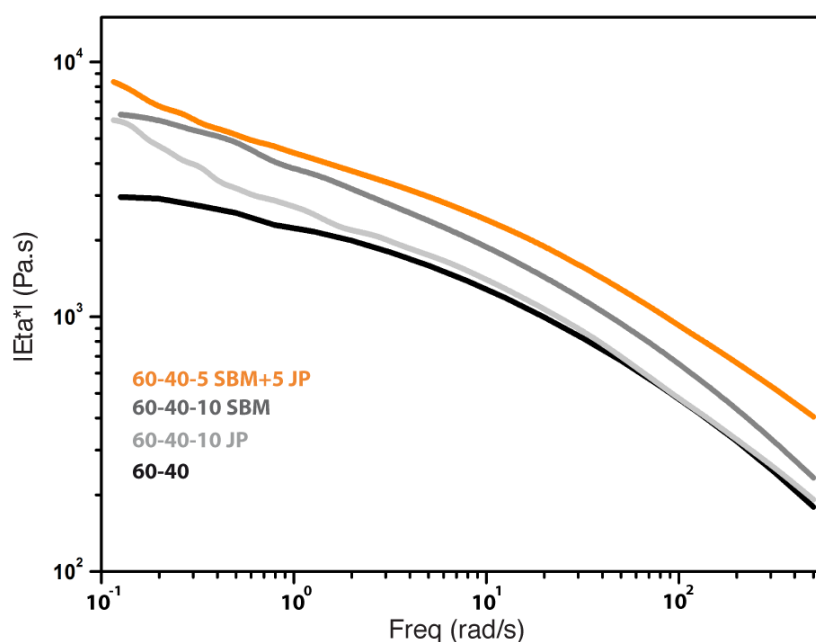


**Figure 60** Absolute shear viscosity of mixed blend (5 wt.% SBM + 5 wt.% JP) compared to SBM (10 wt.%) and JP (10 wt.%) compatibilized blends, as well as the neat blend

### 5.4.3 Mechanical properties of mixed blends

#### DMA analysis

**Figure 61** summarizes the complex modulus of the mixed blend (JPs + SBM) compared to the blends with 10 wt.% compatibilizers and the neat blend. The complex modulus of the mixed blend at room temperature is higher than of neat and SBM compatibilized blends, however unlike the blend with 10 wt.% JPs, the step correlating to the  $T_g$  of JPs is not visible here (probably due to lower amounts of them). The behaviour of material above the  $T_g$  of SAN is similar to what has been discussed in previous sections, and shows that the blend has solely PPE droplet morphology.

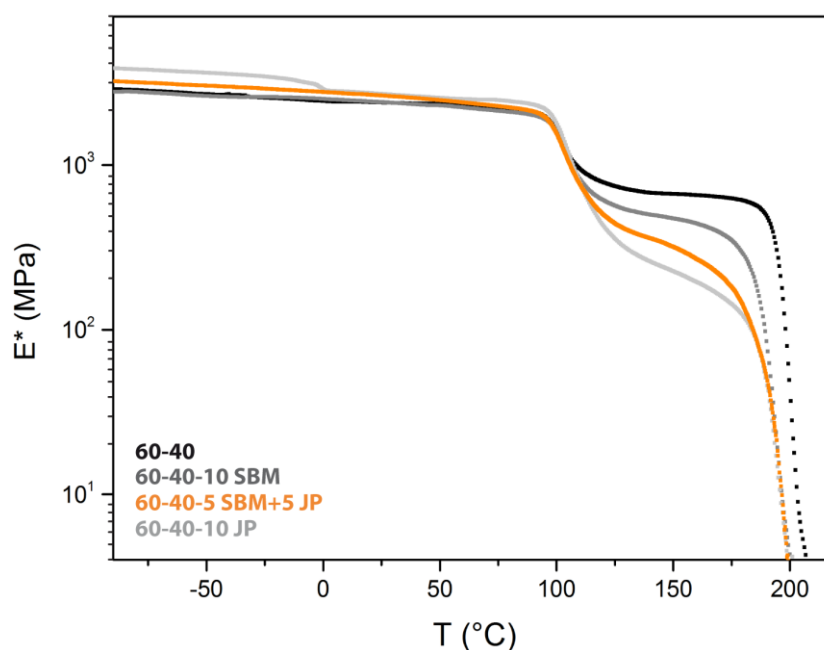


**Figure 61** Complex modulus of mixed blend (5 wt.% SBM + 5 wt.% JP) compared to SBM (10 wt.%) and JP (10 wt.%) compatibilized blends, as well as the neat blend

#### Low strain (tensile) properties

The tensile modulus of the mixed blend is compared to the neat blend and the blends compatibilized with 10 wt.% of each JPs and SBM triblock (**Figure 62**). The increase in modulus is attributed to the higher modulus of the JPs. At the same time, the raspberry morphology prevents a drop in modulus after compatibilization. According to TEM images and the relative thick interface layer corresponding to SBM and JPs at the interface, one can suppose that the

possible stress concentration or failure spots are minimized in number. Due to homogenization of the morphology, the value of the blend modulus is closer to theoretical value of the blend modulus obtained from the rule of mixture. Hence, the mentioned synergistic effects result in higher modulus for the mixed blend compared to neat, or compatibilized blends with coarser morphologies.

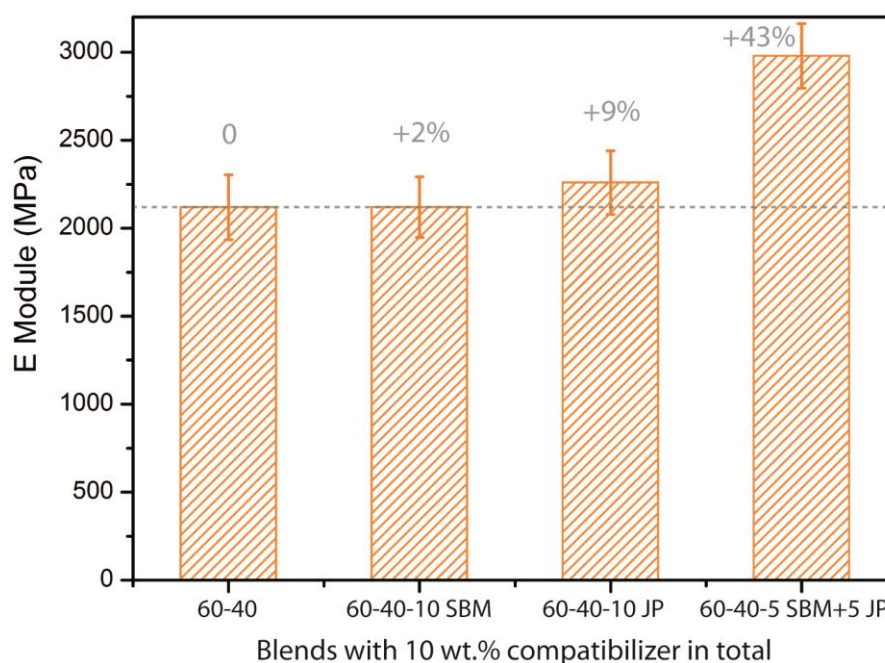


**Figure 62** Tensile modulus of mixed blend (5 wt.% SBM + 5 wt.% JP) compared to SBM (10 wt.%) and JP (10 wt.%) compatibilized blends, as well as the neat blend

### Fracture toughness

The fracture toughness studies in **Figure 63** also show an improvement in the  $K_{Ic}$  value of the mixed blend (JPs + SBM) compared to the neat blend, as well as the blends compatibilized with 10 wt.% of each compatibilizers. Here, the synergistic effects of using both JPs and SBM triblock terpolymers could be due to the homogenization of the blend morphology. Also, smaller PPE droplets with more flexible interfaces can result in several deformation mechanisms in both phases, which will be discussed. Additionally, the thick, strong blend interface result in good adhesion of the phases to each other. The SBM triblock terpolymers maintain enough flexibility at the interface for effective stress transfer between the phases and generation of multiple deformation mechanisms in both phases.

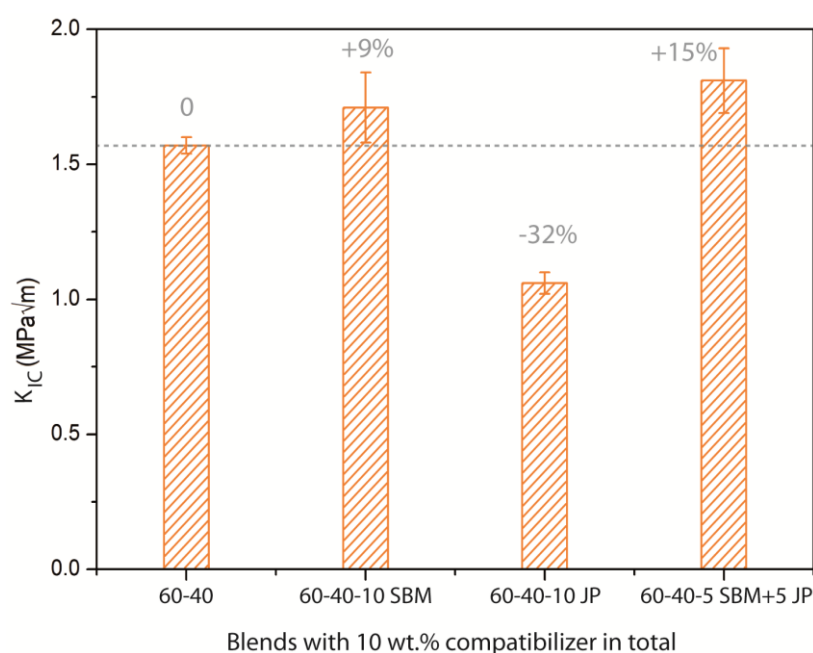


**Figure 63** Critical stress intensity factor of mixed blend (5 wt.% SBM + 5 wt.% JP) compared to SBM (10 wt.%) and JP (10 wt.%) compatibilized blends, as well as the neat blend

In order to determine the deformation mechanisms in the mixed blends, the fracture surface after  $K_{IC}$  measurements is investigated under SEM in **Figure 64**. In an overview, the main deformation mechanism seems to be macro cracks that are extended all over the blend system. **Figure 64a** shows the fractured surface at the starting point of the test. The orange line marks the border between the sharp notch produced by the operator (left side of the line), and crack propagated under the test conditions (right side of the line). It clearly shows how the small PPE droplets as well as the matrix homogenize and show similar crazing due to the strong adhesion at the interface. Therefore, differentiation between the phases is not possible. **Figure 64b** shows the PPE droplets and their interface at higher magnifications. Unlike the JP compatibilized blends discussed in the previous chapter, here the PPE particles are probably still fully embedded in the SAN matrix and make it deform and plasticize. This phenomenon uses up a lot of energy and contributes to the increase of the fracture toughness value compared to the other blends discussed.

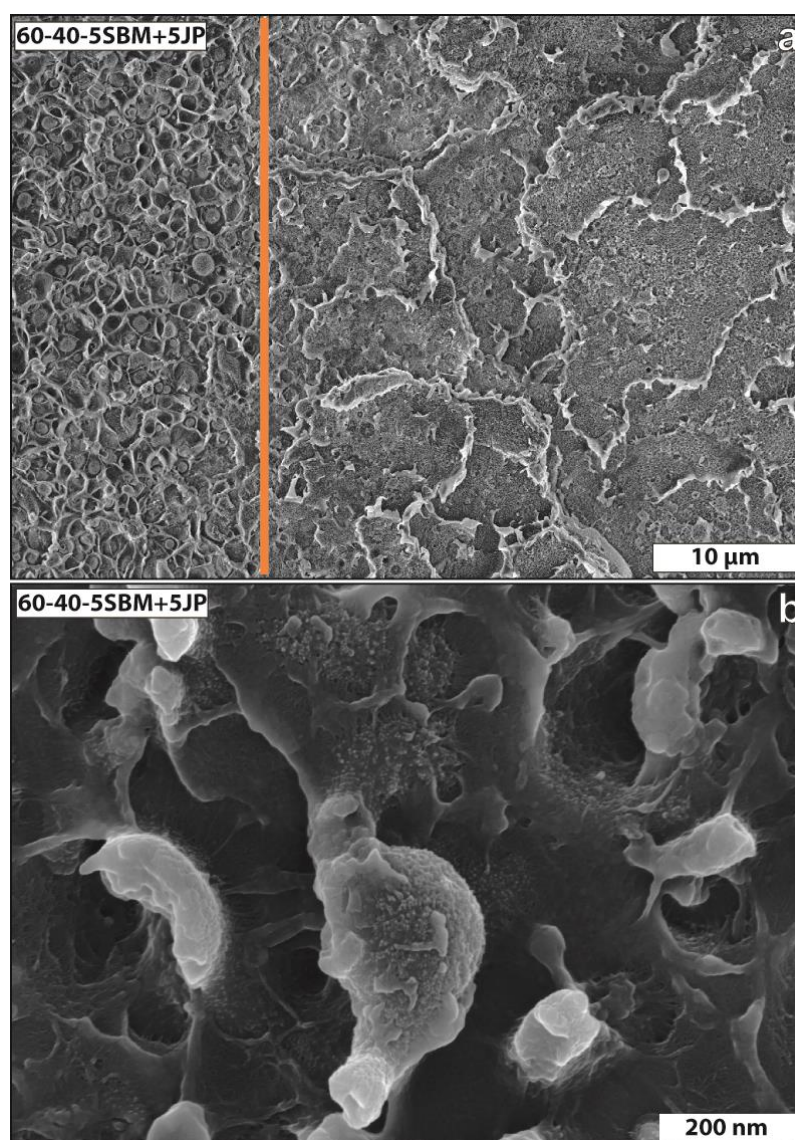


**Figure 64** SEM images of the fractured surface of mixed blend (5 wt.% SBM + 5 wt.%JP) after  $K_{IC}$  measurement. The images are from the area right after the crack initiation point

Even though the fracture toughness is an important test that can compare and determine the ductility of blend systems, their complex morphology and presence of multiple components call for more precise testing methods. Therefore, the blends containing 10 wt.% compatibilizers (SBM triblock terpolymers, JPs, and mixed blends), together with the neat blend as reference material are chosen for more elaborated FCP tests. The morphological study of fractured surfaces at different crack propagation speed gives a wide overview of possible deformation mechanisms in raspberry structures depending on the interface flexibility and the droplet size.

### Fatigue crack propagation (FCP)

The FCP behaviour of the blend containing both compatibilizers (5 wt.% SBM + 5 wt.% JPs) is compared to the neat, SBM, and JP compatibilized blends with 10 wt.% of each compatibilizer system (**Figure 65**). The behaviour of JP compatibilized blends are compared to the neat material in detail previously. The SBM compatibilized blend shows an improved FCP behaviour in the first and second regions compared to the neat and JP compatibilized blends. SBM improves the FCP behaviour in regions I and II, but the steep increase in crack speed in region III (similar to the neat blend) shows its low effectiveness in this higher crack velocity range prior to fracture. In this third region, the crack propagation rate increases (indicated by the steeper slope of the curve) and the SBM compatibilized blend does not show an improved behaviour compared to the neat blend. This might be a result of the different morphologies of the neat and SBM compatibilized blends with smaller PPE droplets ( $R_{PPE;SBM} = 670 \pm 230$  nm compared to very large partially co-continuous PPE phase in the neat blend). However, these PPE particles in the blend with 10 wt.% SBM are still larger than the ones in JP compatibilized blends ( $R_{PPE;JP} = 155 \pm 85$  nm), and, thus, can contribute to the toughening as the size of the plastic zone and the crack propagation rate increases in the first and second regions.

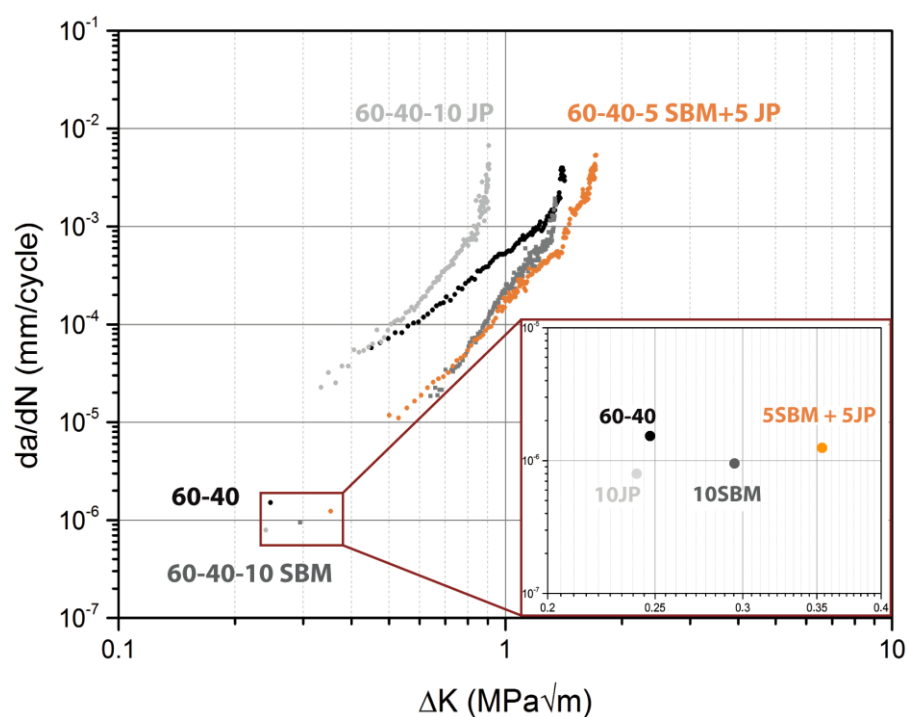


**Figure 65** FCP behaviour of the blends with both compatibilizers (5 wt.% SBM + 5 wt.% JPs) compared to the blends with SBM (10 wt.%), JP (10 wt.%), as well as neat blend. The zoom in of the threshold region is located on the bottom right side of the graph

Interestingly, the FCP behaviour of the mixed blend is improved in all three regions compared to all of the previously discussed blends. Both the threshold region (region I) and the area of critical fracture (region III) show significant improvements (43% and 20%, respectively) compared to the neat blend (**Figure 66**), indicating synergistic effects of combining JPs and SBM. In addition, similar to the JP compatibilized blends, measurement up to very high crack propagation speeds is possible, which confirms the presence of the strong JP mediated linkage at the interface.

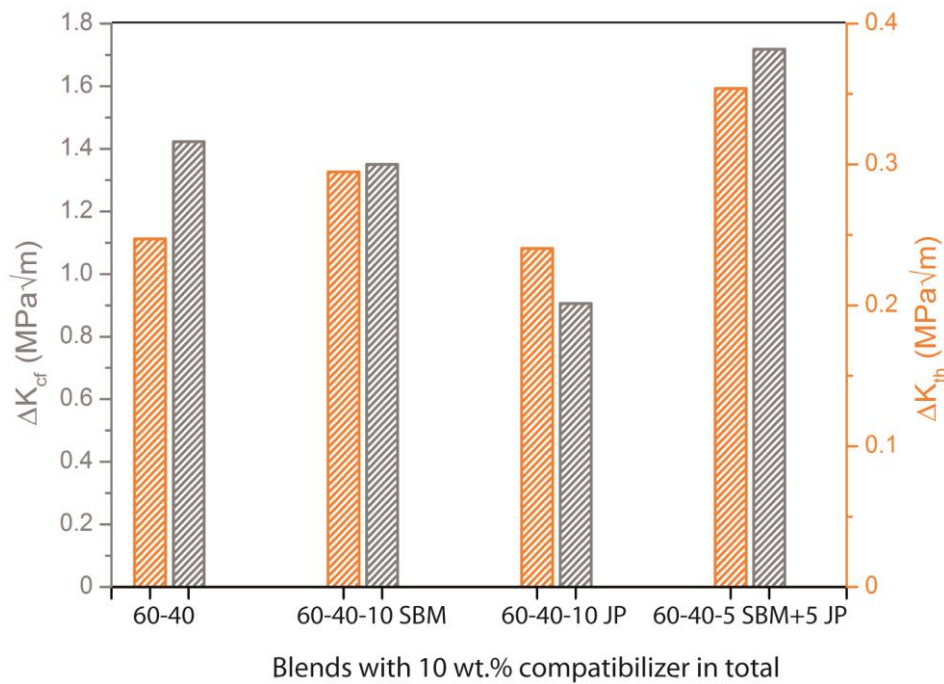


**Figure 66** Stress intensity factor ratio values at the threshold ( $\Delta K_{th}$ ) and critical fracture ( $\Delta K_{cf}$ ) regions for mixed blend (5 wt.% SBM + 5 wt.% JP) compared to SBM (10 wt.%) and JP (10 wt.%) compatibilized blends, as well as the neat blend

Fractured surfaces of the samples in each relevant region after the FCP tests were analysed *via* SEM to determine the reasons behind observed synergistic effects. **Figure 67** shows the neat blend in the region I (threshold) and the region III (instable fast crack growth). Here, large PPE particles dispersed in the SAN matrix are visible. In both regions, there are large cracks and macro deformations (indicated by orange arrows) visible in the blend structure propagating mainly in the SAN matrix (**Figure 67a, b**). At higher magnifications, it is visible that these large cracks usually originate from the PPE/SAN interface, where in this case, debonding occurs due to the lack of or insufficient linkage between the phases. The debonding occurs partially in the first region (**Figure 67c**), and develops into fully debonded PPE particles in the third region (**Figure 67d**) as the crack propagation speed increases. Additionally, in the first region there are embryonal crazes visible on the surface of the PPE domains due to the inherent ductility of this polymer (**Figure 67c**).

In summary, there are several effective (and strong) deformation mechanisms (macro cracks, debonding, and undeveloped embryonal crazing in PPE) in the neat blend that contribute to its plastification.

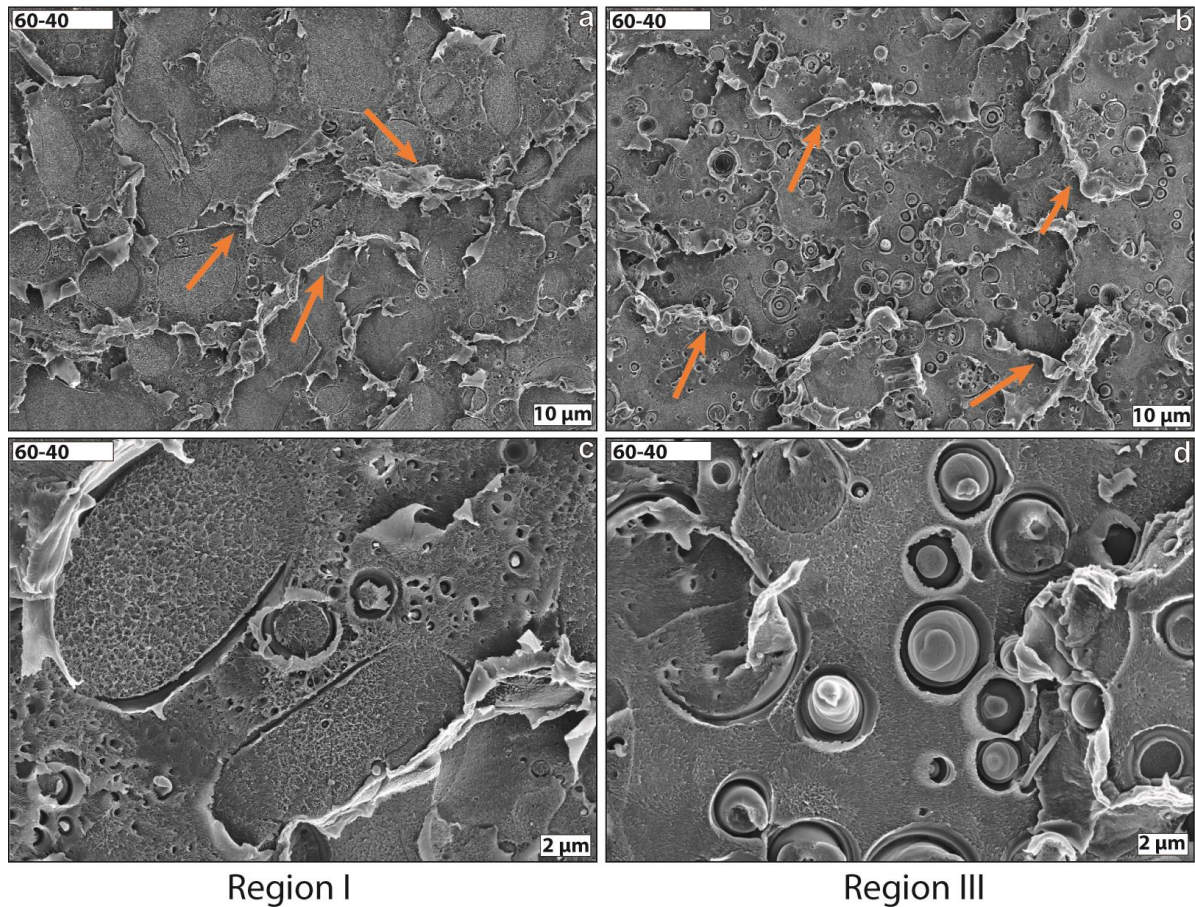


**Figure 67** SEM micrographs of the fractured surface of neat PPE/SAN blend (60/40) at a, c) first (threshold) region, and b, d) third (fast and instable crack growth) region after FCP

In the case of the compatibilized blends, the blend morphology strongly depends on both the amount and the type of compatibilizer (JP or SBM triblock terpolymer) resulting in different toughening mechanisms. Here, different sizes of the PPE domains and different PPE/SAN interfaces (JPs vs. SBM triblock terpolymer chains) could play a very important role. While the neat blend consists of a random partially co-continuous morphology with inhomogeneous large PPE regions, the morphology exclusively turns into PPE droplets dispersed within the SAN matrix when a compatibilizer is used [5]. The influence of interfacial adhesion and droplet size in dependence of the compatibilizer is discussed. The SBM compatibilized blend results in a morphology where the PPE droplets are dispersed within the SAN matrix ( $R_{PPE;SBM} = 670 \pm 230$  nm). The fractured surfaces of this blend in the regions I and III are shown in **Figure 68**. Comparable to the neat blend, the presence of macro deformations and a rough surface structure due to macro cracks is visible in the threshold and critical fracture regions (**Figure**

68a, b), respectively. At higher magnifications, spherical PPE droplets are visible in the SAN matrix. Due to the elastic nature of the interface (raspberry morphology with elastic PB domains at the interface) and its lower stiffness in the interphase region, there are some detached particles visible (the holes left behind) even at low crack propagation speeds (**Figure 68c**). This correlates to the elastic properties of the PB middle block of the SBM compatibilizer that tends to tear apart upon application of stress instead of crazing [40]. The large cracks also initiate at the PPE/SAN interface between the PPE particles and SAN matrix. However, since the PPE particle size has decreased, there is more interface available for crack initiation and, thus, the increased number of cracks leads to a rougher fracture surface with higher amount of plastic deformation in the first region (**Figure 68c**). This result in an improved FCP behaviour of the SBM compatibilized blend (comparable to the material's toughness) in the threshold region (I) (**Figure 65**). On the other hand, as the crack propagation speed increases, more and more PPE particles are detached, and in the last region, since almost all particles are either fully debonded or have torn up SBM interfaces (**Figure 68d**), the behaviour of the blend is very similar to the neat blend (with unmodified interface), which also has shown fully debonded PPE particles in the critical fracture (third) region and has unmodified interface. Consequently, in case of SBM compatibilization, the weaker, elastic PB block at the interface can only withstands small crack propagation speeds and influence the material's behaviour in the first two regions.

In summary, the deformation mechanisms in SBM compatibilized blends also sum up to macro cracks and debonding, which are results of the interface tearing that consumes a lot of energy. The SBM compatibilization will result in larger interface (due to smaller PPE droplets) and would further increase the consumed energy while tearing and debonding.

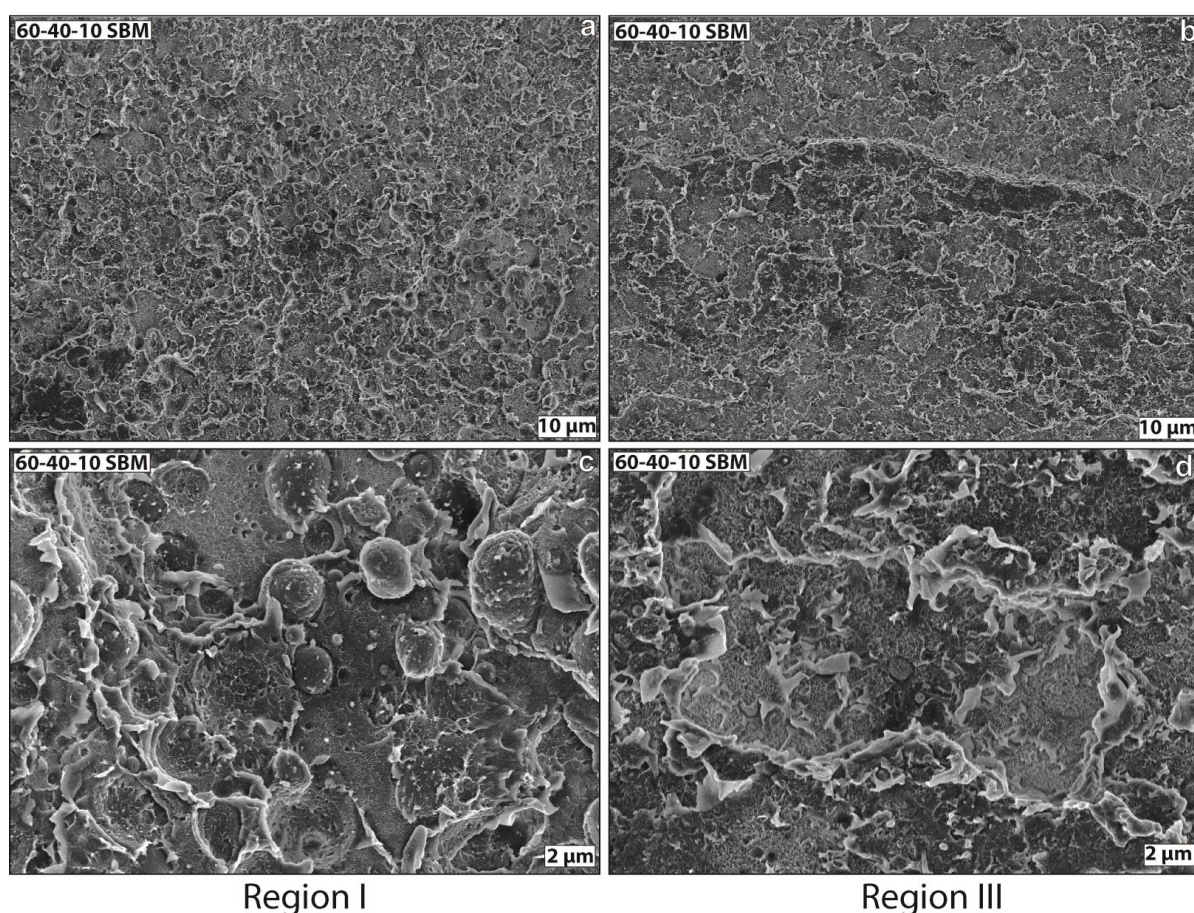


**Figure 68** SEM micrographs of the fractured surface of SBM compatibilized (10 wt.%) PPE/SAN (60/40) blend at a, c) first (threshold) region, and b, d) third (fast and instable crack growth) region after FCP

For the JP compatibilized blends, the fractured surface after FCP measurement looks quite different in both the threshold (first) and the critical fracture (third) regions (**Figure 69**). In both regions, the fine-textured structure of the fractured surface does not indicate any macro deformations or pronounced surface roughness after plasticization (**Figure 69a, b**). The small PPE particles are still completely embedded in the SAN matrix, as evidenced by the higher magnification images shown in **Figure 69c, d**. There are some ligaments (**Figure 69e, f**), where JPs link the PPE and SAN phases to each other, available at the interface showing some crazing in these regions. However, there is no debonding visible between the phases at both regions. The presence of these ligaments at the interface confirms entanglements between the PS and PMMA sides of JPs with the PPE and SAN phases, respectively. Consequently, the enhanced adhesion between the PPE and SAN phase is caused by the strong JP mediated linkage at the interface of

the blends. This is a result of superior interfacial activity of JPs (combination of the Pickering effect with the biphasic structure (amphiphilicity) of the JP corona). Therefore, more desorption energy is necessary to separate JPs from the PPE/SAN interface as compared to the pure SBM triblock terpolymers [138]. Moreover, the entanglement density at the interface is expected to be higher than that of blends with SBM. This is due to the fact that there are several PS or PMMA chains available on each side of JPs as a result of the crosslinking process, which is known to improve the strength of the interface. The JPs provide an increased entanglement density at the blend interface that can effectively improve the strength of the interface. The fact that high entanglement density, improve the strength have been already studied in literature [255–257]. In contrast, for the linear SBM triblock terpolymers, even though they can self-assemble at the interface and form multiple bonds, they have a lower interfacial activity as compared to the JPs.

In the first region (**Figure 69e**) the craze ligaments at the interface show a clear fibrillation where JPs bind the PPE particles to the matrix. The crosslinked PB core of the JPs (which is generated during the synthesis process) is stiffer than the elastic PB patch at the interface of the SBM compatibilized blend and crazes into long and thin fibrils instead of tearing up. This individual craze formation mechanism can compensate for the lack of debonding in the initial stage of crack propagation, where the crack grows slowly. As the crack propagation speed increases, the stiffer nature of the JPs at the interface hinders further transfer of the force between the phases and limits the deformation of either phase. As a result, large amounts of fibrils are visible between the PPE particles and the SAN matrix.

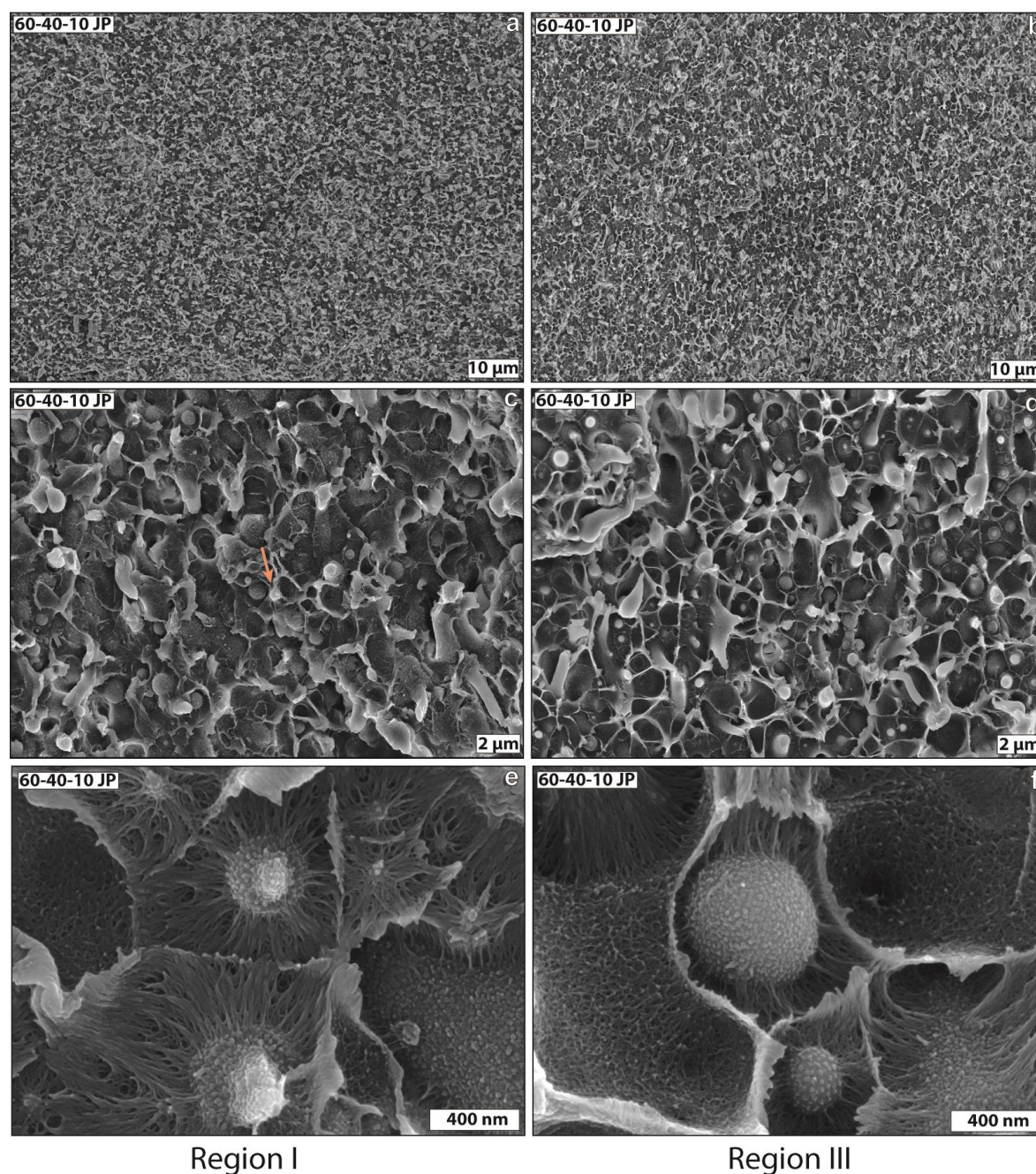


**Figure 69** SEM micrographs of the fractured surface of JP compatibilized (10 wt.%) PPE/SAN (60/40) blend at a, c, e) first (threshold) region, and b, d, f) third (fast and instable crack growth) region after FCP

The dynamic-mechanical analysis of JPs in **Figure 22** shows the influence of partial crosslinking on the  $T_g$  and stiffness of the PB elastomer block. The partially crosslinked PB core in the JPs has a glass transition temperature of around 0 °C which is almost 80 °C higher than that of the non-

crosslinked PB block in SBM. In addition, the decrease in modulus at its  $T_g$  is relatively small. Consequently, JPs have a higher modulus due to their semi crosslinked PB core and as a result higher stiffness as compared to the SBM triblock terpolymer at room temperature, where the FCP behaviour was investigated. Hence, the strong JP mediated linkage at the interface hinders chain scission and interface tear up. At the same time, as the crack propagation speed increases, the craze fibrils are under stress to stretch further, but cannot due to their lower elasticity. Therefore, the rates of deformation of craze tips at the craze/bulk interface decreases and craze fibrils turn into crazes. In the third region (**Figure 69f**), exclusively crazing is observed. At higher crack propagation speeds, the stiff interface appears more brittle under stress and the size of the crazing area around PPE particles decreases. The strong JP mediated linkage prevents debonding and therefore, compared to the neat and SBM compatibilized blends, the FCP behaviour and in turn the toughness of the JP blends deteriorates. On the other hand, the advantage of the strong bond is that it makes measurements up to very high crack propagation rates possible, which is usually not possible for thermoplastic materials due to their high ductility. The fact that the material withstands such fast crack propagations again underlines the high efficiency and strength of the JPs at the interface; however, on a macro scale they result in deteriorated FCP behaviour. To sum up the JPs behaviour, the deformation mechanism here is only limited to a small crazing area around the PPE domains, which build fibrils at the interface. In order to be able to better visualize **Figure 69f** in colour, a schematic raspberry structures and morphology of the PPE, SAN, and JPs together is shown in **Figure 70**.

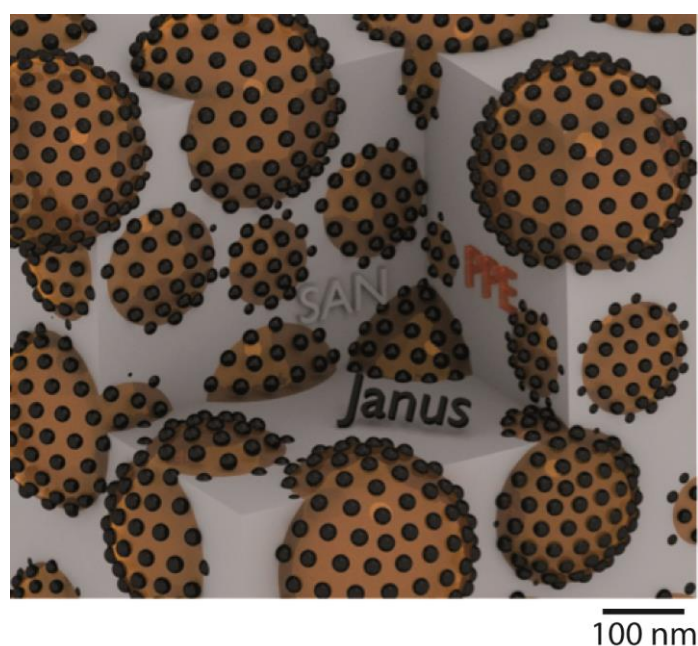


**Figure 70** Schematic structure of JP (10 wt.%) compatibilized PPE/SAN blends (60/40)

In summary, the stiff JP mediated linkage at the interface promotes crazing and fibrillation of the interface area but prevents macro crack formations and debonding; resulting in deteriorated material's behaviour. These macro cracks usually initiate at the interface due to debonding (in case of neat), and tearing of the PB middle block (in case of SBM compatibilized blends) shown by the holes left behind by the debonded PPE particles, and effectively increase the SAN matrix plastification.

**Figure 71** shows SEM images of the fractured surface after the FCP test in the blend containing both compatibilizers (5 wt.% SBM + 5 wt.% JPs) in the threshold and the third region. In the overview images, both regions show macro deformations with large cracks and a rough surface structure indicating massive plastification (**Figure 71a, b**). On a smaller scale, the blend has an apparent continuity and shows a homogenous structure where the PPE particles and the interface are not recognizable in the blend structure anymore. However, it is assumed that the initiation of these large cracks takes place at the PPE/SAN interface, where SBM triblock terpolymer chains are located (**Figure 71c, d**), i. e., in analogy to the SBM compatibilized blend. A closer look at the fractured surface in **Figure 71e** shows premature broken vertical crazes all over the blend surface. In addition, crack bridging is visible for a very long crack of around 10  $\mu\text{m}$  (orange arrow in **Figure 71c**). The fibrils (**Figure 71e**), which are bridging the crack, look very similar to the crazing ligaments found at the interface for the JP compatibilized blend in

**Figure 69e, f.** We assume that the very small PPE particles with JP bonds at their interfaces are aligned at the sides of the crack (which propagates in the SAN matrix) and promote fibril structures between the phases as the crack propagates in the matrix. These fibrils from the strong JP mediated linkage can bridge such a long crack through the SAN matrix. This type of fibril deformation can consume a lot of energy, which contributes to the improved performance in crack growth and thus material's toughness. This is a very effective deformation mechanism that contributes to the improved behaviour of the blend in the threshold region (region I). In region III, where the crack propagates faster (**Figure 65**), the undeveloped vertical crazes would further grow into shear bands and promote massive plastic deformation all over the surface (**Figure 71f**). Therefore, the deformation mechanisms contributing to the improved FCP behaviour of this blend system include macro cracks, embryonal crazes all over the surface due to fine morphology and homogenization, interface fibrillation, and crack bridging.

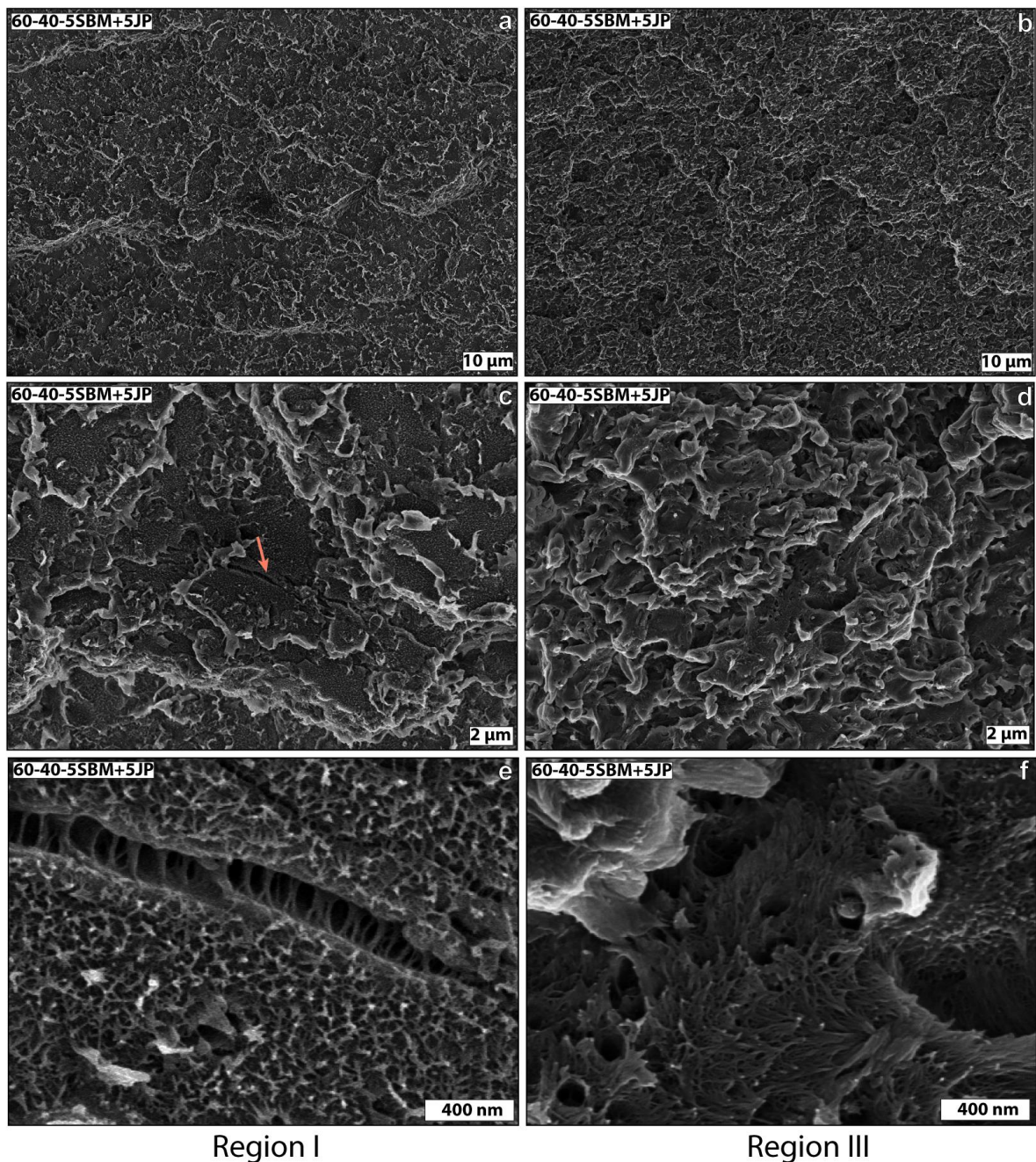


**Figure 71** SEM micrographs of the fractured surface of the mixed PPE/SAN (60/40) blend (5 wt.% SBM + 5 wt.% JP) at a, c, e) first (threshold) region, and b, d, f) third (fast and instable crack growth) region after FCP

**Figure 72a**, shows the areas where the large macro cracks that consume lots of energy are originated. One can say that even though strong adhesion between the phases results in homogenization of the blend morphology and embryonal crazing in both phases (**Figure 72b**), there are still available defect points where these cracks can originate from.

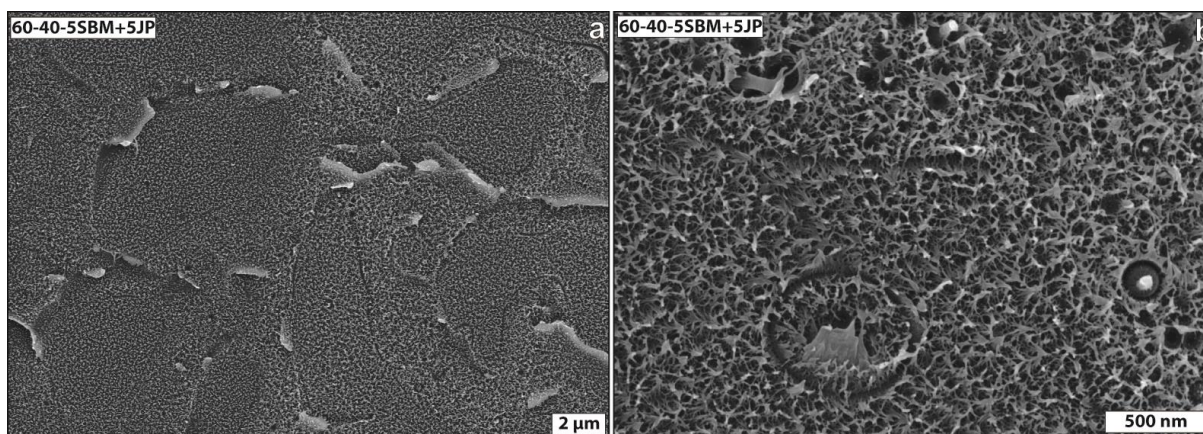


**Figure 72** SEM micrographs of the fractured surface of the mixed PPE/SAN (60/40) blend (5 wt.% SBM + 5 wt.% JP) after FCP measurements: a) areas where macro cracks are originated, b) embryonal crazes in both phases and blend homogenization

These multiple mechanisms are only possible by combining the strong JP mediated linkage at the interface with the high elasticity of the PB middle block in the SBM triblock terpolymer, which can promote formation of macro cracks, in the fine, homogenous morphology of the blend. The direct result of these synergistic effects is the improvement of the materials crack propagation resistance in all three regions.

#### 5.4.4 Conclusion

Enhanced macro mechanical properties are induced when a combination of JPs and a linear SBM triblock terpolymer are used together as compatibilizers. Synergetic stabilization capabilities of JPs and SBM triblock terpolymer mixtures are proven as the morphology of the blend compatibilized with mixed materials shows the smallest PPE droplets with  $R_{PPE} = 100 \pm 50$  nm. Rheological characterizations correlate the fine, homogeneous morphology of the blend to its high viscosity, and as a result increased shear forces during the process. In addition, the lack of slipping effects generated by excess JPs in the system (as discussed previously) further contributes to the finer morphology. Similar to the JP compatibilized blends, here also DMA analysis confirmed the solely droplet morphology and absence of the semi-continuous structure in blend morphology. Investigation of the mechanical properties confirmed simultaneous increase in the tensile modulus as well as the fracture toughness,  $K_{IC}$ , (45 % and 18 % compared to neat blend, respectively) of the mixed blend compared to both blends compatibilized with only JPs or SBM triblock terpolymers. FCP measurements of the blend material allow insights

into the important role of interface stiffness and flexibility influencing the underlying deformation mechanisms. With the knowledge that the elastic PB block is also needed at the interface to improve the FCP behaviour (especially at low crack propagation speeds), the mixed blend is compared to the blends compatibilized with each 10 wt.% of SBM triblock terpolymers or JPs. The mixed blend shows improved FCP behaviour in all three regions (43 % in the threshold and 20 % in the critical fracture region compared to neat blend). Different deformation mechanisms are acting at the same time during fatigue crack propagation. Macro crack development, crack bridging, embryonal crazing all over the surface, and at higher crack speeds additionally shear yielding are observed. The SBM compatibilized blend shows improved behaviour compared to the neat blend only in regions I and II. This was attributed to the tearing of the elastic PB middle block at higher crack propagation speeds (in region III). In case of the JP compatibilized blends, extreme crazing and fibril formation around the interface area was attributed to the partially crosslinked PB block and, thus, higher stiffness of the JPs compared to the SBM triblock terpolymer. The strong JP mediated linkage at the blend interface is promoted by the high interfacial activity of these particles and hinders debonding of the PPE particles from the SAN matrix and initiation of macro cracks which can consume a lot of energy. These macro cracks usually initiate at the interface due to debonding (in case of neat), and tearing of the PB middle block (in case of SBM compatibilized blends) shown by the holes left behind by the debonded PPE particles, and effectively increase the SAN matrix plastification. The improved fatigue crack propagation behaviour of the immiscible blends is achieved through the presence of both an elastic (attributed to the soft PB part in the SBM triblock terpolymer) and a stiff linkage (caused by the JPs) between the phases at the blend interface.

**Figure 73a-f** summarizes schematically the deformation mechanisms during  $da/dN$  measurements for different blend systems. Macro cracks in the matrix (**Figure 73a**) happens in neat and SBM compatibilized blends. Molecular crazing (**Figure 73b**) mainly appears in neat and JP compatibilized blends. Tearing of the PB middle block (**Figure 73c**) happens only in the SBM compatibilized blends, whereas fibrillation of the JP mediated linkage at the interface (**Figure 73d**) appears in the JP compatibilized blends. The blend compatibilized with both SBM and JPs show all of the mentioned deformation mechanisms plus shear yielding all over the matrix (**Figure 73e**), and crack bridging (**Figure 73f**). Therefore, it shows best FCP behaviour compared to the other blends mentioned which proves the synergistic effects of combining the JPs with SBM triblocks.

Tailoring blend morphologies with multiple compatibilizer systems is proven to lead to synergistic effects of the macro-mechanical properties and improved mechanical behaviour in immiscible polymer blends. Understanding these basic relationships between the blend recipe and the used compatibilizer systems allows targeting desired materials properties and may act as a helpful toolbox for potential applications.

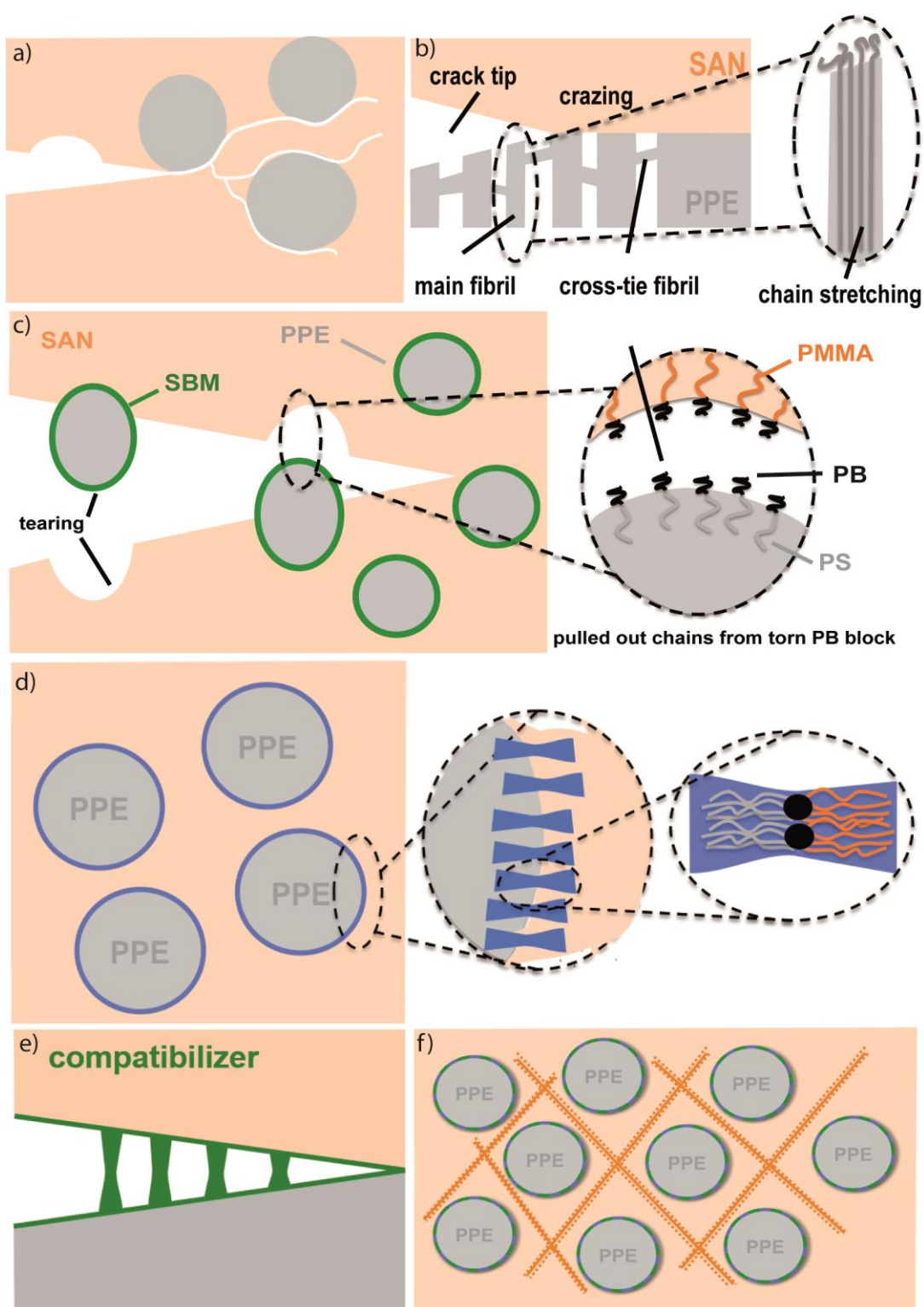


**Figure 73** Schematic overview of deformation mechanisms in blend systems: a) macro cracks in the matrix, b) molecular crazing, c) droplet debonding as a result of interface tearing, d) JP mediated linkage (JP fibrils at the blend interface), e) crack bridging, f) shear yielding (shear bonds)

## 6 Summary and Outlook

### 6.1 Summary

Novel Janus particles show great potential in the compatibilization of technically relevant, immiscible PPE/SAN polymer blends. They are more effective than state of the art SBM triblock terpolymers in terms of homogenizing the morphology and reducing the PPE droplet size, as well as preventing the formation of micelles within the PPE and SAN phases. The small PPE droplets, which form a disperse phase, are ca. 150 nm in radius and are densely packed in the SAN matrix. Unlike expectations, at PPE weight contents of 50 % and higher (up to 70 %), PPE phase still forms droplets in the SAN matrix. The much higher viscosity of PPE compared to SAN and the large viscosity ratio of the blend is responsible for this droplet morphology formation. The high viscosity mismatch also causes a second plateau of the complex modulus (obtained *via* DMA analysis) after  $T_g$  of SAN. The rheological characterization of the blends confirms the effective compatibilization with JPs and increase in the blend viscosity. The JPs are exclusively located at the PPE/SAN interface and form a raspberry structure that prevents any decrease of the modulus in the compatibilized blends. Nevertheless, because of the higher  $T_g$  of the crosslinked PB core in the JPs compared to the PB block in SBM triblock terpolymers, a further increase in the modulus of the JP compatibilized blends is also observed below the  $T_g$  of the PB block. Fracture mechanics investigation of the blends shows that due to the stiff nature of JPs, and as a result a stiffer interface, major deformation mechanisms such as formation of macro cracks are hindered. Deformation in JP compatibilized blends is limited to craze formation around the small area at the interface between PPE and SAN. Therefore, even though the larger number of droplets (and their smaller size) increases the blend interface and shows excellent adhesion, it makes the blend system unable to generate large cracks. The large cracks are usually generated at the points where PPE droplets are detached from the matrix, which in case of JP compatibilized blends can not happen due to the strong JP mediated linkage at the interface. Furthermore, the raspberry morphology prevents the deformation of a ductile PPE phase. In an attempt to tailor a blend with improved toughness and fatigue crack propagation behaviour, the JPs and SBM triblock terpolymers are both used as compatibilizers. Each compatibilizer leads to unique advantages in the blend structure and its properties. Hence, their combination results in finer blend morphologies with thick interfaces. The small size of PPE droplets, together with the combination of elastic and strong interfaces enables several effective deformation mechanisms in the blend during fracture toughness and FCP measurements. Therefore, it is proven that

combining both compatibilizers results in multiple, synergistic improvements in different properties compared to the neat blend as well as the blend components.

## 6.2 Outlook

### 6.2.1 Nanocellular foams from JP compatibilized blends

Foaming polymer blends has a high potential for better control over properties such as the size of the cellular structure, open or closed cell content, etc., as well as foam density [258–260]. Depending on their properties, foams can be used in applications such as energy absorption, thermal and acoustic insulation and packaging. Recently, polymer foams have received more attention due to their lightness, that promotes material saving and other positive environmental aspects. Foaming polymer blends can be very challenging due to their complex nature and several parameters influencing the foaming behaviour of the involved compounds. Especially in terms of immiscible polymer blend systems, the foaming process is strongly influenced by the morphology and the interactions between the phases. The influence of different linear SBM triblock terpolymers on the foaming behaviour of PPE/SAN blends using different blowing agents has been previously investigated [261–263]. They could either achieve low foam densities of about 200 kg/m<sup>3</sup> with large cell sizes using solvents like ethanol and pentane as blowing agents, or nanocellular foams with large densities of 600 kg/m<sup>3</sup> using CO<sub>2</sub> as blowing agents. Heterogeneous nucleation, which is favoured to produce a more homogenous, finer foam structure, can occur at the interphase between the two blend phases [260,264]. During the nucleation and foaming process the dissolution of the blowing agent in the highly viscous PPE phase does not lead to foaming, but most likely interfacial enrichment of CO<sub>2</sub> between the PPE and SAN [262]. Also, differences in the glass transition temperature of amorphous polymers can be used in the batch process for selective foaming of one phase, which was studied more intensely by Ohshima et al. [265–267]. The compatibilizer in immiscible blend systems reduces the stress at the interface, affecting the interfacial tension, the foaming behaviour of the blend components and the foam morphology [53,107,108,110,113,117,221,253,254,255].

With this background, the effect of Janus particle compatibilization on the morphology and density of PPE/SAN polymer blend foams is highly interesting. Since these particles provide finer morphologies compared to the other compatibilizers and have higher interfacial activities, it is interesting to investigate their effect during the complex foaming process in blends. Some

preliminary studies have been performed and the detailed discussion of the results are given in the published article by the author [270]. However, the topic has high potentials and many more aspects that can be the subject of future studies are yet to be studied. Few points are discussed briefly below, however, they are only preliminary studies to initiate further questions for the follow up work.

In summary, immiscible PPE/SAN blends (60/40 w/w) compatibilized with JPs were foamed using  $CO_2$  as physical blowing agent. The small PPE domains in the compatibilized blend could act as potential nucleating sites during foaming and provide a homogenous foam structure with small cells. The sorption measurements showed that the carbon dioxide solubility in the solid blend at room temperature increased with adding up to 2 wt.% of JPs. This is due to an extra surface generated by crazes at the interface. JP mediated linkage at the blend interface act as stress concentration points and after  $CO_2$  absorption (that causes swelling) would fail and cause crazes in the material. These crazes provide extra free volume that results in higher solubility of the gas in the polymer blend. In the case that the PPE/SAN interface is densely covered by JPs (5 and 10 wt.% of JPs), the stress concentration points where these cracks could have initiated did not exist and therefore a lower free volume caused the  $CO_2$  solubility to decrease. **Figure 74** shows the schematic explanation of the proposed theory. The diffusion coefficient shows a similar trend and decreases with 5 and 10 wt.% of JPs, due to the barrier effect of the partially crosslinked PB middle block in the compatibilizer.

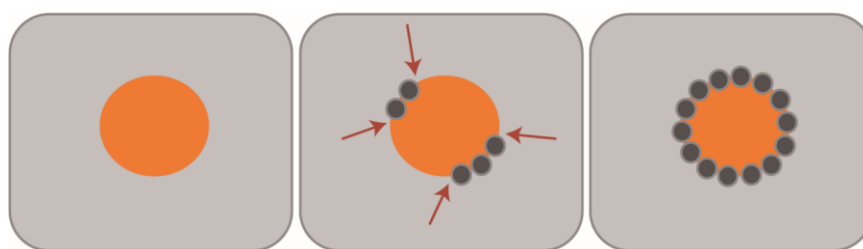


**Figure 74** Effect of raspberry morphology on the  $CO_2$  sorption behaviour of PPE/SAN blends: stress concentration at areas marked by red arrows leads to micro crazes in  $CO_2$  loaded blends with 1 and 2 wt.% JPs, where as the strong Jp mediated bond in blends with full raspberry structure prevents the formation of micro crazes

The average foam cell size decreased with increasing the amount of JPs, due to the fact that smaller PPE domain sizes provide an increased number of foam nucleation sites for foaming. JPs

can also initiate cell nucleation in blend foams and due to their strong linkage (JP mediated linkage discussed in 5.3.3) between the phases during foaming, fibril-like structures were produced, resulting in foams with partial open cell contents (**Figure 75**). The open cell structures resemble spider web morphologies, where the JPs are linking the blend phases together.

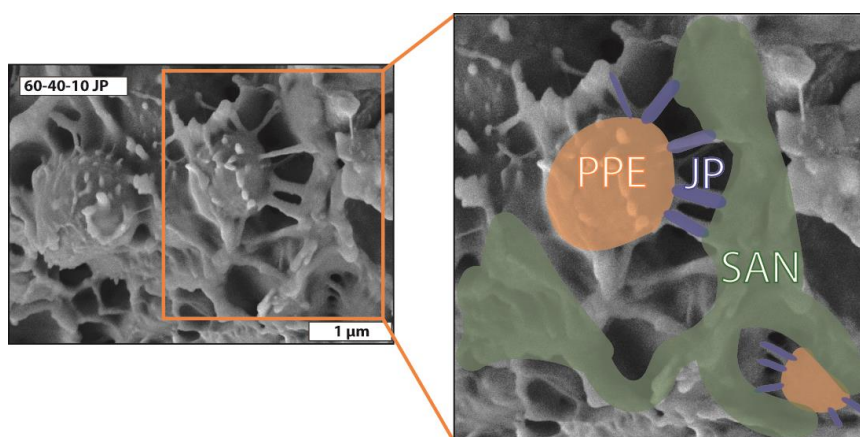


**Figure 75** SEM micrographs of PPE/SAN compatibilized with 10 wt.% JP showing open cells and spider webs (foamed at 140 °C for 10 s with density of 650 kg/m<sup>3</sup>), the magnification shows a small PPE domain (round particle) attached to the SAN matrix by JPs

The lowest cell size (900 nm) with a homogeneous cell structure was achieved in the blend compatibilized with 5 wt.% JPs. The addition of more JPs (10 wt.%) led to densely packed PPE domains with very small inter-domain distances hindering further foam growth. **Figure 76** compares the cellular structure of the blends with 2 and 10 wt.% JPs (foamed at 140°C for 10s) as an example. In case of an insufficient coverage of the interface by JPs, the cellular structure is strongly bimodal and inhomogeneous. Larger cells correspond to SAN areas that have a lower viscosity and can expand better, and the smaller cell sizes represent PPE regions (**Figure 76a**). In case of the blend with 10 wt.% JPs, due to complete adhesion of the phases and the JP mediated linkage, both phases can foam together, which results in a more homogenous cellular structure (**Figure 76b**).

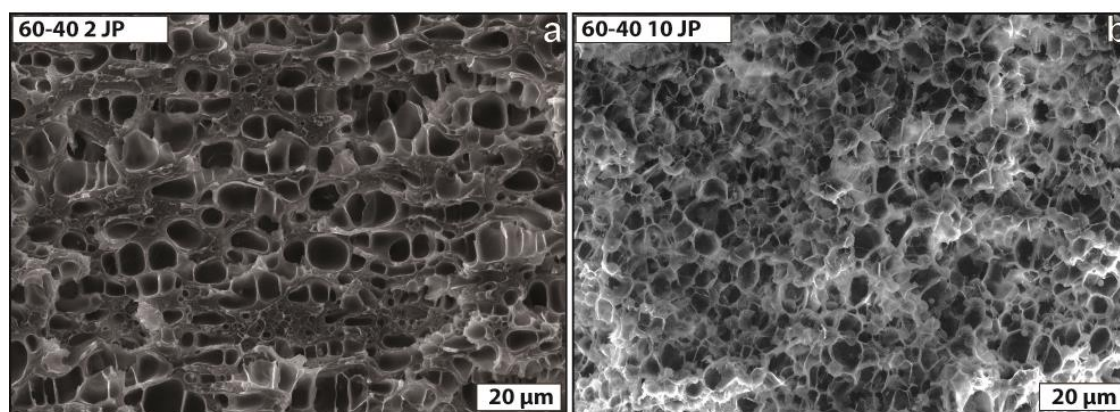


**Figure 76** Cellular structure of PPE/SAN (60/40) foams with a) 2 (density of 535 kg/m<sup>3</sup>) and b) 10 wt.% JPs (density of 650 kg/m<sup>3</sup>)

The minimum foam density was achieved with the PPE/SAN (60/40) blend containing 2 wt.% JPs (535 kg/m<sup>3</sup>), which contains cells with a diameter of 1.7 µm. In this case, the SAN phase is predominantly foamed into larger cell sizes due to the weak attachment of the PPE phase to it. In the end, it is concluded that a foaming temperature of 140 °C and foaming time of 10 s is the best combination to obtain homogeneous foams of PPE/SAN blends compatibilized with JPs, with a very small cell sizes of 1.8-0.9 µm but at relatively high densities of 350 – 650 kg/m<sup>3</sup>. **Figure 77** summarizes the densities and cell sizes of JP compatibilized blend foams at optimum processing conditions.

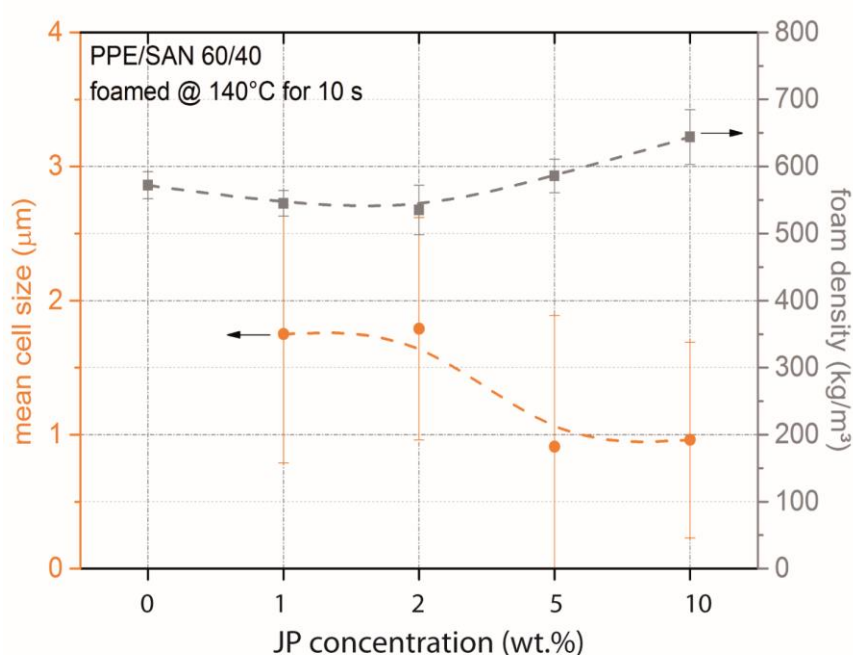


**Figure 77** Correlation of mean cell size and foam density with a focus on the effect of compatibilization of PPE/SAN blend with JPs

One can conclude that the use of highly interfacial active JPs as compatibilizer promotes a better nucleation compared to the neat blend during foaming. At the same time, the strong binding of the JPs at the interface would allow for production of open cellular foam structures. Even though these results give a first positive impression of the role of JPs during foaming, the role of having both JPs and SBM triblock terpolymers in the blend may lead to synergistic effects similar to the ones observed in case of fracture toughness behaviour of the materials. Hence, further studies in this area would be of high interest.

### 6.2.2 Different JPs and JP modified structures

Beside symmetrical JPs used in this work, there has been many advances regarding synthesizing JPs with unsymmetrical geometries, and other complex compartmentalized nanostructures [133,136]. It is expected that the use of Janus nanoparticles with unequal-sized volume ratios of the corona hemispheres (Janus balance) could result in even smaller droplets than the ones reported in the current study. Synergetic effects of JPs in combination with other conventional compatibilizers, especially JPs with Janus balance in favour of the stabilizing patch is an

interesting case study that can be followed. Ruhland et. al investigated the self-assembly behaviour of Janus particles with different geometries at a liquid-liquid interface. They have shown that Janus particles with different geometries such as cylinders and discs (**Figure 78**) have even higher interfacial activities than the spherical particles used in this study [154]. Therefore, it is of high scientific interest to study them as compatibilizers during melt blending. However, currently the bottle neck in conducting such research would be synthesizing such particles on a larger scale in order to be able to test them under industrially relevant conditions. Effect of such novel particles on the melt blending process, rheological, morphological, and mechanical properties of different polymer blends is of high scientific interest.

Additionally, these multicompartiment structures could be patched on fillers such as carbon nanotubes to improve their dispersion in polymer blends [271]. It has been shown that self-assembled worm like micelles with patchy PS/PMMA coronas have interfacial activities comparable of Janus cylinders [272]. Using similar patchy coronas on carbon nanotubes would lead to multi functionality of fillers in polymers where compatibilization and reinforcement are addressed simultaneously. These particles and their behaviours in PPE/SAN blends could also be an interesting topic to follow.

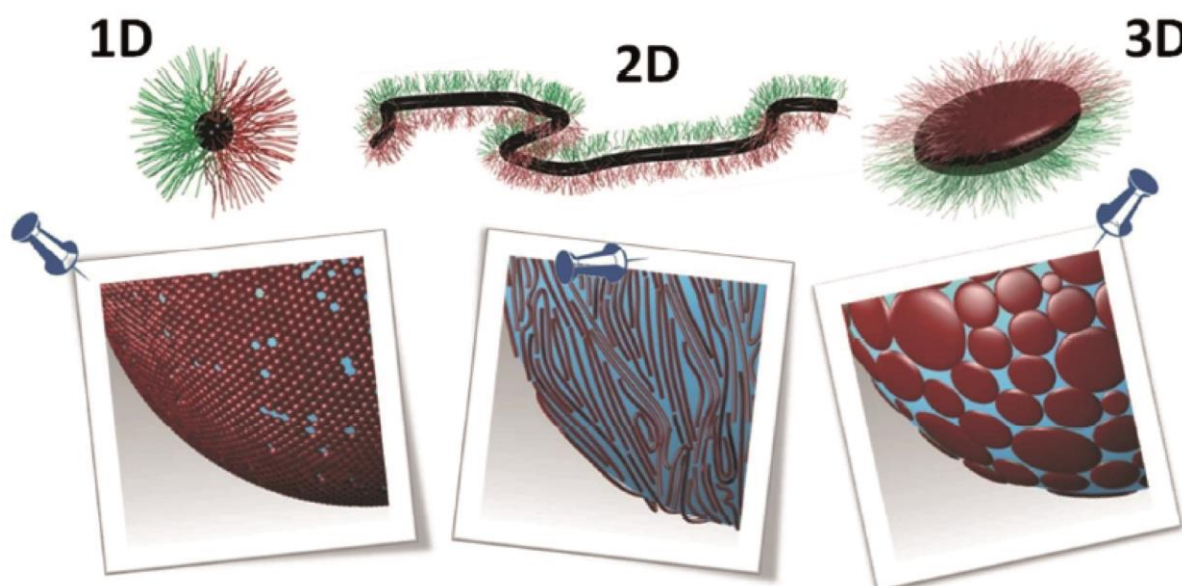


**Figure 78** Overview of possible Janus architectures and their correlating packing behaviour at liquid/liquid interfaces [154]

## 7 Bibliography

- [1] Wang J, Huang Z, Duan H, Yu S, Feng X, Wang G, et al. Surface stress effect in mechanics of nanostructured materials. *Acta Mech Solida Sin* 2011;24:52–82.
- [2] Gleiter H. Nanostructured materials: state of the art and perspectives. *Nanostructured Mater* 1995;6:3–14.
- [3] Gleiter H. Nanostructured materials: basic concepts and microstructure. *Acta Mater* 2000;48:1–29.
- [4] Kuncser V, Miu L. Size effects in nanostructures. vol. 205. Berlin, Heidelberg: Springer Berlin Heidelberg; 2014.
- [5] Yu L, Dean K, Li L. Polymer blends and composites from renewable resources. *Prog Polym Sci* 2006;31:576–602.
- [6] Berggren M, Inganäs O, Gustafsson G, Rasmusson J, Andersson MR, Hjertberg T, et al. Light-emitting diodes with variable colours from polymer blends. *Nature* 1994;372:444–6.
- [7] Paul DR, Newman S. *Polymer blends*. Elsevier Inc.; 1978.
- [8] Li G, Shrotriya V, Huang J, Yao Y, Moriarty T, Emery K, et al. High-efficiency solution processable polymer photovoltaic cells by self-organization of polymer blends. *Nat Mater* 2005;4:864–8.
- [9] Manson JA, Sperling LH. *Polymer Blends and Composites*. Boston, MA: Springer US; 1976.
- [10] Geddes C. Why does PPO have to be modified?  
<https://hardiepolymers.wordpress.com/2013/01/03/why-does-ppo-have-to-be-modified/>.
- [11] Ruckdäschel H, Sandler JKW, Altstädt V, Rettig C, Schmalz H, Abetz V, et al. Compatibilisation of PPE/SAN blends by triblock terpolymers: Correlation between block terpolymer composition, morphology and properties. *Polymer* 2006;47:2772–90.
- [12] Lach R, Grellmann W, Weidisch R, Altstädt V, Kirschnick T, Ott H, Stadler R, Mehler C. Poly(styrene-block-butadiene-block-styrene-block-butadiene) and poly(styrene-block-butadiene-block-methyl methacrylate) copolymers as compatibilizers in PPO–SAN Blends: I. Morphology and fracture behavior. *J Appl Polym Sci* 2000;78:2037–45.
- [13] Gottschalk A, Mühlbach K, Seitz F, Stadler R, Auschra C. Blends of poly(2,6-dimethyl-1,4-phenylene oxide) with styrene copolymers. *Macromol Symp* 1994;83:127–46.
- [14] Walther A, Matussek K, Müller AHE. Engineering nanostructured polymer blends with controlled nanoparticle location using Janus particles. *ACS Nano* 2008;2:1167–78.
- [15] Leibler L. Nanostructured plastics: Joys of self-assembling. *Prog Polym Sci* 2005;30:898–914.
- [16] Paul DR, Bucknall CB. *Polymer Blends*. New York: Wiley; 2000.

- 
- [17] Utracki LA. Commercial polymer blends. 1st ed. London: Chapman and Hall; 1998.
- [18] Robeson LM. Polymer blends: a comprehensive review. Hanser Verlag; 2007.
- [19] Harrats C, Sabu T, Groeninckx G. Micro- and nanostructured multiphase polymer blend systems. Taylor & Francis Group; 2006.
- [20] Utracki LA. Polymer alloys and blends (Thermodynamics and rheology). Hanser Verlag; 1990.
- [21] Shonaike GO, Simon GP. Polymer blends and alloys. Marcel Dekker Inc.; 1999.
- [22] Shultz AR, Gendron BM. Thermo-optical and differential scanning calorimetric observations of mobility transitions in polystyrene-poly(2,6-dimethyl-1,4-phenylene oxide) blends. *J Appl Polym Sci* 1972;16:461–71.
- [23] Prest WM, Porter RS. Rheological properties of poly(2,6-dimethylphenylene oxide)—polystyrene blends. *J Polym Sci Part B Polym Phys* 1972;10:1639–55.
- [24] Van de Grampel HT. Blends and Alloys of Engineering Thermoplastics. Rapra Technology Limited; 1992.
- [25] Alberti D. Modifizierte aromatische Polyether. *Kunststoffe* 1987;10.
- [26] Suess M, Kressler J, Kammer HW. The miscibility window of poly(methylmethacrylate)/poly(styrene-co-acrylonitrile) blends. *Polymer* 1987;28:957–60.
- [27] Cowie JMG, Lath D. Miscibility mapping in some blends involving poly(styrene-co-acrylonitrile). *Macromol Symp* 1988;16:103–12.
- [28] Zheng SX, Li J, Guo QP, Mi YL. In situ polymerization preparation of blends of poly(methyl methacrylate) and poly(styrene-co-acrylonitrile). *J Mater Sci* 1997;32:3463–8.
- [29] Zhang Q, Du M, Yang B, Wu G. Relationship between dynamic rheological behavior and phase separation of poly(methyl methacrylate)/poly(styrene-co-acrylonitrile) blends. *Polmer* 2001;42:5743–7.
- [30] Kumaraswamy GN, Ranganathaiah C, Deepa Urs M V., Ravikumar HB. Miscibility and phase separation in SAN/PMMA blends investigated by positron lifetime measurements. *Eur Polym J* 2006;42:2655–66.
- [31] Merfeld GD, Karim A, Majumdar B, Satija SK, Paul DR. Interfacial thickness in bilayers of poly(phenylene oxide) and styrenic copolymers. *J Polym Sci Part B Polym Phys* 1998;36:3115–25.
- [32] Flory PJ. Thermodynamics of high polymer solutions. *J Chem Phys* 1942;10:51–61.
- [33] Huggins ML. Some properties of solutions of long-chain compounds. *J Phys Chem* 1942;46:151–8.
- [34] Coleman MM, Graf JF, Painter PC. Specific interactions and the miscibility of polymer blends. CRC Press; 1991.
- [35] Datta S, Lohse DJ. Polymeric compatibilizers: Uses and benefits in polymer blends. Hanser

- Verlag; 1996.
- [36] Utracki LA. History of commercial polymer alloys and blends (from a perspective of the patent literature). *Polym Eng Sci* 1995;35:2–17.
- [37] Utracki LA. *Polymer blends handbook*. Kluwer Academic Pub; 2002.
- [38] Macosko CW. Morphology development and control in immiscible polymer blends. *Macromol Symp* 2000;149:71–184.
- [39] Paul D, Newman S. *Polymer blends*. Elsevier Inc.; 1978.
- [40] Mark HF, Bikales NM. *Encyclopedia of polymer science and technology*. John Wiley & Sons Inc.; 1987.
- [41] Shields RJ, Bhattacharyya D, Fakirov S. Fibrillar polymer-polymer composites: morphology, properties and applications. *J Mater Sci* 2008;43:6758–70.
- [42] Monticciolo A, Cassagnau P, Michel A. Fibrillar morphology development of PE/PBT blends: Rheology and solvent permeability. *Polym Eng Sci* 1998;38:1882–9.
- [43] Hong JS, Ahn KH, Lee SJ. Strain hardening behavior of polymer blends with fibril morphology. *Rheol Acta* 2005;45:202–8.
- [44] Liu X, Fan X-D, Tang M-F, Nie Y. Synthesis and characterization of core-shell acrylate based latex and study of its reactive blend. *Int J Mol Sci* 2008;9:342–54.
- [45] Luzinov I, Pagnouille C, Jérôme R. Ternary polymer blend with core-shell dispersed phases: effect of the core-forming polymer on phase morphology and mechanical properties. *Polymer* 2000;41:7099–109.
- [46] Li L-P, Yin B, Yang M-B. Morphology prediction and the effect of core-shell structure on the rheological behavior of PP/EPDM/HDPE ternary blends. *Polym Eng Sci* 2011;51:2425–33.
- [47] Macosko CW, Gue P, Khandpur AK, Nakayama A, Marechal P, Inoue T. Compatibilizers for Melt Blending: Premade Block Copolymers. *Macromolecules* 1996;29:5590–8.
- [48] Luciani A, Jarrin J, Dewimille B. Morphology development during polymer blending. *Le J Phys IV* 1993;3:C7-1577-C7-1580.
- [49] Luciani A, Jarrin J. Morphology development in immiscible polymer blends. *Polym Eng Sci* 1996;36:1619–26.
- [50] Tucker III CL, Moldenaers P. Microstructure evolution in polymer blends. *Annu Rev Fluid Mech* 2002;34:177–210.
- [51] Puyvelde P Van, Moldenaers P. Rheology and morphology development in immiscible polymer blends. *Rheol Rev* 2005:101–45.
- [52] Pötschke P, Paul DR. Formation of co-continuous structures in melt-mixed immiscible polymer blends. *J Macromol Sci Part C Polym Rev* 2003;43:87–141.
- [53] Lyngaae-Jørgensen J, Utracki LA. Dual phase continuity in polymer blends. *Makromol Chemie Macromol Symp* 1991;48–49:189–209.

- 
- [54] Palierne JF. Linear rheology of viscoelastic emulsions with interfacial tension. *Rheol Acta* 1990;29:204–14.
- [55] Erratum. *Rheol Acta* 1991;30:497–497.
- [56] Graebling D, Muller R, Palierne JF. Linear viscoelastic behavior of some incompatible polymer blends in the melt. Interpretation of data with a model of emulsion of viscoelastic liquids. *Macromolecules* 1993;26:320–9.
- [57] Lacroix C, Bousmina M, Carreau PJ, Favis BD, Michel A. Properties of PETG/EVA blends: 1. Viscoelastic, morphological and interfacial properties. *Polymer* 1996;37:2939–47.
- [58] Lacroix C, Bousmina M, Carreau PJ, Llauro MF, Pétiard R, Michel A. Properties of PETG/EVA blends: 2. Study of reactive compatibilization by n.m.r. spectroscopy and linear viscoelastic properties. *Polymer* 1996;37:2949–56.
- [59] Macaúbas PH., Demarquette N. Morphologies and interfacial tensions of immiscible polypropylene/polystyrene blends modified with triblock copolymers. *Polymer* 2001;42:2543–54.
- [60] Friedrich C, Honerkamp J, Weese J. New ill-posed problems in rheology. *Rheol Acta* 1996;35:186–93.
- [61] Vinckier I, Moldenaers P, Mewis J. Relationship between rheology and morphology of model blends in steady shear flow. *J Rheol* 1996;40:613–631.
- [62] Janssen JJM, Boon A, Agterof WGM. Influence of dynamic interfacial properties on droplet breakup in plane hyperbolic flow. *AIChE J* 1997;43:1436–47.
- [63] Grace HP. Dispersion phenomena in high viscosity immiscible fluid systems and application of static mixers as dispersion devices in such systems. *Chem Eng Commun* 1982;14:225–77.
- [64] Janssen JMH. Dynamics of liquid-liquid mixing. Technische Universiteit Eindhoven, 1993.
- [65] Duin VAN, Jerome R. Strategies for compatibilization polymer blends. *Prog Polym Sci* 1998;23:707–57.
- [66] Lohse DJ, Datta S, Kresge EN. Graft copolymer compatibilizers for blends of polypropylene and ethylene-propylene copolymers. *Macromolecules* 1991;24:561–6.
- [67] Crist B, Nesarikar AR. Coarsening in polyethylene-copolymer blends. *Macromolecules* 1995;28:890–6.
- [68] Yu W, Zhou C, Inoue T. A coalescence mechanism for the coarsening behavior of polymer blends during a quiescent annealing process. I. Monodispersed particle system. *J Polym Sci Part B Polym Phys* 2000;38:2378–89.
- [69] Milner ST, Xi H. How copolymers promote mixing of immiscible homopolymers. *J Rheol* 1996;40:663–687.
- [70] Scott CE, Macosko CW. Morphology development during the initial stages of polymer-polymer blending. *Polymer* 1995;36:461–70.
- [71] Cerclé C, Favis BD. Generalizing interfacial modification in polymer blends. *Polymer*

- 2012;53:4338–43.
- [72] Cai X, Li B, Pan Y, Wu G. Morphology evolution of immiscible polymer blends as directed by nanoparticle self-agglomeration. *Polymer* 2012;53:259–66.
- [73] Kim BJ, Bang J, Hawker CJ, Chiu JJ, Pine DJ, Jang SG, et al. Creating surfactant nanoparticles for block copolymer composites through surface chemistry. *Langmuir* 2007;23:12693–703.
- [74] Jang SG, Kramer EJ, Hawker CJ. Controlled supramolecular assembly of micelle-like gold nanoparticles in PS-*b*-P2VP diblock copolymers via hydrogen bonding. *J Am Chem Soc* 2011;133:16986–96.
- [75] Zhao Y, Thorkelsson K, Mastroianni AJ, Schilling T, Luther JM, Rancatore BJ, et al. Small-molecule-directed nanoparticle assembly towards stimuli-responsive nanocomposites. *Nat Mater* 2009;8:979–85.
- [76] Cao Y, Zhang J, Feng J, Wu P. Compatibilization of immiscible polymer blends using graphene oxide sheets. *ACS Nano* 2011;5:5920–7.
- [77] Du B, Handge UA, Majeed S, Abetz V. Localization of functionalized MWCNT in SAN/PPE blends and their influence on rheological properties. *Polymer* 2012;53:5491–501.
- [78] Balazs AC, Emrick T, Russell TP. Nanoparticle polymer composites: where two small worlds meet. *Science* 2006;314:1107–10.
- [79] Kao J, Thorkelsson K, Bai P, Rancatore BJ, Xu T. Toward functional nanocomposites: taking the best of nanoparticles, polymers, and small molecules. *Chem Soc Rev* 2013;42:2654–78.
- [80] Auschra C, Stadler R, Voigt-Martin IG. Poly(styrene-*b*-methyl methacrylate) block copolymers as compatibilizing agents in blends of poly(styrene-*co*-acrylonitrile) and poly(2,6-dimethyl-1,4-phenylene ether): 1. Location of block copolymers in ternary blends — compatibilization versus micelle for. *Polymer* 1993;34:2081–93.
- [81] Utracki LA. Compatibilization of polymer blends. *Can J Chem Eng* 2002;80:1008–16.
- [82] Utracki LA. *Polymer Alloys and Blends*. Hanser Gardner Publications ; 1989.
- [83] Koning C, van Duin M, Pagnouille C, Jerome R. Strategies for compatibilization of polymer blends. *Prog Polym Sci* 1998;23:707–57.
- [84] Osswald TA, Menges G. *Material science of polymers for engineers*. Hanser Publishers; 2012.
- [85] Kim H, Ryu JG, Lee JW. Evolution of phase morphology and in-situ compatibilization of polymer blends during ultrasound-assisted melt mixing. *Korea-Australia Rheol J* 2002;14:121–8.
- [86] Clark JN, Higgins JS, Peiffer DG. Reduction in domain size in polymer mixtures via charge transfer interactions. *Polym Eng Sci* 1992;32:49–56.
- [87] El-Sabbagh SH. Compatibility study of natural rubber and ethylene-propylene-diene rubber blends. *J Appl Polym Sci* 2003;90:1–11.

- [88] Lo D-W, Chiang C-R, Chang F-C. Reactive compatibilization of PET and PPE blends by epoxy couplers. *J Appl Polym Sci* 1997;65:739–53.
- [89] Galloway JA, Jeon HK, Bell JR, Macosko CW. Block copolymer compatibilization of cocontinuous polymer blends. *Polymer* 2005;46:183–91.
- [90] Lombeck F, Sepe A, Thomann R, Friend RH, Sommer M. Compatibilization of all-conjugated polymer blends for organic photovoltaics. *ACS Nano* 2016;10:8087–96.
- [91] Yousfi M, Livi S, Dumas A, Crépin-Leblond J, Greenhill-Hooper M, Duchet-Rumeau J, et al. Ionic compatibilization of polypropylene/polyamide 6 blends using an ionic liquids/nanotalc filler combination: morphology, thermal and mechanical properties. *RSC Adv* 2015;5:46197–205.
- [92] Shumigin D, Tarasova E, Krumme A, Meier P. Rheological and mechanical properties of poly(lactic) acid/cellulose and LDPE/cellulose composites. *Mater Sci* 2011;17:1392–1320.
- [93] Xavier P, Rao P, Bose S, Balazs AC, Emrick T, Russell TP, et al. Nanoparticle induced miscibility in LCST polymer blends: critically assessing the enthalpic and entropic effects. *Phys Chem Chem Phys* 2016;18:47–64.
- [94] Wang J, Velankar SS. Strain recovery of model immiscible blends: effects of added compatibilizer. *Rheol Acta* 2006;45:741–53.
- [95] Velankar S, Van Puyvelde P, Mewis J, Moldenaers P. Steady-shear rheological properties of model compatibilized blends. *J Rheol* 2004;48:725–744.
- [96] Martin JD, Velankar SS. Effects of compatibilizer on immiscible polymer blends near phase inversion. *J Rheol* 2007;51:669–692.
- [97] Münstedt H. Rheological and morphological properties of dispersed polymeric materials : filled polymers and polymer blends. Hanser Verlag; 2016.
- [98] Starý Z, Pemsel T, Baldrian J, Münstedt H. Influence of a compatibilizer on the morphology development in polymer blends under elongation. *Polymer* 2012;53:1881–9.
- [99] Duvall J, Sellitti C, Myers C, Hiltner A, Baer E. Interfacial effects produced by crystallization of polypropylene with polypropylene-g-maleic anhydride compatibilizers. *J Appl Polym Sci* 1994;52:207–16.
- [100] Duvall J, Sellitti C, Myers C, Hiltner A, Baer E. Effect of compatibilization on the properties of polypropylene/polyamide-66 (75/25 wt/wt) blends. *J Appl Polym Sci* 1994;52:195–206.
- [101] Jeon HK, Feist BJ, Koh SB, Chang K, Macosko CW, Dion RP. Reactively formed block and graft copolymers as compatibilizers for polyamide 66/PS blends. *Polymer* 2004;45:197–206.
- [102] Hussain AI, Tawfic ML, Khalil AA, Awad TE. High Performance Emulsified EPDM grafted with vinyl acetate as compatibilizer for EPDM with polar rubber. *Nat Sci* 2010;8:348–357.
- [103] Fu X, Hu K, Kong W, Bao L, Wang J, Lei J. Synthesis and characterization of poly(styrene-block-n-butyl acrylate) pentablock copolymer via RAFT emulsion polymerization

- mediated by amphiphilic macroRAFT agent combined with pre-emulsion technology. *Polym Bull* 2016;73:1649–71.
- [104] Fenouillot F, Cassagnau P, Majesté J-C. Uneven distribution of nanoparticles in immiscible fluids: Morphology development in polymer blends. *Polymer* 2009;50:1333–50.
- [105] Zuza E, Lejardi A, Ugartemendia JM, Monasterio N, Meaurio E, Sarasua J-R. Compatibilization through specific interactions and dynamic fragility in poly(D,L-lactide)/polystyrene blends. *Macromol Chem Phys* 2008;209:2423–33.
- [106] Pearce EM, Kwei TK, Min BY. Polymer compatibilization through hydrogen bonding. *J Macromol Sci Part A - Chem* 1984;21:1181–216.
- [107] Xu X. Compatibilization of PBT / PP blends by adding side-chain liquid crystalline ionomer with quaternary pyridinium groups. *Chem Res Chinese Univ* 2011;27:140–4.
- [108] Gemeinhardt GC, Moore AA, Moore RB. Influence of ionomeric compatibilizers on the morphology and properties of amorphous polyester/polyamide blends. *Polym Eng Sci* 2004;44:1721–31.
- [109] Lee Y-D, Chen C-M. Properties of PVC/CPE/EPDM polyblends. *J Appl Polym Sci* 1987;33:1231–40.
- [110] Zenkert D, Burman M. Tension, compression and shear fatigue of a closed cell polymer foam. *Compos Sci Technol* 2009;69:785–92.
- [111] Chow WS, Mohd Ishak ZA. Polyamide blend-based nanocomposites: A review. *Express Polym Lett* 2015;9:211–32.
- [112] Karger-Kocsis J (József), Fakirov S. Nano- and micro-mechanics of polymer blends and composites. Hanser; 2009.
- [113] Laoutid F, Picard A, Persenaire O, Dubois P. Investigation of the alumina nanoparticle role in the enhancement of the mechanical properties of polyamide/polycarbonate blends. *Polym Degrad Stab* 2015;112:137–44.
- [114] Goodarzi V, Jafari SH, Khonakdar HA, Seyfi J. Morphology, rheology and dynamic mechanical properties of PP/EVA/clay nanocomposites. *J Polym Res* 2011;18:1829–39.
- [115] Anastasiadis SH, Gancarz I, Koberstein JT. Interfacial tension of immiscible polymer blends: temperature and molecular weight dependence. *Macromolecules* 1988;21:2980–7.
- [116] Creton C, Kramer EJ, Hadziioannou G. Critical molecular weight for block copolymer reinforcement of interfaces in a two-phase polymer blend. *Macromolecules* 1991;24:1846–53.
- [117] Auschra C, Stadler R, Chemie O, Becherweg JJ. New ordered morphologies in ABC triblock copolymers. *Macromolecules* 1993;9:2171–4.
- [118] Auschra C, Stadler R, Voigt-Martin IG. Poly(styrene-*b*-methyl methacrylate) block copolymers as compatibilizing agents in blends of poly(styrene-*co*-acrylonitrile) and poly(2,6-dimethyl-1,4-phenylene ether): 2. Influence of concentration and molecular weight of symmetric block copolymers. *Polymer* 1993;34:2094–110.

- [119] Stadler R, Auschra C, Beckmann J, Krappe U, Voigt-Martin I, Leibler L. Morphology and thermodynamics of symmetric poly ( A-block-B-block-C) triblock copolymers. *Macromolecules* 1995;28:3080–97.
- [120] Breiner U, Krappe U, Abetz V, Stadler R. Cylindrical morphologies in asymmetric ABC triblock copolymers. *Macromol Chem Phys* 1997;198:1051–83.
- [121] Abetz V, Goldacker T. Formation of superlattices via blending of block copolymers. *Macromol Rapid Commun* 2000;21:16–34.
- [122] Liang Z, Williams HL. Dynamic mechanical properties of polypropylene–polyamide blends: Effect of compatibilization. *J Appl Polym Sci* 1992;44:699–717.
- [123] Kalfoglou NK, Skafidas DS, Kallitsis JK, Lambert J-C, Van der Stappen L. Comparison of compatibilizer effectiveness for PET/HDPE blends. *Polymer* 1995;36:4453–62.
- [124] Papadopoulou CP, Kalfoglou NK. Comparison of compatibilizer effectiveness for PET/PP blends: their mechanical, thermal and morphology characterization. *Polymer* 2000;41:2543–55.
- [125] Pang YX, Jia DM, Hu HJ, Hourston DJ, Song M. Effects of a compatibilizing agent on the morphology, interface and mechanical behaviour of polypropylene/poly(ethylene terephthalate) blends. *Polymer* 2000;41:357–65.
- [126] Lee JB, Lee YK, Choi GD, Na SW, Park TS, Kim WN. Compatibilizing effects for improving mechanical properties of biodegradable poly (lactic acid) and polycarbonate blends. *Polym Degrad Stab* 2011;96:553–60.
- [127] Del Castillo-Castro T, Castillo-Ortega MM, Herrera-Franco PJ, Rodríguez-Félix DE. Compatibilization of polyethylene/polyaniline blends with polyethylene-graft-maleic anhydride. *J Appl Polym Sci* 2011;119:2895–901.
- [128] Auschra C, Stadler R. Polymer alloys based on poly( 2,6-dimethyl-1,4-phenylene ether) and poly(styrene-co-acrylonitrile) using poly(styrene-b-(ethylene-co-butylene)-b-methyl methacrylate) triblock copolymers as compatibilizers. *Macromolecules* 1993;26:6364–77.
- [129] Auschra C, Stadler R. Synthesis of block copolymers with poly(methyl methacrylate): P(B-b-MMA), P(EB-b-MMA), P(S-b-B-b-MMA) and P(S-b-EB-b-MMA). *Polym Bull* 1993;30:257–64.
- [130] Breiner U, Krappe U, Jakob T, Abetz V, Stadler R. Spheres on spheres - a novel spherical multiphase morphology in polystyrene-block-polybutadiene-block-poly(methyl methacrylate) triblock copolymers. *Polym Bull* 1998;40:219–26.
- [131] Krappe U, Stadler R, Voigt-Martin I. Chiral assembly in amorphous ABC triblock copolymers. Formation of a helical morphology in polystyrene-block-polybutadiene-block-poly(methyl methacrylate) block copolymers. *Macromolecules* 1995;28:4558–61.
- [132] Breiner U, Krappe U, Stadler R. Evolution of the “knitting pattern” morphology in ABC triblock copolymers. *Macromol Rapid Commun* 1996;17:567–75.
- [133] Gröschel AH, Schacher FH, Schmalz H, Borisov O V., Zhulina EB, Walther A, et al. Precise hierarchical self-assembly of multicompartiment micelles. *Nat Commun* 2012;3:710–20.

- [134] Löbbling TI, Borisov O, Haataja JS, Ikkala O, Gröschel AH, Müller AHE. Rational design of ABC triblock terpolymer solution nanostructures with controlled patch morphology. *Nat Commun* 2016;7:12097–12107.
- [135] Gröschel AH. Bottom-up self-assembly across hierarchies: From triblock terpolymers to patchy particles to colloidal (co-)polymers. Bayreuth University, 2012.
- [136] Walther A, Gödel A, Müller AHE. Controlled crosslinking of polybutadiene containing block terpolymer bulk structures: A facile way towards complex and functional nanostructures. *Polymer* 2008;49:3217–27.
- [137] Löbbling TI. Exploring the structural complexity of compartmentalized nanostructures of triblock terpolymers. Bayreuth University, 2016.
- [138] Binks BP, Fletcher PDI. Particles adsorbed at the oil–water interface: A theoretical comparison between spheres of uniform wettability and “Janus” particles. *Langmuir* 2001;17:4708–10.
- [139] Pickering SU. CXCVI.—Emulsions. *J Chem Soc, Trans* 1907;91:2001–21.
- [140] Walther A, Müller AHE, Hektor HJ, Scholtmeijer K, Casagrande C, Veyssié M, et al. Janus particles. *Soft Matter* 2008;4:663–8.
- [141] Walther A, Hoffmann M, Müller AHE. Emulsion polymerization using Janus particles as stabilizers. *Angew Chem Int Ed* 2008;47:711–4.
- [142] Gröschel AH, Löbbling TI, Petrov PD, Müllner M, Kuttner C, Wieberger F, et al. Janus micelles as effective supracolloidal dispersants for carbon nanotubes. *Angew Chem Int Ed* 2013;52:3602–6.
- [143] Kim S, Lee SY, Yang S. Janus microspheres for a highly flexible and impregnable water-repelling interface. *Angew Chem Int Ed* 2010;49:2535–8.
- [144] Hirsemann D, Shylesh S, Souza RA De, Diar-bakerly B, Biersack B, Mueller DN, et al. Large-scale, low-cost fabrication of Janus-type emulsifiers by selective decoration of natural kaolinite platelets. *Angew Chem Int Ed* 2012;51:1348–52.
- [145] Walther A, Müller AHE. Janus particles: Synthesis, self-assembly, physical properties, and applications. *Chem Rev* 2013;113:5194–261.
- [146] Wurm F, Kilbinger AFM. Polymeric Janus particles. *Angew Chemie* 2009;121:8564–74.
- [147] Jiang BS, Chen Q, Tripathy M, Luijten E, Schweizer KS, Granick S. Janus particle synthesis and assembly. *Adv Mater* 2010;22:1060–71.
- [148] Kim J, Matsen M. Positioning Janus nanoparticles in block copolymer scaffolds. *Phys Rev Lett* 2009;102:78303–4.
- [149] Xu K, Guo R, Dong B, Yan L-T. Directed self-assembly of Janus nanorods in binary polymer mixture: towards precise control of nanorod orientation relative to interface. *Soft Matter* 2012;8:9581–8.
- [150] Yan L-T, Popp N, Ghosh S-K, Böker A. Self-assembly of Janus nanoparticles in diblock copolymers. *ACS Nano* 2010;4:913–20.

- 
- [151] Huang M, Li Z, Guo H. The effect of Janus nanospheres on the phase separation of immiscible polymer blends via dissipative particle dynamics simulations. *Soft Matter* 2012;8:6834–6845.
- [152] Nicole Glaser, Dave J. Adams, Alexander Böker, Georg Krausch. Janus particles at liquid–liquid interfaces. *Langmuir* 2006;22:5227–9.
- [153] Ruhland TM, Gröschel AH, Walther A, Müller AHE. Janus Cylinders at liquid–liquid interfaces. *Langmuir* 2011;27:9807–14.
- [154] Ruhland TM, Gröschel AH, Ballard N, Skelton TS, Walther A, Müller AHE, et al. Influence of Janus particle shape on their interfacial behavior at liquid–liquid interfaces. *Langmuir* 2013;29:1388–94.
- [155] Bahrami R, Löblich TI, Gröschel AH, Schmalz H, Müller AHE, Altstädt V. The impact of Janus nanoparticles on the compatibilization of immiscible polymer blends under technologically relevant conditions. *ACS Nano* 2014;8:10048–56.
- [156] Bryson KC, Löblich TI, Müller AHE, Russell TP, Hayward RC. Using Janus nanoparticles to trap polymer blend morphologies during solvent-evaporation-induced demixing. *Macromolecules* 2015;48:4220–7.
- [157] Pawar AB, Kretschmar I. Fabrication, assembly, and application of patchy particles. *Macromol Rapid Commun* 2010;31:150–68.
- [158] Park S, Lim J-H, Chung S-W, Mirkin CA. Self-assembly of mesoscopic metal-polymer amphiphiles. *Science* 2004;303:348–51.
- [159] Bryson KC. Controlling the Assembly of nanoparticles in polymer blends. University of Massachusetts, 2016.
- [160] Wang H, Dong W, Li Y. Compatibilization of immiscible polymer blends using in situ formed Janus nanomicelles by reactive blending. *ACS Macro Lett* 2015;4:1398–403.
- [161] Gröschel AH, Walther A, Löblich TI, Schmelz J, Hanisch A, Schmalz H, et al. Facile, solution-based synthesis of soft, nanoscale Janus particles with tunable Janus balance. *J Am Chem Soc* 2012;134:13850–60.
- [162] Utracki LA, Wilkie CA. *Polymer blends handbook*. 2014.
- [163] Michler GH (Goerg H, Baltá-Calleja FJ). *Nano- and micromechanics of polymers : structure modification and improvement of properties*. Hanser; 2012.
- [164] Bucknall CB. *Toughened plastics*. Applied Science Publishers; 1977.
- [165] Haward RN, Young RJ. *The Physics of glassy polymers*. Dordrecht: Springer Netherlands; 1997.
- [166] Kinloch AJ. *Fracture behaviour of polymers*. Applied Science Publishers, London and New York; 1983.
- [167] Argon AS. *The physics of deformation and fracture of polymers*. Cambridge University Press; 2013.
- [168] Kausch HH. *Crazing in Polymers*. vol. 52–53. Berlin/Heidelberg: Springer-Verlag; 1983.

- [169] Kausch HH, Argon AS. *Crazing in polymers Vol. II*. Springer-Verlag; 1997.
- [170] Bubeck RA, Buckley DJ, Kramer EJ, Brown HR. Modes of deformation in rubber-modified thermoplastics during tensile impact. *J Mater Sci* 1991;26:6249–59.
- [171] Wu S. Chain structure, phase morphology, and toughness relationships in polymers and blends. *Polym Eng Sci* 1990;30:753–61.
- [172] Wu S. Control of intrinsic brittleness and toughness of polymers and blends by chemical structure: A review. *Polym Int* 1992;29:229–47.
- [173] Kirschnick T, Gottschalk A, Ott H, Abetz V, Puskas J, Altstädt V. Melt processed blends of poly(styrene-co-acrylonitrile) and poly(phenylene ether) compatibilized with polystyrene-*b*-polybutadiene-*b*-poly(methyl methacrylate) triblock terpolymers. *Polymer* 2004;45:5653–60.
- [174] Wellinghoff ST, Baer E. Microstructure and its relationship to deformation processes in amorphous polymer glasses. *J Appl Polym Sci* 1978;22:2025–45.
- [175] Knott JF. *Fundamentals of fracture mechanics*. Butterworth & Co Publishers Ltd; 1973.
- [176] Anderson TL, Ted L. *Fracture mechanics: fundamentals and applications*. Taylor & Francis; 2005.
- [177] Irwin GR. *Fracture dynamics. Fracture of metals*. Am Soc Met (Cleveland) 1948:147–66.
- [178] Orowan E. *Fracture and strength of solids. Reports Prog Phys* 1948;12:185–232.
- [179] Orowan E. Energy criterion of fracture, welding criterion of fracture. *Weld Res Suppl* 1955;34:157–60.
- [180] D5045-14 AS. *Standard test methods for plane-strain fracture toughness and strain energy release rate of plastic materials*.
- [181] ASTM Standard: 399-90. *Standard test method for plane-strain fracture toughness of metallic materials 1. 399–90*, 1997.
- [182] Handge UA, Sailer C, Steininger H, Weber M, Scholtyssek S, Seydewitz V, et al. Micromechanical processes and failure phenomena in reactively compatibilized blends of polyamide 6 and styrenic polymers. II. Polyamide 6/styrene-acrylonitrile copolymer blends. *J Appl Polym Sci* 2010;115:2529–39.
- [183] Michler GH. Microstructural construction of polymers with improved mechanical properties. *Polym Adv Technol* 1998;9:812–22.
- [184] Tiejun W, Kishimoto K, Notomi M. Effect of triaxial stress constraint on the deformation and fracture of polymers. *Acta Mech Sin* 2002;18:480–93.
- [185] Handge UA, Galeski A, Kim SC, Dijkstra DJ, Götz C, Fischer F, et al. Melt processing, mechanical, and fatigue crack propagation properties of reactively compatibilized blends of polyamide 6 and acrylonitrile-butadiene-styrene copolymer. *J Appl Polym Sci* 2012;124:740–54.
- [186] Takayama T, Todo M, Tsuji H. Effect of annealing on the mechanical properties of PLA/PCL and PLA/PCL/LTI polymer blends. *J Mech Behav Biomed Mater* 2011;4:255–60.

- [187] Todo M, Takayam T. Fracture Mechanisms of Biodegradable PLA and PLA/PCL Blends. *Biomater. - Phys. Chem., InTech*; 2011:375–394.
- [188] Richard HA, Sander M. *Ermüdungsrisse*. Wiesbaden: Teubner Verlag; 2012.
- [189] ISO 15850. *Plastics - Determination of tension-tension fatigue crack propagation -- Linear elastic fracture mechanics (LEFM) approach*. 2014.
- [190] Hertzberg RW, Manson JA. *Fatigue of engineering plastics*. Academic Press; 1980.
- [191] Richard HA, Sander M. *Ermüdungsrisse: erkennen, sicher beurteilen, vermeiden*. Springer Vieweg; 2012.
- [192] Paris P, Erdogan F. A critical analysis of crack propagation laws. *J Basic Eng* 1963;85:528–533.
- [193] Kothmann MH, Zeiler R, Anda AR De, Brückner A, Altstädt V. Fatigue crack propagation behaviour of epoxy resins modified with silica-nanoparticles. *Polymer* 2015;60:157–63.
- [194] Saxena A, Hudak SJ. Review and extension of compliance information for common crack growth specimens. *Int J Fract* 1978;14:453–68.
- [195] E1820 AS. *Standard Test Method for Measurement of Fracture Toughness*.
- [196] Zehnder AT. *Fracture Mechanics*. vol. 62. Dordrecht: Springer Netherlands; 2012.
- [197] Schwalbe KH, editor. *The crack tip opening displacement in elastic-plastic fracture mechanics*. Springer Berlin Heidelberg; 1986.
- [198] Hertzberg RW, Nordberg H, Manson JA. Fatigue crack propagation in polymeric materials. *J Mater Sci* 1907;5:521–6.
- [199] Bureau MN, Dickson JI. Fatigue propagation behaviour of polystyrene/polyethylene blends. *J Mater Sci* 1998;33:1405–19.
- [200] Bureau MN, DI Francesco E, Denault J, Dickson JI. Mechanical behaviour of injection-molded polystyrene/polyethylene blends: Fracture toughness vs. fatigue crack propagation. *Polym Eng Sci* 1999;39:1119–29.
- [201] Koster C, Altstädt V, Kausch HH, Cantwell WJ. Split rate fatigue propagation in polymer blends. *Polym Bull* 1995;34:243–8.
- [202] Morelli TA, Takemori MT. Fatigue crack advance mechanisms in polymers: rubber toughening mechanisms in blends of poly (2, 6-dimethy1-1, 4-phenylene oxide) and polystyrene. *J Mater Sci* 1983;18:1836–44.
- [203] Wyzguski MG, Novak GE. Fatigue-resistant nylon alloys. *J Appl Polym Sci* 1994;51:873–85.
- [204] Ramsteiner F, Armbrust T. Fatigue crack growth in polymers. *Polym Test* 2001;20:321–7.
- [205] Ruckdäschel H, Fischer F, Altstädt V, Müller AHE. Fatigue crack growth behavior of multiphase blends. *J Solid Mech Mater Eng* 2008;2:417–27.
- [206] Bahrami R, Löbbling TI, Schmalz H, Müller AHE, Altstädt V. Micromechanics of “raspberry” morphology in PPE/SAN polymer blends compatibilized with linear ABC triblock terpolymers. *Polymer* 2015;80:52–63.

- [207] Shariatpanahi H, Nazokdast H, Hemmati M. Relationship between interfacial tension and dispersed- phase particle size in polymer blends . II . PP/PA6. *J Appl Polym Sci* 2003;88:54–63.
- [208] Kolarik J, Fambri L, Pegoretti A, Penati A. Ternary polymer blends: Prediction of mechanical properties for various phase structures. *Polym Adv Technol* 2000;11:75–81.
- [209] Bucknall CB, Altstädt V. Blends containing core-shell impact modifiers. Part 4 - Fatigue crack growth behaviour. *Plast Rubber Compos* 2004;33:234–41.
- [210] Woishnis W, Ebnesajjad S. Chemical resistance of thermoplastics. William Andrew; 2011.
- [211] Burke J. Solubility parameters: Theory and application. Am Inst Conserv 1984.
- [212] Baur E (Erwin), Ruhrberg K, Woishnis W. Chemical resistance of engineering thermoplastics. William Andrew; 2016.
- [213] Ehrenstein GW (Gottfried W, Pongratz S, Pongratz S. Resistance and stability of polymers. Carl Hanser ; 2013.
- [214] Krebs C, Leu KW. Langzeitverhalten von Thermoplasten: Alterungsverhalten und Chemikalienbeständigkeit. Hanser; 1999.
- [215] Beaucage G, Stein RS, Hashimoto T, Hasegawa H. Tacticity effects on polymer blend miscibility. *Macromolecules* 1991;24:3443–8.
- [216] Laughner MK, Farah H. Impact resistant blends of high heat polycarbonate and aromatic polyester. CA2101321 A1, 1992.
- [217] Laughner MK. Acrylate polymers modified with poly(phenylene ether). US5286790 A, 1992.
- [218] Manjunatha Nanjegowda L, Bommulu R, Juikar V, Hatna S. Investigation on the influence of different compatibilizers on polycarbonate and high density polyethylene blends: Mechanical properties, thermal properties, morphology, and chemical resistance. *Ind Eng Chem Res* 2013;52:5672–82.
- [219] Samsudin SA, Hassan A, Mokhtar M, Jamaluddin SMS. Chemical resistance evaluation of polystyrene/polypropylene blends: Effect of blend compositions and SEBS content. *Malaysian Polym J* 2006;1:11–24.
- [220] Wang H, Shi H. New impact-modified polycarbonate/polyester blends. *Plast Res Online* 2014.
- [221] Mittal V. Functional polymer blends : synthesis, properties, and performances. CRC Press; 2012.
- [222] Ruckdäschel H, Sandler JKW, Altstädt V, Schmalz H, Abetz V, Müller AHE. Toughening of immiscible PPE/SAN blends by triblock terpolymers. *Polymer* 2007;48:2700–19.
- [223] Fowler ME, Barlow JW, Paul DR. Kinetics of adhesion development at PMMA-SAN interfaces. *Polymer* 1987;28:2145–50.
- [224] Dobkowski Z. Determination of critical molecular weight for entangled macromolecules using the tensile strength data. *Rheol Acta* 1995;34:578–85.

- [225] Wool RP. Polymer interfaces. 1st ed. Munich: Carl Hanser; 1995.
- [226] Fischer F, Beier U, Wolff-Fabris F, Altstädt V. Toughened high performance epoxy resin system for aerospace applications. *Sci Eng Compos Mater* 2011;18:209–15.
- [227] Gödel A, Ruckdäschel H, Müller AHE, Pötschke P, Altstädt V. Controlling the phase morphology of immiscible poly(2,6-dimethyl-1,4-phenylene ether)/poly(styrene-co-acrylonitrile) blends via addition of polystyrene. *E-Polymers* 2008;151:1–17.
- [228] Ruckdäschel H. Micro- and nanostructured polymer blends – Processing, properties and foaming behaviour. Bayreuth University, 2008.
- [229] Freeman BD, Hill AJ. Free volume and transport properties of barrier and membrane polymers, 1999, p. 306–25.
- [230] Vallée RAL, Tomczak N, Kuipers L, Vancso GJ, van Hulst NF. Single molecule lifetime fluctuations reveal segmental dynamics in polymers. *Phys Rev Lett* 2003;91:38301–5.
- [231] Vallée RAL, Cotlet M, Hofkens J, De Schryver FC, Müllen K. Spatially heterogeneous dynamics in polymer glasses at room temperature probed by single molecule lifetime fluctuations. *Macromolecules* 2003;36:7752–8.
- [232] Tant MR, Hill AJ. Structure and properties of glassy polymers. American Chemical Society; 1998.
- [233] Vidal Russell E, Israeloff NE. Direct observation of molecular cooperativity near the glass transition. *Nature* 2000;408:695–8.
- [234] Lin B, Sundararaj U. Effect of mixing protocol on compatibilized polymer blend morphology. *Polym Eng Sci* 2006;46:691–702.
- [235] Sundararaj U, Macosko CW, Rolando RJ, Chan HT. Morphology development in polymer blends. *Polym Eng Sci* 1992;32:1814–23.
- [236] Wu S. Formation of dispersed phase in incompatible polymer: Interfacial and rheological effects. *Polym Eng Sci* 1987;27:335–43.
- [237] Favis BD, Chalifoux JP. The effect of viscosity ratio on the morphology of polypropylene/polycarbonate blends during processing. *Polym Eng Sci* 1987;27:1591–600.
- [238] Thomas S, Groeninckx G. Nylon 6/ethylene propylene rubber (EPM) blends: Phase morphology development during processing and comparison with literature data. *J Appl Polym Sci* 1999;71:1405–29.
- [239] Yee M, Souza AMC, Valera TS, Demarquette NR. Stress relaxation behavior of PMMA/PS polymer blends. *Rheol Acta* 2009;48:527–41.
- [240] Burch HE, Scott CE. Effect of viscosity ratio on structure evolution in miscible polymer blends. *Polymer* 2001;42:7313–25.
- [241] Kirchberger A, Münstedt H. Droplet deformation under extensional flow in immiscible and partially miscible polymer blends based on poly(styrene-co-acrylonitrile). *J Rheol* 2010;54:687–704.

- [242] Heino MT, Hietaoja PT, Vainio TP, Seppälä J V. Effect of viscosity ratio and processing conditions on the morphology of blends of liquid crystalline polymer and polypropylene. *J Appl Polym Sci* 1994;51:259–70.
- [243] Utracki LA. On the viscosity-concentration dependence of immiscible polymer blends. *J Rheol* 1991;35:1615–38.
- [244] Chen TH, Su AC. Morphology of poly(p-phenylene sulfide)/polyethylene blends. *Polymer* 1993;34:4826–31.
- [245] Liang J-Z. Predictions of storage modulus of glass bead-filled low-density-polyethylene composites. *Mater Sci Appl* 2010;1:343–9.
- [246] Lewis TB, Nielsen LE. Dynamic mechanical properties of particulate-filled composites. *J Appl Polym Sci* 1970;14:1449–71.
- [247] Payne AR. Effect of dispersion on the dynamic properties of filler-loaded rubbers. *J Appl Polym Sci* 1965;9:2273–84.
- [248] Heinrich G, Vilgis TA. A statistical mechanical approach to the Payne effect in filled rubbers. *Express Polym Lett* 2015;9:291–9.
- [249] Wang Z, Li S, Wei D, Zhao J. Mechanical properties, Payne effect, and Mullins effect of thermoplastic vulcanizates based on high-impact polystyrene and styrene-butadiene rubber compatibilized by styrene-butadiene-styrene block copolymer. *J Thermoplast Compos Mater* 2015;28:1154–72.
- [250] Lipetzky P, Schmauder S. Crack-particle interaction in two-phase composites Part I: Particle shape effects. *Int J Fract* 1994;65:345–58.
- [251] Angola JC, Fujita Y, Sakai T, Inoue T. Compatibilizer-aided toughening in polymer blends consisting of brittle polymer particles dispersed in a ductile polymer matrix. *J Polym Sci Part B Polym Phys* 1988;26:807–16.
- [252] Tjong SC, Xu SA. Ternary polymer composites: PA6,6/maleated SEBS/glass beads. *J Appl Polym Sci* 2001;81:3231–7.
- [253] Nachlis WL, Kambour RP, MacKnight WJ. In situ polymerization of bisphenol-A-carbonate cyclic oligomers in miscible blends with a styrene-acrylonitrile copolymer: phase separation dynamics and the influence of phase dispersion on ductility. *Polymer* 1994;35:3643–57.
- [254] Münstedt H. Rheology of rubber-modified polymer melts. *Polym Eng Sci* 1981;21:259–70.
- [255] Jud K, Kausch HH, Williams JG. Fracture mechanics studies of crack healing and welding of polymers. *J Mater Sci* 1981;16:204–10.
- [256] Kausch HH. *Polymer fracture*, 2nd revised and enlarged edition. Springer-Verlag Heidelberg; 1987.
- [257] Michler GH, Balta-Calleja FJ. *Mechanical Properties of Polymers Based on Nanostructure and Morphology*. Taylor & Francis Group; 2005.
- [258] Lee M, Tzoganakis C, Park CB. Extrusion of PE/PS blends with supercritical carbon

- dioxide. *Polym Eng Sci* 1998;38:1112–20.
- [259] Tejada EH, Sahagun CZ, Gonzales-Nunez R, Rodrigue D. Morphology and mechanical properties of foamed polyethylene-polypropylene blends. *J Cell Plast* 2005;41:417–35.
- [260] Jiang X-L, Xu Z-M, Yuan W-K. Effects of blend morphology on the foaming of polypropylene/low-density polyethylene blends during a batch foaming process. *J Cell Plast* 2009;45:225–41.
- [261] Ruckdaeschel H, Rausch J, Sandler JKW, Altstaedt V, Schmalz H, Mueller a HE. Foaming of miscible and immiscible polymer blends. *Mater Res Soc Symp Proc* 2006;977:46–52.
- [262] Ruckdaeschel H, Rausch J, Sandler JKW, Altstaedt V, Schmalz H, Mueller AHE. Correlation of the melt rheological properties with the foaming behavior of immiscible blends of poly(2,6-dimethyl-1,4-phenylene ether) and poly(styrene-co-acrylonitrile). *Polym Eng Sci* 2008;48:2111–25.
- [263] Gutmann P, Hildebrandt K, Altstädt V, Müller AHE. Foaming of an immiscible blend system using organic liquids as blowing agents. *J Cell Plast* 2010;46:239–58.
- [264] Ramesh NS, Rasmussen DH, Campbell GA. The heterogeneous nucleation of microcellular foams assisted by the survival of microvoids in polymers containing low glass transition particles. Part I: Mathematical modeling and numerical simulation. *Polym Eng Sci* 1994;34:1685–97.
- [265] Nemoto T, Takagi J, Ohshima M. Control of bubble size and location in nano-/microscale cellular poly(propylene)/rubber blend foams. *Macromol Mater Eng* 2008;293:574–80.
- [266] Nemoto T, Takagi J, Ohshima M. Nanocellular foams — Cell structure difference between immiscible and miscible PEEK/PEI polymer blends. *Polym Eng Sci* 2010;50:2408–16.
- [267] Otsuka T, Taki K, Ohshima M. Nanocellular foams of PS/PMMA polymer blends. *Macromol Mater Eng* 2008;293:78–82.
- [268] Panzer U. Polypropylene foams 2002;42:1481–92.
- [269] Lach R, Grellmann W, Weidisch R, Altstädt V, Kirschnick T, Ott H, et al. Poly (styrene-block-butadiene- block-styrene-block-butadiene ) and poly (styrene-block-butadiene-block-methyl methacrylate ) copolymers as compatibilizers in PPO – SAN blends . I . morphology and fracture behavior. *J Appl Polym Sci* 2000;78:2037–45.
- [270] Bärwinkel S, Bahrami R, Löbling TI, Schmalz H, Müller AHE, Altstädt V. Polymer foams made of immiscible polymer blends compatibilized by Janus particles-effect of compatibilization on foam morphology. *Adv Eng Mater* 2016;18:814–25.
- [271] Gegenhuber T, Krekhova M, Schöbel J, Gröschel AH, Schmalz H. “Patchy” carbon nanotubes as efficient compatibilizers for polymer blends. *ACS Macro Lett* 2016;5:306–10.
- [272] Schmelz J, Schacher FH, Schmalz H, Tsai R, Tewari M, Minko T, et al. Cylindrical crystalline-core micelles: pushing the limits of solution self-assembly. *Soft Matter* 2013;9:2101–7.

## Curriculum Vitae

<b>Personal data</b>	Ronak Bahrami born on May/14/1986 in Tehran, Iran
<b>Marital status</b>	Married
<b>Nationality</b>	German/Iranian
<b>Education</b>	2000 - 2004 Sianat Highschool Diploma in Mathematics & Physics
	2004 - 2009 Amirkabir University of Technology, AUT (Tehran Polytechnic) B.Sc. in Polymer Engineering, Industrial Polymers
	2009 - 2011 Friedrich-Alexander University Erlangen- Nürnberg, FAU M.Sc. (honors) in Advance Materials and Processes (MAP)
<b>Professional experience</b>	2012 - 2016 Scientific staff member/Group leader of Polymer Foams Polymer Engineering, University of Bayreuth
	2016 - present Manager R&D Packaging Development Schwan STABILO Cosmetics

# Publications

## Reviewed Publications:

*R. Bahrami, T. I. Löbbling, A. H. Gröschel, H. Schmalz, A. H. E. Müller, V. Altstädt*

**The impact of Janus nanoparticles on the compatibilization of immiscible polymer blends under technologically relevant conditions**

ACS Nano 8(10), pp. 10048-10056, 2014

*R. Bahrami, T. I. Löbbling, H. Schmalz, A. H. E. Müller, V. Altstädt*

**Micromechanics of “raspberry” morphology in PPE/SAN polymer blends compatibilized with linear ABC triblock terpolymers**

Polymer 80, pp. 52-63, 2015

*R. Bahrami, S. Bärwinkel, T. I. Löbbling, H. Schmalz, A. H. E. Müller, V. Altstädt*

**Polymer foams made of immiscible polymer blends compatibilized by Janus particles- effect of compatibilization foam morphology**

Advanced Engineering Materials 18(5), pp. 814-825, 2016

*R. Bahrami, T. I. Löbbling, H. Schmalz, A. H. E. Müller, V. Altstädt*

**Synergistic effects of Janus particles and triblock terpolymers on toughness of immiscible polymer blends**

Polymer 109, pp. 229-237, 2017

## Conference Contributions:

*R. Bahrami, M. L. Stumpf (Lang), V. Altstädt*

**Morphology characterization of PPE/SAN immiscible polymer blends compatibilized by Janus particles**

Poster: 18th International Conference on Ternary and Multinary Compounds (ICTMC18), Salzburg, Austria, 2012

*R. Bahrami, T. I. Löbbling, H. Schmalz, A. H. E. Müller, V. Altstädt*

**Nano-scale Janus particles as compatibilizers for tailoring the microstructure of PPE/SAN immiscible polymer blends**

Oral presentation: Polymer Processing Society (PPS-29), Nürnberg, Germany, 2013

*V. Altstädt, R. Bahrami, T. I. Löbling, H. Schmalz, A. H. E. Müller*

**Tailoring the microstructure of PPE/SAN polymer blends with nano-scale Janus particles**

Oral presentation: 15. Problemseminar Polymermischungen, Halle (Saale), Germany, 2014

*R. Bahrami, T. I. Löbling, H. Schmalz, A. H. E. Müller, V. Altstädt*

**Janus particles as blend compatibilizers: Micromechanics of raspberry morphology**

Oral presentation: Polymer Processing Society (PPS-30), Cleveland, USA, 2014

*R. Bahrami, T. I. Löbling, H. Schmalz, A. H. E. Müller, V. Altstädt*

**Effect of Janus particles and SBM triblock terpolymers compatibilization on the micromechanics of PPE/SAN blends**

Oral presentation: European Polymer Congress (epf 2015), Dresden, Germany, 2015

*R. Bahrami, T. I. Löbling, H. Schmalz, A. H. E. Müller, V. Altstädt*

**Fatigue crack propagation behaviour of multiphase immiscible blends compatibilized with Janus particles**

Oral presentation: Polymertec16, Merseburg, Germany, 2016